Stochastic models of intracellular transport

Paul C. Bressloff[1,2] and Jay M. Newby[2]

[1]*Department of Mathematics,*
University of Utah
155 South 1400 East
Salt Lake City
UT 84112

[2]*Mathematical Institute,*
University of Oxford,
94-96 St. Giles',
Oxford,
OX1 3LS UK

The interior of a living cell is a crowded, heterogenuous, fluctuating environment. Hence, a major challenge in modeling intracellular transport is to analyze stochastic processes within complex environments. Broadly speaking, there are two basic mechanisms for intracellular transport: passive diffusion and motor-driven active transport. Diffusive transport can be formulated in terms of the motion of an over-damped Brownian particle. On the other hand, active transport requires chemical energy, usually in the form of ATP hydrolysis, and can be direction specific, allowing biomolecules to be transported long distances; this is particularly important in neurons due to their complex geometry. In this review we present a wide range of analytical methods and models of intracellular transport. In the case of diffusive transport, we consider narrow escape problems, diffusion to a small target, confined and single-file diffusion, homogenization theory, and fractional diffusion. In the case of active transport, we consider Brownian ratchets, random walk models, exclusion processes, random intermittent search processes, quasi-steady-state reduction methods, and mean field approximations. Applications include receptor trafficking, axonal transport, membrane diffusion, nuclear transport, protein-DNA interactions, virus trafficking, and the self–organization of subcellular structures.

CONTENTS

I. INTRODUCTION

The efficient delivery of proteins and other molecular products to their correct location within a cell (intracellular transport) is of fundamental importance to normal cellular function and development (Alberts *et al.*, 2008). Moreover, the breakdown of intracellular transport is a major contributing factor to many degenerative diseases. Broadly speaking, there are two basic mechanisms for intracellular transport; passive diffusion within the cytosol

or the surrounding plasma membrane of the cell, and active motor–driven transport along polymerised filaments such as microtubules and F-actin that comprise the cytoskeleton. Newly synthesised products from the nucleus are mainly transported to other intracellular compartments or the cell membrane via a microtubular network that projects radially from organising centres (centrosomes). The same network is used to transport degraded cell products back to the nucleus. Moreover, various animal viruses including HIV take advantage of microtubule-based transport in order to reach the nucleus from the cell surface and release their genome through nuclear pores (Damm and Pelkmans, 2006). The challenges of intracellular transport are particularly acute for brain cells (neurons), which are amongst the largest and most complex cells in biology, in particular, with regards to the efficient trafficking of newly synthesized proteins from the cell body or soma to distant locations on the axon or dendrites. In healthy cells, the regulation of protein trafficking within a neuron provides an important mechanism for modifying the strength of synaptic connections between neurons (Bredt and Nicoll, 2003; Choquet and Triller, 2003; Newpher and Ehlers, 2008; Triller and Choquet, 2005), and synaptic plasticity is generally believed to be the cellular substrate of learning and memory. On the other hand, various types of dysfunction in protein trafficking appear to be a major contributory factor to a number of neurodegenerative diseases associated with memory loss including Alzheimers (de Vos *et al.*, 2008).

Over the past 20 years, intracellular transport has been a major application area within the statistical physics community, and has driven a large number of papers on the stochastic modeling and analysis of molecular motors and diffusion in complex environments. Many excellent reviews have been written on topics relevant to intracellular transport including anomalous diffusion (Bouchaud and Georges, 1990; Metzler and Klafter, 2000, 2004), molecular motors (Julicher *et al.*, 1997; Keller and Bustamante, 2000; Kolomeisky and Fisher, 2007; Lipowsky and Klumpp, 2005; Reimann, 2002), reaction kinetics (Hanggi *et al.*, 1990), confined diffusion (Burada *et al.*, 2009), random intermittent search processes (Benichou *et al.*, 2011b), and exclusion processes (Chou *et al.*, 2011; Evans and Hanney, 2005; Schadschneider *et al.*, 2010). However, as far as we are aware, there has not been a substantial review in which intracellular transport itself is the central topic.

The overall goal of the current review is to provide an up to date and unified perspective on stochastic models of intracellular transport. One of the major aims is to cover a wide range of models and analytical methods, highlighting links between them wherever possible. Although it is not possible to cover every topic in complete detail, sufficient details are provided to make the review as self-contained and pedagogical as possible. Another aim of the review is to highlight aspects of stochastic processes that are particularly relevant to intracellular transport, some of which have not been emphasised in other reviews. These include the following:

1. Since the aqueous environment (cytosol) of a cell is highly viscous at the length scale of macromolecules (low Reynolds number), a diffusing particle can be treated as an overdamped Brownian particle where inertial effects are ignored.

2. One of the characteristics of diffusive transport inside the cell is that often a particle is confined to a domain with small exits on the boundary of the domain. Examples include an ion looking for an open ion channel within the cell membrane (Grigoriev *et al.*, 2002), the transport of newly transcribed mRNA from the nucleus to the cytoplasm via nuclear pores (Gorski *et al.*, 2006; Mistelli, 2008), the confinement of neurotransmitter receptors within a synapse of a neuron (Holcman and Schuss, 2004), and the confinement of calcium and other signaling molecules within sub cellular compartments such as dendritic spines (Biess *et al.*, 2011). This has led to recent interest in using Green's function and asymptotic methods to solve the so–called narrow escape problem (Benichou and Voituriez, 2008; Grigoriev *et al.*, 2002; Holcman and Schuss, 2004; Pillay *et al.*, 2010; Schuss *et al.*, 2007; Singer *et al.*, 2006a,b).

3. A related class of problems involves the search for a small target within the interior of a cellular domain. In this case it is necessary to extend the Smoluchowski theory of diffusion limited reaction rates to bounded domains or to more complex transport processes than simple diffusion. One example is the arrival of a receptor at a localised reaction site on the surface of an immune cell, which is a key step in the signaling cascade responsible for activating the cell (Coombs *et al.*, 2009). Another important example is a promotor protein searching for its binding site on DNA, which is facilitated by an intermittent search process in which the particle switches between 3D and 1D diffusion (Berg *et al.*, 1981; Coppey *et al.*, 2004; Halford and Marko, 2004; Kolomeisky, 2011; Mirny *et al.*, 2009; Sheinman *et al.*, 2012).

4. The intracellular environment is extremely crowded with macromolecules, subcellular compartments and confinement domains, suggesting that anomalous subdiffusion is likely to occur (Dix and Verkman, 2008). The plasma membrane is also a complex heterogeneous environment (Jacobson *et al.*, 2007; Kusumi *et al.*, 2005; Vereb *et al.*, 2003). Thus, many papers model diffusion in such environments in terms of continuous time random walks and fractional Brownian motion. However, it is still unclear to what extent intracellular diffusion is anomalous in the long–time limit rather than just at intermediate times. This motivates studying diffusion in the presence of obstacles and transient traps whereby normal diffusion is recovered asymptotically (Bressloff and Earnshaw, 2007; Santamaria *et al.*, 2006; Saxton, 1994, 2007).

5. Another common form of diffusion within cells is the transport of particles through a narrow biological pore or channel (Hille, 2001; Roux *et al.*, 2004; Schuss *et al.*, 2001). Restricting the volume of the phase space available to the diffusing particles by means of confining boundaries or obstacles causes striking entropic effects (Burada *et al.*, 2009). Moreover, various mechanisms of facilitated diffusion can occur through interactions between a diffusing particle and proteins within the channel, as exemplified by nuclear pore complexes, which are the sole mediators of exchange between the nucleus and cytoplasm (Fahrenkrog *et al.*, 2004; Macara, 2001; Rout *et al.*, 2003; Tran and Wente, 2006). When a channel becomes sufficiently narrow, particles are no longer able to pass each other (single-file diffusion), which imposes strong constraints on the diffusive motion. In particular, a tagged particle exhibits anomalous subdiffusion on long time scales (Barkai and Silbey, 2009; Harris, 1965; Lebowitz and Percus, 1967; Levitt, 1973)

6. There have been many stochastic models of motor-driven transport at multiple spatial and temporal scales, ranging from Brownian ratchet models (Reimann, 2002) to random walk models (Lipowsky and Klumpp, 2005; Muller *et al.*, 2008b) to systems of partial differential equations (PDEs) (Reed *et al.*, 1990; Smith and Simmons, 2001). However, many of these treatments neglect the fact that the goal of such transport is to deliver molecular cargo to specific sites. This then naturally leads to a connection with random intermittent search processes (Bressloff and Newby, 2009; Loverdo *et al.*, 2008; Newby and Bressloff, 2010a,b). It also raises the important question regarding signaling mechanisms responsible for localizing a motor complex at a target. Another issue in active transport involves exclusion effects due to multiple motors moving along the same filament track (Blythe and Evans, 2007; Chou *et al.*, 2011; Schadschneider *et al.*, 2010).

7. Most cellular structures including the cytoskeleton and various organelles are highly dynamic, open systems that are constantly exchanging energy and molecules with the cytosol or other compartments. The formation and maintenance of such dynamic structures have properties suggestive of far from equilibrium self-organizing systems (Heinrich and Rapoport, 2005; Mistelli, 2001; Semplice *et al.*, 2012). One of the challenges in cellular biology is understanding how the coupling of diffusive or vesicular transport with chemical reactions and cell signaling generates self-organizing structures within a cell. One clear example is given by the actin and microtubular cytoskeletons, which not only provide tracks for intracellular transport, but also determine cell shape and polarity (Lacayo *et al.*, 2007), drive cell motility (Mogilner and Edelstein-Keshet, 2002; Rafelski and Theriot, 2004), and form the spindle apparatus during cell division (Eggert *et al.*, 2006; Glotzer, 2009). Self-organization of the cytoskeleton and its regulation by cell signaling also plays a crucial role in axonal growth and guidance during neurogenesis and cortical development (Goldberg, 2003; Graham *et al.*, 2006; Suter and Miller, 2011).

The structure of the paper is as follows. In Sec. II, diffusive transport is developed from the perspective of the Langevin equation for an overdamped Brownian particle, and various first passage time problems are considered (points 1-3). In Sec. III, the anomalous effects of molecular crowding, trapping and confinement are discussed (points 4 and 5). The differences in diffusive behavior at multiple timescales are highlighted. In Sec. IV, the theory of motor-driven active transport is reviewed, emphasizing the connection with random intermittent search processes (point 6). A method for reducing the complexity of molecular motor models is also described, and used to study the effects of local signaling. Finally, in Sec. V some examples illustrating the role of intracellular transport in self-organizing systems are presented (point 7).

II. DIFFUSIVE TRANSPORT: FIRST-PASSAGE PROBLEMS

A. Derivation of the diffusion equation

1. Random walks

Consider a particle that hops at discrete times between neighboring sites on a one–dimensional (1D) lattice with unit spacing. At each step, the random walker moves a unit distance to the right with probability p or to the left with probability $q = 1 - p$. Let $P_n(r)$ denote the probability that the particle is at site r at the Nth time step. The evolution of the probability distribution is described by the discrete-time master equation

$$P_N(r) = pP_{N-1}(r-1) + qP_{N-1}(r+1), \quad r \in \mathbb{Z}. \quad (2.1)$$

If $q = p = 1/2$ then the random walk is symmetric or unbiased, whereas for $p > q$ $(p < q)$ it is biased to the right (left). In order to solve this equation, introduce the discrete Laplace-Fourier transform

$$\widetilde{P}(k, z) = \sum_{N=0}^{\infty} z^N \sum_{r=-\infty}^{\infty} e^{ikr} P(r, N). \quad (2.2)$$

Applying this transform to the master equation and multiplying by an extra factor of z, it is straightforward to show that

$$\widetilde{P}(k, z) - \sum_{r=-\infty}^{\infty} P_0(r)e^{ikr} = z(pe^{ik} + qe^{-ik})\widetilde{P}(k, z).$$

Assuming that the particle starts at the origin so that $P_0(r) = \delta_{r,0}$, we have

$$\widetilde{P}(k, z) = \frac{1}{1 - zu(k)}, \quad u(k) = pe^{ik} + qe^{-ik}. \quad (2.3)$$

Here $u(k)$ is the Fourier transform of the single-step hopping probability. The original probability distribution can now be reconstructed using the inverse transform

$$P_N(r) = \oint \frac{dz}{2\pi i z^{N+1}} \int_{-\pi}^{\pi} \frac{dk}{2\pi} \mathrm{e}^{-ikr} \widetilde{P}(k,z) \qquad (2.4)$$

with the z-contour taken around the unit circle. Taylor expanding the solution for $\widetilde{P}(k,z)$ in terms of z thus yields

$$P_N(r) = \frac{1}{2\pi} \int_{-\pi}^{\pi} \mathrm{e}^{-ikr} u(k)^N dk \qquad (2.5)$$

$$= \frac{1}{2\pi} \int_{-\pi}^{\pi} \mathrm{e}^{-ikr} \sum_{m=0}^{N} \binom{N}{m} p^m q^{N-m} \mathrm{e}^{-ik(N-2m)} dk$$

$$= \frac{N!}{\left(\dfrac{N+r}{2}\right)! \left(\dfrac{N-r}{2}\right)!} p^{(N+r)/2} q^{(N-r)/2}.$$

Using Stirling's approximation for large N,

$$\log n! \approx n \log n - n + \frac{1}{2} \log(2\pi n),$$

and assuming $p, q \approx 1/2$, it can be shown that

$$P_N(r) \sim \frac{1}{\sqrt{2\pi N}} \mathrm{e}^{[r-N(p-q)]^2/2N}.$$

(To be more precise, $P_N(r)$ should be multiplied by a factor of 2, since $N-r$ must be even). Indeed, the Gaussian form of $P_N(r)$ in the large time limit arises universally whenever the mean and variance of the displacement Δr in a single step are finite. This is basically a statement of the central-limit theorem. One way to see this is to note that when $\langle \Delta r \rangle$ and $\langle \Delta r^2 \rangle$ are both finite, $u(k)$ has the small-k series expansion

$$u(k) = 1 + ik\langle \Delta r \rangle - \frac{1}{2} k^2 \langle \Delta r^2 \rangle + \ldots \sim \mathrm{e}^{ik\langle \Delta r \rangle - \frac{1}{2} k^2 \langle \Delta r^2 \rangle}.$$

Substituting this approximation into the first line of equation (2.5) using the fact that the integral is dominated by the behavior in the region around $k = 0$ when N is large, the resulting Gaussian integral yields the approximation

$$P_N(r) \sim \frac{1}{\sqrt{2\pi N\langle \Delta r^2 \rangle}} \mathrm{e}^{(r-N\langle \Delta r \rangle)^2/2N\langle \Delta r^2 \rangle}. \qquad (2.6)$$

Having analyzed the discrete random walk, it is now possible to take an appropriate continuum limit to obtain a diffusion equation in continuous space and time. First, introduce infinitesimal step lengths δx and δt for space and time and set $P_N = \rho(x,t)\delta x$ with $x = r\delta x, t = N\delta t$. Substituting into the master equation (2.1) gives the following equation for the probability density $\rho(x,t)$:

$$\rho(x,t) = p\rho(x - \delta x, t - \delta t) + q\rho(x + \delta x, t - \delta t)$$

$$\approx (p+q) \left[\rho(x,t) - \frac{\partial \rho}{\partial t} \delta t \right] - (p-q)\frac{\partial \rho}{\partial x}\delta x$$

$$+ \frac{(p+q)}{2} \frac{\partial^2 \rho}{\partial x^2} \delta x^2,$$

where ρ has been Taylor expanded to first order in δt and to second order in δx. Note that $p + q = 1$. Dividing through by δt and taking the continuum limit $\delta x, \delta t \to 0$ such that the quantities V, D are finite, where

$$V = \lim_{\delta x, \delta t \to 0} (p-q)\frac{\delta x}{\delta t}, \quad D = \lim_{\delta x, \delta t \to 0} \frac{\delta x^2}{2\delta t},$$

yields the Fokker–Planck (FP) equation with constant drift

$$\frac{\partial \rho(x,t)}{\partial t} = -V \frac{\partial [\rho(x,t)]}{\partial x} + D \frac{\partial^2 \rho(x,t)}{\partial x^2}. \qquad (2.7)$$

Note that $p = 0.5 + \kappa\delta x$ and $q = 0.5 - \kappa\delta x$ with $\kappa = \mathcal{O}(1)$. Applying the same continuum limit to the Gaussian distribution (2.6) gives the density

$$\rho(x,t) = \frac{1}{\sqrt{4\pi Dt}} \mathrm{e}^{-(x-Vt)^2/4Dt}, \qquad (2.8)$$

which is the fundamental solution of equation (2.7) under the initial condition $\rho(x,0) = \delta(x)$. Although we will mainly consider continuum models of diffusion, it should be noted that random walk models are particularly helpful in developing theories of diffusion in complex heterogeneous media and associated phenomena such as anomalous diffusion (Bouchaud and Georges, 1990; Hughes, 1995; Metzler and Klafter, 2000), see also section IIIA.

2. Langevin equation

Consider a microscopic particle moving in a water solution such as found in the interior of cells (the cytoplasm). Suppose that it is subject to some external force of size F. Collisions with fluid molecules have two distinct effects. First, they induce an apparent diffusive or Brownian motion of the particle, and second they generate an effective frictional force that opposes motion induced by the external force. In the case of microscopic particles, water acts as a highly viscous medium (low Reynolds number) so that any particle quickly approaches terminal velocity and inertial effects can be ignored. The effects of all collisions on the motion of the particle can then be represented in terms of the Langevin or stochastic differential equation (Gardiner, 2009)

$$\frac{dX(t)}{dt} = \frac{F(X(t))}{\gamma} + \xi(t), \qquad (2.9)$$

where $X(t)$ is the stochastic position of the particle at time t, γ is a drag coefficient, and $\xi(t)$ is a Gaussian noise term with

$$\langle \xi(t) \rangle = 0, \quad \langle \xi(t)\xi(t') \rangle = 2D\delta(t - t'). \quad (2.10)$$

Suppose, for the moment, that F is a constant. Formally integrating equation (2.9) with $X(0) = 0$ shows that

$$X(t) = Vt + \int_0^t \xi(t')dt'$$

with $V = F/\gamma$ the terminal velocity. Averaging with respect to the noise then implies that

$$\langle X(t) \rangle = Vt, \quad \langle (X(t) - Vt)^2 \rangle = 2Dt.$$

Thus the mean-square displacement about the deterministic trajectory $x(t) = Vt$ is given by $\langle \Delta X(t) \rangle = 2Dt$, which suggests identifying D as a diffusion coefficient. Moreover, $X(t)$ is itself a Gaussian process whose probability density $p(x, t)$ evolves according to the FP equation (2.7). Under the initial condition $p(x, 0) = \delta(x)$, this can be solved to give the Gaussian distribution (2.8).

We now present a more formal derivation of the FP equation applicable to position–dependent forces $F(x)$. Since $X(t)$ is a stochastic variable, each simulation of the Langevin equation generates one sample out of the set of all possible trajectories. This motivates an alternative way of thinking about such a stochastic process, namely in terms of the conditional probability density $p(x, t|x_0, t_0)$ that the particle is at x at time t, given that it started at x_0 at time t_0. Exploiting the fact that the stochastic process is Markovian, that is, $X(t + \delta t)$ only depends on the state at the previous time step $X(t)$, it follows that $p(x, t|x_0, t_0)$ satisfies the Chapman–Kolmogorov equation

$$p(x, t|x_0, t_0) = \int_{-\infty}^{\infty} p(x, t|x', t')p(x', t'|x_0, t_0)dx' \quad (2.11)$$

for any $t' \in [t_0, t]$. Such an equation is a defining property of a Markov process. Consider an infinitesimal version of this equation by taking $t \to t + \delta t, t' \to t$ and setting $w(x, t; u, \delta t) = p(x + u, t + \delta t|x, t)$:

$$p(x, t + \delta t) = \int_{-\infty}^{\infty} w(x - u, t; u, \delta t)p(x - u, t)du,$$

where the initial argument (x_0, t_0) has been suppressed. Now suppose that over a sufficiently small time window δt, large jumps u in position are highly unlikely, so that u can be treated as a small variable. Performing a Taylor expansion with respect to u gives

$$p(x, t + \delta t) = \alpha_0(x, t)p(x, t) - \partial_x[\alpha_1(x, t)p(x, t)]$$
$$+ \frac{1}{2}\partial_{xx}^2[\alpha_2(x, t)p(x, t)] + \dots \quad (2.12)$$

where

$$\alpha_n(x, t) = \int_{-\infty}^{\infty} w(x, t; u, \delta t)u^n du. \quad (2.13)$$

The Langevin Eq. (2.9) can be used to calculate the coefficients α_n. First, rewrite Eq. (2.9) in the infinitesimal form

$$X(t + \delta t) = x + F(x)\delta t/\gamma + \delta t\xi(t),$$

given that $X(t) = x$. This implies that the transition probability w can be written as

$$w(x, t; u, \delta t) = \langle \delta(x + u - X(t + \delta t)) \rangle_\xi$$
$$= \langle \delta(u - F(x)\delta t/\gamma - \delta t\xi(t)) \rangle_\xi.$$

Discretizing time in units of δt means that $\xi(t)$ becomes a Gaussian random variable with zero mean and variance $2D/\delta t$. The corresponding probability density is

$$p(\xi) = \sqrt{\delta t/4\pi D}\,\mathrm{e}^{-\xi^2 \delta t/4D}.$$

Hence, averaging with respect to $\xi(t)$,

$$w(x, t; u, \delta t) = \sqrt{\frac{1}{4\pi D\delta t}}\,\mathrm{e}^{-(u - F(x)\delta t/\gamma)^2/4D\delta t}.$$

It follows that

$$\alpha_0 = 1, \quad \alpha_1 = F(x)\delta t/\gamma, \quad \alpha_2 = 2D\delta t + \alpha_1^2, \quad (2.14)$$

and $\alpha_m = \mathcal{O}(\delta t^2)$ for $m > 2$. Substituting these results into Eq. (2.12) and taking the limit $\delta t \to 0$ finally leads to the Fokker–Planck (FP) equation

$$\frac{\partial p(x, t)}{\partial t} = -\frac{1}{\gamma}\frac{\partial[F(x)p(x, t)]}{\partial x} + D\frac{\partial^2 p(x, t)}{\partial x^2}. \quad (2.15)$$

Note that it is straightforward to generalize the above analysis to higher dimensions. Assuming for simplicity isotropic diffusion and friction, Eq. (2.9) becomes

$$\frac{dX_i}{dt} = \frac{F_i(\mathbf{X})}{\gamma} + \xi_i(t), \quad i = 1, \dots, d \quad (2.16)$$

with $\langle \xi_i(t) \rangle = 0$ and $\langle \xi_i(t)\xi_j(t') \rangle = 2D\delta_{i,j}\delta(t - t')$. The corresponding multivariate FP equation is

$$\frac{\partial p(\mathbf{x}, t)}{\partial t} = -\frac{1}{\gamma}\boldsymbol{\nabla} \cdot [\mathbf{F}(\mathbf{x})p(\mathbf{x}, t)] + D\boldsymbol{\nabla}^2 p(\mathbf{x}, t). \quad (2.17)$$

The 1D FP Eq. (2.15) can be rewritten as a probability conservation law according to

$$\frac{\partial p(x, t)}{\partial t} = -\frac{\partial J(x, t)}{\partial x}, \quad (2.18)$$

where

$$J(x, t) = \frac{1}{\gamma}F(x)p(x, t) - D\frac{\partial p(x, t)}{\partial x} \quad (2.19)$$

is the probability flux. An equilibrium steady-state solution corresponds to the conditions $\partial p / \partial t = 0$ and $J \equiv 0$. This leads to the first-order ODE for the equilibrium density $P(x)$: $DP'(x) - \gamma^{-1}F(x)P(x) = 0$, which has the solution

$$P(x) = \mathcal{N}e^{-\Phi(x)/\gamma D}. \qquad (2.20)$$

Here $\Phi(x) = -\int^x F(y)dy$ is a potential energy function and $\mathcal{N}$ is a normalization factor (assuming that it exists). Comparison of the equilibrium distribution with the Boltzmann-Gibbs distribution of statistical mechanics yields the Einstein relation

$$D\gamma = k_B T, \qquad (2.21)$$

where T is the temperature (in degrees Kelvin) and $k_B \approx 1.4 \times 10^{-23} J K^{-1}$ is the Boltzmann constant. This formula relates the variance of environmental fluctuations to the strength of dissipative forces and the temperature. In the case of a sphere of radius R moving in a fluid of viscosity η, Stoke's formula can be used, that is, $\gamma = 6\pi\eta R$. For water at room temperature, $\eta \sim 10^{-3} kg\, m^{-1}s^{-1}$ so that a particle of radius $R = 10^{-9}m$ has a diffusion coefficient $D \sim 100\mu m^2 s^{-1}$.

So far, we have considered diffusive–like motion from the probabilistic perspective of a single microscopic particle moving in a fluid medium. However, it is possible to reinterpret Eq. (2.15) or (2.17) as a deterministic advection–diffusion equation for the concentration $u(x,t)$ of many particles. That is, ignoring any interactions or correlations between the particles, set $u(x,t) = Np(x,t)$ where N is the total number of particles (assumed large). Multiplying both sides of Eq. (2.15) by N then leads to the corresponding advection–diffusion (or Smoluchowski) equation for $u(x,t)$ with $NJ(x,t)$ interpreted as the particle flux arising from a combination of advection and Fickian diffusion. In this review we will often switch between the microscopic probabilistic formulation of diffusion and the macroscopic deterministic formulation, which can be viewed as a mean-field limit of the former. However, the relationship between macroscopic and microscopic formulations is more complicated when chemical reactions are included. Macroscopically, reactions are described in terms of the deterministic law of mass action, whereas microscopically they are modeled stochastically using a chemical master equation. Differences between the two levels of modeling become significant when the number of interacting molecules becomes small (Kampen, 1992).

Finally, note that another important issue arises in the case of space–dependent diffusion coefficients. From the macroscopic picture of Fickian diffusion, the conservation equation $\partial_t u = -\nabla \cdot \mathbf{J}$ can lead to two different forms of the diffusion equation, depending on whether $\mathbf{J}(\mathbf{x},t) = \boldsymbol{\nabla}[D(\mathbf{x})u(\mathbf{x},t)]$ or $\mathbf{J}(\mathbf{x},t) = D(\mathbf{x})\boldsymbol{\nabla}u(\mathbf{x},t)$. (These are equivalent when D is a constant). In order to distinguish between the two cases, it is necessary to incorporate details regarding the microscopic dynamics using, for example, kinetic theory (Bringuier, 2009; van Milligen et al., 2005). From the perspective of the FP equation, a space–dependent diffusion coefficient arises when the corresponding Langevin equation is driven by multiplicative (state-dependent) noise, and the position of the diffusion coefficient will depend on whether the noise is interpreted in the sense of Ito or Statonovich (Gardiner, 2009; Kampen, 1992). The situation is even more complicated in anisotropic heterogeneous media, where it is no longer possible to characterize the rate of diffusion in terms of a single coefficient. One now needs to consider a diffusion tensor, see Sec. IVE.

B. First passage times

One of most important ways of quantifying the efficacy of diffusive transport is in terms of the first passage time to reach a target (Gardiner, 2009; Redner, 2001). In the case of intracellular transport, such a target could represent a substrate for a subsequent biochemical reaction or an exit from some bounded domain such as a chemical synapse. (Although we will focus on spatially continuous processes, an analogous theory of first passage times can be developed for spatially discrete random walks (Hughes, 1995; Kampen, 1992)). Consider a particle whose position evolves according to the 1D Langevin Eq. (2.9) with motion restricted to the bounded domain $x \in [0, L]$. Suppose that the corresponding FP Eq. (2.15) has a reflecting boundary condition at $x = 0$ and an absorbing boundary condition at $x = L$:

$$J(0,t) = 0, \quad p(L,t) = 0. \qquad (2.22)$$

We would like to determine the stochastic time $T(y)$ for the particle to exit the right hand boundary given that it starts at location $y \in [0, L]$ at time t. As a first step, we introduce the survival probability $\mathbb{P}(y,t)$ that the particle has not yet exited the interval at time t:

$$\mathbb{P}(y,t) = \int_0^L p(x,t|y,0)dx. \qquad (2.23)$$

It follows that $\text{Prob}[T(y) \leq t] = 1 - \mathbb{P}(y,t)$ and we can define the first passage time (FPT) density according to

$$f(y,t) = -\frac{\partial \mathbb{P}(y,t)}{\partial t}. \qquad (2.24)$$

The FPT density satisfies a backwards FP equation, which can be derived from the Chapman-Kolmogorov Eq. (2.11) by differentiating boths sides with respect to the intermediate time t' and using the forwards equation. Using the fact that $\partial_{t'}p(x,t|x',t') = -\partial_t p(x,t|x',t')$, which follows from time-translation invariance, then yields the

backwards FP equation for p:

$$\partial_t p(x,t|x',t') = A(x')\partial_{x'} p(x,t|x',t') + D\partial^2_{x'x'} p(x,t|x',t'),$$
(2.25)

where $A(x) = F(x)/\gamma$. Taking $x' \to y$, $t' = 0$ and integrating with respect to x shows that $\mathbb{P}(y,t)$, and hence $f(y,t)$, also satisfy a backwards FP equation:

$$\frac{\partial \mathbb{P}(y,t)}{\partial t} = A(y)\frac{\partial \mathbb{P}(y,t)}{\partial y} + D\frac{\partial^2 \mathbb{P}(y,t)}{\partial y^2}.$$
(2.26)

A quantity of particular interest is the mean first passage time (MFPT) $\tau(y)$ defined according to

$$\tau(y) = \langle T(y) \rangle \equiv \int_0^\infty f(y,t)t\,dt$$
(2.27)
$$= -\int_0^\infty t\frac{\partial \mathbb{P}(y,t)}{\partial t}dt = \int_0^\infty \mathbb{P}(y,t)dt,$$

after integration by parts. Hence, integrating both sides of Eq. (2.26) shows that the MFPT satisfies the ODE

$$A(y)\frac{d\tau(y)}{dy} + D\frac{d^2\tau(y)}{dy^2} = -1.$$
(2.28)

Eq. (2.28) is supplemented by reflecting and absorbing boundary conditions for the backwards FP equation:

$$\tau'(0) = 0, \quad \tau(L) = 0.$$
(2.29)

It is straightforward to solve Eq. (2.28) by direct integration (Gardiner, 2009). First, introduce the integration factor

$$\psi(y) = \exp\left(\frac{1}{D}\int_0^y A(y')dy'\right) = \exp\left(-V(y)/k_B T\right),$$

where $D^{-1}A(y) = (D\gamma)^{-1}F(y) = -(k_B T)^{-1}V'(y)$ and $V(y)$ is a potential energy. Eq. (2.28) becomes

$$\frac{d}{dy}[\psi(y)\tau'(y)] = -\frac{\psi(y)}{D}$$

so that

$$\psi(y)\tau'(y) = -\frac{1}{D}\int_0^y \psi(y')dy',$$

where the boundary condition $\tau'(0) = 0$ has been used. Integrating once more with respect to y and using $\tau(L) = 0$ then gives

$$\tau(y) = \int_y^L \frac{dy'}{\psi(y')}\int_0^{y'} \frac{\psi(y'')}{D}dy''.$$
(2.30)

In the case of pure diffusion ($A(x) = 0$), we have $\psi(y) = 1$ and $\tau(y) = (L^2 - y^2)/2D$. It follows that for any finite $L - y$, $\tau(y) \to \infty$ as $L \to \infty$. Thus, although 1D diffusion is recurrent i.e. the particle surely reaches the origin, the average time it takes is infinite. (This can also be understood in terms of the scaling properties of the FPT density, see below). Now suppose that L is finite and the particle starts at the left–hand boundary. The corresponding MFPT is then $\tau = L^2/D$. Within the cytosol of cells, macromolecules such as proteins tend to have diffusivities $D < 1\mu m^2 s^{-1}$, which is due to effects such as molecular crowding, see Sec. III. This implies that the mean time for a diffusing particle to travel a distance $100\mu m$ is at least $10^4 s$ (a few hours), whereas to travel a distance $1mm$ is at least $10^6 s$ (10 days). Since neurons, which are the largest cells in humans, have axonal and dendritic protrusions that can extend from $1mm$ up to $1m$, the mean travel time due to passive diffusion becomes prohibitively large, and an active form of transport becomes essential.

It is also possible to extend the above analysis to the case where the particle can exit from either end (Gardiner, 2009; Redner, 2001). It is often of interest to keep track of which end the particle exits, which leads to the concept of a splitting probability. Let $G_0(x,t)$ denote the probability that the particle exits at $x = 0$ after time t, having started at the point x. Then

$$G_0(x,t) = -\int_t^\infty J(0,t'|x,0)dt'$$
(2.31)

with

$$J(0,t|x,0) = A(0)p(0,t|x,0) - D\left.\frac{\partial p(y,t|x,0)}{\partial y}\right|_{y=0}.$$

Differentiating with respect to t and using the backwards FP Eq. (2.25) gives

$$\frac{\partial G_0(x,t)}{\partial t} = J(0,t|x,0) = -\int_t^\infty \frac{\partial J(0,t'|x,0)}{\partial t'}dt'$$
$$= A(x)\frac{\partial G_0(x,t)}{\partial x} + D\frac{\partial^2 G_0(x,t)}{\partial x^2}.$$
(2.32)

The hitting or splitting probability that the particle exits at $x = 0$ (rather than $x = L$) is $\Pi_0(x) = G_0(x,0)$. Moreover, the probability that the particle exits at time t through $x = 0$, is $\text{Prob}(T_0(x) > t) = G_0(x,t)/G_0(x,0)$, where $T_0(x)$ is the corresponding conditional FPT. Since the conditional MFPT satisfies

$$\tau_0(x) = -\int_0^\infty t\frac{\partial \text{Prob}(T_0(x) > t)}{\partial t}dt = \int_0^\infty \frac{G_0(x,t)}{G_0(x,0)}dt,$$

Eq. (2.32) is integrated with respect to t to give

$$A(x)\frac{\partial \Pi_0(x)\tau_0(x)}{\partial x} + D\frac{\partial^2 \Pi_0(x)\tau_0(x)}{\partial x^2} = -\Pi_0(x), \quad (2.33)$$

with boundary conditions $\Pi_0(0)\tau_0(0) = \Pi_0(L)\tau_0(L) = 0$. Finally, taking the limit $t \to 0$ in Eq. (2.32) and noting that $J(0,0|x,0) = 0$ for $x \neq 0$,

$$A(x)\frac{\partial \Pi_0(x)}{\partial x} + D\frac{\partial^2 \Pi_0(x)}{\partial x^2} = 0,$$
(2.34)

with boundary conditions $\Pi_0(0) = 1, \Pi_0(L) = 0$. A similar analysis can be carried out for exit through the other end $x = L$ such that $\Pi_0(x) + \Pi_L(x) = 1$.

The above formalism extends to higher spatial dimensions. In particular, suppose that a particle evolves according to the Langevin Eq. (2.16) in a compact domain Ω with boundary $\partial\Omega$. Suppose that at time $t = 0$ the particle is at the point $\mathbf{y} \in \Omega$ and let $T(\mathbf{y})$ denote the first passage time to reach any point on the boundary $\partial\Omega$. The probability that the particle has not yet reached the boundary at time t is then

$$\mathbb{P}(\mathbf{y}, t) = \int_\Omega p(\mathbf{x}, t | \mathbf{y}, 0) d\mathbf{x}, \qquad (2.35)$$

where $p(\mathbf{x}, t | \mathbf{y}, 0)$ is the solution to the multivariate FP Eq. (2.17) with an absorbing boundary condition on $\partial\Omega$. The FPT density is again $f(\mathbf{y}, t) = -d\mathbb{P}(\mathbf{y}, t)/dt$ which, on using Eq. (2.17) and the divergence theorem, can be expressed as

$$f(\mathbf{y}, t) = -\int_{\partial\Omega} [-\mathbf{A}(\mathbf{x}) p(\mathbf{x}, t | \mathbf{y}, 0) + D\nabla p(\mathbf{x}, t | \mathbf{y}, 0)] \cdot d\sigma$$

with $\mathbf{A} = \mathbf{F}/\gamma$. Similarly, by constructing the corresponding backwards FP equation, it can be shown that the MFPT satisfies the equation

$$\mathbf{A}(\mathbf{y}) \cdot \nabla\tau(\mathbf{y}) + D\nabla^2\tau(\mathbf{y}) = -1 \qquad (2.36)$$

with $\partial_n\tau(\mathbf{y}) = 0$ for $\mathbf{y} \in \partial\Omega$.

In the case of 1D diffusion, it is straightforward to calculate the FPT density explicitly. In the absence of boundaries we can set the conditional probability density $p(x, t | x_0, 0) = p(x - x_0, t)$. Similarly the FPT density of arriving for the first time at x at time τ starting from x_0 can be written as $f(x, \tau | x_0, 0) = f(x - x_0, \tau)$. The densities p and f are related according to the integral equation

$$p(x - x_0, t) = \int_0^t p(x - x', t - \tau) f(x' - x_0, \tau) d\tau. \quad (2.37)$$

Taking Laplace transforms,

$$\widetilde{p}(x - x_0, s) = \widetilde{p}(x - x', s) \widetilde{f}(x' - x_0, s). \qquad (2.38)$$

Laplace transforming the Gaussian distribution (2.8) for $V = 0$ yields $\widetilde{p}(x, s) = \frac{1}{\sqrt{4\pi Ds}} e^{-\sqrt{x^2 s/D}}$, so that

$$\widetilde{f}(x - x_0, s) = e^{-\sqrt{(x - x_0)s/D}}.$$

The inverse Laplace transform then yields the Levy-Smirnov distribution

$$f(x - x_0, t) = \frac{1}{t} \sqrt{\frac{(x - x_0)^2}{4\pi Dt}} e^{-(x - x_0)^2/4Dt}. \qquad (2.39)$$

This inverse-Gaussian decays asymptotically as $f(x, t) \sim t^{-3/2}$, which immediately establishes that it does not have a finite first moment, that is, the MFPT from x_0 to x diverges. On the other hand, $\int_0^\infty f(x - x_0, t)dt = 1$ so that the diffusing particle will almost surely hit any point x during its motion.

C. Narrow escape problems

Within the context of intracellular transport, there has been a growing interest in a particular class of first passage processes, namely, the escape of a freely diffusing molecule from a 2D or 3D bounded domain through small absorbing windows on an otherwise reflecting boundary (Benichou and Voituriez, 2008; Grigoriev et al., 2002; Holcman and Schuss, 2004; Schuss et al., 2007). Examples include the FPT for an ion to find an open ion channel situated within the cell membrane or the FPT of a protein receptor to locate a particular target binding site. Within the context of intracellular transport in neurons, recent applications include analyzing the confinement of neurotransmitter receptors within the synapse of a neuron (Bressloff and Earnshaw, 2009; Holcman and Schuss, 2004; Holcman and Triller, 2006) and the the role of dendritic spines in confining signaling molecules such as calcium (Biess et al., 2007; Holcman et al., 2005). (A related class of problems is the FPT for a particle to find a small target within the interior of a cellular domain. One example concerns the arrival of receptors at a localized reaction site on the surface of an immune cell, which is a key step in the signaling cascade leading to the activation of the cell (Coombs et al., 2009), see Sec. II.D). In order to develop the basic theory, we will focus on diffusion in a two–dimensional domain $\Omega \subset \mathbb{R}^2$ whose boundary can be decomposed as $\partial\Omega = \partial\Omega_r \cup \partial\Omega_a$, where $\partial\Omega_r$ represents the reflecting part of the boundary and $\partial\Omega_a$ the absorbing part. We then have a narrow escape problem in the limit that the measure of the absorbing set $|\partial\Omega_a| = \mathcal{O}(\varepsilon)$ is asymptotically small, that is, $0 < \varepsilon \ll 1$. It follows from the analysis of exit times, see Eq. (2.36), that the MFPT to exit the boundary $\partial\Omega_a$ satisfies the equation (in the absence of external forces)

$$\boldsymbol{\nabla}^2\tau(\mathbf{x}) = -\frac{1}{D}, \quad \mathbf{x} \in \Omega \qquad (2.40)$$

with boundary conditions

$$\tau(\mathbf{x}) = 0, \quad \mathbf{x} \in \partial\Omega_a = \cup_{j=1}^N \partial\Omega_j \qquad (2.41)$$

and

$$\partial_n\tau(\mathbf{x}) = 0, \quad \mathbf{x} \in \partial\Omega_r. \qquad (2.42)$$

The absorbing set is assumed to consist of N small disjoint absorbing windows $\partial\Omega_j$ centered at $\mathbf{x}_j \in \partial\Omega$. In the 2D case, each window is a small absorbing arc of length $|\partial\Omega_j| = \varepsilon l_j$ with $l_j = \mathcal{O}(1)$. It is also assumed that the windows are well separated, that is, $|\mathbf{x}_i - \mathbf{x}_j| = \mathcal{O}(1)$ for all $i \neq j$. An example of a Brownian particle in a 2D unit disk with small absorbing windows on the circular boundary is illustrated in Fig. 1.

Since the MFPT diverges as $\varepsilon \to 0$, the calculation of $\tau(\mathbf{x})$ requires solving a singular perturbation problem. There have been a number of studies of the narrow
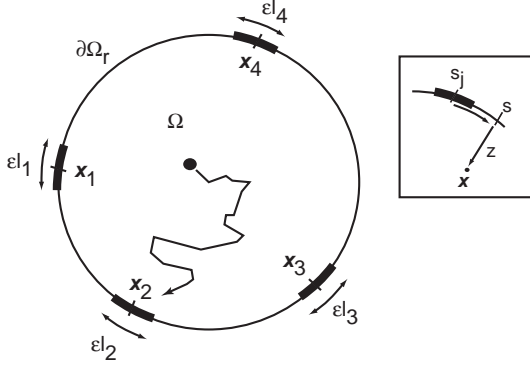
FIG. 1 Example trajectory of a Brownian particle moving in a 2D unit disk with small absorbing windows on an otherwise reflecting circular boundary. Inset: a local coordinate system around the jth arc.

escape problem using a combination of singular perturbation theory and Green's function methods for a variety of geometries in two and three dimensions (Benichou and Voituriez, 2008; Chevalier *et al.*, 2011; Cheviakov *et al.*, 2010; Holcman and Schuss, 2004; Pillay *et al.*, 2010; Schuss *et al.*, 2007; Singer *et al.*, 2006a,b). Here we will review the particular approach of Ward and collaborators (Pillay *et al.*, 2010; Ward, 2000). The basic idea is to construct the asymptotic solution for the MFPT in the limit $\varepsilon \to 0$ using the method of matched asymptotic expansions. That is, an inner or local solution valid in a $\mathcal{O}(\varepsilon)$ neighborhood of each absorbing arc is constructed and then these are matched to an outer or global solution that is valid away from each neighborhood.

In order to construct an inner solution near the jth absorbing arc, Eq. (2.40) is rewritten in terms of a local orthogonal coordinate system (z, s), in which s denotes arc length along $\partial\Omega$ and z is the minimal distance from $\partial\Omega$ to an interior point $\mathbf{x} \in \Omega$, as shown in the inset of Fig. 1. Now introduce stretched coordinates $\widehat{z} = z/\varepsilon$ and $\widehat{s} = (s - s_j)/\varepsilon$, and write the solution to the inner problem as $\tau(\mathbf{x}) = w(\widehat{z}, \widehat{s})$. Neglecting terms of $\mathcal{O}(\varepsilon)$, it can be shown that w satisfies the homogeneous equation (Pillay *et al.*, 2010)

$$\frac{\partial^2 w}{\partial^2 \widehat{z}} + \frac{\partial^2 w}{\partial^2 \widehat{s}} = 0, \quad 0 < \widehat{z} < \infty, \quad -\infty < \widehat{s} < \infty \quad (2.43)$$

with the following boundary conditions on $\widehat{z} = 0$:

$$\frac{\partial w}{\partial \widehat{z}} = 0 \text{ for } |\widehat{s}| > l_j/2, \quad w = 0 \text{ for } |\widehat{s}| < l_j/2. \quad (2.44)$$

The resulting boundary value problem can be solved by introducing elliptic cylinder coordinates. However, in order to match the outer solution we need only specify the far-field behavior of the inner solution, which takes the form

$$w(\mathbf{x}) \sim A_j \left[\log |\mathbf{y}| - \log d_j + o(1)\right] \text{ as } |\mathbf{y}| \to \infty, \quad (2.45)$$

where $d_j = l_j/4$, $|\mathbf{y}| = |\mathbf{x} - \mathbf{x}_j|/\varepsilon = \sqrt{\widehat{z}^2 + \widehat{s}^2}$ and A_j is an unknown constant (that is determined by matching with the outer solution).

As far as the outer solution is concerned, each absorbing arc shrinks to a point $\mathbf{x}_j \in \partial\Omega$ as $\varepsilon \to 0$. Each point $\mathbf{x}_j$ effectively acts as a point source that generates a logarithmic singularity resulting from the asymptotic matching of the outer solution to the far–field behavior of the inner solution. Thus the outer solution satisfies

$$\nabla^2 \tau(\mathbf{x}) = -\frac{1}{D}, \quad \mathbf{x} \in \Omega, \quad (2.46)$$

with reflecting boundary condition

$$\partial_n \tau = 0 \text{ for } \mathbf{x} \in \partial\Omega \backslash \{\mathbf{x}_1, \ldots, \mathbf{x}_N\} \quad (2.47)$$

and

$$\tau(\mathbf{x}) \sim \frac{A_j}{\mu_j} + A_j \log |\mathbf{x} - \mathbf{x}_j| \text{ as } \mathbf{x} \to \mathbf{x}_j, \, j = 1, \ldots, N, \quad (2.48)$$

where

$$\mu_j \equiv -\frac{1}{\log(\varepsilon d_j)}. \quad (2.49)$$

This can be solved in terms of the Neumann Green's function, defined as the unique solution of

$$\nabla^2 G(\mathbf{x}, \mathbf{x}') = \frac{1}{|\Omega|} - \delta(\mathbf{x} - \mathbf{x}'), \quad x \in \Omega \quad (2.50a)$$

$$G(\mathbf{x}, \mathbf{x}_j) \sim -\frac{1}{\pi} \log |\mathbf{x} - \mathbf{x}_j| + R(\mathbf{x}_j, \mathbf{x}_j) \text{ as } \mathbf{x} \to \mathbf{x}_j \in \partial\Omega \quad (2.50b)$$

$$\partial_n G(\mathbf{x}, \mathbf{x}') = 0, \, \mathbf{x} \in \partial\Omega, \quad \int_\Omega G(\mathbf{x}, \mathbf{x}_j) d\mathbf{x} = 0, \quad (2.50c)$$

where $R(\mathbf{x}, \mathbf{x}')$ is the regular part of $G(\mathbf{x}, \mathbf{x}')$. It follows that the outer solution can be expressed in terms of the Green's function G and an unknown constant χ,

$$\tau(\mathbf{x}) = -\pi \sum_{j=1}^N A_i G(\mathbf{x}, \mathbf{x}_j) + \chi. \quad (2.51)$$

Integrating both sides of Eq. (2.51) shows that χ is the MFPT averaged over all possible starting positions:

$$\chi = \overline{\tau} \equiv \frac{1}{|\Omega|} \int_\Omega \tau(\mathbf{x}) d\mathbf{x}. \quad (2.52)$$

The problem has reduced to solving $N+1$ linear equations for $N+1$ unknowns A_i, χ. The first N equations are obtained by matching the near-field behavior of the outer solution as $\mathbf{x} \to \mathbf{x}_j$ with the far–field behavior of the corresponding inner solution (2.45). After cancellation of the logarithmic terms, we have

$$-\pi A_j R_j - \pi \sum_{i \neq j} A_i G_{ji} + \chi = \frac{A_j}{\mu_j}, \quad (2.53)$$

for $j = 1, \ldots, N$, where $G_{ji} \equiv G(\mathbf{x}_j, \mathbf{x}_i)$ and $R_j \equiv R(\mathbf{x}_j, \mathbf{x}_j)$. The remaining equation is obtained by noting that $\boldsymbol{\nabla}^2 \tau(\mathbf{x}) = -\pi \sum_{j=1}^{N} A_j \boldsymbol{\nabla}^2 G(\mathbf{x}, \mathbf{x}_j)$ and, hence

$$\pi |\Omega|^{-1} \sum_{j-1}^{N} A_j = \frac{1}{D}. \tag{2.54}$$

In the case of a single absorbing window of arc length 2ε ($d = 1/2$), Eqs. (2.53) and (2.54) are easily solved to give $A_1 = \Omega|/\pi D$ and

$$\tau(\mathbf{x}) \sim \frac{|\Omega|}{D} \left[-\frac{1}{\pi} \log(\varepsilon/2) + R(\mathbf{x}_1, \mathbf{x}_1) - G(\mathbf{x}, \mathbf{x}_1) \right], \tag{2.55}$$

$$\overline{\tau} \sim \frac{|\Omega|}{D} \left[-\frac{1}{\pi} \log(\varepsilon/2) + R(\mathbf{x}_1, \mathbf{x}_1) \right].$$

All that remains is to calculate the regular part of the Neumann Green's function $R(\mathbf{x}, \mathbf{x}_j)$, which will depend on the geometry of the domain Ω. In certain cases such as the unit disk or a rectangular domain, explicit formulae for R can be obtained, otherwise numerical methods are required (Holcman and Schuss, 2004; Pillay *et al.*, 2010; Singer *et al.*, 2006a,b). The Green's function for a unit disk when the source $\mathbf{x}_j$ is on the unit circle has the well known formula

$$G(\mathbf{x}, \mathbf{x}_j) = -\frac{1}{\pi} \log |\mathbf{x} - \mathbf{x}_j| + \frac{|\mathbf{x}|^2}{4\pi} - \frac{1}{8\pi}. \tag{2.56}$$

It immediately follows that $R(\mathbf{x}_j, \mathbf{x}_j) = 1/8\pi$ (since $|\mathbf{x}_j|^2 = 1$) and

$$\overline{\tau} = \frac{1}{D} \left[-\log(\varepsilon) + \log 2 + 1/8 \right]. \tag{2.57}$$

For a rectangular domain of width L_2 and height L_1, the Green's function can be solved using separation of variables and expanding the result in terms of logarithms, see (Bressloff and Newby, 2011; Pillay *et al.*, 2010).

D. Diffusion-limited reaction rates

Another important type of first passage process arises in Smoluchowski rate theory for diffusion–controlled reactions (Collins and Kimball, 1949; Keizer, 1982; Redner, 2001; Rice, 1985; Smoluchowski, 1917). The simplest version of the theory concerns the bimolecular reaction $A + B \to AB$ for which the concentrations evolve according to the following law of mass action:

$$\frac{d[AB]}{dt} = k[A][b]. \tag{2.58}$$

We assume that an A molecule and a B molecule react immediately to form the complex AB when they encounter each other within a reaction radius, so that the speed of reaction k is limited by their encounter rate via diffusion. (Also note that k has units of volume s^{-1}). One can then formulate the problem as an idealized first passage process, in which one molecule is fixed and treated as the target, whilst the other reactants diffuse and are absorbed if they hit the target. It is assumed that the density of the particles is sufficiently small, so that reactions amongst the diffusing particles can be neglected, that is, a reaction only occurs if one of the background diffusing particles comes within the reaction radius of the target molecule. The steady–state flux to the target (if it exists) is then identified as the reaction rate k. Let Ω denote the target domain (which is often treated as a sphere of radius a) and $\partial\Omega$ its absorbing boundary. We then need to solve the diffusion equation for the concentration $c(\mathbf{x}, t)$ of background molecules exterior to the domain Ω:

$$\frac{\partial c(\mathbf{x}, t)}{\partial t} = D\boldsymbol{\nabla}^2 c(\mathbf{x}, t), \quad c(\mathbf{x} \in \partial\Omega, t) = 0, \, c(\mathbf{x}, 0) = 1, \tag{2.59}$$

subject to the far–field boundary condition $c(\mathbf{x}, t) = 1$ for $\mathbf{x} \to \infty$. The flux through the target boundary is

$$J = D \int_{\partial\Omega} \boldsymbol{\nabla} c \cdot d\mathbf{S}. \tag{2.60}$$

Note the sign, which is due to the fact that the flux is from the exterior to interior of the target.

Let d denote the spatial dimension of the target. For $d > 2$, a diffusing particle is transient, which means that there is a non-zero probability of never reaching the target. Hence, the loss of reactants by target absorption is balanced by their resupply from infinity. It follows that there exists a steady state in which the reaction rate is finite. On the other hand, for $d \leq 2$, reactants are sure to hit the target (recurrent diffusion) and a depletion zone continuously develops around the target so that the flux and reaction rate decay monotonically to zero with respect to time. Although a reaction rate does not strictly exist, it is still useful to consider the time-dependent flux as a time–dependent reaction rate. The two–dimensional case is particularly important when considering interactions of molecules embedded in the plasma membrane of a cell or the lipid bilayer surrounding an intracellular compartment.

First consider the case of a spherical target of radius a ($d = 3$). Exploiting the radial symmetry of the problem, it is possible to set $u(r, t) = rc(r, t)$ such that the 3D diffusion equation for c reduces to a 1D diffusion equation for u (Redner, 2001):

$$\frac{\partial u(r, t)}{\partial t} = D\frac{\partial^2 u(r, t)}{\partial r^2} \tag{2.61}$$

with $u(r, 0) = r$, $u(a, t) = 0$ and $u(r, t) = r$ as $r \to \infty$. Laplace transforming this equation gives $s\widetilde{u}(r, s) - r =$

$D\widetilde{u}''(r,s)$, which has the solution

$$\widetilde{u}(r,s) = \frac{1}{s}\left[r - ae^{-(r-a)\sqrt{s/D}}\right].$$

Since the inverse Laplace transform of $s^{-1}[1 - e^{-r\sqrt{s/D}}]$ is the error function $\mathrm{erf}(r/\sqrt{4Dt})$, one finds that

$$c(r,t) = \left(1 - \frac{a}{r}\right) + \frac{a}{r}\mathrm{erf}\left[\frac{r-a}{\sqrt{4Dt}}\right]. \qquad (2.62)$$

It follows that the time–dependent flux is

$$J(t) = 4\pi a^2 D \left.\frac{\partial c}{\partial r}\right|_{r=a} \qquad (2.63)$$

$$= 4\pi a D\left(1 + \frac{a}{\sqrt{\pi Dt}}\right) \underset{t\to\infty}{\to} 4\pi a D.$$

Hence, we obtain the Smoluchowski reaction rate $k = 4\pi a D$. As highlighted by Redner (2001), it is straightforward to generalize the steady–state result to other three–dimensional targets by making a connection with electrostatics. That is, setting $\phi(\mathbf{x}) = 1 - c(\mathbf{x})$ in steady–state, it follows that ϕ satisfies Laplace's equation with $\phi = 1$ on the target boundary and $\phi = 0$ at infinity, so that ϕ is equivalent to the electrostatic potential generated by a perfectly conducting object Ω held at unit potential. Moreover, the steady–state reaction rate $k = 4\pi D Q$ where Q is the total charge on the surface of the conductor, which for a unit potential is equal to the capacitance, $Q = C$. Thus, determining the reaction rate for a general 3D target is equivalent to finding the capacitance of a perfect conductor with the same shape; see also (Cheviakov *et al.*, 2010).

Although it is possible to calculate the exact time–dependent flux for $d \leq 2$, a much simpler method is to use a quasi–static approximation (Redner, 2001). Consider, for example a target disk of radius $r = a$. The region exterior to the disk is divided into a *near zone* that extends a distance $\sqrt{Dt}$ from the surface and a complementary *far zone*. In the near zone, it is assumed that diffusing particles have sufficient time to explore the domain before being absorbed by the target so that the concentration in the near zone can be treated as almost steady or quasi–static. Conversely, it is assumed that the probability of a particle being absorbed by the target is negligible in the far zone, since a particle is unlikely to diffuse more than a distance $\sqrt{Dt}$ over a time interval of length t. Thus, $c(r) \approx 1$ for $r > \sqrt{Dt} + a$. The near zone concentration is taken to be a radially symmetric solution of Laplace's equation, which for $d = 2$ is $c(r) = A + B\log r$. Matching the solution to the boundary conditions $c(a) = 0$ and $c(\sqrt{Dt}) = 1$ then gives (for $\sqrt{Dt} \gg a$)

$$c(r,t) \approx \frac{\log(r/a)}{\log(\sqrt{Dt}/a)}. \qquad (2.64)$$

The corresponding time–dependent flux is

$$J(t) \approx \frac{2\pi D}{\log(\sqrt{Dt}/a)}. \qquad (2.65)$$

Over the years there have been various generalizations of Smoluchowski's rate theory. For example, Collins and Kimball (1949) considered the case where molecules in proximity to each other do not react immediately. Thus, the target is assumed to act like an imperfect absorber, which can be taken into account by modifying the boundary condition at the surface of the (spherical) target:

$$4\pi a^2 D \left.\frac{\partial c(r,t)}{\partial r}\right|_{r=a} = k_0 c(a,t), \qquad (2.66)$$

where k_0 is the intrinsic reaction rate. Incorporating this modified boundary condition into Smoluchowski's theory leads to a new expression for the diffusion–controlled reaction rate of the form

$$k = \frac{4\pi D a k_0}{4\pi D a + k_0}. \qquad (2.67)$$

Another important extension was developed by Keizer (1982), who used the theory of nonequilibrium pair correlation functions to include many body effects that become important at higher concentrations of reactants.

So far it has been assumed that the diffusion of the background reactants occurs in an unbounded domain with a uniform concentration at infinity. The analysis becomes considerably more involved when the boundary of the domain is taken into account. Recently, however, Straube *et al.* (2007) have shown how methods similar to the analysis of the narrow escape problem, Sec. II.C, can be used to determine the reaction rate in the asymptotic limit that the target is much smaller than the domain size. Here we sketch the basic steps of their analysis. Consider a target disk Ω_ε of radius $\varepsilon \ll 1$ and center $\mathbf{x}_0$ that is located in the interior of a rectangular domain Ω of size $\mathcal{O}(1)$. The calculation of the reaction rate can be formulated in terms of the solution to the following diffusion equation:

$$\frac{\partial c(\mathbf{x},t)}{\partial t} = D\nabla^2 c(\mathbf{x},t), \quad \mathbf{x} \in \Omega\backslash\Omega_\varepsilon \qquad (2.68)$$

with $\partial_n c = 0$ on the exterior boundary $\partial\Omega$ and $c = 0$ on the interior boundary $\partial\Omega_\varepsilon$. The initial condition is taken to be $c(\mathbf{x},0) = 1$. Following Straube *et al.* (2007), we seek a solution in the form of an eigenfunction expansion,

$$c(\mathbf{x},t) = \sum_{j=0}^{\infty} c_j \phi_j(\mathbf{x}) e^{-\lambda_j Dt} \qquad (2.69)$$

where the eigenfunctions $\phi_j(\mathbf{x})$ satisfy the Helmholtz equation

$$\boldsymbol{\nabla}^2\phi_j + \lambda_j\phi_j = 0, \quad \mathbf{x} \in \Omega\backslash\Omega_\varepsilon \qquad (2.70)$$

subject to the same boundary conditions as $c(\mathbf{r},t)$. The eigenfunctions are orthogonalized as

$$\int_{\Omega\backslash\Omega_\varepsilon} \phi_i(\mathbf{x})\phi_j(\mathbf{x})d\mathbf{x} = \delta_{i,j}. \qquad (2.71)$$

The initial condition then implies that

$$c_j = \int_{\Omega \setminus \Omega_\varepsilon} \phi_j(\mathbf{x}) d\mathbf{x}. \qquad (2.72)$$

Taking the limit $\varepsilon \to 0$ results in an eigenvalue problem in a rectangular domain without a hole. It is well known that the eigenvalues are ordered as $\lambda_0 = 0 < \lambda_1 \leq \lambda_2 \leq \dots$. This ordering will persist when $0 < \varepsilon \ll 1$ so that in the long–time limit, the solution will be dominated by the eigenmode with the smallest eigenvalue:

$$c(\mathbf{x}, t) \sim c_0 \phi_0(\mathbf{x}) e^{-\lambda_0 t}. \qquad (2.73)$$

It can also be shown that the principal eigenvalue has an infinite logarithmic expansion (Ward *et al.*, 1993):

$$\lambda_0 = \nu \Lambda_1 + \nu^2 \Lambda_2 + \dots, \quad \nu \equiv -\frac{1}{\log \varepsilon}. \qquad (2.74)$$

Moreover, the eigenfunction $\phi_0(\mathbf{x})$ will develop a boundary layer in a neighborhood of the target, where it changes rapidly from zero on the boundary $\partial \Omega_\varepsilon$ to a value of $\mathcal{O}(1)$ away from the target. This suggests dividing the domain into inner/outer regions, and using matched asymptotics along analogous lines to the study of the narrow escape problem.

Therefore, introduce stretched coordinates $\mathbf{y} = (\mathbf{x} - \mathbf{x}_0)/\varepsilon$ and write the inner solution of the principal eigenfunction as $\varphi(\mathbf{y}) = \phi_0(\varepsilon \mathbf{y})$. Using the logarithmic expansion of λ_0 shows that the righthand side of the rescaled eigenvalue equation is of $\mathcal{O}(\varepsilon^2 \nu^2) = o(\nu^k)$ for all $k \geq 0$. Thus to logarithmic accuracy, it follows that $\nabla^2 \varphi(\mathbf{y}) = 0$ on $\mathbb{R}^2 \setminus S^1$ where S^1 is the unit circle centered about the origin, and $\varphi = 0$ on $|\mathbf{y}| = 1$. Hence, $\varphi(\mathbf{y}) = A \log |\mathbf{y}|$ and the inner solution has the far–field behavior

$$\varphi \sim A \log(|\mathbf{x} - \mathbf{x}_0|/\varepsilon). \qquad (2.75)$$

The outer solution satisfies the equation

$$\begin{aligned}
\nabla^2 \phi_0 + \lambda_0 \phi_0 &= 0, \quad \mathbf{x} \in \Omega \setminus \{\mathbf{x}_0\}, \\
\phi_0 &\sim A \log(|\mathbf{x} - \mathbf{x}_0|/\varepsilon), \quad \mathbf{x} \to \mathbf{x}_0, \\
\int_\Omega \phi_0^2(\mathbf{x}) d\mathbf{x} &= 1.
\end{aligned} \qquad (2.76)$$

Following the analysis in Sec. II.C, the outer problem can be solved in terms of the Neumann Green's function for the Helmholtz equation:

$$\nabla^2 G(\mathbf{x}, \mathbf{x}_0; \lambda_0) + \lambda_0 G(\mathbf{x}, \mathbf{x}_0; \lambda_0) = -\delta(\mathbf{x} - \mathbf{x}_0), \quad x \in \Omega \qquad (2.77a)$$

$$\partial_n G(\mathbf{x}, \mathbf{x}_0; \lambda_0) = 0, \quad \mathbf{x} \in \partial \Omega \qquad (2.77b)$$

$$G(\mathbf{x}, \mathbf{x}_0; \lambda_0) \sim -\frac{1}{2\pi} \log |\mathbf{x} - \mathbf{x}_0| + R(\mathbf{x}_0, \mathbf{x}_0; \lambda_0), \quad \mathbf{x} \to \mathbf{x}_0. \qquad (2.77c)$$

That is,

$$\phi_0(\mathbf{x}) = -2\pi A G(\mathbf{x}, \mathbf{x}_0; \lambda_0). \qquad (2.78)$$

Matching the near–field behavior of the outer solution with the far–field behavior of the inner solution then yields a transcendental equation for the principal eigenvalue:

$$R(\mathbf{x}_0, \mathbf{x}_0; \lambda_0) = -\frac{1}{2\pi\nu}. \qquad (2.79)$$

Finally, the normalization condition for ϕ_0 determines the amplitude A according to

$$4\pi^2 A^2 \int_\Omega G(\mathbf{x}, \mathbf{x}_0; \lambda_0)^2 d\mathbf{x} = 1. \qquad (2.80)$$

The Helmholtz Green's function and its regular part can be calculated along similar lines to Sec. II.C. Here it is sufficient to note that, since $0 < \lambda_0 \ll 1$ for a small target, the Green's function has the expansion

$$G(\mathbf{x}, \mathbf{x}_0; \lambda_0) = -\frac{1}{\lambda_0 |\Omega_0|} + G_1(\mathbf{x}, \mathbf{x}_0) + \lambda_0 G_2(\mathbf{x}, \mathbf{x}_0) + \mathcal{O}(\lambda_0^2) \qquad (2.81)$$

with $\int_\Omega G_j(\mathbf{x}, \mathbf{x}_0) d\mathbf{x} = 0$. The regular part $R(\mathbf{x}, \mathbf{x}_0; \lambda_0)$ can be expanded in an identical fashion. Hence, neglecting terms of $\mathcal{O}(\lambda_0)$ and higher, substitute $R(\mathbf{x}, \mathbf{x}_0; \lambda_0) \approx -(\lambda_0 |\Omega_0|)^{-1} + R_1(\mathbf{x}, \mathbf{x}_0)$ into the transcendental Eq. (2.79). This yields a linear equation for λ_0 such that

$$\lambda_0 \approx \frac{2\pi\nu}{|\Omega_0|} \frac{1}{1 + 2\pi\nu R_1(\mathbf{x}_0, \mathbf{x}_0)}. \qquad (2.82)$$

Substituting the expansion (2.81) into Eq. (2.80) shows that to leading order in λ_0,

$$A \approx \frac{\sqrt{|\Omega_0|} \lambda_0}{2\pi}. \qquad (2.83)$$

Moreover, using Eqs. (2.78), (2.80) and $\int_\Omega G_j(\mathbf{x}) d\mathbf{x} = 0$, the coefficient c_0 is

$$c_0 = -2\pi A \int_\Omega G(\mathbf{x}, \mathbf{x}_0; \lambda_0) d\mathbf{x} = \frac{2\pi A}{\lambda_0}. \qquad (2.84)$$

We now have all the components necessary to determine the time–dependent reaction rate $k(t)$. That is, using the inner solution $\varphi(\mathbf{x}) = A \log(r/\varepsilon)$, $r = |\mathbf{x} - \mathbf{x}_0|$, we combine Eqs. (2.73), (2.83) and (2.84) to obtain the result (Straube *et al.*, 2007)

$$\begin{aligned}
J(t) &= D c_0 e^{-\lambda_0 t} \int_0^{2\pi} \left(r \frac{\partial \varphi}{\partial r} \right) \Big|_{r=\varepsilon} d\theta \\
&= 2\pi D c_0 e^{-\lambda_0 t} A \approx c_0 |\Omega_0| \lambda_0 e^{-\lambda_0 D t}.
\end{aligned} \qquad (2.85)$$

Note that Straube *et al.* (2007) applied the above analysis to the particular problem of protein receptor clustering on a cylindrical surface membrane. The only modification to the rectangular domain Ω is that the left and right side boundaries are identified by replacing the reflecting boundary conditions with periodic boundary conditions. This generates the topology of a cylinder and modifies the form of the Helmholtz Green's function accordingly.

E. Diffusive search for a protein-DNA binding site

A wide range of cellular processes are initiated by a single protein binding a specific target sequence of base pairs (target site) on a long DNA molecule. The precise mechanism whereby a protein finds its DNA binding site remains unclear. However, it has been observed experimentally that reactions occur at very high rates, of around $k = 10^{10} M^{-1} s^{-1}$ (Richter and Eigen, 1974; Riggs *et al.*, 1974). This is around 100 times faster than the rate based on the Smoluchowski theory of diffusion–limited reaction rates (Sec. II.D), and 1000 times higher than most known protein-protein association rates. (Note, however, that some protein-protein association rates are also much larger than the predictions of Smoluchowski theory (Schreiber *et al.*, 2009)). This apparent discrepancy in reaction rates, suggests that some form of facilitated diffusion occurs. The best known theoretical model of facilitated diffusion for proteins searching for DNA targets was originally developed by Berg, Winter and von Hippel (BHW) (Berg and von Hippel, 1985; Berg *et al.*, 1981; Winter *et al.*, 1981), and subsequently extended by a number of groups (Coppey *et al.*, 2004; Halford and Marko, 2004; Hu *et al.*, 2006; Hu and Shklovskii, 2006; Mirny *et al.*, 2009; Slutsky and Mirny, 2004). The basic idea of the BHW model is to assume that the protein randomly switches between two distinct phases of motion, 3D diffusion in solution and 1D diffusion along DNA (sliding), see Fig. 2. Such a mechanism is one example of a random intermittent search process, see Sec. IVB. The BHW model assumes that there are no correlations between the two transport phases, so that the main factor in speeding up the search is an effective reduction in the dimensionality of the protein motion. However, as recently reviewed by Kolomeisky (2011), there are a number of discrepancies between the BHW model and experimental data, which has led to several alternative theoretical approaches to facilitated diffusion. We first review the BHW model and then briefly discuss these alternative models.

A simple method for estimating the effective reaction rate of facilitated diffusion in the BHW model is as follows (Mirny *et al.*, 2009; Slutsky and Mirny, 2004). Consider a single protein searching for a single binding site on a long DNA strand of N base pairs, each of which has length b. Suppose that on a given search, there are R rounds labeled $i = 1, \ldots, R$. In the ith round the protein spends a time $T_{3,i}$ diffusing in the cytosol followed by a period $T_{1,i}$ sliding along the DNA. The total search time is thus $T = \sum_{i=1}^{R}(T_{3,i} + T_{1,i})$, and the mean search time is $\tau = r(\tau_3 + \tau_1)$. Here r is the mean number of rounds and τ_3, τ_1 are the mean durations of each phase of 3D and 1D diffusion. Let n denote the mean number of sites scanned during each sliding phase with $n \ll N$. If the binding site of DNA following a 3D diffusion phase is distributed uniformly along the DNA, then the prob-
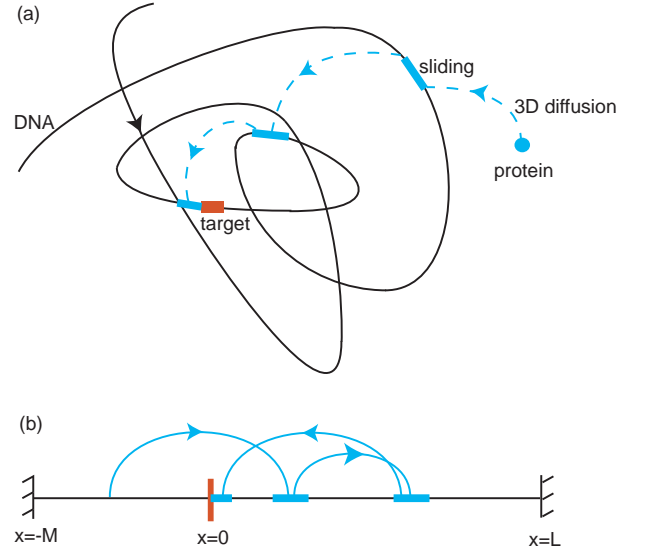

FIG. 2 (a) Mechanism of facilitated diffusion involving alternating phases of 3D diffusion and 1 D diffusion (sliding along the DNA). (b) 1D representation of facilitated diffusion.

ability of finding the specific promoter site is $p = n/N$. It follows that the probability of finding the site after R rounds is $(1-p)^{R-1}p$. Hence, the mean number of rounds is $r = 1/p = N/n$. Assuming that 1D sliding occurs via normal diffusion, then $nb = 2\sqrt{D_1 \tau_1}$ where D_1 is the $1D$ diffusion coefficient, and we have (Mirny *et al.*, 2009)

$$\tau = \frac{N}{n}(\tau_1 + \tau_3), \quad n = 2\sqrt{D_1 \tau_1}/b. \tag{2.86}$$

Since τ_3 depends primarily on the cellular environment and is thus unlikely to vary significantly between proteins, it is reasonable to minimize the mean search time with respect to τ_1 while τ_3 is kept fixed. Setting $d\tau/d\tau_1 = 0$ implies that the optimal search time occurs when $\tau_1 = \tau_3$ with $\tau_{\text{opt}} = 2N\tau_3/n = Nb\sqrt{\tau_3/D_1}$. Comparing with the expected search time for pure 3D diffusion by setting $\tau_1 = 0, n = 1$ gives $\tau_{3D} = N\tau_3$. Thus facilitated diffusion is faster by a factor $n/2$. Further insights to facilitated diffusion may be obtained by using the Smoluchowski formula for the rate at which a diffusing protein can find any one of N binding sites of size N, namely, $\tau_3^{-1} = 4\pi D_3 N b$. Using this to eliminate N shows that the effective reaction rate of facilitated diffusion is (Mirny *et al.*, 2009)

$$k \equiv \tau^{-1} = 4\pi D_3 \left(\frac{\tau_3}{\tau_1 + \tau_3} \right) nb. \tag{2.87}$$

This equation identifies two competing mechanisms in facilitated diffusion. First, sliding diffusion effectively increases the reaction cross-section from 1 to n base pairs, thus accelerating the search process compared to standard Smoluchowski theory. This is also known as the *antenna effect* (Hu *et al.*, 2006). However, the search is

also slowed down by a factor $\tau_3/(\tau_1 + \tau_3)$, which is the fraction of the time the protein spends in solution. That is, a certain amount of time is lost by binding to non-specific sites that are far from the target.

A more complicated analysis is needed in order to take into account the effects of boundaries, for example. Here we review the particular formulation of Coppey *et. al.*, which generalizes the original analysis of Berg *et al.* (1981). Suppose that DNA is treated as a finite track of length $l = L + M$ with reflecting boundaries at $x = -M$ and $x = +L$ and a point–like target at $x = 0$, see Fig. 2. Rather than modeling 3D diffusion explicitly, each time the protein disassociates from DNA it simply rebinds at a random site at a time t later that is generated from an exponential waiting time density. This is based on the assumption that 3D excursions are uncorrelated in space. It might be expected that excursions would be correlated due to the geometric configuration of DNA. However, in solution DNA is a random coil so that even short 3D trips can generate long displacements relative to the linear position of the protein along the DNA strand, resulting in decorrelation of excursions. If $P_3(t)$ denotes the probability density that the protein in solution at time $t = 0$ binds to the DNA at time t at a random position, then

$$P_3(t) = \lambda_3 \mathrm{e}^{-\lambda_3 t}, \qquad (2.88)$$

where $\tau_3 = 1/\lambda_3$ is again the mean time spent in solution. Next, let $P_1(t, x)$ be the conditional probability density that the protein disassociates from the DNA at time t without finding the target, given that it is at linear position x along the DNA at time $t = 0$:

$$P_1(x, t) = \lambda_1 \mathrm{e}^{-\lambda_1 t} \mathbb{P}(x, t) \qquad (2.89)$$

where $\tau_1 = 1/\lambda_1$ is the mean time of each sliding phase, and $\mathbb{P}(t, x)$ is the conditional probability density that the protein starting at x has not met the target at time t. Finally, let $Q_1(x, t)$ be the conditional probability density that the protein starting at x finds the target at time t:

$$Q_1(x, t) = \mathrm{e}^{-\lambda_1 t} f(x, t), \qquad (2.90)$$

where $f(x, t) = -d\mathbb{P}(x, t)/dt$ is the FPT density associated with diffusion along the DNA strand. That is $f(x, t)dt$ is the probability that starting at x at $t = 0$, the protein finds the target during a single phase of sliding diffusion in the time interval $[t, t+dt]$. (Protein-DNA binding is assumed to be diffusion-limited so that as soon as the protein reaches the target site it reacts).

Suppose that in a given trial, a protein starting at x at time $t = 0$ executes $n-1$ excursions before finding the target with $t_1, \ldots, t_n$ the residence times on DNA and $\tau_1, \ldots, \tau_{n-1}$ the excursion times. The probability density for such a sequence of events with $t = \sum_{i=1}^{n} t_i + \sum_{i=1}^{n-1} \tau_n$ is

$$P_n(x, \{t_i, \tau_i\}) = Q_1(t_n) P_3(\tau_{n-1}) P_1(t_{n-1}) \ldots$$
$$\times P_1(t_2) P_3(\tau_1) P_1(x, t_1), \qquad (2.91)$$

where $P_1(t) = \langle P_1(x, t) \rangle, Q_1(t) = \langle Q_1(x, t) \rangle$ and $\langle g(x, t) \rangle \equiv (L+M)^{-1} \int_{-M}^{L} g(x, t) dx$ for an arbitrary function g. In order to determine the FPT density $F(x, t)$ for finding the target, it is necessary to sum over all possible numbers of excursions and intervals of time, given the constraint $t = \sum_{i=1}^{n} t_i + \sum_{i=1}^{n-1} \tau_n$. Thus, setting $F(t) = \langle F(x, t) \rangle$, one finds that

$$F(t) = \sum_{n=1}^{\infty} \int_0^{\infty} dt_1 \ldots dt_n d\tau_1 \ldots d\tau_n \qquad (2.92)$$

$$\delta \left(\sum_{i=1}^{n} t_i + \sum_{i=1}^{n-1} \tau_n - t \right) Q_1(t_n) \prod_{i=1}^{n-1} P_3(\tau_i) \prod_{i=1}^{n-1} P_1(t_i).$$

Finally, Laplace transforming this equation gives (Coppey *et al.*, 2004)

$$\widetilde{F}(s) = \widetilde{f}(\lambda_1 + s) \left[1 - \frac{1 - \widetilde{f}(\lambda_1 + s)}{(1 + s/\lambda_1)(1 + s/\lambda_3)} \right]^{-1}, \quad (2.93)$$

with $\widetilde{f}(s) = \int_0^{\infty} \mathrm{e}^{-st} \langle f(x, t) \rangle dt$. Given $\widetilde{F}(s)$, the MFPT to find the target (averaged over the starting position x) is then

$$\tau = \int_0^{\infty} t F(t) dt = -\left. \frac{d\widetilde{F}(s)}{ds} \right|_{s=0}. \qquad (2.94)$$

which can be evaluated to give

$$\tau = \frac{1 - \widetilde{f}(\lambda_1)}{\widetilde{f}(\lambda_1)} (\lambda_1^{-1} + \lambda_3^{-1}). \qquad (2.95)$$

All that remains is to determine $\widetilde{f}(x, s)$ averaged with respect to x. If $x < 0$ ($x > 0$), then one simply needs to determine the FPT density for a 1D Brownian particle on the interval $[-M, 0]$ ($[0, L]$) with a reflecting boundary at $x = -M$ ($x = L$) and an absorbing boundary at $x = 0$. Recall from Sec. (II.B) that $f(x, t)$ satisfies the backwards FP equation

$$\frac{\partial f(x, t)}{\partial t} = D_1 \frac{\partial^2 f(x, t)}{\partial x^2}, \qquad (2.96)$$

with $f(x, 0) = 0$, $f(0, t) = \delta(t)$ and $\partial_x f(L, t) = 0$ or $\partial_x f(-M, t) = 0$. Taking Laplace transforms,

$$s\widetilde{f}(x, s) = D_1 \frac{\partial^2 \widetilde{f}(x, s)}{\partial x^2}, \qquad (2.97)$$

with $\widetilde{f}(0, s) = 1, \partial_x \widetilde{f}(L, s) = 0$ or $\partial_x \widetilde{f}(-M, s) = 0$. The general solution is $\widetilde{f}(x, s) = A\mathrm{e}^{-\sqrt{s/D_1}x} + B\mathrm{e}^{-\sqrt{s/D_1}x}$ with the coefficients A, B determined by the boundary conditions. Solving for A, B separately when $x < 0$ and $x > 0$ and averaging with respect to x finally gives

$$\widetilde{f}(s) = \frac{1}{L + M} \sqrt{\frac{D_1}{\lambda_1}}$$
$$\times \left[\tanh(L\sqrt{\lambda_1/D_1}) + \tanh(M\sqrt{\lambda_1/D_1}) \right].$$

Thus, setting $\tau_i = 1/\lambda_i$, $i = 1, 3$,

$$\tau = \left[\frac{(L+M)/\sqrt{\tau_1 D_1}}{\tanh(L/\sqrt{\tau_1 D_1}) + \tanh(M/\sqrt{\tau_1 D_1})} - 1 \right] (\tau_1 + \tau_3),$$

which recovers the original result of Berg *et al.* (1981). It also recovers Eq. (2.86) when $L/\sqrt{\tau_1 D_1}, M/\sqrt{\tau_1 D_1} \gg 1$.

There have been a number of extensions of the BHW model that incorporate various biophysical effects. For example, sequence-dependent protein-DNA interactions generate a rugged energy landscape during sliding motion of the protein (Hu and Shklovskii, 2006; Mirny *et al.*, 2009; Slutsky and Mirny, 2004) - see also Sec. III.C. This observation then leads to an interesting speed-stability paradox (Mirny *et al.*, 2009; Sheinman *et al.*, 2012). On the one hand, fast 1D search requires that the variance σ^2 of the protein-DNA binding energy be sufficiently small, that is, $\sigma \sim k_B T$, whereas stability of the protein at the DNA target site requires $\sigma \sim 5 k_B T$. One suggested resolution of this paradox is to assume that a protein-DNA complex has two conformational states: a recognition state with large σ and a search state with small σ (Mirny *et al.*, 2009; Slutsky and Mirny, 2004). If the transitions between the states are sufficiently fast then target stability and fast search can be reconciled. (For a recent review of the speed-stability paradox and its implications for search mechanisms see Sheinman *et al.* (2012)). Other effects include changes in the conformational state of DNA and the possibility of correlated association/disassociation of the protein (Benichou *et al.*, 2011a; Hu *et al.*, 2006), and molecular crowding along DNA (Li *et al.*, 2009) or within the cytoplasm (Isaacson *et al.*, 2011). Molecular crowding will be considered in Sec. IIIB.

The BHW model and its extensions provide a plausible mechanism for facilitated diffusion that has some support from experimental studies, which demonstrate that proteins do indeed slide along DNA (Gorman and Greene, 2008; Gowers *et al.*, 2005; Li *et al.*, 2009; Tafvizi *et al.*, 2008; Winter *et al.*, 1981). In particular, recent advances in single–molecule spectroscopy means that the motion of flourescently labeled proteins along DNA chains can be quantified with high precision, although it should be noted that most of these studies have been performed *in vitro*. A quantitative comparison of the BHW model with experimental data leads to a number of discrepancies, however. For example, it is usually assumed that $D_1 \approx D_3$ in order to obtain a sufficient level of facilitation. On the other hand, single–molecule measurements indicate that $D_1 \ll D_3$ (Elf *et al.*, 2007; Yang *et al.*, 2006). Such experiments have also shown that $\tau_1 \gg \tau_3$, which is significantly different from the optimal condition $\tau_1 = \tau_3$. Hence the intermittent search process could actually result in a slowing down compared to pure 3D diffusion (Hu *et al.*, 2006). The RHW model also exhibits unphysical behavior in certain limits. These issues have motivated a number of alternative models of facilitated diffusion, as recently highlighted by Kolomeisky (2011).

Electrostatic interactions. One alternative hypothesis is that the observed fast association rates are due to electrostatic interactions between oppositely charged molecules, and thus do not violate the 3D diffusion limit (Halford, 2009). This is motivated by the theoretical result that the maximal association rate in Smoluchowski theory when there are long-range interactions between the reacting molecules is

$$k = 4\pi D a / \beta, \quad \beta = \int_a^\infty e^{U(r)/k_B T} \frac{dr}{r^2}, \qquad (2.98)$$

where $U(r)$ is the interaction potential. The standard result is recovered when $U(r) = 0$ for $r > a$, see Eq. (2.63). It follows that long–range attractive interactions can significantly increase diffusion–limited reaction rates. It has been further argued that in vitro experiments tend to be performed at low salt concentrations so that the effects of screening could be small. However, experimentally-based estimates of the Debye length, which specifies the size of the region where electrostatic forces are important, indicate that it is comparable to the size of the target sequence. Hence, electrostatic forces are unlikely to account for facilitated diffusion.

Colocalization Another proposed mechanism is based on the observation that in bacteria, genes responsible for producing specific proteins are located close to the binding sites of these proteins. This colocalization of proteins and binding sites could significantly speed up the search process by requiring only a small number of alternating 3D and 1D phases (Mirny *et al.*, 2009). However, such a mechanism might not be effective in eukaryote cells, where transcription and translation tend to be spatially and temporally well separated. Moreover, colocalization breaks down in cases where proteins have multiple targets on DNA.

Correlations. Yet another theoretical mechanism involves taking into account correlations between 1D sliding and 3D bulk diffusion. These correlations reflect the fact that attractive interactions between a protein and non-specific binding sites means that there is a tendency for a protein to return back to a neighborhood of the DNA site from which it recently disassociated (Cherstvy *et al.*, 2008; Zhou, 2005). Although such interactions tend to slow down proteins moving along DNA, they also increase the local concentration of proteins absorbed to DNA. This suggests that facilitated diffusion can occur at intermediate levels of protein concentration and intermediate ranges of protein–DNA interactions.

III. DIFFUSIVE TRANSPORT: EFFECTS OF MOLECULAR CROWDING, TRAPS AND CONFINEMENT

A. Anomalous diffusion

In normal (unobstructed) diffusion in d dimensions, the mean-square displacement (MSD) of a Brownian particle is proportional to time, $\langle R^2 \rangle = 2dDt$, which is a consequence of the central limit theorem. A general signature of anomalous diffusion is the power law behavior (Bouchaud and Georges, 1990; Metzler and Klafter, 2000)

$$\langle R^2 \rangle = 2dDt^\alpha, \tag{3.1}$$

corresponding to either subdiffusion ($\alpha < 1$) or superdiffusion ($\alpha > 1$). Due to recent advances in single-particle tracking methods, subdiffusive behavior has been observed for a variety of biomolecules and tracers within living cells. Examples include messenger RNA molecules (Golding and Cox, 2006) and chromosomal loci (Weber *et al.*, 2010) moving within the cytoplasm of bacteria, lipid granule motion in yeast cells (Jeon *et al.*, 2011), viruses (Seisenberger *et al.*, 2001), telemores in cell nuclei (Bronstein *et al.*, 2009), and protein channels moving within the plasma membrane (Weigel *et al.*, 2011).

There are currently three subcellular mechansims thought to generate subdiffusive motion of particles in cells, each with its own distinct type of physical model (Weber *et al.*, 2010). The first mechanism, which is typically modeled using the continuous time random walk (CTRW) (Hughes, 1995; Scher and Montroll, 1975), involves transient immobilization or trapping, see Sec. IIIC. That is, if a diffusing particle encounters a binding site then it will pause for a while before disassociating and diffusing away. Multiple binding events with a range of rate constants can generate long tails in the waiting time distribution leading to subdiffusive behavior (Saxton, 1996, 2007). In addition to having a heavy-tailed waiting time distribution, the CTRW is weakly nonergodic; the temporal average of a long particle trajectory differs from the ensemble average over many diffusing particles (He *et al.*, 2008; Jeon and Metzler, 2012; Jeon *et al.*, 2011; Weigel *et al.*, 2011). The second mechanism for subdiffusion in cells is obstructed diffusion (OD) due to molecular crowding or cytoskeletal networks that impose obstacles around which diffusing molecules have to navigate, see Sec. IIIB. If the concentration of obstacles is sufficiently high, then subdiffusive behavior occurs, in which the domain of free diffusion develops a fractal-like structure (Saxton, 1994). Diffusion on a fractal is a stationary process and is thus ergodic. The final mechanism involves the viscoelastic properties of the cytoplasm due to the combined effects of macromolecular crowding and the presence of elastic elements such as nucleic acids and cytoskeletal filaments. As a particle moves through the cytoplasm, the latter "pushes back", thus

generating long-time correlations in the particle's trajectory. This memory effect leads to subdiffusive behavior that can be modeled in terms of fractional Brownian motion (FBM) or the fractional Langevin equation (FLE) (Burov *et al.*, 2011; Mandelbrot and Ness, 1968). In contrast to CTRW and diffusion on fractals, the probability density for unconfined subdiffusion in FBM/FLE is a Gaussian (with a time–dependent diffusivity). Moreover, FBM/FLE are ergodic systems, although under confinement time-averaged quantities behave differently from their ensemble-averaged counterparts (Jeon and Metzler, 2012).

Determining which type of model best fits experimental data is a nontrivial task, particularly since CTRW, OD and FBM/FLE generate similar scaling laws for ensemble-averaged behavior in the long-time limit. Thus other measures such as ergodicity are being used to help identify which model provides the best characterization for anomalous diffusion in living cells. A number of recent studies provide examples where FBM/FLE appears to give a better fit to the data than CTRW (Magdziarz *et al.*, 2009; Szymanski and Weiss, 2009; Weber *et al.*, 2010). However, other studies suggest that both ergodic (OD or FBM/FLE) and nonergodic processes (CTRW) can coexist (Jeon *et al.*, 2011; Weigel *et al.*, 2011).

In this review we are going to focus on biophysical models of the cellular environment and how it effects diffusive transport via molecular crowding, trapping and confinement, rather than on generic models of anomalous transport such as CTRW and FBM/FLE. The reasons are two-fold: (i) there are already a number of comprehensive reviews of such models (Kou, 2008; Mandelbrot and Ness, 1968; Metzler and Klafter, 2000; Scher and Montroll, 1975; Tothova *et al.*, 2011), and (ii) it is still unclear to what extent intracellular diffusion is anomalous in the long–time limit rather than just at intermediate times. This motivates studying diffusion in the presence of obstacles and transient traps whereby normal diffusion is recovered asymptotically. However, before proceeding, we briefly sketch the basic structure of CTRW and FBM/FLE models.

The CTRW considers a particle performing random jumps whose step length is generated by a probability density with finite second moments. However, the waiting times between jumps are assumed to be distributed according to a power law (rather than an exponential waiting time density characteristic of Markovian random walks). The resulting heavy tailed waiting times generate subdiffusive behavior. Consider, for example, a 1D CTRW generated by a sequence of independent identically distributed (iid) positive random waiting times $T_1, T_2, \ldots, T_n$, each having the same probability density function $\phi(t)$, and a corresponding sequence of (iid) random jumps $X_1, X_2, \ldots \in \mathbb{R}$, each having the same probability density $w(x)$. Setting $t_0 = 0$ and $t_n = T_1 + T_2 + \ldots + T_m$ for positive integers n,

the random walker makes a jump of length X_n at time t_n. Hence, its position is $x_0 = 0$ for $0 \leq t < T_1$ and $x_n = X_1 + X_2 + \ldots + X_n$ for $t_n \leq t < t_{n+1}$. It follows that the probability density $p(x,t)$ that the particle is at position x at time t satisfies the integral equation

$$p(x,t) = \delta(x)\Psi(t) \tag{3.2}$$
$$+ \int_0^t \phi(t-t')\left[\int_{-\infty}^\infty w(x-x')p(x',t')dx'\right]dt',$$

where $\Psi(t) = \int_t^\infty \phi(t')dt'$ is the survival probability that at time t the particle has not yet moved from its initial position at $x = 0$. In the special case of an exponential waiting time density $\phi(t) = \tau^{-1}e^{-t/\tau}$, we can differentiate both sides of Eq. (3.2) to obtain

$$\tau\frac{\partial p(x,t)}{\partial t} = \left[-p(x,t') + \int_{-\infty}^\infty w(x-x')p(x',t')dx'\right],$$

Setting $w(x) = 0.5\delta(x-\delta x) + 0.5\delta(x+\delta x)$ then yields a spatially discrete version of the diffusion equation. On the other hand, anomalous subdiffusion occurs if $\phi(t) \sim t^{-\alpha-1}$ with $0 < \alpha < 1$ (Metzler and Klafter, 2000).

In order to motivate the FLE, recall that a molecule moving through a fluid is subject to a frictional force and a random fluctuating force originating from random collisions between the Brownian molecule and particles of the surrounding fluid. In the Langevin Eq. (2.9), the random fluctuations are represented by a zero-mean Gaussian noise term with a two-point correlation function taken to be a Dirac function. Moreover, the amplitude-squared of the noise (diffusion coefficient) is related to the friction coefficient via the Einstein relation, which is an example of the fluctuation-dissipation theorem. It has been suggested that the Langevin equation can be generalized to the case of diffusion in complex heterogeneous media such as the cytoplasm or plasma membrane by considering a Brownian particle subject to frictional and fluctuating forces with long–time correlations that exhibit power-law behavior (Lutz, 2001; Porra *et al.*, 1996; Wang, 1992; Wang and Lung, 1990). For example, consider the following generalized Langevin equation for a Brownian particle with unit mass moving in a 1D medium (Wang and Lung, 1990):

$$\dot{X}(t) = V(t), \tag{3.3a}$$
$$\ddot{X}(t) + \int_0^t \phi(t-t_1)V(t_1)dt_1 = F(t), \tag{3.3b}$$

where $\phi(t)$ represents a friction memory kernel with $\phi(t) = 0$ for $t < 0$. The Gaussian noise term $F(t)$ satisfies

$$\langle F(t)\rangle = 0, \quad \langle F(0)F(t)\rangle = C(t). \tag{3.4}$$

Following Wang (1992); Wang and Lung (1990), the correlation function $C(t)$ is governed by a power law,

$$C(t) = F_0(\alpha)t^{-\alpha}, \quad t > 0, \tag{3.5}$$

with $0 < \alpha < 1$ for subdiffusive behavior and $C(-t) = C(t)$. Using a generalized fluctuation-dissipation theorem, the functions $\phi(t), C(t)$ are related according to

$$C(t) = k_B T\phi(t), \quad t \geq 0. \tag{3.6}$$

We now show how to derive a FP equation for the generalized Langevin equation following Wang (Wang, 1992). Since the fluctuating force is described by a Gaussian process then so is the random variable $X(t)$. Let $p(x,t)$ denote the probability density for $X(t) = x$ and introduce the characteristic function or Fourier transform

$$\Gamma(k,t) \equiv \langle e^{ikX(t)}\rangle = \int_{-\infty}^\infty p(x,t)e^{ikx}dx. \tag{3.7}$$

It follows that Γ is given by the Gaussian

$$\Gamma(k,t) = e^{ik\overline{X}(t)-k^2\sigma^2(t)/2}, \tag{3.8}$$

where

$$\overline{X}(t) = \langle X(t)\rangle, \quad \sigma^2(t) = \langle[X(t)-\overline{X}(t)]^2\rangle. \tag{3.9}$$

The mean and variance can be determined from Laplace transforming the generalized Langevin equation (3.3):

$$s\widetilde{X}(s) - X(0) = \widetilde{V}(s), \tag{3.10a}$$
$$s^2\widetilde{X}(s) - V(0) - sX(0) + \widetilde{\phi}(s)V(s) = \widetilde{F}(s). \tag{3.10b}$$

Rearranging (3.10b) gives

$$\widetilde{X}(s) - s^{-1}X(0) - \widetilde{H}(s)V(0) = \widetilde{H}(s)\widetilde{F}(s),$$

where

$$\widetilde{H}(s) = \frac{1}{s[s+\widetilde{\phi}(s)]}. \tag{3.11}$$

Inverting the equation for $\widetilde{X}(s)$ thus yields

$$X(t) - X(0) - V(0)H(t) = \int_0^t H(t-t_1)F(t_1)dt_1 \tag{3.12}$$

It immediately follows from equation (3.12) that

$$\overline{X}(t) = X(0) + V(0)H(t). \tag{3.13}$$

Calculation of the variance is a little more involved. First, using equations (3.12) and (3.13),

$$\sigma^2(t) = \int_0^t dt_1 \int_0^t dt_2 H(t_1)H(t_2)\langle F(t-t_1)F(t-t_2)\rangle$$
$$= \int_0^t dt_1 \int_0^t dt_2 H(t_1)H(t_2)C(t_1-t_2)$$
$$= 2\int_0^t dt_1 \int_0^{t_1} dt_2 H(t_1)H(t_2)C(t_1-t_2)$$
$$= 2k_B T\int_0^t dt_1 \int_0^{t_1} dt_2 H(t_1)H(t_2)\phi(t_1-t_2)$$

The last two lines follow from the fact that $C(t)$ is an even function and the generalized fluctuation-dissipation theorem, respectively. The final step is to note that

$$A(t_1) \equiv \int_0^{t_1} H(t_2)\phi(t_1 - t_2)dt_2$$

$$\xrightarrow{\mathcal{L}} \widetilde{A}(s) = \widetilde{H}(s)\widetilde{\phi}(s) = \frac{1}{s} - \frac{1}{s + \widetilde{\phi}(s)}$$

$$\xrightarrow{\mathcal{L}^{-1}} A(t_1) = 1 - \frac{dH(t_1)}{dt_1},$$

where $\mathcal{L}$ denotes the Laplace transform operator. Substituting back into the expression for σ^2 gives (Wang, 1992),

$$\sigma^2(t) = k_B T \left[2 \int_0^t H(\tau)d\tau - H(t)^2 \right]. \qquad (3.14)$$

The final step in the analysis is to substitute equations (3.13) and (3.14) into equation (3.8) and to differentiate the resulting expression for $\Gamma(k,t)$ with respect to time t. This gives

$$\frac{\partial \Gamma(k,t)}{\partial t} = \left[ikV(0)h(t) - k^2 k_B T H(t)(1 - h(t)) \right] \Gamma(k,t), \qquad (3.15)$$

where $h(t) = dH(t)/dt$. Finally, carrying out the inverse Fourier transform gives the FPE

$$\frac{\partial p(x,t)}{\partial t} = -h(t)V(0)\frac{\partial p(x,t)}{\partial x}$$

$$+ k_B T H(t)(1 - h(t))\frac{\partial^2 p(x,t)}{\partial x^2}. \qquad (3.16)$$

For a given choice of correlation function $C(t)$ and the asymptotic properties of Laplace transforms in the small s limit, one can determine the large t behavior of the FP equation. For example, if $C(t) = F_0(\alpha)t^{-\alpha}$, it can be shown that when $t \to \infty$ and $0 < \alpha < 1$, the FP equation has the asymptotic form (Wang, 1992)

$$\frac{\partial p(x,t)}{\partial t} = -a_1(\alpha)V(0)t^{\alpha-2}V(0)\frac{\partial p(x,t)}{\partial x}$$

$$b_1(\alpha)k_B T t^{\alpha-1}\frac{\partial^2 p(x,t)}{\partial x^2}, \qquad (3.17)$$

for α–dependent coefficients a_1, b_1. Note in particular that the diffusion coefficient is time–dependent and there is a drift term when $V(0) \neq 0$. Both of these reflect the non–Markovian nature of the process. Given the initial condition $p(x,0) = \delta(x)$, the asymptotic FP equation has the solution

$$p(x,t) = \frac{1}{\sqrt{4\pi D_0 t^\alpha}} \exp\left[-(x + at^{\alpha-1})^2/(4D_0 t^\alpha) \right], \qquad (3.18)$$

where $D_0 = b_1 k_B T/\alpha$, $a = a_1 V(0)/(\alpha - 1)$. It can also be shown that the mean-square displacement $\langle [X(t) - \overline{X}]^2 \rangle = 2D_0 t^\alpha$, thus signifying anomalous subdiffusion.

Finally, note that one can construct a FBM model that exhibits the same Gaussian behavior as the FLE in the long-time limit (Lutz, 2001). The former considers a particle evolving according to a Langevin equation of the form

$$\frac{dX}{dt} = -kX + \xi(t), \qquad (3.19)$$

which is driven by fractional Gaussian noise of zero mean and a slowly decaying, power-law autocorrelation function $(t \neq t')$

$$\langle \xi(t)\xi(t') \rangle \sim \alpha(\alpha - 1)K|t - t'|^{\alpha-2}. \qquad (3.20)$$

In contrast to FLE, this process is driven by external noise without considering the fluctuation-dissipation theorem. Note that the Gaussian solution of FBM breaks down in the case of confined motion.

B. Molecular crowding

One of the characteristic features of the interior aqueous environment of cells (cytoplasm) and intracellular compartments such as the endoplasmic reticulum and mitochondria is that they are crowded with macromolecules and skeletal proteins, which occupy $10\% - 50\%$ of the volume (Dix and Verkman, 2008; Fulton, 1982; Luby-Phelps, 2000). Cell membranes are also crowded environments containing lipids (molecules consisting of nonpolar, hydrophobic hydrocarbon chains that end in a polar hydrophylic head), which are often organized into raft structures, and various mobile and immobile proteins (Kusumi et al., 2005). One consequence of molecular crowding, which we will not consider further here, is that it can drastically alter biochemical reactions in cells (Schnell and Turner, 2004; Zhou et al., 2008). That is, volume or area exclusion effects increase the effective solute concentration, thus increasing the chemical potential of the solute. Another consequence of molecular crowding is that it hinders diffusion, although there is an ongoing debate regarding to what extent this results in anomalous diffusion rather than a simple reduction in the normal diffusion coefficient (Banks and Fradin, 2005; Dix and Verkman, 2008; Weiss et al., 2004).

One of the difficulties in experimentally establishing the existence of anomalous diffusion is that the behavior of $\langle R^2 \rangle$ can depend on the spatial or temporal scale over which observations are made. Consider, for example, the effects of obstacles on protein diffusion (Saxton, 1994; Sung and Yethiraj, 2008). The presence of obstacles reduces the space available for diffusion, and consequently decreases the effective diffusion coefficient. As the volume or area fraction of obstacles ϕ is increased, there is a fragmentation of the available space in the sense that many paths taken by a diffusing protein terminate in a

dead end and thus do not contribute to diffusive transport. The region of free diffusion develops a fractal–like structure resulting in anomalous diffusion at intermediate times, $\langle R^2 \rangle \sim t^\alpha$, $\alpha < 1$. (For sufficiently small times $\sqrt{Dt} \ll \xi$, where ξ is the mean distance between obstacles, so that diffusion is normal). However, assuming that the volume or area fraction is below the percolation threshold, diffusion is expected to be normal on sufficiently long time-scales, $\langle R^2 \rangle \sim t$. On the other hand, above the percolation threshold, proteins are confined and $\langle R^2 \rangle$ saturates as $t \to \infty$. The time it takes to cross over from anomalous to normal diffusion increases with the volume or area fraction ϕ, and diverges at the percolation threshold ϕ_c where $\langle R^2 \rangle \sim t^\alpha$ for all times.

Another difficulty in interpreting experimental data is that there are certain practical limitations of current methods (Dix and Verkman, 2008). The most effective method for describing membrane diffusion is single-particle tracking (SPT). This involves the selective labeling of proteins or lipids with fluorophores such as quantum dots, green fluorescent protein (GFP) or organic dyes so that continuous high resolution tracking of individual molecules can be carried out. SPT can yield nanometer spatial resolution and submillisecond temporal resolution of individual trajectories. However, it is not currently suitable for measuring diffusion in three dimensions due to the relatively rapid speed of 3D diffusion and the problems of imaging in depth. Hence, in the case of diffusion within the cytosol, it is necessary to use a method such as fluorescence recovery after photobleaching (FRAP). Here fluorescently labeled molecules are introduced into the cell and those in some specified volume are bleached by a brief intense laser pulse. The diffusion of unbleached molecules into the bleached volume is then measured. FRAP is limited because it only provides ensemble averaged information of many fluorescent particles, and it also has a restricted measurement time, making it difficult to capture long-tail phenomena expected in anomalous subdiffusion.

Recently, homogenization theory has been used to develop a fast numerical scheme to calculate the effects of excluded volume due to molecular crowding on diffusion in the cytoplasm (Novak et al., 2009). The basic idea is to model the heterogeneous environment in terms of randomly positioned overlapping obstacles. (Note, however, that this is an oversimplification, since single-particle tracking experiments indicate that the cytoplasm is more properly treated as a dynamic, viscoelastic environment). Although obstacles don't overlap physically, when the finite size of a diffusing molecule (tracer) is taken into account, the effective volume excluded by an obstacle increases so that this can result in at least partially overlapping exclusion domains, see Fig. 3(a). In the absence of any restrictions on the degree of overlap, the fraction of inaccessible volume is $\phi = 1 - e^{-V}$, where V is the sum of the individual obstacles per unit volume. A sim-
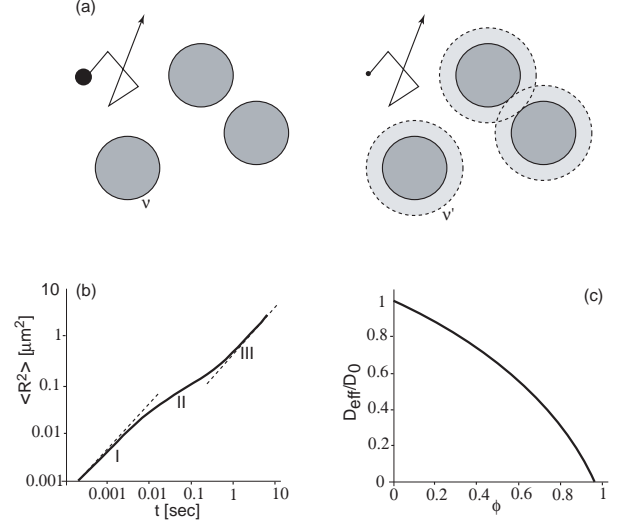

FIG. 3 (a) Diffusion of a finite size particle (tracer) between obstacles of volume ν (left) can be modeled as diffusion of a point particle between effective obstacles of volume ν' (right). Effective obstacles can partially overlap. (b) Sketch of MSD $\langle R^2 \rangle$ against time t, illustrating three different diffusion regimes: unobstructed diffusion (I), anomalous intermediate diffusion (II), and normal effective diffusion (III). (c) Illustrative plot of the normalized effective diffusion coefficient $D_{\text{eff}}(\phi)/D_0$ for random spheres. The scale of the curves in (b,c) are based on the results of Novak et al. (2009).

ple argument for this (Novak et al., 2009) is to consider a set of N identical overlapping objects placed in a box of total volume $|\Omega|$. Let ν denote the volume of each obstacle. The probability $P(x)$ that a randomly selected point $x \in \Omega$ is outside any given obstacle is $1 - \nu/|\Omega|$. Hence, the probability for that point to be outside all obstacles is $P(x)^N = (1 - \nu/|\Omega|)^N$. The volume fraction of accessible space at fixed number density $n = N/|\Omega|$ is then

$$\lim_{N \to \infty} (1 - \nu/|\Omega|)^N = \lim_{N \to \infty} (1 - \nu n/N)^N = e^{-n\nu} = e^{-V}$$

and the result follows. The mean distance between obstacles can then be determined in terms of ϕ and the geometry of each obstacle.

As previously discussed, three regimes of diffusion are expected below the percolation threshold, $\phi < \phi_c$, as illustrated in Fig. 3(b). For sufficiently short times there is unobstructed diffusion, for intermediate times there is anomalous diffusion, and for long times there is normal effective diffusion. Novak et al. (2009) use homogenization theory to estimate the effective diffusion coefficient D_{eff} in the last regime. The starting point for their analysis is to consider a periodic arrangement of identical obstacles in a large rectangular box of volume Ω with accessible volume Ω_1 and $\phi = 1 - |\Omega_1|/|\Omega|$. The spatial periods of the arrangement in Cartesian coordinates are

$a_j, j = 1, 2, 3$ such that the ratio

$$\epsilon = \sqrt{a_1^2 + a_2^2 + a_3^2}/\sqrt[3]{|\Omega|} \ll 1. \qquad (3.21)$$

The heterogeneous diffusion coefficient is

$$D_\epsilon(\mathbf{x}) = \begin{cases} D_0 & \text{if } \mathbf{x} \in \Omega_1 \\ 0, & \text{otherwise.} \end{cases} \qquad (3.22)$$

Inhomogeneous Dirichlet conditions are imposed on the boundaries of the box in order to maintain a steady–state diffusive flux. In the case of a heterogeneous diffusion coefficient, the flux is determined by the steady–state diffusion equation for the tracer distribution $u(\mathbf{x})$:

$$\boldsymbol{\nabla} \cdot (D_\epsilon(\mathbf{x})\boldsymbol{\nabla} u(\mathbf{x})) = 0. \qquad (3.23)$$

The basic idea of the homogenization method is to represent the diffusive behavior of a tracer on two different spatial scales (Pavliotis and Stuart, 2008; Torquato, 2002): one involving a macroscopic slow variable $\mathbf{x}$ and the other a microscopic fast variable $\mathbf{y} \equiv \mathbf{x}/\epsilon$ so that u is periodic with respect to $\mathbf{y}$. Thus, we write

$$u = u(\mathbf{x}, \mathbf{y}), \quad \boldsymbol{\nabla} u = \boldsymbol{\nabla}_{\mathbf{x}} u(\mathbf{x}, \mathbf{y}) + \epsilon^{-1}\boldsymbol{\nabla}_{\mathbf{y}} u(\mathbf{x}, \mathbf{y}).$$

Also $D_\epsilon(\mathbf{x}) \equiv D(\mathbf{x}/\epsilon) = D(\mathbf{y})$ with D and u having the same periodicity in $\mathbf{y}$.

A solution to Eq. (3.23) is then constructed in terms of the asymptotic expansion

$$u = u_0(\mathbf{x}, \mathbf{y}) + \epsilon u_1(\mathbf{x}, \mathbf{y}) + \epsilon^2 u_2(\mathbf{x}, \mathbf{y}) + \dots. \qquad (3.24)$$

Collecting terms of the same order in ϵ then yields a hierarchy of equations, which up to $\mathcal{O}(1)$ are as follows:

$$\boldsymbol{\nabla}_{\mathbf{y}} \cdot [D(\mathbf{y})\boldsymbol{\nabla}_{\mathbf{y}} u_0(\mathbf{x}, \mathbf{y})] = 0 \qquad (3.25a)$$

$$\begin{aligned} \boldsymbol{\nabla}_{\mathbf{y}} \cdot [D(\mathbf{y})\boldsymbol{\nabla}_{\mathbf{y}} u_1(\mathbf{x}, \mathbf{y})] = &-\boldsymbol{\nabla}_{\mathbf{y}} \cdot [D(\mathbf{y})\boldsymbol{\nabla}_{\mathbf{x}} u_0(\mathbf{x}, \mathbf{y})] \\ &- \boldsymbol{\nabla}_{\mathbf{x}} \cdot [D(\mathbf{y})\boldsymbol{\nabla}_{\mathbf{y}} u_0(\mathbf{x}, \mathbf{y})] \end{aligned}$$
$$(3.25b)$$

$$\begin{aligned} \boldsymbol{\nabla}_{\mathbf{y}} \cdot [D(\mathbf{y})\boldsymbol{\nabla}_{\mathbf{y}} u_2(\mathbf{x}, \mathbf{y})] = &-\boldsymbol{\nabla}_{\mathbf{x}} \cdot [D(\mathbf{y})\boldsymbol{\nabla}_{\mathbf{x}} u_0(\mathbf{x}, \mathbf{y})] \\ &- \boldsymbol{\nabla}_{\mathbf{y}} \cdot [D(\mathbf{y})\boldsymbol{\nabla}_{\mathbf{x}} u_1(\mathbf{x}, \mathbf{y})] \\ &- \boldsymbol{\nabla}_{\mathbf{x}} \cdot [D(\mathbf{y})\boldsymbol{\nabla}_{\mathbf{y}} u_1(\mathbf{x}, \mathbf{y})]. \end{aligned}$$
$$(3.25c)$$

Eq. (3.25a) and periodicity with respect to $\mathbf{y}$ establishes that $u_0(\mathbf{x}, \mathbf{y}) \equiv u_0(\mathbf{x})$, that is, u_0 corresponds to an homogenized solution. It follows from Eq. (3.25b) that

$$\boldsymbol{\nabla}_{\mathbf{y}} D(\mathbf{y}) \cdot \boldsymbol{\nabla}_{\mathbf{x}} u_0(\mathbf{x}) + \boldsymbol{\nabla}_{\mathbf{y}} \cdot [D(\mathbf{y})\boldsymbol{\nabla}_{\mathbf{y}} u_1(\mathbf{x}, \mathbf{y})] = 0,$$

which has the solution

$$u_1(\mathbf{x}, \mathbf{y}) = \sum_{i=1}^{3} \frac{\partial u_0(\mathbf{x})}{\partial x_i} w_i(\mathbf{y}), \qquad (3.26)$$

with $w_i(\mathbf{y})$ a periodic function satisfying

$$\frac{\partial D(\mathbf{y})}{\partial y_i} + \sum_{j=1}^{3} \frac{\partial}{\partial y_j}\left[D(\mathbf{y})\frac{\partial w_i(\mathbf{y})}{\partial y_j}\right] = 0. \qquad (3.27)$$

Finally, averaging both sides of Eq. (3.25c) with respect to $\mathbf{y}$ over a unit volume $|\omega_0|/\epsilon^3$ of the periodic structure, using the divergence theorem, and expressing u_1 in terms of u_0 yields the homogenized diffusion equation

$$\sum_{i,j=1}^{3} \widetilde{D}_{\text{eff},ij} \frac{\partial^2 u_0(\mathbf{x})}{\partial x_i \partial x_j} = 0, \qquad (3.28)$$

with the anisotropic diffusion tensor

$$\widetilde{D}_{\text{eff},ij} = \frac{\epsilon^3}{|\omega_0|} \int_{\omega_0} \left(D(\mathbf{y})\delta_{i,j} + D(\mathbf{y})\frac{\partial w_i(\mathbf{y})}{\partial y_j}\right) d\mathbf{y}. \qquad (3.29)$$

Finally, rewriting the diffusion tensor in a more symmetric form using Eq. (3.27) and integration by parts gives (Novak *et al.*, 2009)

$$\widetilde{D}_{\text{eff},ij} = \frac{D_0}{|\omega_0|} \int_{\omega_1} \sum_{k=1}^{3} \left(\delta_{i,k} + \frac{\partial \widehat{w}_i(\mathbf{x})}{\partial x_k}\right)\left(\delta_{j,k} + \frac{\partial \widehat{w}_j(\mathbf{x})}{\partial x_k}\right) d\mathbf{x},$$

where ω_1 is the accessible region of the fundamental domain ω_0. The function $w(x)$ has been rescaled according to $\widehat{w}(\mathbf{x}) = \epsilon w(\mathbf{x}/\epsilon)$ so that

$$\frac{\partial D_\epsilon(\mathbf{x})}{\partial x_i} + \sum_{j=1}^{3} \frac{\partial}{\partial x_j}\left[D_\epsilon(\mathbf{x})\frac{\partial \widehat{w}_i(\mathbf{x})}{\partial x_j}\right] = 0 \qquad (3.30)$$

over a unit cell with periodic boundary conditions. Note that the concentration $u_0(\mathbf{x})$ is only defined in free space so that the macroscopic concentration is actually $u(\mathbf{x}) = (1-\phi)u_0(\mathbf{x})$ and the macroscopic diffusion tensor is $D_{\text{eff},ij} = \widetilde{D}_{\text{eff},ij}/(1-\phi)$. In the case of isotropic periodic structures $D_{\text{eff},ij} = D_{\text{eff}}\delta_{i,j}$.

Novak *et al.* (2009) numerically extended the homogenization method to a random arrangement of obstacles by approximating the disordered medium with a periodic one, in which the unit cell consists of N randomly placed obstacles. N is taken to be sufficiently large so that for a given density of obstacles, one obtains a statistically stationary D_{eff}. Comparing the homogenized diffusion coefficient with that obtained from Monte Carlo simulations, Novak *et. al.* showed that the numerical homogenization method yielded reasonable agreement for $N = \mathcal{O}(100)$. One of the interesting results of their study was that the variation of D_{eff} with the excluded volume fraction ϕ can be approximated by the power law

$$D_{\text{eff}}(\phi) = D_0 \frac{(1 - \phi/\phi_c)^\mu}{1 - \phi}, \qquad (3.31)$$

where the parameters ϕ_c, μ depend on the geometry of the obstacles. For example, for randomly arranged spheres, $\phi_c \approx 0.96$ and $\mu \approx 1.5$. A typical plot of $D_{\text{eff}}(\phi)$ is shown in Fig. 3(c). Previously, the above power law behavior had been predicted close to the percolation threshold (Bouchaud and Georges, 1990), but these results suggest it also holds for a wider range of volume fractions.

C. Diffusion–trapping models

In the Smoluchowski theory of reaction kinetics, it is assumed that when a diffusing particle reacts with the target it disappears, that is, we have the trapping reaction $A + B \rightarrow B$ where A denotes a diffusing particle and B denotes an immobile trap. However, within the context of intracellular transport, there are many examples where there is transient trapping of diffusing particles, resulting in anomalous diffusion on intermediate time-scales and normal diffusion on long time-scales. This has been elucidated by Saxton (1996, 2007), who carried out Monte–Carlo simulations of random walks on a 2D lattice with a finite hierarchy of binding sites, that is binding sites with a finite set of energy levels. This means that there are no traps that have an infinite escape time so that diffusing particles ultimately equilibrate with the traps and diffusion becomes normal. On the other hand, in the case of infinite hierarchies, arbitrarily deep traps exist but are very rare, resulting in a nonequilibrium system in which anomalous subdiffusion occurs at all times (Bouchaud and Georges, 1990). The latter process can be modeled in terms of a continuous-time random walk, see Sec. III.A. Here we will consider some examples of diffusive transport in the presence of transient immobile traps. Note that a related application is calcium buffering, where freely diffusing calcium molecules bind to large proteins in the cytosol that can either be mobile or immobile. In particular, mobile buffering can lead to a nonlinear advection-diffusion equation that changes many properties of the basic diffusion model, as detailed in Keener and Sneyd (2009).

1. Sequence-dependent protein diffusion along DNA

We begin by considering a 1D random walk model used to study sequence-dependent protein diffusion along DNA (Barbi *et al.*, 2004a,b). This concerns the important problem of how a site–specific DNA binding protein locates its target binding site on DNA. As discussed in Sec. II.E, such a search process is thought to involve a combination of mechanisms, including one–dimensional sliding along the DNA and uncorrelated 3D diffusion (Berg *et al.*, 1981; Halford and Marko, 2004). Barbi *et al.* (2004a,b) model the sliding phase of protein movement in terms of a 1D random walk, in which the step probability to neighboring sites depends on an energy landscape that reflects sequence dependent protein-DNA interactions, see Fig. 4. This is motivated by the idea that the protein needs to "read" the underlying sequence of base pairs (bps) as it slides along the DNA in order to be able to detect the target site. Thus each nonspecific site on DNA acts as a potential trap for the sliding protein.

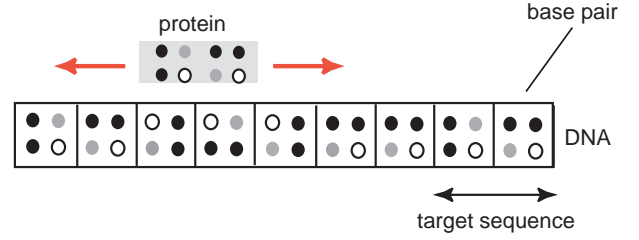The sequence of the target site usually consists of a few (r) consecutive bps, and sequence recognition is of-

FIG. 4 Schematic illustration of Barbi *et al.* (2004a,b) random walk model of sequence-dependent protein diffusion along DNA. Each lattice site corresponds to a base pair with four binding sites that can potentially make hydrogen bonds with the diffusing protein: acceptor sites (black dots), donor sites (gray dots) and missing sites (white dots). In this example, the protein interacts with a base pair sequence of length $r = 2$. The energy of protein-DNA interactions determines the transition rates to nearest neighbor lattice sites.

ten mediated by hydrogen bonds to a set of four specific binding sites on each base pair. Some binding sites form a hydrogen bond as an acceptor, some as a donor and some do not to form a bond. Barbi *et. al.* assume that at each site n of DNA, the protein attempts to form hydrogen bonds with the local sequence of r base pairs. Hence, each potential binding site n is represented as a sequence of r-vectors $\{\mathbf{b}_n, \mathbf{b}_{n+1}, \ldots, \mathbf{b}_{n+r-1}\}$, one for each bp in the sequence, according to the rule

$$\mathbf{b}_n = \left\{ \begin{array}{ll} (1,-1,1,0)^T \text{ for } AT & (0,1,-1,1)^T \text{ for } TA \\ (1,1,-1,0)^T \text{ for } GC & (0,-1,1,1)^T \text{ for } CG \end{array} \right. ,$$

where $+1, -1, 0$ denote, respectively, an acceptor, a donor and a missing hydrogen bond on a given bp. The protein is then represented by a so–called $(r \times 4)$ recognition matrix $\mathbf{R}$ describing the pattern of hydrogen bonds formed by the protein and DNA at the target site where there is optimal matching. The protein-DNA interaction energy is then defined by counting the matching and unmatching bonds between the recognition matrix and the DNA sequence at site n:

$$E(n) = -\epsilon \text{Tr}[\mathbf{R} \cdot \mathbf{B}], \tag{3.32}$$

where $\mathbf{B}$ is the matrix whose r columns are given by the vectors $\{\mathbf{b}_n, \mathbf{b}_{n+1}, \ldots, \mathbf{b}_{n+r-1}\}$, and ϵ denotes each hydrogen bond energy.

Given the above energy landscape, Barbi *et. al.* model the dynamics of protein sliding motion along DNA as a 1D random walk, in which the protein is represented as a particle hopping to its nearest neighboring lattice sites with rates

$$r_{n \rightarrow n'} = \frac{1}{2\tau} e^{-\Delta E_{n \rightarrow n'}/k_B T}, \quad n' = n \pm 1, \tag{3.33}$$

where $\Delta E_{n \rightarrow n'}$ is the effective energy barrier between neighboring sites, k_B is the Boltzmann constant, and T is

the temperature. Various models can be considered relating the barrier energy to the site-dependent energy $E(n)$ (Barbi *et al.*, 2004b). The simplest is to take $\Delta E_{n\rightarrow n'} = \max[E(n') - E(n), 0]$. Monte Carlo simulations may then be used to study the dynamics of the resulting random walk with transient traps (Barbi *et al.*, 2004a,b). In the large time limit, a population of non-interacting random walkers will reach a stationary Boltzmann distribution of the form $\rho(n) \sim e^{-E(n)/k_B T}$ and the associated dynamics will exhibit normal diffusion. However, for large enough values of $\epsilon/k_B T$, some sites along the DNA could trap a protein for significant times, suggesting that anomalous behavior could be observed at intermediate times. This is indeed found to be the case. Defining the MSD according to $\langle \Delta n^2 \rangle = N^{-1} \sum_{i=1}^{N} (n_i(t) - n_i(0))^2$ where N is the number of proteins in the population, it was found numerically that $\langle \Delta n^2 \rangle \sim t^\alpha, \alpha < 1$ at intermediate times, with a crossover to normal diffusion ($\alpha = 1$) at large times. Moreover, using experimentally based model parameters, Barbi *et. al.* showed that the crossover time was sufficiently large that anomalous diffusion occurred on time-scales comparable to the typical sliding phase of target search (Barbi *et al.*, 2004a,b). This suggests that anomalous diffusion is likely to dominate.

2. Diffusion along spiny dendrites

Another recent example of anomalous diffusion in the presence of transient traps has been considered by Santamaria *et al.* (2006). These authors used a combination of experimental and computational modeling to study how the presence of dendritic spines affects the 3D diffusion of signaling molecules along the dendrites of neurons. Neurons are amongst the largest and most complex cells in biology. Their intricate geometry presents many challenges for cell function, in particular with regards to the efficient delivery of newly synthesized proteins from the cell body or soma to distant locations on the axon or dendrites. The axon contains ion channels for action potential propagation and presynaptic active zones for neurotransmitter release, whereas each dendrite contains postsynaptic domains (or densities) where receptors that bind neurotransmitter tend to cluster, see Fig. 5. At most excitatory synapses in the brain, the postsynaptic density (PSD) is located within a dendritic spine, which is a small, sub-micrometer membranous extrusion that protrudes from a dendrite (Sorra and Harris, 2000), see Fig. 6. Typically spines have a bulbous head that is connected to the parent dendrite through a thin spine neck, and there can exist thousands of spines distributed along a single dendrite. It is widely thought that spines act to compartmentalize chemical signals generated by synaptic activity, thus impeding their diffusion into dendrites (Sabatini *et al.*, 2001; Yuste *et al.*, 2000). Conversely, in the case of signaling molecules diffusing along the den-

drite, the spines act as transient traps as illustrated in Fig. 7(a). Following along similar arguments to the case of diffusion in the presence of obstacles, normal diffusion is expected at short and long times and anomalous subdiffusion at intermediate times. Anomalous subdiffusion was indeed observed by Santamaria *et al.* (2006), such that the mean square displacement $\langle \mathbf{x}^2(t) \rangle \sim D_0 t^{2/\beta}$ at intermediate times with $\beta > 2$ and D_0 the free diffusion coefficient. As might be expected, β increases (slower diffusion) with increasing spine density. β also increases when the volume of the spine head is increased relative to the spine neck, reflecting the fact there is an enhanced bottleneck. Note that anomalous diffusion can occur at all times if the reactions within each spine are taken to have a non-exponential waiting time density (Fedotov *et al.*, 2010), see also III.A.

A related problem is the diffusive transport of neurotransmitter protein receptors within the plasma membrane of a dendrite, with each spine acting as a transient trap that localizes the receptors at a synapse. The ma-
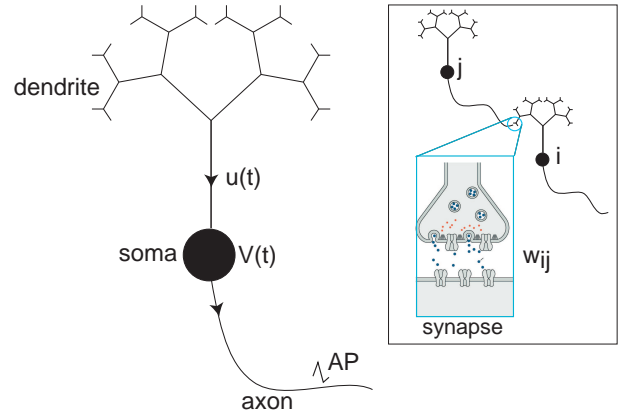

FIG. 5 Basic structure of a neuron. [Inset shows a synaptic connection of strength w_{ij} from an upstream or presynaptic neuron labeled j and a downstream or postsynaptic neuron labeled i]. Neurons in the brain communicate with each other by transmitting electrical spikes (action potentials). An action potential (AP) propagates along the axon of a neuron until it reaches a terminal that forms the upstream or presynaptic component of the synaptic connection to a downstream or postsynaptic neuron. The arrival of the action potential induces the release of chemical transmitters into the synapse. These subsequently bind to protein receptors in the postsynaptic membrane resulting in the opening of various ion channels. This generates a synaptic current that flows along the dendritic tree of the postsynaptic neuron and combines with currents from other activated synapses. If the total synaptic current $u(t)$ forces the membrane potential $V(t)$ at a certain location within the cell body to cross some threshold, then the postsynaptic neuron fires an action potential and the process continues. One can thus view the brain as a vast collection of synaptically–coupled networks of spiking neurons. Moreover, the strength of synaptic connections within and between networks are modifiable by experience (synaptic plasticity).
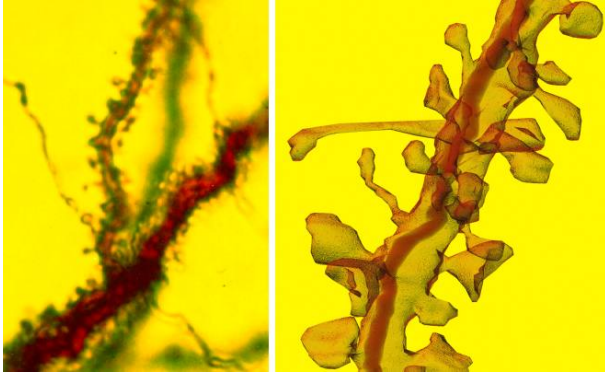
FIG. 6 An example of a piece of spine studded dendritic tissue (from rat hippocampal region CA1 stratum radiatum). The dendrite on the right-hand side is $\sim 5\mu m$ in length. Taken with permission from SynapseWeb, Kristen M. Harris, PI, http://synapses.clm.utexas.edu/

jority of fast excitatory synaptic transmission in the central nervous system is mediated by AMPA (α-amino-3-hydroxy-5-methyl-4-isoxazole-propionic acid) receptors,
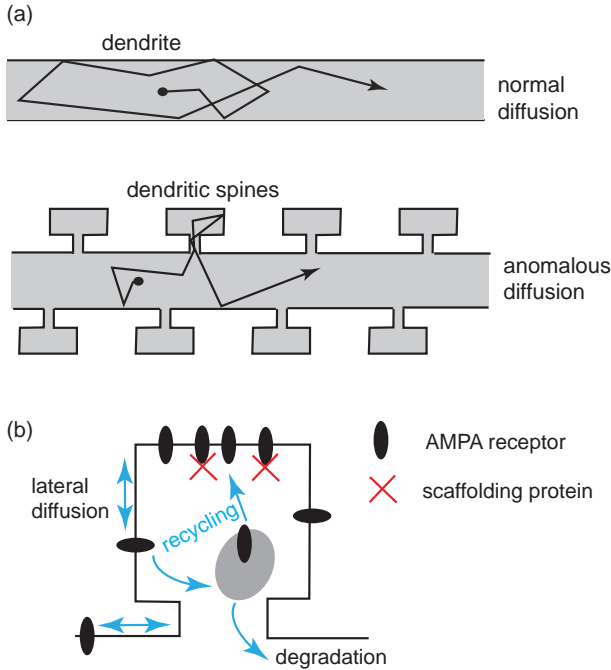

FIG. 7 (a) Schematic illustration of the anomalous diffusion model of Santamaria *et al.* (2006), who carried out detailed 3D simulations of diffusion in a spiny dendrite treated as a system of connected cylinders with the following baseline parameter values: spine neck diameter $0.2\mu m$, neck length $0.6\mu m$, head length and diameter $0.6\mu m$, dendrite diameter $1\mu m$ and a spine density of 15 spines/μm. The dendritic spines act as transient traps for a diffusing particle within the dendrite, which leads to anomalous diffusion on intermediate time scales. (b) Schematic illustration of various pathways of AMPA receptor trafficking at a dendritic spine.

which respond to the neurotransmitter glutamate. There is now a large body of experimental evidence that the fast trafficking of AMPA receptors into and out of spines is a major contributor to activity-dependent, long-lasting changes in synaptic strength (Bredt and Nicoll, 2003; Collinridge *et al.*, 2004; Henley *et al.*, 2011; Shepherd and Huganir, 2007). Single–particle tracking experiments suggest that surface AMPA receptors diffuse freely within the dendritic membrane until they enter a spine, where they are temporarily confined by the geometry of the spine and through interactions with scaffolding proteins and cytoskeletal elements (Choquet and Triller, 2003; Ehlers *et al.*, 2007; Gerrow and Triller, 2010; Groc *et al.*, 2004; Newpher and Ehlers, 2008; Triller and Choquet, 2005). A surface receptor may also be internalized via endocytosis and stored within an intracellular pool, where it is either recycled to the surface via exocytosis or degraded (Ehlers, 2000), see Fig. 7(b). Endocytosis is the physical process whereby vesicles are formed within the plasma membrane and then internalized, and exocytosis is the complementary process in which intracellular vesicles fuse with the plasma membrane and release their contents (Doherty and McMahon, 2009). Molecular motors transport internalized vesicles to intracellular compartments that either recycle vesicles to the cell surface (early endosomes and recycling endosomes) or sort them for degradation (late endosomes and lyososomes) (Maxfield and McGraw, 2004; Soldati, 2006). A number of single spine models have explored the combined effects of diffusion, trapping, receptor clustering and recycling on the number of synaptic AMPA receptors (Burlakov *et al.*, 2012; Czondora *et al.*, 2012; Earnshaw and Bressloff, 2006; Holcman and Triller, 2006; Shouval, 2005). In such models, the synapse is treated as a self-organizing compartment in which the number of AMPA receptors is a dynamic steady-state that determines the strength of the synapse; activity-dependent changes in the strength of the synapse then correspond to shifts in the dynamical set-point. When receptor-receptor interactions are included a synapse can exhibit bistability between a non-clustered and clustered state (Shouval, 2005), which can be understood in terms of a liquid-vapor phase transition (Burlakov *et al.*, 2012).

It is also possible to develop a diffusion–trapping model of receptor trafficking at multiple spines by considering a 2D version of the Santamaria *et al.* (2006) model, in which receptors diffuse on the surface of a cylindrical dendrite containing multiple disk-like traps; when a receptor transiently enters a trap it can undergo various reactions corresponding to processes within a spine such as receptor recycling and binding to anchoring proteins. Using asymptotic methods similar to those of Straube *et al.* (2007), see Sec. II.D, one can show that the 2D model is well approximated by a reduced 1D cable model in which dendritic spines are treated as point–like sources or sinks (Bressloff *et al.*, 2008). The advantage of the 1D

model is that the associated 1D Green's function is non–singular. Therefore, consider a population of N identical spines distributed along a uniform dendritic cable of length L and circumference l, with x_j, $j = 1, \ldots, N$, the position (axial coordinate) of the jth spine. Let $p(x, t)$ denote the probability density (per unit area) that a surface receptor is located within the dendritic membrane at position x at time t. Similarly, let $R_j(t), S_j(t)$ denote the probability that the receptor is trapped at the surface of the jth spine or within an associated intracellular pool, respectively. A simple version of the 1D diffusion–trapping model of AMPA receptor trafficking takes the form (Bressloff and Earnshaw, 2007; Earnshaw and Bressloff, 2008)

$$\frac{\partial p}{\partial t} = D_0 \frac{\partial^2 p}{\partial x^2} - \sum_{j=1}^{N} \Omega[p_j - R_j/A]\delta(x - x_j), \quad (3.34\text{a})$$

$$\frac{dR_j}{dt} = \Omega[p_j - R_j/A] - kR_j + \sigma S_j, \quad (3.34\text{b})$$

$$\frac{dS_j}{dt} = -\sigma S_j + kR_j, \quad (3.34\text{c})$$

where D_0 is the surface diffusivity and $p_j(t) = p(x_j, t)$. The term $\Omega(p_j - R_j/A)$ with A the surface area of a spine represents the probability flux into the jth spine with Ω an effective hopping rate. (This rate depends on the detailed geometry of the dendritic spine (Ashby et al., 2006)). It is assumed that surface receptors within the jth spine can be recycled with respect to the intracellular pool with k, σ the rates of endocytosis and exocytosis, respectively. Eq. (3.34a) is supplemented by reflecting boundary conditions at the ends of the cable: $D\partial_x p(0, t) = 0$ and $D\partial_x p(L, t) = 0$.

The effective diffusivity of a receptor in the long-time limit, which takes into account the effects of trapping at spines, can be determined by calculating the MFPT $\tau(X)$ to travel a distance X from the soma. Introducing an absorbing boundary condition at $x = X$, the function

$$\mathbb{P}(X, t) \equiv l \int_0^X p(x, t)dx + \sum_{j=1}^{N_X} [R_j(t) + S_j(t)] \quad (3.35)$$

is then the probability that $t < \tau(X)$; i.e., the probability that a receptor which was initially at the origin has not yet reached the point $x = X$ in a time t. Here N_X is the number of spines in the interval $[0, X)$. The MFPT is then $\tau(X) = \int_0^\infty \mathbb{P}(X, t)dt$. It follows that the MFPT can be expressed in terms of Laplace transforms;

$$\tau(X) = \int_0^X \widetilde{p}(x, 0)dx + \sum_{j=1}^{N_X} \left[\widetilde{R}_j(0) + \widetilde{S}_j(0) \right] \quad (3.36)$$

where $\widetilde{f}(z) \equiv \int_0^\infty e^{-zt} f(t)dt$. Laplace transforming Eqs.

(3.34a), (3.34c) and using the initial conditions, gives

$$-z\widetilde{p} + D_0 \frac{\partial^2 \widetilde{p}}{\partial x^2} = \sum_{j=1}^{N_X} \Omega[\widetilde{p}_j - \widetilde{R}_j/A]\delta(x - x_j) - l^{-1}\delta(x),$$
$$(3.37\text{a})$$

$$z\widetilde{R}_j = \Omega[\widetilde{p}_j - \widetilde{R}_j/A] - k\widetilde{R}_j + \sigma\widetilde{S}_j, \quad (3.37\text{b})$$

$$z\widetilde{S}_j = -\sigma\widetilde{S}_j + k\widetilde{R}_j, \quad (3.37\text{c})$$

where $\widetilde{p}_j(z) = \widetilde{p}(x_j, z)$. In the limit $z \to 0$, Eqs. (3.37b)–(3.37c) imply that $A\widetilde{p}_j(0) = \widetilde{R}_j(0) = \sigma\widetilde{S}_j(0)/k$, and Eq. (3.37a) becomes

$$lD_0 \frac{\partial^2 \widetilde{p}(x, 0)}{\partial x^2} = -\delta(x). \quad (3.38)$$

Imposing the boundary conditions at $x = 0, X$ gives $l\widetilde{p}(x, 0) = (X - x)/D_0$. Combining these results,

$$\tau(X) = \frac{X^2}{2D_0} + \frac{\eta}{D_0} \sum_{j=1}^{N_X}(X - x_j), \quad (3.39)$$

where $\eta = A[1 + k/\sigma]/l$. The first term on the right–hand side of this equation is the MFPT in the absence of any spines, whereas the remaining terms take into account the effects of being temporarily trapped at a spine.

In order to calculate an effective diffusivity, consider the simple example of identical spines distributing uniformly along the cable with spacing d. That is, $x_j = jd$, $j = 1, \ldots, N$ such that $Nd = L$ and $N_X = X/d$ for $X \gg d$. Eq. (3.39) then becomes (for $N_X \gg 1$)

$$\tau(X) \equiv \frac{X^2}{2D} = \frac{X^2}{2D_0} + \frac{\eta}{D_0} \sum_{j=1}^{N_X}(X - jd).$$

Using the approximation

$$\sum_{j=1}^{N_X}(X - jd) = N_X X - \frac{(N_X + 1)N_X d}{2} \approx \frac{X^2}{2d}$$

finally gives (Bressloff and Earnshaw, 2007)

$$D = D_0 \left[1 + \frac{A}{ld}\left(1 + \frac{k}{\sigma}\right) \right]^{-1}. \quad (3.40)$$

As expected, the presence of traps reduces the effective diffusivity of a receptor. In particular, the diffusivity is reduced by increasing the ratio k/σ of the rates of endocytosis and exocytosis or by increasing the surface area A of a spine relative to the product of the spine spacing d and circumference of the cable l. Interestingly, D does not depend on the hopping rate Ω. Taking typical measured values of the diffusivity ($D = 0.1\mu m^2 s^{-1}$) (Ashby et al., 2006; Groc et al., 2004), the area of a spine ($A = 1\mu m^2$), the spacing between spines ($d = 1\mu m$) and the circumference of a dendrite ($l = 1\mu m$) (Sorra and

Harris, 2000), it follows that $D_{eff} = 0.5D$ when $k = \sigma$, whereas $D \ll D_0$ when $k \gg \sigma$. There is experimental evidence that the rates of exo/endocytsosis are activity–dependent (Ehlers *et al.*, 2007) so that the ratio k/σ, and hence D, may be modifiable by experience.

There have been various generalizations of the above model to include the effects of binding/unbinding to cytoskeletal proteins (Earnshaw and Bressloff, 2008) and dendritic branching (Bressloff, 2009). In the latter case, homogenization theory can be used to replace the discrete distribution of spines by a continuum density. One major simplification of the diffusing–trapping model is that it neglects the detailed structure of a spine and the associated PSD. A more comprehensive model would need to take into the complex organization of the PSD, interactions with scaffolding proteins, and the geometry of the spine (Freche *et al.*, 2011; Kerr and Blanpied, 2012; MacGillavry *et al.*, 2011; Sekimoto and Triller, 2009). Finally, note that the coupling between exocytosis and endocytosis during AMPA receptor recycling is one example of a more general transport mechanism that occurs in neurons (and other secretory cells) via the so–called endocytic pathway (Gundelfinger *et al.*, 2003). Other examples include the insertion and removal of membrane proteins during axonal elongation and guidance (Bloom and Morgan, 2011), see also Sec. V.A, and the stimulus-induced release of secretory molecules (neurotransmitters) at the presynaptic terminal of a synapse (see Fig. 5). The latter is regulated by the exocytosis of synaptic vesicles; endocytic processes then have to be coordinated so that there is an efficient reuptake of vesicles in order to restore functionality of the synapse. For a detailed discussion of whole cell kinetic models of receptor recycling and its role in chemical signaling see Lauffenburger (1996); Wiley *et al.* (2003).

3. Diffusion in the plasma membrane

At the simplest level, the plasma membrane can be treated as a 2D lipid sheet into which proteins are embedded. In the fluid mosaic model of Singer and Nicolson (1972), the membrane lipids are treated as the solvent (water concentrations are very low within the membrane) into which proteins are dissolved. One of the consequences of the fluid mosiac model is that protein clustering, which alters the effective size of a diffusing particle, has only a weak effect on diffusion in the plasma membrane. This follows from the hydrodynamic membrane diffusion model of Saffman and Delbruck (Saffman and Delbruck, 1975), which implies that the diffusion coefficient for a cylinder of radius r in a 2D membrane varies as $\log r$. Although the diffusion of lipids appears to be Brownian in pure lipid bilayers, single-particle tracking experiments indicate that lipids and proteins undergo anomalous diffusion in the plasma membrane (Feder *et al.*, 1996; Kusumi *et al.*, 2005; Saxton and Ja-
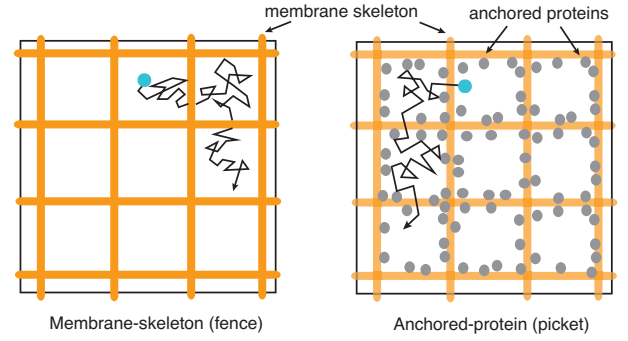

FIG. 8 Picket-fence model of membrane diffusion. The plasma membrane is parceled up into compartments whereby both transmembrane proteins and lipids undergo short-term confined diffusion within a compartment and long-term hop diffusion between compartments. This corralling is assumed to occur by two mechanisms. (a) The membrane-cytoskeleton (fence) model: transmembrane proteins are confined within the mesh of the actin-based membrane skeleton. (b) The anchored-protein (picket) model: transmembrane proteins, anchored to the actin-based cytoskeleton, effectively act as rows of pickets along the actin fences.

cobson, 1997). This has led to a modification of the original fluid mosaic model, whereby lipids and transmembrane proteins undergo confined diffusion within, and hopping between, membrane microdomains or corrals (Kusumi *et al.*, 2005, 2010; Vereb *et al.*, 2003); the corraling could be due to "fencing" by the actin cytoskeleton or confinement by anchored protein "pickets", see Fig. 8. These microdomains could also be associated with lipid rafts (Jacobson *et al.*, 2007; Kusumi *et al.*, 2010).

Partitioning the membrane into a set of corrals implies that anomalous diffusion of proteins will be observed on intermediate timescales, due to the combined effects of confinement and binding to the actin cytoskeleton. However, on time-scales over which multiple hopping events occur, normal diffusion will be recovered. A rough estimate of the corresponding diffusion coefficient is $D \sim L^2/\tau$, where L is the average size of a microdomain and τ is the mean hopping rate between microdomains. A typical range of values for various types of mammalian cell are $L \sim 30 - 240$ nm and $\tau \sim 1 - 20$ ms. In the case of confinement by anchored protein pickets, τ can be estimated by treating each corral as a domain with a set of small holes (gaps) between anchored proteins, and solving the narrow escape problem (Holcman and Schuss, 2004; Holcman and Triller, 2006). (Another approach to estimating τ has been developed by Kalay *et al.* (2008); Kenkre *et al.* (2008), based on a random walker moving on a 1D lattice with either periodically or randomly distributed semipermeable barriers). On the other hand, the membrane cytoskeleton surrounding a corral is usually modeled as an effective energy barrier over which a diffusing protein must escape. For exam-

ple, Saxton (1995) carried out a computational study of a particle diffusing inside a corral surrounded by a static energy barrier. It was assumed that when the particle hit the barrier it had a fixed probability of escape. The MFPT out of the corral was numerically determined for a wide range of corral sizes, shapes and escape probabilities. In earlier work, Saxton (1989, 1990) considered a static fence model in which a protein could only move from one corral to another if the particular barrier separating the two corrals was dissociated. In this particular model, large-scale diffusion only occurs if there exists a percolation network. However, estimates of the density of the actin cytoskeleton in red blood cells (erythrocytes), for example, suggests that the fraction of disassociated cytoskeleton is below the percolation threshold. Hence, it is necessary to modify the percolation model by considering time-dependent, fluctuating energy barriers.

Consider, for example, the spatially homogeneous stochastic gating model of Brown *et al.* (2000); Leitner *et al.* (2000). Let $P_n(t)$ denote the probability that there are n free particles within the corral at time t. Denote the time-dependent rates of protein influx and loss by $\lambda(t)$ and $\mu(t)$, respectively. The probability distribution is then taken to evolve according to the master equation

$$\frac{dP_n}{dt} = \sigma(t)P_{n-1} + \mu(t)(n+1)P_{n+1}(t) - [\sigma(t) + \mu(t)n]P_n \tag{3.41}$$

with $n \geq 0$ and $P_{-1}(t) \equiv 0$. The positive terms on the right-hand side represent the various transitions into the state (n) whereas the negative terms represent the various transitions from the state (n). The initial condition is $P_n(0) = \delta_{n,n_0}$; i.e., at time $t = 0$ there are n_0 free particles within the corral. In the model of Brown *et al.* (2000); Leitner *et al.* (2000), the escape of a protein from the corral is controlled by a stochastic gate that can be in two states, an open state for which $\mu(t) = \mu_o > 0$ and a closed state for which $\mu(t) = \mu_c = 0$. The opening and closing of the stochastic gate is governed by the rate equations

$$\frac{d\mathcal{P}^o}{dt} = -\gamma_-\mathcal{P}^o + \gamma_+\mathcal{P}^c,$$
$$\frac{d\mathcal{P}^c}{dt} = \gamma_-\mathcal{P}^o - \gamma_+\mathcal{P}^c, \tag{3.42}$$

where $\mathcal{P}^o(t)$ ($\mathcal{P}^c(t)$) is the probability that the gate is open (closed) at time t, and $\gamma_\pm$ are the transition rates between the two states. Thus the time-dependent escape rate $\mu(t)$ describes a dichotomous noise process. From detailed balance, the rate at which receptors enter the PSD is then taken to be $\sigma(t) = C\mu(t)$ with C fixed. (At equilibrium C can be identified with the mean number of particles in the corral). One possible interpretation of the stochastic gate is that it represents the random opening and closing of a small hole within the boundary of the PSD. This suggests that one could consider a multi–state version of the stochastic gate, which corresponds to the random opening and closing of multiple small holes within the PSD boundary. The master Eq. (3.41) is solved for a single realization of the stochastic process described by Eq. (3.42). As a consequence, different realizations of $\mu(t)$ will yield different probability distributions P_n.

In order to analyze the above model, introduce the generating function

$$G(u,t) = \sum_{n=0}^{\infty} u^n P_n(t), \tag{3.43}$$

It follows from the master Eq. (3.41) that G satisfies the first-order linear partial differential equation

$$\frac{\partial G}{\partial t} + \mu(t)(u-1)\frac{\partial G}{\partial u} = \sigma(t)(u-1)G \tag{3.44}$$

with initial condition $G(u,v,0) = u^{n_0}$. Eq. (3.44) can be solved using the method of characteristics (Kampen, 1992):

$$G(u,t) = [1 + \mathcal{N}(t)(u-1)]^{n_0} e^{C(1-\mathcal{N}(t))(u-1)}, \tag{3.45}$$

where

$$\mathcal{N}(t) = \exp\left(-\int_0^t \mu(t')dt'\right). \tag{3.46}$$

Given $G(u,t)$, the mean and variance of n can be calculated according to the formulae

$$\mathrm{E}_\mu(n) = \left.\frac{\partial G}{\partial u}\right|_{u=v=1}, \mathrm{E}_\mu(n^2-n) = \left.\frac{\partial^2 G}{\partial u^2}\right|_{u=v=1},$$

where the subscript μ indicates that these means are calculated with respect to a single realization of the random variable μ only, and may therefore take on different values for different realizations of μ. Calculating these derivatives yields

$$\mathrm{E}_\mu(n) = (n_0 - C)\mathcal{N}(t) + C, \ \mathrm{Var}_\mu(n) = \mathrm{E}_\mu(n) - n_0\mathcal{N}(t)^2.$$

A more useful characterization of the means and variances can be obtained by averaging $\mathcal{N}(t)$ with respect to all possible stochastic realizations of the gate, which is denoted by $\langle\mathcal{N}\rangle$. This can be performed using a method originally developed by Kubo (1962) in the study of spectral line broadening in a quantum system, and subsequently extended to chemical rate processes with dynamical disorder by Zwanzig (1990). One thus finds that the μ-averaged mean and variance are

$$\mathrm{E}(n) = (n_0 - C)\langle w \rangle + C, \quad \mathrm{E}(N) = \mathrm{E}(n) + L,$$
$$\mathrm{Var}(n) = \mathrm{E}(n) - n_0\langle w^2 \rangle + (n_0 - C)^2 \left(\langle w^2 \rangle - \langle w \rangle^2\right),$$

where

$$\langle w(t)^j \rangle = \begin{pmatrix} 1 \\ 1 \end{pmatrix}^T \exp\left[-t\begin{pmatrix} j\mu_o + \gamma_- & -\gamma_+ \\ -\gamma_- & \gamma_+ \end{pmatrix}\right]\begin{pmatrix} \Pi_o \\ \Pi_c \end{pmatrix}$$

for $j = 1, 2$. Here Π_l, $l = o, c$, are the stationary probability distributions for the dichotomous noise process of Eq. (3.42):

$$\Pi_o = \frac{\gamma_+}{\gamma_+ + \gamma_-}, \quad \Pi_c = \frac{\gamma_-}{\gamma_+ + \gamma_-}.$$

The averages $\langle w^j \rangle$, $j = 1, 2$, approach zero as time increases, hence the steady-state means and variances are $E_\infty(n) = \text{Var}_\infty(n) = C$. There have been a number of extensions of the stochastic gating model. For example, Bressloff and Earnshaw (2009) have considered the effects of proteins binding to scaffolding proteins within a corral, whereas Reingruber and Holcman (2010) have analyzed the narrow escape problem for a particle that can switch between different conformational states and can only exit a domain in one of these states.

D. Diffusion in confined geometries

Another common form of diffusion within cells is the transport of particles through a narrow biological pore or channel. Examples include membrane transport through ion channels and pumps (Hille, 2001), and the translocation of structured polynucleotides through nanopores (Peskin *et al.*, 1993), which is an important technique for investigating the translocation dynamics of biologically relevant macromolecules (Gerland *et al.*, 2004; Keyser *et al.*, 2006). In such examples, changes in the motion of a particle occur mainly in the axial direction along the channel, whereas local equilibrium is rapidly reached in the transverse directions. Thus transport is quasi one–dimensional and the effects of the boundaries of the channel can be incorporated by introducing an entropic barrier into the dynamics of a Brownian particle, leading to the so–called Fick–Jacobs equation (Burada *et al.*, 2009, 2007; Jacobs, 1967; Kalinay and Percus, 2006; Reguera and Rubi, 2001; Rubi and Reguera, 2010; Zwanzig, 1992). Typically a 3D narrow channel is represented by a cylinder that extends axially in the x–direction and has a periodically varying cross section that is rotationally symmetric about the x-axis, see Fig. 9(a). Denoting the space–dependent radius by $w(x)$, the cross-section varies as $A(x) = \pi w(x)^2$. In the case of a corresponding 2D channel, $w(x)$ represents the half–width of the channel. An extreme version of confined diffusion along a channel is single–file diffusion, in which the channel is so narrow that particles cannot pass each other. In other words, the longtitudinal motion of each particle is hindered by the presence of its neighbors, which act as moving obstacles, see Fig. 9(b). Hence, interparticle interactions can suppress Brownian motion and lead to subdiffusive behavior (Barkai and Silbey, 2009; Jepsen, 1965; Levitt, 1973; Percus, 1974; Rodenbeck *et al.*, 1998; Taloni and Marchesoni, 2006).

1. Fick-Jacobs equation

We begin by deriving the Fick-Jacobs equation for a Brownian particle diffusing in a 2D channel as shown in Fig. 9(a). We follow the particular derivation of Zwanzig (1992), see also (Reguera and Rubi, 2001). It is assumed that the channel walls at $y = \pm w(x)$ confine the motion of the particle but do not exchange energy with it. Thus the probability flux normal to the boundary is zero. This condition can be imposed by introducing a confining potential $U(x, y)$ such that $U(x, y) = 0$ for $|y| < w(x)$ and $U(x, y) = \infty$ for $|y| \geq w(x)$. Let $p(x, y, t)$ denote the probability that the particle is located at position $\mathbf{x} = (x, y)$ at time t with periodic boundary conditions in the longtitudinal direction, $p(x + L, y, t) = p(x, y, t)$. For a general potential $U(x, y)$, the 2D FP equation takes the form

$$\frac{\partial p}{\partial t} = -\frac{1}{\gamma} \left[\frac{\partial [F_x p]}{\partial x} + \frac{\partial [F_y p]}{\partial y} \right] + D_0 \left[\frac{\partial^2 p}{\partial x^2} + \frac{\partial^2 p}{\partial y^2} \right],$$

where $F_x = -\partial_x U, F_y = -\partial_y U$. Using the Einstein relations $D_0 \gamma = k_B T = \beta^{-1}$, the FP equation can be rewritten as

$$\frac{\partial p}{\partial t} = D_0 \frac{\partial}{\partial x} e^{-\beta U(x,y)} \frac{\partial}{\partial x} e^{\beta U(x,y)} p(x, y, t)$$
$$+ D_0 \frac{\partial}{\partial y} e^{-\beta U(x,y)} \frac{\partial}{\partial y} e^{\beta U(x,y)} p(x, y, t). \quad (3.47)$$

In order to reduce to a 1D equation, first integrate both sides of the FP equation with respect to the transverse coordinate y:

$$\frac{\partial P(x,t)}{\partial t} = D_0 \frac{\partial}{\partial x} \int_{-w(x)}^{w(x)} e^{-\beta U(x,y)} \frac{\partial}{\partial x} e^{\beta U(x,y)} p(x, y, t) dy,$$

where $P(x, t)$ is the reduced probability density

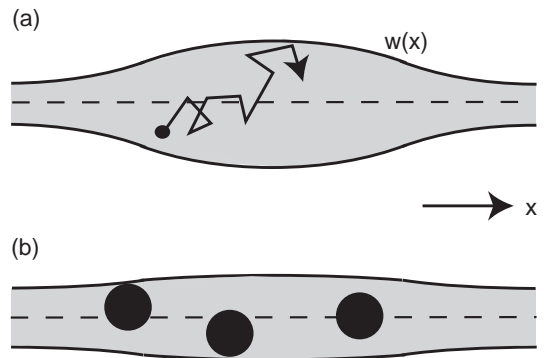$$P(x, t) = \int_{-w(x)}^{w(x)} p(x, y, t) dy. \quad (3.48)$$

(a)

(b)

FIG. 9 Confined diffusion in a narrow cylindrical channel with a periodically modulated boundary $w(x)$ in the axial direction. (a) Small diffusing particle. (b) Single-file diffusion.

The major step in the reduction is to assume that the probability density reaches equilibrium in the transverse direction. That is, $p(x, y, t)$ is assumed to factorize as follows:

$$p(x, y, t) \approx P(x, t)\rho(x, y), \qquad (3.49)$$

where $\rho(x, y)$ is a normalized Boltzmann-Gibbs probability density:

$$\rho(x, y) = \frac{e^{-\beta U(x,y)}}{A_0 e^{-\beta \mathcal{F}(x)}}, \quad e^{-\beta \mathcal{F}(x)} = \frac{1}{A_0} \int_{-w(x)}^{w(x)} e^{-\beta U(x,y)} dy, \qquad (3.50)$$

where $A_0 = 2 \int_0^L w(x) dx$ and $\mathcal{F}(x)$ interpreted as an effective x–dependent free energy. Under this factorization the averaged FP equation becomes

$$\frac{\partial P(x, t)}{\partial t} \approx D_0 \frac{\partial}{\partial x} e^{-\beta \mathcal{F}(x)} \frac{\partial}{\partial x} e^{\beta \mathcal{F}(x)} P(x, t). \qquad (3.51)$$

This holds for a general potential energy function $U(x, y)$ (Reguera and Rubi, 2001).

If U is now taken to be the confining potential of the channel boundary, then $e^{-\beta \mathcal{F}(x)} = 2w(x)/A_0 \equiv \sigma(x)$ and we obtain the Fick–Jacobs equation

$$\frac{\partial P(x, t)}{\partial t} = \frac{\partial}{\partial x} D_0 \sigma(x) \frac{\partial}{\partial x} \frac{P(x, t)}{\sigma(x)}. \qquad (3.52)$$

The same equation is obtained in 3D with $\sigma(x) = A(x)/A_0$ with $A(x) = \pi w(x)^2$ and A_0 the mean cross-sectional area. The Fick–Jacobs equation is valid provided that $|w'(x)| \ll 1$. However, it has been shown that the introduction of an x–dependent diffusion coefficient into the Fick-Jacobs equation can considerably increase the accuracy of the reduced FP equation and thus extend the domain of validity (Kalinay and Percus, 2006; Reguera and Rubi, 2001; Zwanzig, 1992):

$$D(x) = \frac{D_0}{[1 + w'(x)^2]^\alpha}, \qquad (3.53)$$

with $\alpha = 1/3, 1/2$ for 2D and 3D respectively. Note that in the absence of any external forces, the effective free energy $\mathcal{F}(x) = \mathcal{V}(x)$, where $\mathcal{V}(x) \equiv -k_B T \log[A(x)/A_0]$ reflects the existence of an entropic barrier to diffusion (Reguera and Rubi, 2001). That is, using the standard thermodynamic definition of free energy $\mathcal{F} = E - TS$, where E is internal energy and S is the entropy, it follows that $S(x) \sim \log A(x)$ where $A(x)$ is the cross-sectional area of the channel at x. This is consistent with the microcanonical ensemble definition of entropy. That is, in equilibrium there is a uniform probability density ρ_0 in the channel, so that the equilibrium x–dependent density $P_{eq}(x) = \rho_0 A(x)/A_0$ and the number of microstates available to a diffusing particle at location x is proportional to the area of the channel. It also follow that when there is a constant external force F_0 in

the x direction, then Eq. (3.51) still holds except that $\mathcal{F}(x) = -F_0 x - k_B T \log \sigma(x)$.

Given an external force F_0 and the periodic entropic barrier potential $\mathcal{V}(x)$, it remains to determine the mean and variance of the particle position in the long time limit, which naturally leads to the following definitions of the drift mobility and diffusion coefficient of the particle:

$$\mu(F_0) \equiv \frac{\langle \dot{X} \rangle}{F_0}, \quad \langle \dot{X} \rangle = \lim_{t \to \infty} \frac{\langle X(t) \rangle}{t}, \qquad (3.54)$$

and

$$D(F_0) = \lim_{t \to \infty} \frac{\langle X(t)^2 \rangle - \langle X(t) \rangle^2}{2t}. \qquad (3.55)$$

Note that the relationship between $\langle \dot{X} \rangle$ and the long time limit of $\langle X(t) \rangle/t$ is a consequence of ergodicity (Reimann, 2002). In order to determine μ and D, it is necessary to extend the classical problem of Brownian motion in a periodic potential with tilt (Burada *et al.*, 2007; Hanggi *et al.*, 1990; Reimann *et al.*, 2002; Stratonovich, 1958), see also III.D.2. The force–dependence of the mobility and diffusion coefficient have been studied both analytically and numerically in the case of a sinusoidal boundary function (Burada *et al.*, 2007; Reguera *et al.*, 2006)

$$w(x) = a[\sin(2\pi x/L) + b], \quad a > 0, b > 1. \qquad (3.56)$$

The basic results are sketched in Fig. 10. A number of interesting observations emerge from this study. First, the mobility only depends on the temperature via the dimensionless parameter $F_0 L/k_B T$. Hence, increasing the temperature reduces the mobility. Second, as the force is increased the effective diffusion coefficient $D(F_0)$ exceeds the free diffusion coefficient D_0. Using scaling arguments, it can also be shown that the analysis based on the Fick-Jacobs equation begins to break down at a critical force $F_{0,c}$ where (Burada *et al.*, 2009)

$$\frac{F_{0,c} L}{k_B T} \approx \frac{1}{2(1 + b)^2} \left(\frac{L}{a} \right)^2. \qquad (3.57)$$

The Fick-Jacobs equation represents diffusion through a narrow channel in terms of a 1D overdamped Brownian particle moving in an effective potential $U(x)$ that arises from entropic effects. Such a 1D model has also been the starting point for a series of studies of channel-facilitated membrane transport, where now $U(x)$ reflects the constructive role of attractive interactions between permeating particles and proteins forming the channel pore (Berezhkovskii and Bezrukov, 2005; Berezhkovskii *et al.*, 2003, 2002; Bezrukov *et al.*, 2000). In these studies, mixed boundary conditions are assumed at the ends $x = 0, L$ of the channel: $J(0, t) = -\kappa_0 P(0, t)$ and $J(L, t) = -\kappa_L P(L, t)$. The probability of crossing the channel and the mean time in the channel can then be calculated using the standard theory of first passage times
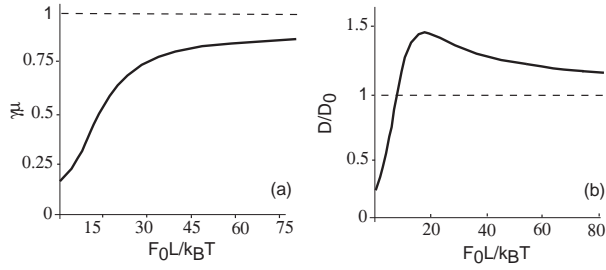
FIG. 10 Illustrative sketches of how mobility and diffusivity vary with non-dimensionalized applied force $F_0 L/k_B T$ in the case of a 2D channel with a sinusoidally varying half-width (3.56). (a) Effective mobility μ in units of γ. In the limit $F_0 \to \infty$, $\mu \to \gamma^{-1}$. (b) Diffusion coefficient D in units of free diffusivity D_0. In the limit $F_0 \to \infty$, $D \to D_0$. Sketches are based on numerical results of (Reguera *et al.*, 2006) for $a = L/2\pi$ and $b = 1.02$.

and splitting probabilities, see Sec. II.B. It can be shown that there is an optimal form of the interaction potential that maximizes the flux through the channel, and involves a play off between increasing the translocation probability through the channel and decreasing the average time particles spend in the channel (Berezhkovskii and Bezrukov, 2005). For a complementary approach to studying channel-facilitated transport that is based on spatially discrete stochastic site-binding models, see (Chou, 1998; Kolomeisky, 2007). Finally, note that stochastic models of confined diffusion through channels have also been developed for charged particles flowing through a nanopore connected to two large reservoirs of electrolyte solutions (Nadler *et al.*, 2004; Schuss *et al.*, 2001). The motion of the ions is sensitive to the specific nanoscale geometry and the charge distribution around the channel so that standard continuum mean-field models breakdown. Two of the most common mean-field models are the equilibrium Poisson-Boltzmann equation and the non-equilibrium Poisson-Nernst-Planck equation (Roux *et al.*, 2004). These equations assume a constitutive relation between the average ion flux and an effective mean field potential that satisfies Poisson's equation for the average charge concentrations. We will not consider ion transport further in this review. See for example Keener and Sneyd (2009) for a detailed discussion of the role of ion transport in cell physiology.

2. Brownian motion in a periodic potential with tilt

Motivated by the problem of a particle diffusing in a narrow channel with a periodically varying boundary, consider the 1D FP equation

$$\frac{\partial p}{\partial t} = D_0 \left[\frac{1}{k_B T} \frac{\partial [V'(x) - F_0]p}{\partial x} + \frac{\partial^2 p}{\partial x^2} \right], \qquad (3.58)$$

where $V(x)$ is an L–periodic potential, $V(x + L) = V(x)$ for all x, and F_0 is a constant external force, see Fig. 11. For the moment, we will take the diffusion coefficient to be constant. Within the context of motion through a narrow channel $V(x)$ can be identified with the entropic potential $\mathcal{V}(x) = -k_B T \log[A(x)/A_0]$. However, there are many other important applications where a periodic potential arises, including Brownian ratchet models of molecular motors (Reimann, 2002), see Sec. IV.A.1. Again we will focus on spatially continuous processes. Note, however, that an alternative approach has been developed in a seminal paper by Derrida (1983), which is concerned with calculating the effective diffusion and velocity of particles on a discrete lattice, and is a spatilly discrete version of the processes considered here. The approach of Derrida has many applications, including motor protein modeling (Kolomeisky and Fisher, 2007).
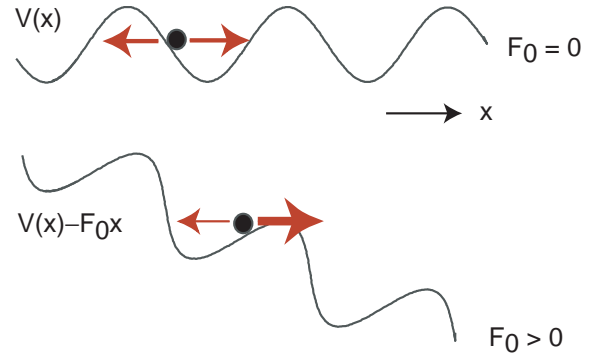

FIG. 11 Brownian particle moving in a periodic potential $V(x)$. In the absence of tilt ($F_0 = 0$) the mean velocity in the long time limit is zero. On the other hand, in the presence of a tilt ($F_0 \neq 0$) the net motion of the particle is in the direction of the force.

We begin by considering the standard Stratonovich-based calculation of the mean velocity (Hanggi *et al.*, 1990; Stratonovich, 1958). Introduce the effective potential or free energy $\mathcal{F}(x) = V(x) - F_0 x$ and note that $\mathcal{F}'(x)$ is periodic even though $\mathcal{F}$ is not. Next consider the reduced probability density and currents

$$\widehat{p}(x,t) = \sum_{n=-\infty}^{\infty} p(x+nL,t), \quad \widehat{J}(x,t) = \sum_{n=-\infty}^{\infty} J(x+nL,t) \tag{3.59}$$

with

$$J(x,t) = -D_0 \left[\frac{1}{k_B T} \mathcal{F}'(x)p + \frac{\partial p}{\partial x} \right].$$

It immediately follows that

$$\widehat{p}(x + L, t) = \widehat{p}(x,t), \quad \int_0^L \widehat{p}(x,t)dx = 1. \tag{3.60}$$

Moreover, multiplying both sides of the FP equation by x and integrating with respect to x gives

$$\frac{d\langle X(t)\rangle}{dt} = \int_{-\infty}^{\infty} J(x,t)dx = \int_0^L \widehat{J}(x,t)dx. \qquad (3.61)$$

(Using the identity $J(x,t) = \langle \dot{X}(t)\delta(x - X(t))\rangle$ and integrating both sides with respect to x, it follows that $\langle \dot{X}(t)\rangle = d\langle X(t)\rangle/dt$ (Reimann, 2002)). The periodicity of $\mathcal{F}'(x)$ implies that if $p(x,t)$ is a solution of the FP equation, then so is $p(x + nL, t)$. The principle of superposition for a linear PDE then shows that $\widehat{p}$ satisfies the FP equation

$$\frac{\partial \widehat{p}(x,t)}{\partial t} + \frac{\partial \widehat{J}(x,t)}{\partial x} = 0, \qquad (3.62)$$

with

$$\widehat{J}(x,t) = -D_0 \left[\frac{1}{k_B T}\mathcal{F}'(x)\widehat{p} + \frac{\partial \widehat{p}}{\partial x} \right] \qquad (3.63)$$

and periodic boundary conditions at $x = 0, L$. There exists a stationary solution $\widehat{p}_0$ of the reduced FP equation with constant flux $\widehat{J}_0$ such that

$$\frac{d}{dx}\left(e^{\mathcal{F}(x)/k_B T}\widehat{p}_0(x) \right) = -\frac{\widehat{J}_0}{D_0}e^{\mathcal{F}(x)/k_B T}. \qquad (3.64)$$

Integrating this equation from x to $x + L$ and using periodicity yields the stationary solution

$$\widehat{p}_0(x) = \frac{\widehat{J}_0 \mathcal{N}(x)}{\left[1 - e^{-F_0 L/k_B T} \right]}, \qquad (3.65)$$

where

$$\mathcal{N}(x) = \frac{1}{D_0}e^{-\mathcal{F}(x)/k_B T}\int_x^{x+L} e^{\mathcal{F}(y)/k_B T}dy. \qquad (3.66)$$

Finally, $\widehat{J}_0$ is determined by imposing the normalization condition on $\widehat{p}_0$. Since $\langle \dot{X}(t)\rangle = L\widehat{J}_0$ for constant current,

$$\langle \dot{X}(t)\rangle = L\frac{1 - e^{-F_0 L/k_B T}}{\int_0^L \mathcal{N}(x)dx}. \qquad (3.67)$$

It can be seen that there is no net motion in a purely periodic potential, since the numerator vanishes when $F_0 = 0$. Moreover the net direction of motion for $F_0 \neq 0$ is in the direction of the applied force. Note that in the case of a space–dependent diffusion coefficient $D(x)$, the above analysis is easily extended with $\mathcal{N}(x)$ now given by (Burada et al., 2007)

$$\mathcal{N}(x) = e^{-\mathcal{F}(x)/k_B T}\int_x^{x+L} \frac{1}{D(y)}e^{\mathcal{F}(y)/k_B T}dy. \qquad (3.68)$$

The calculation of the diffusion coefficient is considerably more involved. However, an elegant method for determing D (as well as the mobility μ) is to exploit a well-known recursion relation for the moments of the first passage time (Burada et al., 2007; Reguera et al., 2006; Reimann et al., 2002). Let $T(x_0 \to b)$ denote the first passage time for the diffusing particle to reach the point b given that it started at x_0 with $x_0 < b$. The nth moment of the first passage time is $\tau_n(x_0 \to b) = \langle T^n(x_0 \to b)\rangle$. It can then be shown that for the stochastic process described by the FP Eq. (3.58), the moments satisfy the recursion relation (Hanggi et al., 1990)

$$\tau_n(x_0 \to b) = \frac{n}{D_0}\int_{x_0}^b dx\, e^{\mathcal{F}(x)/k_B T}\int_{-\infty}^x dy\, e^{\mathcal{F}(y)/k_B T}$$
$$\times \tau_{n-1}(y \to b), \quad n = 1, 2\ldots, \qquad (3.69)$$

with $\tau_0(y \to b) = 1$. Note for $n = 1$, $x_0 = y$, $b = L$ we recover Eq. (2.30) (after taking the left hand boundary to $-\infty$). The basic derivation proceeds as follows. First, it can be shown that $T(x_0 \to x_0 + lL)$, integer l is statistically equivalent to a sum of (iid) random variables $T(x_0 \to x_0 + L), T(x_0 + L \to x_0 + 2L), \ldots, T(x_0 + (l - 1)L \to x_0 + lL)$. Hence, for large l, the central limit theorem (Gardiner, 2009) implies that the FPT $T(x_0 \to x_0 + lL)$ approaches a Gaussian distribution with mean $l\tau_1(x_0 \to x_0 + L)$ and variance $l\Delta\tau_2(x_0 \to x_0 + L)$ where $\Delta\tau_2 = \tau_2 - \tau_1^2$. Second, since μ and D are defined in the large t limit, the evaluation of $\langle x(t)\rangle$ and $\langle x^2(t)\rangle$ can be partitioned into a set of large but finite steps over which the statistics of the corresponding FPT is well approximated by a Gaussian distribution. This has the important implication that if any two stochastic processes described by an FP equation of the form (3.58) have the same mean $\tau_1(x_0 \to x_0 + L)$ and variance $\Delta\tau_2(x_0 \to x_0 + L)$, then they have the same $\langle \dot{X}\rangle$ and D. It finally follows that (Reimann et al., 2002)

$$\langle \dot{X}\rangle = \frac{L}{\tau_1(x_0 \to x_0 + L)}, \quad D = \frac{L^2}{2}\frac{\Delta\tau_2(x_0 \to x_0 + L)}{[\tau_1(x_0 \to x_0 + L)]^3}.$$

The proof of the last step simply consists of verifying that these formulae hold when $V(x) = 0$ (no periodic potential), for which $\langle \dot{X}\rangle = F/\gamma$ and $D = k_B T/\gamma$. Having obtained D in terms of the first and second order moments of the FPT, Eq. (3.69) can now be used to calculate D. After some algebra (see appendix A of (Reimann et al., 2002)), one finds that

$$D = D_0 \frac{\int_{x_0}^{x_0+L} \mathcal{N}(x)^2 \overline{\mathcal{N}}(x)dx/L}{\left[\int_{x_0}^{x_0+L} \mathcal{N}(x)dx/L \right]^3}, \qquad (3.70)$$

with $\mathcal{N}(x)$ given by Eq. (3.66) and

$$\overline{\mathcal{N}}(x) = \frac{1}{D_0}e^{\mathcal{F}(x)/k_B T}\int_{x-L}^x e^{-\mathcal{F}(y)/k_B T}dy. \qquad (3.71)$$

3. Single-file diffusion

When a pore or channel becomes sufficiently narrow, particles are no longer able to pass each other, which imposes strong constraints on the diffusive motion. An idealized model of single–file diffusion considers a 1D collection of diffusing particles with hard-core repulsion. The many–body problem of single–file diffusion was originally tackled by relating the dynamics of the interacting system with the effective motion of a free particle (Harris, 1965; Jepsen, 1965; Lebowitz and Percus, 1967; Levitt, 1973; Percus, 1974). In particular, in the case of an infinite system and a uniform initial particle density, it was shown that a tagged particle exhibits anomalous subdiffusion on long time scales, $\langle X^2(t)\rangle \sim t^{1/2}$. (On the other hand, the center of mass of the system of particles exhibits normal diffusion). More recently, a variety of complementary approaches to analyzing single-file diffusion have been developed (Barkai and Silbey, 2009; Centres and Bustingorry, 2010; Lizana and Ambjornsson, 2008; Rodenbeck *et al.*, 1998; Taloni and Lomholt, 2008). Here we review the particular formulation of Barkai and Silbey (Barkai and Silbey, 2009), which develops the analysis of a tagged particle in terms of classical reflection and transmission coefficients.
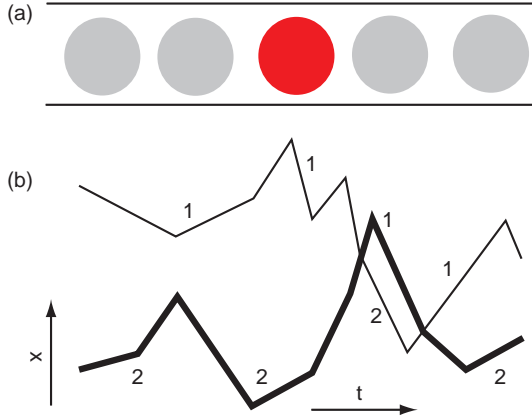

FIG. 12 (a) Single-file diffusion of a tagged particle (red) surrounded by other impenetrable particles. (b) Equivalent noninteracting picture, in which each trajectory is treated as a non-interacting Brownian particle by keeping track of the exchange of particle label.

Suppose that the tagged particle is initially at the origin with N particles to its left and N particles to its right, see Fig. 12(a). The motion of each particle in the absence of hard core interactions is taken to be overdamped Brownian motion as described by the Langevin Eq. (2.9) or the corresponding FP Eq. (2.15). As a further simplification, the potential energy function $V(x) = \int^x F(x')dx'$ is taken to be symmetric, $V(x) = V(-x)$, as is the initial distribution of particles. That is, if the initial position x_0 of a particle is drawn from $f_R(x_0)$ for $x_0 > 0$ and from $f_L(x_0)$ for $x_0 < 0$, then $f_R(x_0) = f_L(-x_0)$. This reflection symmetry ensures that $\langle X(t)\rangle = 0$, where $X(t)$ is the stochastic position of the tagged particle at time t. The main underlying idea is to map the many-body problem to a non-interacting one by allowing particles to pass through each other and keeping track of the particle label, see Fig. 12(b). That is, assuming that collisions are elastic and neglecting n-body interactions for $n > 2$, it follows that when two particles collide they exchange momenta and this is represented as an exchange of particle labels. The probability density for the tagged particle to be at $X(t) = X_T$ at time t then reduces to the problem of finding the probability that the number of free particle trajectories that started at $x_0 < 0$ and are now to the right of X_T is balanced by the number of free particle trajectories that started at $x_0 > 0$ and are now to the left of X_T.

Thus, let $P_{LL}(x_0^{-j})$ $(P_{LR}(x_0^{-j}))$ denote the probability that the jth free particle trajectory starting from $x_0^{-j} < 0$ at $t = 0$ is to the left (right) of X_T at time t. Similarly, let $P_{RR}(x_0^j)$ $(P_{RL}(x_0^j))$ denote the probability that the jth free particle trajectory starting from $x_0^j > 0$ at $t = 0$ is to the right (left) of X_T at time t. Let α be the net number of free particle trajectories that are on the opposite side of X_T at time t compared to their starting point (with left to right taken as positive). The associated probability distribution for α given $2N$ untagged particles is (Barkai and Silbey, 2009)

$$P_N(\alpha) = \frac{1}{2\pi}\int_{-\pi}^{\pi}\prod_{j=1}^{N}\Gamma(\phi, x_0^{-j}, x_0^j)e^{i\alpha\phi}d\phi, \qquad (3.72)$$

where

$$\Gamma(\phi, x_0^{-j}, x_0^j) = e^{i\phi}P_{LR}(x_0^{-j})P_{RR}(x_0^j) + P_{LL}(x_0^{-j})P_{RR}(x_0^j)$$
$$+ P_{LR}(x_0^{-j})P_{RL}(x_0^j) + e^{-i\phi}P_{LL}(x_0^{-j})P_{RL}(x_0^j). \qquad (3.73)$$

The integration with respect to ϕ ensures that the net number of crossings is α, that is, $\int_{-\pi}^{\pi}e^{i\phi n} = \delta_{n,0}$. Since the trajectories are independent and the initial conditions are (iid) random variables, $P_N(\alpha)$ can be averaged with respect to the initial conditions to give

$$\langle P_N(\alpha)\rangle = \frac{1}{2\pi}\int_{-\pi}^{\pi}\langle\Gamma(\phi)\rangle^N e^{i\alpha\phi}d\phi, \qquad (3.74)$$

where

$$\langle\Gamma(\phi)\rangle = \left(\langle P_{RR}\rangle + e^{-i\phi}\langle P_{RL}\rangle\right)\left(\langle P_{LL}\rangle + e^{i\phi}\langle P_{LR}\rangle\right). \qquad (3.75)$$

The averages $\langle P_{LR}\rangle$ etc. can be calculated using the Green's function $G(x, x_0, t)$ of the corresponding FP Eq. (2.15) with $G(x, x_0, 0) = \delta(x - x_0)$. For example,

$$\langle P_{LR}\rangle = \int_{-l}^{0} f_L(x_0)\int_{X_T}^{l} G(x, x_0, t)dx\,dx_0, \qquad (3.76)$$

where $2l$ is the length of the 1D domain, which can be taken to be infinity.

Eq. (3.74) takes the form of the generating function for a discrete random walk of N steps and a net displacement of α. Hence, for large N, application of the central limit theorem leads to the Gaussian approximation

$$P_N(0) \sim \frac{1}{\sqrt{2\pi N \sigma^2}} \exp(-N\mu_1^2/2\sigma^2), \qquad (3.77)$$

where $\sigma^2 = \mu_2 - \mu_1^2$ and μ_1, μ_2 are the first two moments of the structure function:

$$\langle \Gamma(\phi) \rangle = 1 + i\mu_1 \phi - \frac{1}{2}\mu_2 \phi^2 + \mathcal{O}(\phi^3). \qquad (3.78)$$

Hence,

$$\mu_1 = \langle P_{LR} \rangle - \langle P_{RL} \rangle, \ \sigma^2 = \langle P_{RR} \rangle \langle P_{RL} \rangle + \langle P_{LL} \rangle \langle P_{LR} \rangle. \qquad (3.79)$$

Since $\langle X(t) \rangle = 0$ and N is assumed to be large, μ_1 and σ^2 can be Taylor expanded with respect to X_T about $X_T = 0$. Reflection symmetry then implies that

$$\langle P_{LL} \rangle|_{X_T=0} = \langle P_{RR} \rangle|_{X_T=0} \equiv \mathcal{R},$$

$$\langle P_{LR} \rangle|_{X_T=0} = \langle P_{RL} \rangle|_{X_T=0} \equiv \mathcal{T} = 1 - \mathcal{R},$$

$$\partial_{X_T} \langle P_{LR} \rangle|_{X_T=0} = -\partial_{X_T} \langle P_{RL} \rangle|_{X_T=0} \equiv \mathcal{J}.$$

The time–dependent functions $\mathcal{R}$ and $\mathcal{T}$ may be interpreted as reflection and transmission coefficients determining whether or not a free particle trajectory crosses $X_T = 0$. The resulting mean and variance are

$$\mu_1 = -2\mathcal{J} X_T + \mathcal{O}(X_T^2), \quad \sigma^2 = 2\mathcal{R}(1 - \mathcal{R}) + \mathcal{O}(X_T). \qquad (3.80)$$

Thus, $\langle P_N(\alpha) \rangle$ for $\alpha = 0$ reduces to a Gaussian distribution for the position $X(t) = X_T$:

$$P(X_T, t) = \frac{1}{\sqrt{2\pi \langle X(t)^2 \rangle}} \exp\left[-\frac{X_T^2}{2\langle X(t)^2 \rangle} \right], \qquad (3.81)$$

with

$$\langle X(t)^2 \rangle = \frac{\mathcal{R}(1 - \mathcal{R})}{2N\mathcal{J}^2}. \qquad (3.82)$$

Finally, using Eq. (3.76),

$$\mathcal{R} = \int_0^l f(x_0) \int_0^l G(x, x_0, t) dx dx_0 \qquad (3.83)$$

$$\mathcal{J} = \int_0^l f(x_0) G(0, x_0, t) dx_0. \qquad (3.84)$$

In the special case of zero external forces, the free particle Green's function is

$$G(x, x_0, t) = \frac{1}{\sqrt{4\pi Dt}} e^{-(x-x_0)^2/4Dt}. \qquad (3.85)$$

Taking a uniform initial distribution $f(x_0) = 1/l$ with $l \to \infty$ and fixed particle density $\rho = N/l$, one finds anomalous subdiffusion for large times t (Harris, 1965):

$$\langle X(t)^2 \rangle \sim \frac{2}{\sqrt{\pi}} \frac{\sqrt{Dt}}{\rho}. \qquad (3.86)$$

On the other hand, for particles initially centered at the origin, $f(x_0) = \delta(x_0)$, diffusion is normal

$$\langle X(t)^2 \rangle \sim \frac{\pi Dt}{2N}. \qquad (3.87)$$

In the case of a bounded domain or a Gaussian initial condition, anomalous diffusion occurs at intermediate times only (Barkai and Silbey, 2009).

E. Nuclear transport

The nucleus of eukaryotes is surrounded by a protective nuclear envelope (NE) within which are embedded nuclear pore complexes (NPCs). The NPCs are the sole mediators of exchange between the nucleus and cytoplasm. In general small molecules of diameter $\sim 5nm$ can diffuse through the NPCs unhindered, whereas larger molecules up to around $40nm$ in diameter are excluded unless they are bound to a family of soluble protein receptors known as karyopherins (kaps), see the reviews (Fahrenkrog et al., 2004; Macara, 2001; Rout et al., 2003; Tran and Wente, 2006). Within the cytoplasm kap receptors bind cargo to be imported via a nuclear localization signal (NLS) that results in the formation of a kap-cargo complex. This complex can then pass through an NPC to enter the nucleus. A small enzyme RanGTP then binds to the kap, causing a conformational change that releases the cargo. The sequence of events underlying the import of cargo is shown in Fig. 13(a). In the case of cargo export from the nucleus, kaps bind to cargo with a nuclear export signal (NES) in the presence of RanGTP, and the resulting complex passes through the NPC. Once in the cytoplasm, RanGTP undergoes hydrolysis to form RanGDP, resulting in the release of the cargo. The export process is illustrated in Fig. 13(b). Finally, RanGDP is recycled to the nucleus by another molecule NFT2 and is reloaded with GTP to begin another import/export cycle. This cycle allows a single NPC to support a very high rate of transport on the order of 1000 translocations/sec (Ribbeck and Gorlich, 2001). Since the transportation cycle is directional and accumulates cargo against a concentration gradient, an energy source combined with a directional cue is required. Both of these are provided by the hydrolysis of RanGTP and the maintenance of a concentration gradient of RanGTP across the NPC. The RanGTP gradient is continuously regenerated by GTP hydrolysis in the cytoplasm, translocation of RanGTD into the nucleus by NFT2, and replacement of GDP by GTP in the nucleus. It is important to note that the energy generated

from RanGTP hydrolysis is ultimately used to create a concentration gradient of kap-cargo complexes between the nucleus and cytoplasm, so that the actual translocation across the NPC occurs purely via diffusion.
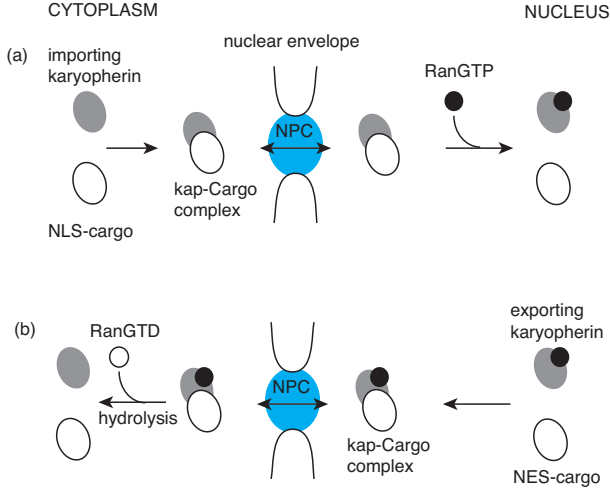

FIG. 13 Schematic illustration of the (a) import and (b) export process underlying the karyopherin-mediated transportation of cargo between the nucleus and cytoplasm via a nuclear pore complex (NPC). See text for details.

Although the above basic picture is now reasonably well accepted, the detailed mechanism underlying facilitated diffusion of kap-cargo complexes within the NPC is still not understood. The NPC is composed of about 30 distinct proteins known collectively as nucleoporins (nups). It has emerged in recent years that individual nups are directly related to a number of human diseases including influenza and cancers such as leukemia (Cronshaw and Matunis, 2004), as well as playing an important role in viral infections by providing docking sites for viral capsids (Whittaker *et al.*, 2000). Associated with many of the nups are natively unfolded phenylalanine-glycine (FG) repeats, known collectively as FG-repeats. The FG-repeats set up a barrier to diffusion for large molecules so that the key ingredient in facilitated diffusion through the NPC is the interaction between kap receptors with the FG-repeats. In essence, the major difference between the various theoretical models of NPC transport concerns the built in assumptions regarding the properties and spatial arrangements of FG-repeats within the NPC, and the nature of interactions with kaps during translocation through the NPC (Becskei and Mattaj, 2005). Current models include the Entropic Gate model (Rout *et al.*, 2003; Zilman *et al.*, 2007), Selective Phase models (Bickel and Bruinsma, 2002; Kustanovich and Rabin, 2004; Ribbeck and Gorlich, 2001, 2002), Dimensionality Reduction model (Peters, 2005), and the Polymeric Brush model (Lim *et al.*, 2007, 2006). A number of computational models and molecular-based simulations are also being developed (Grunwald and Singer,

2011; Moussavi-Baygi *et al.*, 2011). Here we will review the first two types of model in a little more detail.

Entropic gate model. Recall from Sec. III.D that a macromolecule diffusing in a confined geometry (such as a nuclear pore) experiences an entropic barrier due to excluded volume effects. Within the NPC this would be enhanced by the densely packed FG-repeats. One way to counteract the effects of the entropic barrier is for the kaps to have an affinity for and bind to the FG-repeat regions (Rout *et al.*, 2003; Zilman *et al.*, 2007), thus lowering the effective Gibbs free energy of the cargo-complex within the NPC. The degree of affinity has to be sufficiently high to overcome the entropic barrier but not too high otherwise the complex can be trapped within the NPC and the rate of translocation would be too small. One possible solution, is to have a large number of low–affinity binding sites within the nuclear pore. Recently, a mathematical model for the effects of binding on diffusion within the NPC has been developed by Zilman *et al.* (2007), based on diffusion through an effective energy landscape. This is based on the assumption that the binding/unbinding rates are relatively fast compared to the diffusion rate. The simplest version of the model is illustrated in Fig. 14 for the case of nuclear import. The effective potential energy $U(X)$ is taken to be a flat potential well of depth E along an NPC, and zero outside the NPC. Absorbing boundary conditions are placed at the points $x = 0, L$ a distance R from either side of the NPC, which has length $L - 2R$. The left-hand boundary takes into account the fact that not all complexes entering the NPC will reach the nucleus, that is, some will eventually return to the cytoplasm. Diffusion within the NPC is described by a standard Smoluchowski equation for the density of cargo-complexes $\rho(x)$, $x = [0, L]$, see Sec. II.A.2:

$$\frac{\partial \rho}{\partial t} = -\frac{\partial J}{\partial x}, \; J = -D\frac{\partial \rho}{\partial x} - D\rho\frac{\partial U}{\partial x}, \qquad (3.88)$$

with U measured in units of $k_B T$. This equation is supplemented by the boundary conditions $\rho(0) = \rho(L) = 0$.
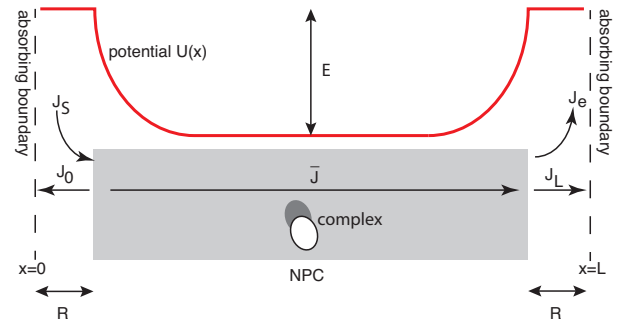

FIG. 14 Model of Zilman *et al.* (2007). Transport of cargo-complex through the NPC is modeled as diffusion in an energy landscape. See text for details.

The steady-state solution is obtained by assuming that there are constant fluxes J_0 in $[0, R]$, J_L in $[L-R, L]$ and $\overline{J}$ in $[R, L-R]$ with $J_0 < 0$. These fluxes are related according to $J_S = \overline{J} - |J_0|$ and $\overline{J} = J_L + J_e$, where J_S is the total flux of complexes injected into the NPC from the cytoplasm, which is proportional to density of complexes in the cytoplasm, and J_e denotes the flux due to active removal of complexes from the nucleus end of the NPC by RanGTP. The latter depends on the number of complexes at the nuclear exit, the rate J_{ran} at which RanGTP molecules hit the exit: $J_e = J_{\mathrm{ran}}\rho(L-R)R$. The steady-state rate of transport $\overline{J}$ can now be determined by solving for $\rho(x)$ in terms of $J_0, J_L, \overline{J}$ in each of the three domains and imposing continuity of the density at $x = R$ and $x = R - L$. The result is that the fraction of complexes reaching the nucleus is given by (Zilman *et al.*, 2007)

$$P = \frac{\overline{J}}{J_S} = \left[2 - \frac{K}{1+K} + \frac{1}{R}\int_R^{L-R} e^{U(x)}dx\right]^{-1}, \quad (3.89)$$

with $K = J_{\mathrm{ran}}R^2/D$. It follows that for a sufficiently deep well (large E), where the integral term is negligible, and for sufficiently large K (large J_{ran}), the probability of translocation is $P \approx 1$. On the other hand, if K is small so that RanGTP does not facilitate entry of complexes into the nucleus then $P_{\max} = 0.5$. As previously indicated, it is not possible to arbitrarily increase the affinity of binding sites and thus the well depth E, since this will lead to trapping of the complexes so that they accumulate within the NPC, resulting in molecular crowding and an unrealistically long time for an individual molecule to pass through the NPC. Thus there is some optimal well depth that balances an increase of transport probability P with increased time spent in the NPC (Zilman *et al.*, 2007). Finally, note that the model is robust with regards the particular shape of the potential well. For example, one could represent transport through the NPC as diffusion in an array of overlapping potential wells that represent flexible FG-repeat regions. The shape of each well will depend on the number and affinity of binding sites on each FG-repeat, and the degree of flexibility of the polymers which will determine the entropic costs of bending and stretching the FG-repeats. It can be shown that for relatively fast binding/unbinding, the multi-well potential can be replaced by a single well along the lines of Fig. 14.

Selective phase models. The basic assumption of these models is that the NPC can be treated as a channel filled with a hydrophobic medium consisting of a concentrated polymer solution; the latter is composed of the natively unfolded, flexible protein domains of FG-repeats (Bickel and Bruinsma, 2002; Kustanovich and Rabin, 2004; Reichenbach *et al.*, 2006; Ribbeck and Gorlich, 2001, 2002). The FG-repeats form weak bonds with each other sug-

gesting that they act approximately like a weak reversible gel. Particles smaller than the mesh size of the network can diffuse freely through the NPC, whereas non-selective macromolecules larger than the mesh size cannot. On the other hand, kap-cargo complexes can 'dissolve' in the gel due to the presence of hydrophobic domains on the surface of the kap receptors, and then diffuse through the pore by breaking the weak bonds of the reversible gel (Ribbeck and Gorlich, 2001, 2002). However, as pointed out by Bickel and Bruinsma (2002), the observed high permeability of the NPC with respect to the transport of kap-cargo complexes is inconsistent with the basic theory of reversible gels. The argument proceeds as follows (see appendix of Bickel and Bruinsma (2002)). For a homogeneous pore filled with reversible gel, the flux of particles through the pore is given by $J = D\Delta\phi/L$, where L is the length of the pore, D is the diffusivity of dissolved complexes, and $\Delta\phi = \phi_L - \phi_R$ is the difference in concentrations of dissolved complexes at the ends of the pore. The permeability Π, however, is defined in terms of the difference in concentrations of exterior particle reservoirs on either side of the pore, $\Delta c = c_L - c_R$. That is, $J = \Pi\Delta c$. In order to relate Δc and $\Delta\phi$, it is necessary to consider the fluxes entering and exiting the pore. Equating the fluxes at the left and right ends gives

$$J = k_{\mathrm{in}}c_L - k_{\mathrm{out}}\phi_L = k_{\mathrm{out}}\phi_R - k_{\mathrm{in}}c_R \qquad (3.90)$$

This allows one to express $\Delta\phi$ in terms of Δc such that

$$\Pi = \frac{k_{\mathrm{in}}}{2 + k_{\mathrm{out}}L/D}. \qquad (3.91)$$

From detailed balance the ratio of the rates is $k_{\mathrm{in}}/k_{\mathrm{out}} = e^{\beta\Delta F}$ where ΔF is the free energy gain (assuming $\Delta F > 0$) of entering the gel. Ignoring other contributions to the free energy, $\Delta F = n\epsilon$, where n is the number of interactions of strength ϵ between a kap receptor and the gel. It can also be shown that the diffusivity of a spherical kap-cargo complex moving through a reversible gel is

$$D = D_0(1 + e^{-n\epsilon})^{-1} \approx D_0 e^{-\beta n\epsilon}. \qquad (3.92)$$

Suppose that in the high affinity regime k_{out} is given by the Arrhenius law $k_{\mathrm{out}} \sim (D/\delta)e^{-\beta\Delta F}$, where Δ is taken to be the size of the boundary layer at either end of the pore. Combining all of these results then shows that (Bickel and Bruinsma, 2002)

$$\Pi = \frac{D_0}{L + 2\delta e^{\beta n\epsilon}}. \qquad (3.93)$$

Thus the permeability decreases with the number of sites n, implying that increasing the affinity of the complex moving in a reversible gel should decrease the permeability; this contradicts the high permeabilities seen experimentally (Ribbeck and Gorlich, 2002). One suggestion for modifying the original selective phase model is
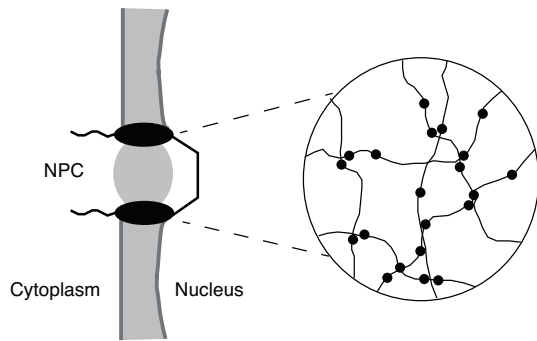
FIG. 15 Selective phase model (Bickel and Bruinsma, 2002; Ribbeck and Gorlich, 2001, 2002), in which the FG repeats within a NPC are treated as a reversible polymer gel. See text for details.

to assume that the polymer gel is under tension due to pinning of the polymers to the container walls (Bickel and Bruinsma, 2002). Thermal fluctuations would then lead to local rearrangements of the stretched polymer network, resulting in rearrangements of the associated tension field. This, in turn, could generate force fluctuations on a dissolved macromolecule that could enhance its effective diffusivity. Such a mechanism has not yet been confirmed experimentally. However, single particle tracking of individual complexes moving through the NPC shows that cargo bound to more kap receptors diffuse more freely (Lowe *et al.*, 2010). This is consistent with the tensile gel model but inconsistent with the entropic gate model, for which greater affinity implies slower transport of individual complexes.

Chaperone–assisted translocation of polymers through nanopores. Finally, note that here and in Sec. IIID we have considered diffusion of particles that are smaller than or comparable in size to the diameter of the channel. However, there are many examples where it is necessary to consider translocation of an unfolded (or partially folded) polymer through a nanopore, including the translocation of RNA through the nuclear pore membrane, as well as newly synthesized proteins into the endoplasmic reticulum (see also Sec. VB). Polymer translocation through a nanopore involves a large entropic barrier due to the loss of many conformational states, so that some form of driving force is required. One suggested driving mechanism involves the binding of chaperone proteins to the translocating polymer on the far side of the nanopore, which prohibits the polymer diffusing backward through the pore, thus speeding up translocation (Matlack *et al.*, 1999). This rectified stochastic motion was orginally analyzed in terms of a Brownian ratchet by Peskin *et al.* (1993), and has subsequently been developed in a number of studies (Ambjornsson and Metzler, 2004; D'Orsogna *et al.*, 2007; Elston, 2000b; Krapivsky and Mallick, 2010).

IV. ACTIVE INTRACELLULAR TRANSPORT

A. Modeling molecular motors at different scales

Diffusion inside the cytosol or along the plasma membrane of a cell is a means by which dissolved macromolecules can be passively transported without any input of energy. However, there are two main limitations of passive diffusion as a mechanism for intracellular transport. First, it can take far too long to travel the long distances necessary to reach targets within a cell, which is particularly acute in the case of the axons and dendrites of neurons. Second, diffusive transport tends to be unbiased, making it difficult to sort resources to specific areas within a cell. Active intracellular transport can overcome these difficulties so that movement is both faster and direct specific, but does so at a price. Active transport cannot occur under thermodynamic equilibrium, which means that energy must be consumed by this process, typically via the hydrolysis of adenosine triphosphate (ATP). The main type of active intracellular transport involves the molecular motors kinesin and dynein carrying resources along microtubular filament tracks. Microtubules are polarized polymeric filaments with biophysically distinct $(+)$ and $(-)$ ends, and this polarity determines the preferred direction in which an individual molecular motor moves. In particular, kinesin moves towards the $(+)$ end whereas dynein moves towards the $(-)$ end (Howard, 2001). Each motor protein undergoes a sequence of conformational changes after reacting with one or more ATP molecules, causing it to step forward along the microtubule in its preferred direction. Thus, ATP provides the energy necessary for the molecular motor to do work in the form of pulling its cargo along the microtubule in a biased direction.

The movement of molecular motors and motor/cargo complexes occur over several length and time scales (Julicher *et al.*, 1997; Keller and Bustamante, 2000; Kolomeisky and Fisher, 2007; Lipowsky and Klumpp, 2005). In the case of a single motor there are at least three regimes: (i) the mechanicochemical energy transduction process that generates a single step of the motor; (ii) the effective biased random walk along a filament during a single run; (iii) the alternating periods of directed motion along the filament and diffusive or stationary motion when the motor is unbound from the filament. A popular model for the stochastic dynamics of a single motor step in regime (i) is the so–called Brownian ratchet (Reimann, 2002), which extends the theory of overdamped Brownian motion in periodic potentials that was reviewed in Sec. III.D.2. In the case of dimeric or double–headed kinesin, a single step is of length $8\mu m$ and the total conformational cycle takes around $10 ms$. In the second regime (ii), multiple steps are taken before a motor disassociates from the filament. For example, kinesin takes around 100 steps in a single run, covering

a distance of around $1\mu m$. Walking distances can be substantially increased if several molecular motors pull the cargo. In the third motility regime (iii), molecular motors repeatedly unbind and rebind to filaments. In the unbound state a motor diffuses in the surrounding aqueous solution with a diffusion coefficient of the order $1\mu m^2 s^{-1}$. However, molecular crowding tends to confine the motor so that it stays close to its detachment point. At these longer length and time scales, the motion of the motor can be represented in terms of a system of PDEs. This combines a discrete Markov process for the transitions between bound and unbound states with an FP equation for the advective or diffusive motion in the different states (Newby and Bressloff, 2010b; Reed et al., 1990; Smith and Simmons, 2001). In bidirectional transport, there may be more than one type of bound state.

1. Brownian ratchets

In performing a single step along a filament track, a molecular motor cycles through a sequence of conformational states before returning to its initial state (modulo the change in spatial location). Suppose that there is a total of M conformational states in a single cycle labeled $i = 1, \ldots, M$. Given a particular state i, the motor is modeled as an overdamped, driven Brownian particle moving in a periodic potential $V_i(x)$. The Langevin equation for the location of the particle $X(t)$ assuming that it remains in the given state is

$$\frac{dX}{dt} = -\frac{V_i'(X)}{\gamma}dt + \xi(t), \tag{4.1}$$

with $\langle \xi(t) \rangle = 0$ and $\langle \xi(t)\xi(t') \rangle = 2Dt\delta(t - t')$. The corresponding FP equation is

$$\frac{\partial p_i(x,t)}{\partial t} = -\frac{\partial J_i(x,t)}{\partial x}, \tag{4.2}$$

where $p_i(x,t)$ is the probability density that the motor particle is in internal state i and at location x at time t, and $J_i(x,t)$ is the probability flux

$$J_i(x,t) = \frac{1}{\gamma}\left[-V_i'(x) - k_B T\frac{\partial}{\partial x}\right]p_i(x,t). \tag{4.3}$$

If the state transitions between the conformational states are now introduced according to a discrete Markov process, then it is necessary to add source terms to the FP equation:

$$\frac{\partial p_i(x,t)}{\partial t} = -\frac{\partial J_i(x,t)}{\partial x} \tag{4.4}$$
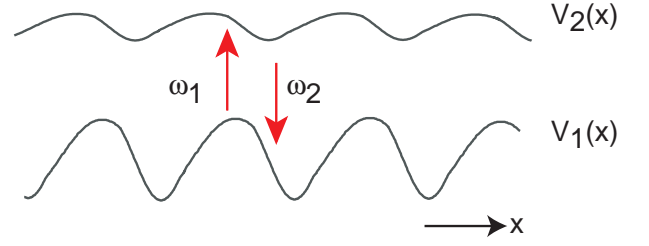$$+ \sum_{j \neq i}\left[\omega_{ij}(x)p_j(x,t) - \omega_{ji}(x)p_i(x,t)\right],$$

FIG. 16 Brownian ratchet model of a molecular motor that can exist in two internal states with associated l–periodic potentials $V_1(x)$ and $V_2(x)$. State transition rates are denoted by ω_1 and ω_2.

where $\omega_{ij}(x)$ is the rate at which the motor switches from state j to state i.

In order to develop the basic theory, consider the simple case of two internal states $N = 2$ following along the lines of Julicher et al. (1997); Parmeggiani et al. (1999); Prost et al. (1994). Then

$$\frac{\partial p_1(x,t)}{\partial t} + \frac{\partial J_1(x,t)}{\partial x} = -\omega_1(x)p_1(x,t) + \omega_2(x)p_2(x,t) \tag{4.5a}$$

$$\frac{\partial p_2(x,t)}{\partial t} + \frac{\partial J_2(x,t)}{\partial x} = \omega_1(x)p_1(x,t) - \omega_2(x)p_2(x,t). \tag{4.5b}$$

Note that adding the pair of equations together and setting $p = p_1 + p_2$, $J = J_1 + J_2$ leads to the conservation equations $\partial_t p + \partial_x J = 0$. An example of l–periodic ratchet (asymmetric) potentials $V_1(x), V_2(x)$ is shown in Fig. 16, with l the basic step length of a cycle along the filament track. The analysis of the two–state model proceeds along similar lines to the one state model considered in Sec. III.D.2. That is, set

$$\widehat{p}_j(x,t) = \sum_{n=-\infty}^{\infty} p_j(x+nl,t), \quad \widehat{J}_j(x,t) = \sum_{n=-\infty}^{\infty} J_j(x+nl,t). \tag{4.6}$$

The total probability flux can then be written as

$$\widehat{J}(x,t) \tag{4.7}$$
$$= -\frac{1}{\gamma}\left[V_1'(x)\widehat{p}_1(x,t) + V_2'(x)\widehat{p}_2(x,t) + k_B T\frac{\partial \widehat{p}(x,t)}{\partial x}\right].$$

Consider the steady-state solution for which there is a constant total flux $\widehat{J}_0$ so that

$$V_1'(x)\widehat{p}_1(x) + V_2'(x)\widehat{p}_2(x) + k_B T\frac{\partial \widehat{p}(x)}{\partial x} = -\widehat{J}_0\gamma.$$

Defining $\lambda(x) = \widehat{p}_1(x)/\widehat{p}(x)$, this equation can be rewritten as

$$V_{\text{eff}}'(x)\widehat{p}(x) + k_B T\frac{\partial \widehat{p}(x)}{\partial x} = -\widehat{J}_0\gamma, \tag{4.8}$$

where

$$V_{\text{eff}}(x) = \int_0^x [\lambda(y)V_1'(y) + (1 - \lambda(y))V_2'(y)]\, dy. \quad (4.9)$$

Suppose that the system is in thermodynamic equilibrium so that detailed balance holds. That is, the state transition rates and steady-state probabilities satisfy
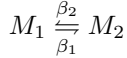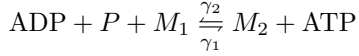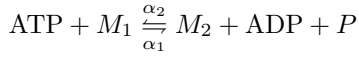
$$\frac{\omega_1(x)}{\omega_2(x)} = e^{[V_1(x) - V_2(x)]/k_B T} = \frac{p_2(x)}{p_1(x)}. \quad (4.10)$$

Therefore,

$$\lambda(x) = \frac{1}{1 + e^{-[V_1(x) - V_2(x)]/k_B T}}, \quad (4.11)$$

and, in particular, $\lambda(x)$ reduces to an l–periodic function. It follows that $V_{\text{eff}}(x)$ in Eq. (4.8) is also an l-periodic potential and hence there is no net motion in a particular direction (in the absence of an external force or tilt), see Sec. III.D.2. In conclusion, in order for a molecular motor to sustain directed motion that can pull against an applied load, we require a net positive supply of chemical energy that maintains the state transition rates away from detailed balance - this is the role played by ATP.

Therefore, consider the situation in which transitions between the two states occur as a result of chemical reactions involving ATP hydrolysis. Denoting the two conformational states of the motor by M_1, M_2, the scheme is taken to be (Parmeggiani *et al.*, 1999)

$$\text{ATP} + M_1 \underset{\alpha_1}{\overset{\alpha_2}{\rightleftharpoons}} M_2 + \text{ADP} + P$$

$$\text{ADP} + P + M_1 \underset{\gamma_1}{\overset{\gamma_2}{\rightleftharpoons}} M_2 + \text{ATP}$$

$$M_1 \underset{\beta_1}{\overset{\beta_2}{\rightleftharpoons}} M_2$$

with $\alpha_j, \gamma_j, \beta_j$ x–dependent. The first reaction pathway involves ATP hydrolysis with chemical free energy gain $\Delta\mu$ and a corresponding transition from state 1 to state 2, the second involves hydrolysis in the opposite direction, while the third involves thermal state transitions without any change in chemical potential. Basic chemical kinetics implies that

$$\frac{\alpha_1}{\alpha_2} = e^{(V_1 - V_2 + \Delta\mu)/k_B T}, \quad \frac{\gamma_1}{\gamma_2} = e^{(V_1 - V_2 - \Delta\mu)/k_B T},$$

$$\frac{\beta_1}{\beta_2} = e^{(V_1 - V_2)/k_B T}. \quad (4.12)$$

It follows that the net transition rates between the two conformational states are

$$\omega_1 = \alpha_2 e^{(V_1 - V_2 + \Delta\mu)/k_B T} + \gamma_2 e^{(V_1 - V_2 - \Delta\mu)/k_B T}$$
$$+ \beta_2 e^{(V_1 - V_2)/k_B T} \quad (4.13)$$
$$\omega_2 = \alpha_2 + \gamma_2 + \beta_2. \quad (4.14)$$

Clearly detailed balance no longer holds. In general, it is now necessary to determine the steady–state solution of the pair of Eqs. (4.5) numerically. Given such a solution, the efficiency of the motor doing work against a load F may be determined as follows. First the flux (4.3) has an additional term of the form $F p_i(x,t)/\gamma$. The mechanical work done per unit time against the external force is then $\dot{W} = Fv$ where $v = l\hat{J}_0$ is the velocity of the motor. On the other hand, the chemical energy consumed per unit time is $\dot{Q} = r\Delta\mu$, where r is the steady–state rate of ATP consumption:

$$r = \int_0^l [(\alpha_1(x) - \gamma_1(x))\hat{p}_1(x) - (\alpha_2(x) - \gamma_2(x))\hat{p}_2(x)]dx.$$

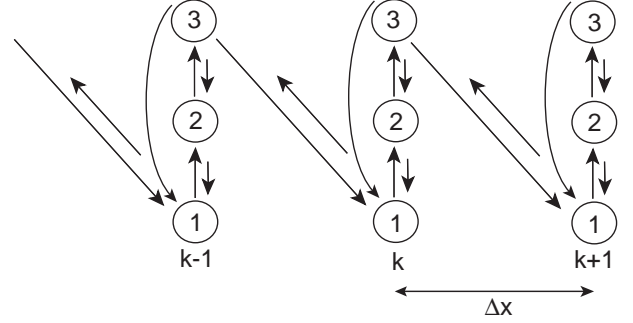The efficiency of the motor is then defined to be (Julicher *et al.*, 1997) $\eta = \frac{Fv}{r\Delta\mu}$.

FIG. 17 State transition diagram for a discrete Brownian ratchet that cycles through $M = 3$ internal states and makes a single step of length Δx

It is often convenient to simplify the generalized ratchet model further by taking the transition rate functions to be localized at the discrete set of positions $x = x_k$, $k = 1, \ldots, K$, and to replace the continuum diffusion and drift terms by hopping rates between nearest lattice sites (Liepelt and Lipowsky, 2007; Lipowsky and Klumpp, 2005). The resulting discrete Brownian ratchet model can be mapped on to a stochastic network of KM states as shown in Fig. 17; (see (Kolomeisky and Fisher, 2007) for an alternative approach to stochastic network models of molecular motors). The stochastic dynamics is now described by a master equation, an example of which is

$$\frac{dP_{km}(t)}{dt} = \sum_{n \neq m} [P_{kn}(t)W_{km;kn} - P_{km}(t)W_{kn;km}] \quad (4.15)$$
$$+ P_{k+1,1}(t)W_{kM;k+1,1} + P_{k-1,M}(t)W_{k1;k-1,M}$$
$$- P_{k,1}(t)W_{k-1,M;k,1} - P_{k,M}(t)W_{k+1,1;k,M},$$

where $P_{km}(t) = p_m(x_k, t)$ and for "vertical" transitions $W_{km;kn} = \omega_{mn}(x_k)$. In this example steps along the filament (power strokes) only occur between states $m = 1$ and $m = M$. Observing a molecular motor's motion

along a filament on longer time-scales (several cycles) suggests that its macroscopic dynamics can be approximated by diffusion with constant drift (Peskin and Oster, 1995; Wang *et al.*, 1998). That is, in the long-time limit, the probability density $\rho(x = k\Delta x, t) = \sum_{m=1}^{M} P_{km}(t)$ satisfies the FP equation

$$\frac{\partial \rho}{\partial t} = -V\frac{\partial \rho}{\partial x} + D\frac{\partial^2 \rho}{\partial x^2}. \qquad (4.16)$$

Such an equation can be derived analytically (Elston, 2000a) by considering the vector $\boldsymbol{F}(z,t)$ with components $F_m(z,t) = \sum_{k=-\infty}^{\infty} P_{km}(t)z^k$. This is related to the probability generating function $F(z,t) = \sum_{m=1}^{M} F_m(z,t)$ for the moments of the discrete location $K(t)$. The vector $\boldsymbol{F}(z,t)$ satisfies a matrix equation of the form $\partial_t \boldsymbol{F}(z,t) = A(z)\boldsymbol{F}(z,t)$ such that the long time behavior of $\boldsymbol{F}(z,t)$ is dominated by the leading eigenvalue $\lambda_0(z)$ of the matrix $A(z)$. From this it can be shown that to leading order the drift $V = \lambda_0'(1)\Delta x$ and the diffusion coefficient $D = \Delta x^2(\lambda_0''(1) + \lambda_0'(1))/2$ (Elston, 2000a).

2. PDE models of active transport

Over much longer time-scales a molecular motor alternates between phases where it is bound to a filament and undergoing several cycles of mechanicochemical transduction, and phases where it is unbound and diffusing in the cytosol. As a further level of complexity, several molecular motors may be attached to a vesicular cargo at the same time, which means that the active transport of the motor/cargo complex will exhibit different velocity states depending on which combination of motors are currently bound to the filament (Mallik and Gross, 2004; Welte, 2004). Indeed, experimental observations of the dynamic behavior of motor/cargo complexes transported along microtubules reveal intermittent behavior with constant velocity movement in both directions along the microtubule (bidirectional transport), interrupted by brief pauses or fast oscillatory movements that may precede localization at specific targets (Bannai *et al.*, 2004; Dynes and Steward, 2007; Gennerich and Schild, 2006; Knowles *et al.*, 1996; Rook *et al.*, 2000). In the axon and distal end of dendrites one finds that microtubule filaments all have the same polarity, with the (+) end oriented away from the cell body (Goldstein and Yang, 2000). This suggests a model of bidirectional transport in which kinesin and dynein motors transport a cargo in opposite directions along a single track. On the other hand, dendritic microtubules located close to the cell body tend to have mixed polarities (Baas *et al.*, 1988), suggesting a model in which motors of the same directional preference are distributed among two parallel microtubules of opposite polarity. In both of the above scenarios, there has to be some mechanism for coordinating the action of the various motors as part of a larger motor complex. One possibility is that the motors interact through a tug–of–war competition, where individual motors influence each other through the force they exert on the cargo (Hendricks *et al.*, 2010; Kural *et al.*, 2005; Muller *et al.*, 2008a,b; Soppina *et al.*, 2009; Welte, 2004), see Sec. IV.B. When a force is exerted on a motor opposite to its preferred direction, it is more likely to detach from its microtubule. Ultimately the motion of the cargo is determined by the random attachments and force–dependent detachments from the microtubule of each motor in the motor complex. (An alternative coordination mechanism could involve a fast molecular switch that alternatively turns off kinesin and dynein).

When considering the active transport of intracellular cargo over relatively long distances, it is often convenient to ignore the microscopic details of how a motor performs a single step (as described by Brownian ratchet models), and to focus instead on the transitions between different types of motion (eg. anterograde vs. retrograde active transport, diffusion vs. active transport). This has motivated a class of mesoscopic models that take the form of a system of PDEs (Bressloff and Newby, 2009; Friedman and Craciun, 2006; Jung and Brown, 2009; Kuznetsov and Avramenko, 2008; Loverdo *et al.*, 2008; Newby and Bressloff, 2010b; Reed *et al.*, 1990; Smith and Simmons, 2001). For the sake of illustration, consider a simple 3-state model of a particle moving on a 1D track of length L. Such a track could represent a single microtubular filament. Within the interior of the track, $0 < x < L$, the particle is taken to be in one of three states labeled by $n = 0, \pm$: unbound from the track and diffusing ($n = 0$), bound to the track and moving to the right (anterograde) with speed v_+ ($n = +$), or bound to the track and moving to the left (retrograde) with speed $-v_-$ ($n = -$). For simplicity, take $v_\pm = v > 0$. Transitions between the three states are governed by a discrete Markov process. Let $Z(t)$ and $N(t)$ denote the random position and state of the particle at time t and define $\mathbb{P}(x, n, t \mid y, m, 0)dx$ as the joint probability that $x \leq Z(t) < x + dx$ and $N(t) = n$ given that initially the particle was at position $Z(0) = y$ and was in state $N(0) = m$. Setting

$$p_n(x,t) \equiv \sum_m \mathbb{P}(x,t,n|0,0,m)\sigma_m \qquad (4.17)$$

with initial condition $p_n(x,0) = \delta(x)\sigma_n$, $\sum_{m=1}^{n} \sigma_m = 1$, the evolution of the probability is described by the following system of PDEs for $t > 0$:

$$\frac{\partial p_+}{\partial t} = -v\partial_x p_+ - \beta_+ p_+ + \alpha p_0 \qquad (4.18a)$$

$$\frac{\partial p_-}{\partial t} = v\partial_x p_- - \beta_- p_- + \alpha p_0 \qquad (4.18b)$$

$$\frac{\partial p_0}{\partial t} = \beta_+ p_+ + \beta_- p_- - 2\alpha p_0 + D_0 \frac{\partial^2 p_0}{\partial x^2}. \qquad (4.18c)$$

Here $\alpha, \beta_\pm$ are the transition rates between the stationary and mobile states. Eq. (4.18) is supplemented by

appropriate boundary condition at $x = 0, L$. For example, a reflecting boundary at $x = 0$ and an absorbing boundary at $x = L$ means that

$$p_-(0, t) = p_+(0, t), \quad p_-(L, t) = 0. \qquad (4.19)$$

In the general case that the velocities $v_\pm$ in the two directions are different, the transport will be biased in the anterograde (retrograde) direction if $v_+/\beta_+ > v_-/\beta_-$ $(v_+/\beta_+ < v_-/\beta_-)$.

It is straightforward to generalize the 3–state model to the case of n distinct velocity states as found for example in the tug–of-war model, see IV.B. Introducing the n–component probability density vector $\mathbf{p}(x, t) \in \mathbb{R}^n$ the corresponding system of PDEs takes the form

$$\frac{\partial \mathbf{p}}{\partial t} = A\mathbf{p} + \mathcal{L}(\mathbf{p}), \qquad (4.20)$$

where $A \in \mathbb{R}^{n \times n}$ specifies the transition rates between each of the n internal motor states and the differential operator $\mathcal{L}$ has the structure

$$\mathcal{L} = \begin{bmatrix} \mathcal{L}_1 & 0 & \cdots & & 0 \\ 0 & \mathcal{L}_2 & 0 & \cdots & 0 \\ \vdots & & \ddots & & \vdots \\ & & & \mathcal{L}_{n-1} & 0 \\ 0 & \cdots & & 0 & \mathcal{L}_n \end{bmatrix}, \qquad (4.21)$$

where the scalar operators are given by

$$\mathcal{L}_j = [-v_j \partial_x + D_{0,j} \partial_x^2]. \qquad (4.22)$$

Here v_j is the velocity of internal state j and $D_{0,j}$ is the corresponding diffusivity.

B. Tug-of-war model of bidirectional transport

Suppose that a certain vesicular cargo is transported along a one–dimensional track via N_+ right–moving (anterograde) motors and N_- left–moving (retrograde motors). At a given time t, the internal state of the cargo–motor complex is fully characterized by the numbers n_+ and n_- of anterograde and retrograde motors that are bound to a microtubule and thus actively pulling on the cargo. Assume that over the time–scales of interest all motors are permanently bound to the cargo so that $0 \leq n_\pm \leq N_\pm$. The tug–of–war model of Muller *et. al.* (Muller *et al.*, 2008a,b) assumes that the motors act independently other than exerting a load on motors with the opposite directional preference. (However, some experimental work suggests that this is an oversimplification, that is, there is some direct coupling between motors (Driver *et al.*, 2010)). Thus the properties of the motor complex can be determined from the corresponding properties of the individual motors together with a specification of the effective load on each motor. There

are two distinct mechanisms whereby such bidirectional transport could be implemented (Muller *et al.*, 2008a). First, the track could consist of a single polarized microtubule filament (or a chain of such filaments) on which up to N_+ kinesin motors and N_- dynein motors can attach, see Fig. 18. Since individual kinesin and dynein motors have different biophysical properties, with the former tending to exert more force on a load, it follows that even when $N_+ = N_-$ the motion will be biased in the anterograde direction. Hence, this version is referred to as an asymmetric tug–of–war model. Alternatively, the track could consist of two parallel microtubule filaments of opposite polarity such that N_+ kinesin motors can attach to one filament and N_- to the other. In the latter case, if $N_+ = N_-$ then the resulting bidirectional transport is unbiased resulting in a symmetric tug–of–war model.
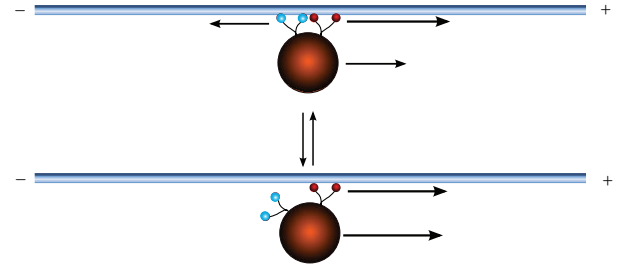

FIG. 18 Schematic diagram of an asymmetric tug–of–war model. Two kinesin and two dynein motors transport a cargo in opposite directions along a single polarized microtubule track. Transitions between two possible motor states are shown.

When bound to a microtubule, the velocity of a single molecular motor decreases approximately linearly with force applied against the movement of the motor (Visscher *et al.*, 1999). Thus, each motor is assumed to satisfy the linear force-velocity relation

$$v(F) = \begin{cases} v_f(1 - F/F_s) & \text{for } F \leq F_s \\ v_b(1 - F/F_s) & \text{for } F \geq F_s \end{cases} \qquad (4.23)$$

where F is the applied force, F_s is the stall force satisfying $v(F_s) = 0$, v_f is the forward motor velocity in the absence of an applied force in the preferred direction of the particular motor, and v_b is the backward motor velocity when the applied force exceeds the stall force. The original tug–of–war model assumes the binding rate is independent of the applied force, whereas the unbinding rate is taken to be an exponential function of the applied force:

$$\pi(F) = \pi_0, \quad \gamma(F) = \gamma_0 e^{\frac{F}{F_d}}, \qquad (4.24)$$

where F_d is the experimentally measured force scale on which unbinding occurs. The force dependence of the unbinding rate is based on measurements of the walking distance of a single motor as a function of load (Schnitzer *et al.*, 2000), in agreement with Kramers rate theory

(Hanggi *et al.*, 1990). Let F_c denote the net load on the set of anterograde motors, which is taken to be positive when pointing in the retrograde direction. Suppose that the molecular motors are not directly coupled to each other so that they act independently and share the load; however, see (Driver *et al.*, 2010). It follows that a single anterograde motor feels the force F_c/n_-, whereas a single retrograde motor feels the opposing force $-F_c/n_+$. Eq. (4.24) implies that the binding and unbinding rates for both types of motor take the form

$$\widehat{\gamma}(n, F_c) = n\gamma(F_c/n), \quad \widehat{\pi}(n) = (N - n)\pi_0. \quad (4.25)$$

The parameters associated with kinesin and dynein motors will be different, so that it is necessary to add the subscript $\pm$ to these parameters. The cargo force F_c is determined by the condition that all the motors move with the same cargo velocity v_c. Suppose that $N_+ \geq N_-$ so that the net motion is in the anterograde direction, which is taken to be positive. In this case, the forward motors are stronger than the backward motors so that $n_+F_{s+} > n_-F_{s-}$. Eq. (4.23) implies that

$$v_c = v_{f+}(1 - F_c/(n_+F_{s+})) = -v_{b-}(1 - F_c/(n_-F_{s-})). \quad (4.26)$$

This generates a unique solution for the load F_c and cargo velocity v_c:

$$F_c(n_+, n_-) = (\mathcal{F}n_+F_{s+} + (1 - \mathcal{F})n_-F_{s-}), \quad (4.27)$$

where

$$\mathcal{F} = \frac{n_-F_{s-}v_{f-}}{n_-F_{s-}v_{f-} + n_+F_{s+}v_{b-}}, \quad (4.28)$$

and

$$v_c(n_+, n_-) = \frac{n_+F_{s+} - n_-F_{s-}}{n_+F_{s+}/v_{f+} + n_-F_{s-}/v_{b-}}. \quad (4.29)$$

The corresponding expressions when the backward motors are stronger, $n_+F_{s+} < n_-F_{s-}$, are found by interchanging v_f and v_b.

The original study of Muller *et al.* (2008a,b) considered the stochastic dynamics associated with transitions between different internal states (n_+, n_-) of the motor complex, without specifying the spatial position of the complex along a 1D track. This defines a Markov process with a corresponding master equation for the time evolution of the probability distribution $P(n_+, n_-, t)$. They determined the steady-state probability distribution of internal states and found that the motor complex exhibited at least three different modes of behavior: (i) the motor complex spends most of its time in states with approximately zero velocity; (ii) the motor complex exhibits fast backward and forward movement interrupted by stationary pauses, which is consistent with experimental studies of bidirectional transport; (iii) the motor complex alternates between fast backward and forward movements. The transitions between these modes

of behavior depend on motor strength, which primarily depends upon the stall force. More recently, Newby and Bressloff (2010a,b) have constructed a system of PDEs describing the evolution of the probability density $p(n_+, n_-, x, t)$ that the motor complex is in the internal state (n_+, n_-) and has position x at time t. This version of the tug–of–war model simultaneously keeps track of the internal state of the motor complex and its location along a 1D track. In order to write the model in the general form (4.20), it is convenient to introduce the label $i(n_+, n_-) = (N_+ + 1)n_- + (n_+ + 1)$ and set $p(n_+, n_-, x, t) = p_{i(n_+,n_-)}(x, t)$. This then gives an n–component probability density vector $\mathbf{p} \in \mathbb{R}^n$ with $n = (N_+ + 1)(N_- + 1)$, which satisfies Eq. (4.20). The internal velocity of internal state $j = j(n_+, n_-)$ is $v_j = v_c(n_+, n_-)$, and the diffusivities D_j are taken to be zero unless all motors are detached from the microtubule: $D_i = D_0\delta_{i,1}$. The components $a_{i,j}$, $i, j = 1, \ldots, n$, of the state transition matrix A are given by the corresponding binding/unbinding rates of Eqs. (4.25). That is, setting $i = i(n_+, n_-)$, the non–zero off–diagonal terms are

$$a_{i,j} = \pi_+(n_+ - 1) \text{ for } j = i(n_+ - 1, n_-), \quad (4.30a)$$
$$a_{i,j} = \pi_-(n_- - 1), \text{ for } j = i(n_+, n_- - 1), \quad (4.30b)$$
$$a_{i,j} = \gamma_+(n_+ + 1, F_c), \text{ for } j = i(n_+ + 1, n_-), \quad (4.30c)$$
$$a_{i,j} = \gamma_-(n_- + 1, F_c), \text{ for } j = i(n_+, n_- + 1). \quad (4.30d)$$

The diagonal terms are then given by $a_{i,i} = -\sum_{j \neq i} a_{j,i}$.

One of the useful features of the tug-of-war model is that it allows various biophysical processes to be incorporated into the model (Newby and Bressloff, 2010a,b; Posta *et al.*, 2009), see also Sec. IV.H.2. For example, a convenient experimental method for changing the stalling force (and hence the mode of motor behavior) is to vary the level of ATP available to the motor complex. At low [ATP] the motor has little fuel and is weaker, resulting in mode (i) behavior; then, as [ATP] increases and more fuel is available, mode (ii) behavior is seen until the stall force saturates at high values of [ATP] where mode (iii) behavior takes over. Thus, [ATP] provides a single control parameter that tunes the level of intermittent behavior exhibited by a motor complex. There are a number of models of the [ATP] and force-dependent motor parameters that closely match experiments for both kinesin (Fisher and Kolomeisky, 2001; Mogilner *et al.*, 2001; Schnitzer *et al.*, 2000; Visscher *et al.*, 1999) and dynein (Gao, 2006; King and Schroer, 2000). It is found that [ATP] primarily affects the stall force, forward motor velocity, and unbinding rate. For example, based on experimental data, the forward velocity may be modeled using Michaelis-Menten kinetics

$$v_f([ATP]) = \frac{v_f^{max}[ATP]}{[ATP] + K_v}, \quad (4.31)$$

where $v_f^{max} = 1\mu m/s$, $K_v = 79.23\mu M$ for kinesin and $v_f^{max} = 0.7\mu m/s$, $K_v = 38\mu M$ for dynein. (The

backward velocity of both kinesin and dynein is small, $v_b \approx \pm 0.006 \mu m/s$, so that the [ATP] dependence can be neglected). The binding rate is determined by the time necessary for an unbound motor to diffuse within range of the microtubule and bind to it, which is assumed to be independent of [ATP]. The unbinding rate of a single motor under zero load can be determined using the [ATP] dependent average run length $L_k([ATP]) = L_k^{max}/([ATP] + K_u)$. The mean time to detach from the microtubule is $v_f([ATP])/L_k([ATP])$ so that

$$\gamma_0([ATP]) = \frac{v_f^{max}([ATP] + K_u)}{L_k^{max}([ATP] + K_v)}, \qquad (4.32)$$

where $L_k^{max} = 0.86 \mu m$, $K_u = 3.13 \mu M$ for kinesin and $L_k^{max} = 1.5 \mu m$, $K_u = 1.5 \mu M$ for dynein. Finally, a model for the [ATP]-dependent stall force of kinesin is

$$F_s([ATP]) = F_s^0 + \frac{(F_s^{max} - F_s^0)[ATP]}{K_s + [ATP]}, \qquad (4.33)$$

where $F_s^0 = 5.5 pN$, $F_s^{max} = 8 pN$, $K_s = 100 \mu M$ for kinesin and $F_s^0 = 0.22 pN$, $F_s^{max} = 1.24 pN$, $K_s = 480 \mu M$ for dynein.

C. Quasi–steady–state (QSS) reduction of PDE models of active transport

Two important quantities characterizing the effectiveness of motor-driven active transport are the hitting probability and MFPT to deliver cargo to a specific target within a cell, see Sec. IVH. In the case of the 3-state model (4.18), in which the number of internal states of the motor-cargo complex is sufficiently small, it is possible to derive exact analytical expressions for the MFPT and hitting probability using Laplace transforms or solving a corresponding system of backwards equations (Benichou *et al.*, 2005; Bressloff and Newby, 2009). However, if the number of internal velocity states becomes large, as in the tug-of-war model, then some form of approximation is needed. This also holds for active transport in higher spatial dimensions where the direction of motion is random, see Sec. IVE. In this section, we review a quasi–steady–state (QSS) method for reducing equations of the general form (4.20) to a scalar FP equation under the assumption that the state transition rates are faster than the velocity of motile states on an appropriate length scale (Newby and Bressloff, 2010a,b). A number of authors have analyzed such equations in this regime. For example, Reed *et al.* (1990) used singular perturbation theory to show that the transport of a chemical along an axon can be analyzed in terms of an approximate traveling-wave solution of a scalar advection diffusion equation for the chemical concentration. Subsequent work rigorously established the validity of this scalar reduction for a wide range of PDE models of active transport (Brooks, 1999; Friedman and Craciun, 2006; Friedman and Hu, 2007). More recently, Newby and Bressloff (2010a,b) have carried out a QSS reduction of the tug-of-war model and used this to study the efficiency of intracellular active transport within the context of random intermittent search processes, see also IV.H. For a more general discussion of the QSS and projection methods for reducing the dimensionality of stochastic models, also referred to as adiabatic reduction, see Gardiner (2009).

The first step in the QSS reduction is to fix the units of space and time by setting $l = 1$ and $l/v = 1$, where $v = \max_{i=1}^n v_i$. This corresponds to non–dimensionalizing Eq. (4.18) by performing the rescalings $x \to x/l$ and $t \to tv/l$. Furthermore, suppose that for the given choice of units, $a_{ij} = \mathcal{O}(1/\varepsilon)$ whereas $\mathcal{L}_{ij} = \mathcal{O}(1)$ for some small parameter $\varepsilon \ll 1$, and set $A = \varepsilon^{-1}\widehat{A}$. Eq. (4.18) can then be rewritten in the dimensionless form (after dropping hat on $\widehat{A}$)

$$\frac{\partial \mathbf{p}}{\partial t} = \frac{1}{\epsilon}A\mathbf{p} + \mathcal{L}(\mathbf{p}), \qquad (4.34)$$

The transition matrix A is assumed to be irreducible and conservative so that $\boldsymbol{\psi} = (1, 1, \cdots, 1)^T$ is in the nullspace $\mathcal{N}(A^T)$. Moreover, A has one zero eigenvalue and the remaining eigenvalues have negative real part. Let $\mathbf{p}^{ss} \in \mathcal{N}(A)$ and choose $\mathbf{p}^{ss}$ so that $\boldsymbol{\psi}^T\mathbf{p}^{ss} = 1$. The next step is to introduce the decomposition $\mathbf{p} = u\mathbf{p}^{ss} + \mathbf{w}$ where $u \equiv \boldsymbol{\psi}^T\mathbf{p}$ and $\boldsymbol{\psi}^T\mathbf{w} = 0$. Thus u is the component of $\mathbf{p}$ in the left nullspace of A, whereas $\mathbf{w}$ is in the orthogonal complement. Multiplying both sides of (4.34) by $\boldsymbol{\psi}^T$ yields the equation

$$\partial_t u = \boldsymbol{\psi}^T \mathcal{L}(u\mathbf{p}^{ss} + \mathbf{w}). \qquad (4.35)$$

Substituting $\mathbf{p} = u\mathbf{p}^{ss} + \mathbf{w}$ into (4.34) gives

$$\partial_t\mathbf{w} + (\partial_t u)\mathbf{p}^{ss} = \frac{1}{\epsilon}A(\mathbf{w} + u\mathbf{p}^{ss}) + \mathcal{L}(\mathbf{w} + u\mathbf{p}^{ss}).$$

Using equation (4.35) and the fact that $\mathbf{p}^{ss}$ is in the right null space of A, shows that

$$\partial_t\mathbf{w} = \frac{1}{\epsilon}A\mathbf{w} + (\mathbb{I}_n - \mathbf{p}^{ss}\boldsymbol{\psi}^T)\mathcal{L}(\mathbf{w} + u\mathbf{p}^{ss}), \qquad (4.36)$$

where $\mathbb{I}_n$ is the $n \times n$ identity matrix.

Now introduce an asymptotic expansion for $\mathbf{w}$:

$$\mathbf{w} \sim \mathbf{w}_0 + \epsilon\mathbf{w}_1 + \epsilon^2\mathbf{w}_2 + \dots. \qquad (4.37)$$

Substituting this expansion into (4.36) and collecting $\mathcal{O}(\epsilon^{-1})$ terms gives $A\mathbf{w}_0 = 0$. Since $\mathbf{w}$ is in the orthogonal complement of the left nullspace of A, it follows that $\mathbf{w}_0 = 0$. Now collecting terms of $\mathcal{O}(1)$ yields the equation

$$A\mathbf{w}_1 = -(\mathbb{I}_n - \mathbf{p}^{ss}\boldsymbol{\psi}^T)\mathcal{L}(u\mathbf{p}^{ss}), \qquad (4.38)$$

where $\mathbb{I}_n$ is the $n \times n$ identity matrix. The orthogonal projection $\mathbb{I}_n - \mathbf{p}^{ss}\boldsymbol{\psi}^T$ ensures that the right–hand side

of the above equation is in the range of A, and a unique solution for $\mathbf{w}_1$ is obtained by requiring that $\boldsymbol{\psi}^T \mathbf{w}_1 = 0$. It is convenient to define the mean of an n-vector $\mathbf{z}$ with respect to the stationary distribution $\mathbf{p}^{ss}$ according to $\langle z \rangle \equiv \mathbf{z}^T \mathbf{p}^{ss}$ Substituting $\mathbf{w} \sim \varepsilon \mathbf{w}_1$ into Eq. (4.35) then yields

$$\partial_t u = -\langle v \rangle \partial_x u + \langle D_0 \rangle \partial_x^2 u + \varepsilon \sum_{j=1}^n \mathcal{L}_j w_{1,j}. \qquad (4.39)$$

From Eq. (4.38) it can be seen that the components of $\mathbf{w}_1$ are linear combinations of $\partial_x u$ and $\partial_x^2 u$ so that

$$w_{1,j} = -\theta_j \partial_x u + q_j \partial_x^2 u \qquad (4.40)$$

where θ_j and q_j, $j = 1, \ldots, n$, are u–independent. Collecting $\partial_x u$ terms in Eq. (4.38) yields an equation for $\boldsymbol{\theta} = (\theta_1, ..., \theta_n)^T$,

$$A\boldsymbol{\theta} = -((\langle v \rangle - v_1)p_1^{ss}, \cdots, (\langle v \rangle - v_n)p_n^{ss})^T. \qquad (4.41)$$

The condition $\boldsymbol{\psi}^T \mathbf{w}_1 = 0$ implies that $\boldsymbol{\psi}^T \boldsymbol{\theta} = 0$ and hence there exists a unique solution for $\boldsymbol{\theta}$. Likewise the equation for $\boldsymbol{q}$ is given by

$$A\boldsymbol{q} = -((\langle D_0 \rangle - D_{0,1})p_1^{ss}, \cdots, (\langle D_0 \rangle - D_{0,n})p_n^{ss})^T.$$

Finally, assuming that the diffusivity $D_{0,j} = \mathcal{O}(\varepsilon)$ and keeping only lowest order terms, leads to the scalar FP equation (Newby and Bressloff, 2010a,b)

$$\frac{\partial u}{\partial t} = -V \frac{\partial u}{\partial x} + D \frac{\partial^2 u}{\partial x^2} \qquad (4.42)$$

with

$$V = \langle v \rangle + \mathcal{O}(\varepsilon^2),\ D = \langle D_0 \rangle + \varepsilon \boldsymbol{v}^T \boldsymbol{\theta} + \mathcal{O}(\varepsilon^2). (4.43)$$

In order to compute the $\mathcal{O}(\varepsilon)$ contribution to D, the rank deficient Eqs. (4.41) can be solved numerically using the full singular value decomposition of the matrix A, see below. The probability density function u is the total probability of being in any motor state at position x and time t. Suppose that the particle was initially injected on to the track at $x = 0$ and $\sigma_m = p_m^{ss}$ in equation (4.17) so that the initial state lies in the slow manifold. The initial condition for u is then $u(x,0) = \delta(x)$. Similarly, typical boundary conditions for u on a finite track of length L will be $Vu - D\partial_x u\ |_{x=0} = 0$ (reflecting) and $u(L,t) = 0$ (absorbing). These boundary conditions follow from substituting $\mathbf{p} = u\mathbf{p}^{ss} + \varepsilon \mathbf{w}_1$ into the corresponding boundary conditions of Eq. (4.34).

QSS reduction of 3–state model. In the case of the 3–state model given by Eq. (4.18), the steady–state probability distribution is

$$\mathbf{p}^{ss} = \frac{1}{\gamma} \begin{pmatrix} \frac{1}{\beta_+} \\ \frac{1}{\beta_-} \\ \frac{1}{\alpha} \end{pmatrix}, \gamma = \frac{1}{\beta_+} + \frac{1}{\beta_-} + \frac{1}{\alpha}. \qquad (4.44)$$

The resulting 2-rank system of equations for the 3-vector $\mathbf{w}_1$, Eq. (4.38), can be solved up to the arbitrary element $[\mathbf{w}_1]_0$ using Gaussian elimination:

$$[\mathbf{w}_1]_\pm = \mp \frac{1 \mp \langle v \rangle}{\beta_\pm^2 \gamma} \partial_x u + \frac{\alpha \Omega}{\beta_\pm}, \quad [\mathbf{w}_1]_0 = \Omega \qquad (4.45)$$

where

$$\langle v \rangle = \frac{v}{\gamma} \left(\frac{1}{\beta_+} - \frac{1}{\beta_-} \right).$$

Ω is determined by imposing the condition $\psi^T \mathbf{w} = 0$:

$$\alpha \Omega = \frac{1}{\gamma^2} \left(\frac{1 - \langle v \rangle}{\beta_+^2} - \frac{1 + \langle v \rangle}{\beta_-^2} \right) \partial_x u \qquad (4.46)$$

Substituting equations (4.45) and (4.46) into (4.35) yields the FP Eq. (4.42) with (to $\mathcal{O}(\epsilon^2)$)

$$D = \frac{\alpha D_0}{\gamma} + \epsilon \left(\frac{(v - \langle v \rangle)^2}{\gamma \beta_+^2} + \frac{(v + \langle v \rangle)^2}{\gamma \beta_-^2} \right) \qquad (4.47)$$

QSS reduction of tug-of-war model. The reduction of the tug–of–war model presented in Sec. IV.B is more involved (Newby and Bressloff, 2010a,b). In particular, it is necessary to compute the vector $\boldsymbol{\theta}$ by solving equation (4.41), which has the general form $A\boldsymbol{\theta} = \boldsymbol{b}$. The standard numerical method for solving a rank deficient linear system using singular valued decomposition (SVD) must be modified slightly. The Fredholm-Alternative theorem implies that a solution to equation (4.41) exists but is not unique. In the case of a standard least squares solution, uniqueness is obtained by requiring the solution to be orthogonal to the nullspace of A. However, in this case a unique solution must be obtained by requiring the solution be orthogonal to the nullspace of A^T. The following procedure may be used. Let $U\Sigma H^T = A$ be a full singular value decomposition of A. Let $\boldsymbol{z} = U^T \boldsymbol{b}$ and $\boldsymbol{y} = H^T \boldsymbol{\theta}$ so that $\Sigma \boldsymbol{y} = \boldsymbol{z}$. It follows that $y_i = z_i/\sigma_i$, $i = 1, ..., n-1$, where σ_i are the non-zero singular values of A. The last component y_n is arbitrary since $\sigma_n = 0$. The standard least squares solution is obtained by setting $y_n = 0$. To determine y_n here, one requires that $\sum_{i=1}^n \theta_i = 0$. Since $\boldsymbol{\theta} = H\boldsymbol{y}$,

$$\theta_i = \sum_{j=1}^{n-1} h_{ij} y_j + h_{in} y_n. \qquad (4.48)$$

where h_{ij} are the components of the matrix H. Since $\sum_{i=1}^n \theta_i = 0$, it follows that

$$y_n = -\frac{\sum_{i=1}^n \sum_{j=1}^{n-1} h_{ij} y_j}{\sum_{i=1}^n h_{in}}. \qquad (4.49)$$

The QSS reduction determines the generic parameters V, D of the scalar FP equation (4.42) as functions of the

various biophysical parameters of the tug–of–war model. These include the stall force F_s, the detachment force F_d, the maximum forward and backward velocities v_f, v_b, and the single motor binding/unbinding rates γ_0, π_0. These, in turn will depend on environmental factors such as the concentration of [ATP] and various signaling molecules, see also Sec. IV.H.2.

D. Fast and slow axonal transport

Axons of neurons can extend up to 1m in large organisms but synthesis of many of its components occur in the cell body. Axonal transport is typically divided into three main categories based upon the observed speed (Brown, 2003; Sheetz et al., 1998): fast transport $(1 - 9\mu\text{m/s})$ of organelles and vesicles and slow transport $(0.004 - 0.6\mu\text{m/s})$ of soluble proteins and cytoskeletal elements. Slow transport is further divided into two groups; actin and actin-bound proteins are transported in slow component A while cytoskeletal polymers such as microtubules and neurofilaments are transported in slow component B. It had originally been assumed that the differences between fast and slow components were due to differences in transport mechanisms, but direct experimental observations now indicate that they all involve fast motors but differ in how the motors are regulated. Membranous organelles, which function primarily to deliver membrane and protein components to sites along the axon and at the axon tip, move rapidly in a unidirectional manner, pausing only briefly. In other words, they have a high duty ratio – the proportion of time a cargo complex is actually moving. On the other hand, cytoskeletal polymers and mitochondria move in an intermittent and bidirectional manner, pausing more often and for longer time intervals, as well as sometimes reversing direction. Such transport has a low duty ratio.

Neurofilaments are space-filling cytoskeletal polymers that increase the cross-sectional area of axons, which then increases the propagation speed of action potentials. Radioisotopic pulse labeling experiments provide information about the transport of neurofilaments at the population level, which takes the form of a slowly moving Gaussian-like wave that spreads out as it propagates distally. A number of authors have modeled this slow transport in terms of a unidirectional mode similar to the 3–state model of Eqs. (4.18) (Blum and Reed, 1989; Craciun et al., 2005; Reed et al., 1990). For example, Blum and Reed (1989) considered the following system on the semi-infinite domain $0 \le x < \infty$:

$$\epsilon \left[\frac{\partial p_1}{\partial t} - v \frac{\partial p_1}{\partial x} \right] = \sum_{j=1}^n A_{1j} p_j \tag{4.50a}$$

$$\epsilon \frac{\partial p_i}{\partial t} = \sum_{j=1}^n A_{ij} p_j, \quad 1 < i \le N, \tag{4.50b}$$

where p_1 represents the concentration of moving neurofilament proteins, and $p_i, i > 1$ represent the concentrations in $n - 1$ distinct stationary states. Conservation of mass implies that $A_{jj} = -\sum_{i \ne j} A_{ij}$. The initial condition is $p_i(x,0) = 0$ for all $1 \le i \le n$, $0 < x < \infty$. Moreover $p_1(0,t) = 1$ for $t > 0$. Reed et al. (1990) carried out an asymptotic analysis of Eqs. (4.50) that is related to the QSS reduction method of Sec. IV.C. Suppose that p_1 is written in the form

$$p_1(x,t) = Q_\epsilon \left(\frac{x - ut}{\sqrt{\epsilon}}, t \right),$$

where u is the effective speed, $u = v p_1^{\text{ss}} / \sum_{j=1}^n p_j^{\text{ss}}$, and $\mathbf{p}^{\text{ss}}$ is the steady-state solution for which $\mathbf{A}\mathbf{p}^{\text{ss}} = \mathbf{0}$. They then showed that $Q_\epsilon(s,t) \to Q_0(s,t)$ as $\epsilon \to 0$, where Q_0 is a solution to the diffusion equation

$$\frac{\partial Q_0}{\partial t} = D \frac{\partial^2 Q_0}{\partial x^2}, \quad Q_0(s,0) = H(-s)$$

with H the Heaviside function. The diffusivity D can be calculated in terms of v and the transition matrix $\mathbf{A}$. Hence the propagating and spreading waves observed in experiments could be interpreted as solutions to an effective advection-diffusion equation. More recently, Friedman and Craciun (2005, 2006) have developed a more rigorous analysis of spreading waves.
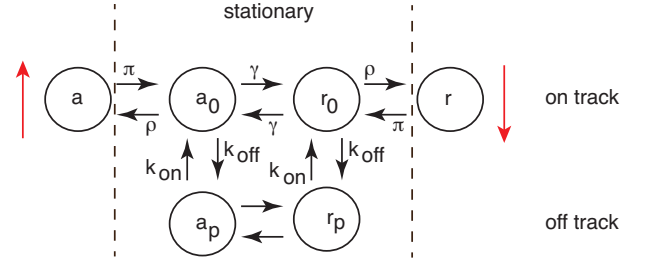

FIG. 19 Transition diagram of 'stop-and-go' moldel for the slow axonal transport of neurofilaments. See text for definition of different states.

In contrast to the above population models, direct observations of neurofilaments in axons of cultured neurons using fluorescence microscopy has demonstrated that individual neurofilaments are actually transported by fast motors but in an intermittent fashion (Wang and Brown, 2001; Wang et al., 2000). Hence, it has been proposed that the slow rate of movement of a population is an average of rapid bidirectional movements interrupted by prolonged pauses, the so-called stop-and-go hypothesis (Brown, 2000; Jung and Brown, 2009; Li et al., 2012). Computational simulations of an associated system of PDEs shows how fast intermittent transport can account for the slowly spreading wave seen at the population level. One version of the model assumes that the neurofilaments can be in one of six states (Brown, 2000; Li et al., 2012): anterograde moving on track (state a), anterograde pausing on track (a_0 state), anterograde pausing off track

(state a_p), retrograde pausing on track (state r_0), retrograde pausing off track (state r_p), and retrograde moving on track (state r). The state transition diagram is shown in Fig. 19.

E. Active transport on microtubular networks

In the case of axonal or dendritic transport in neurons, the microtubles tend to be aligned in parallel (Goldstein and Yang, 2000) so that one can treat the transport process as effectively 1D. On the other hand, intracellular transport within the soma of neurons and most non–polarized animal cells occurs along a microtubular network that projects radially from an organizing center (centrosome) with outward polarity (Alberts *et al.*, 2008). This allows the delivery of cargo to and from the nucleus. Moreover, various animal viruses including HIV take advantage of microtubule-based transport in order to reach the nucleus from the cell surface and release their genome through nuclear pores (Damm and Pelkmans, 2006; Lagache *et al.*, 2009a). In contrast, the delivery of cargo from the cell membrane or nucleus to other localized cellular compartments requires a non–radial path involving several tracks. It has also been found that microtubules bend due to large internal stresses, resulting in a locally disordered network. This suggests that *in vivo* transport on relatively short length scales may be similar to transport observed *in vitro*, where microtubular networks are not grown from centrosomes, and thus exhibit orientational and polarity disorder (Kahana *et al.*, 2008; Salman *et al.*, 2005). Another example where a disordered microtubular network exists is within the *Drosophila* oocyte (Becalska and Gavis, 2009). Kinesin and dynein motor-driven transport along this network is thought to be one of the mechanisms for establishing the asymmetric localization of four maternal mRNAs - *gurken, oskar, bicoid* and *nanos*- which are essential for the development of the embryonic body axes.

A detailed microscopic model of intracellular transport within the cell would need to specify the spatial distribution of microtubular orientations and polarity, in order to specify which velocity states are available to a motor-cargo complex at a particular spatial location. However, a simplified model can be obtained under the "homogenization" assumption that the network is sufficiently dense so that the set of velocity states (and associated state transitions) available to a motor complex is independent of position. In that case, one can effectively represent the active transport and delivery of cargo to an unknown target within the cell in terms of a two– or three-dimensional model of active transport (Benichou *et al.*, 2007, 2011b; Loverdo *et al.*, 2008). This also provides motivation for extending the QSS analysis of Sec. IV.C to higher–dimensions (Bressloff and Newby, 2011).

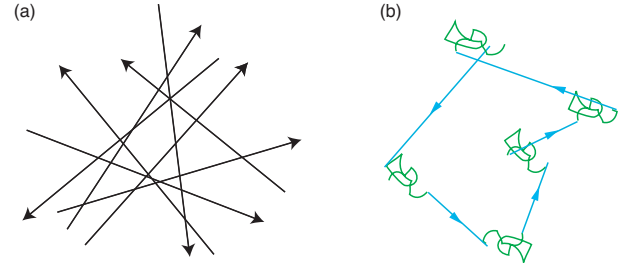For simplicity, consider a disordered 2D microtubular

FIG. 20 Active transport on a disordered microtubular network. (a) Random orientational arrangement of microtubules. (b) Effective 2D random intermittent search in which a particle switches between diffusion and ballistic motion in a random direction.

network as illustrated in Fig. 20. (The extension to 3D networks is relatively straightforward). Suppose that after homogenization, a molecular motor at any point $\mathbf{r} = (x, y)$ in the plane can bind to a microtubule with any orientation θ, resulting in ballistic motion with velocity $\mathbf{v}(\theta) = v(\cos\theta, \sin\theta)$ and $\theta \in [0, 2\pi)$. If the motor is unbound then it acts as a Brownian particle with diffusion coefficient D_0. Transitions between the diffusing state and a ballistic state are governed by a discrete Markov process. The transition rate β from a ballistic state with velocity $\mathbf{v}(\theta)$ to the diffusive state is taken to be independent of θ, whereas the reverse transition rate is taken to be of the form $\alpha\mathcal{Q}(\theta)$ with $\int_0^{2\pi}\mathcal{Q}(\theta)d\theta = 1$. Suppose that at time t the motor is undergoing ballistic motion. Let $(X(t), Y(t))$ be the current position of the searcher and let $\Theta(t)$ denote the corresponding velocity direction. Introduce the conditional probability density $p(x, y, \theta, t)$ such that $p(x, y, \theta, t)dxdyd\theta$ is the joint probability that $(x, y, \theta) < (X(t), Y(t), \Theta(t)) < (x + dx, y + dy, \theta + d\theta)$ given that the particle is in the ballistic phase. Similarly, take $p_0(x, y, t)$ to be the corresponding conditional probability density if the particle is in the diffusive phase. (For the moment the initial conditions are left unspecified). The evolution of the probability densities for $t > 0$ can then be described in terms of the following 2D system of PDEs (Bressloff and Newby, 2011):

$$\frac{\partial p}{\partial t} = -\boldsymbol{\nabla} \cdot (\mathbf{v}(\theta)p) - \frac{\beta}{\epsilon}p(\mathbf{r}, \theta, t) + \frac{\alpha\mathcal{Q}(\theta)}{\epsilon}p_0(\mathbf{r}, t) \tag{4.51a}$$

$$\frac{\partial p_0}{\partial t} = \epsilon D_0\boldsymbol{\nabla}^2 p_0 + \frac{\beta}{\epsilon}\int_0^{2\pi} p(\mathbf{r}, \theta', t)d\theta' - \frac{\alpha}{\epsilon}p_0(\mathbf{r}, t). \tag{4.51b}$$

In the case of a uniform density, $\mathcal{Q}(\theta) = 1/(2\pi)$, Eqs. (4.51a) and (4.51b) reduce to the 2D model considered by Benichou *et. al.* (Benichou *et al.*, 2007, 2011b; Loverdo *et al.*, 2008). In order to carry out a quasi steady–state (QSS) reduction of Eqs. (4.51a) and (4.51b), see Sec. IV.C, we have fixed the units of space and time according

to $l = 1$ and $l/v = 1$, where l is again a typical run length. Furthermore, for the given choice of units, we have assumed that there exists a small parameter $\epsilon \ll 1$ such that all transition rates are $\mathcal{O}(\epsilon^{-1})$, the diffusivity is $\mathcal{O}(\epsilon)$ and all velocities are $\mathcal{O}(1)$.

In the limit $\epsilon \to 0$, the system rapidly converges to the space-clamped (i.e. $\boldsymbol{\nabla} p = \boldsymbol{\nabla} p_0 = 0$) steady–state distributions $(p^{\mathrm{ss}}(\theta), p_0^{\mathrm{ss}})$ where

$$p_0^{\mathrm{ss}} = \frac{\beta}{\alpha + \beta} \equiv b, \quad p^{\mathrm{ss}}(\theta) = \frac{\alpha \mathcal{Q}(\theta)}{\alpha + \beta} \equiv a\mathcal{Q}(\theta). \quad (4.52)$$

The QSS approximation is based on the assumption that for $0 < \epsilon \ll 1$, solutions remain close to the steady–state solution. Hence,

$$p(\mathbf{r}, \theta, t) = u(\mathbf{r}, t)p^{\mathrm{ss}}(\theta) + \epsilon w(\mathbf{r}, \theta, t) \quad (4.53)$$
$$p_0(\mathbf{r}, t) = u(\mathbf{r}, t)p_0^{\mathrm{ss}} + \epsilon w_0(\mathbf{r}, t), \quad (4.54)$$

where

$$u(\mathbf{r}, t) \equiv \int_0^{2\pi} p(\mathbf{r}, \theta, t)d\theta + p_0(\mathbf{r}, t), \quad (4.55)$$

and

$$\int_0^{2\pi} w(\mathbf{r}, \theta, t)d\theta + w_0(\mathbf{r}, t) = 0. \quad (4.56)$$

Furthermore, the initial conditions are taken to be

$$u(\mathbf{r}, 0) = \delta(\mathbf{r} - \mathbf{r}_0), \quad w(\mathbf{r}, 0) = w_0(\mathbf{r}, 0) = 0, \quad (4.57)$$

which are equivalent to the following initial conditions for the full probability densities:

$$p(\mathbf{r}, \theta, 0) = \delta(\mathbf{r} - \mathbf{r}_0)p^{\mathrm{ss}}(\theta), \; p_0(\mathbf{r}, 0) = \delta(\mathbf{r} - \mathbf{r}_0)p_0^{\mathrm{ss}}. \quad (4.58)$$

Thus, the initial internal state of the motor (diffusive or ballistic with velocity $\mathbf{v}(\theta)$) is generated according to the steady–state distributions $p^{ss}(\theta)$ and p_0^{ss}. In other words, the motor starts on the slow manifold of the underlying dynamics. If this were not the case, then one would need to carry out a multiscale analysis in order to take into account the initial transient dynamics transverse to the slow manifold (Gardiner, 2009).

Perturbation and projection methods can now be used to derive a closed equation for the scalar component $u(\mathbf{r}, t)$ (Bressloff and Newby, 2011). First, integrating equation (4.51a) with respect to θ and adding equation (4.51b) yields

$$\frac{\partial u}{\partial t} = \epsilon D_0 \boldsymbol{\nabla}^2 p_0 - \langle\langle \mathbf{v} \cdot \boldsymbol{\nabla} p \rangle\rangle \quad (4.59)$$
$$= \epsilon b D_0 \boldsymbol{\nabla}^2 u - a \langle \mathbf{v} \rangle \cdot \boldsymbol{\nabla} u - \epsilon \langle\langle \mathbf{v} \cdot \boldsymbol{\nabla} w \rangle\rangle + \mathcal{O}(\epsilon^2),$$

where $\langle f \rangle = \int_0^{2\pi} \mathcal{Q}(\theta)f(\theta)d\theta$ and $\langle\langle f \rangle\rangle = \int_0^{2\pi} f(\theta)d\theta$ for any function or vector component $f(\theta)$. Next, substituting equations (4.53) and (4.54) into equations (4.51a)

and (4.51b) yields

$$a\mathcal{Q}(\theta)\frac{\partial u}{\partial t} + \epsilon \frac{\partial w}{\partial t} = -\mathbf{v}(\theta) \cdot \boldsymbol{\nabla} [a\mathcal{Q}(\theta)u + \epsilon w] - \beta w$$
$$+ \alpha \mathcal{Q}(\theta)w_0. \quad (4.60)$$

and

$$b\frac{\partial u}{\partial t} + \epsilon \frac{\partial w_0}{\partial t} = \epsilon D_0 \boldsymbol{\nabla}^2 (bu + \epsilon w_0) \quad (4.61)$$
$$+ \beta \langle w \rangle - \alpha w_0.$$

Now substitute (4.59) into (4.60) and (4.61). Collecting terms to leading order in ϵ and using Eq. (4.56) then gives

$$w_0(\mathbf{r}, t) \sim \frac{ab}{\alpha + \beta} [\langle \mathbf{v} \rangle \cdot \boldsymbol{\nabla} u], \quad (4.62)$$

and

$$w(\mathbf{r}, \theta, t) \sim \frac{\mathcal{Q}(\theta)}{\beta} \left(a^2(1 + b) \langle \mathbf{v} \rangle - a\mathbf{v}(\theta) \right) \cdot \boldsymbol{\nabla} u. \quad (4.63)$$

Finally, substituting equations (4.63) and (4.62) into (4.59) yields to $\mathcal{O}(\epsilon)$ the FP equation

$$\frac{\partial u}{\partial t} = -\boldsymbol{\nabla} \cdot (\mathbf{V} u) + \epsilon b D_0 \boldsymbol{\nabla}^2 u + \epsilon \boldsymbol{\nabla} \cdot (\mathbf{D}\boldsymbol{\nabla} u). \quad (4.64)$$

The diffusion tensor $\mathbf{D}$ has components $D_{kl}, k = x, y, l = x, y$

$$D_{kl} \sim \frac{a}{\beta} \left(\langle v_k v_l \rangle - \langle v_k \rangle \langle v_l \rangle + b^2 \langle v_k \rangle \langle v_l \rangle \right), \quad (4.65)$$

to lowest order in ϵ, whilst the effective drift velocity is given by $\mathbf{V} \sim a \langle \mathbf{v} \rangle$.

In the case of a uniform direction distribution $\mathcal{Q}(\theta) = 1/(2\pi)$, the diffusion tensor reduces to a scalar. This follows from the fact that $v_x = v \cos \theta, v_y = v \sin \theta$ so $\langle v_x \rangle = \langle v_y \rangle = \langle v_x v_y \rangle = 0$ and to leading order

$$D_{xx} = \frac{av^2}{2\beta} = D_{yy}, \quad D_{xy} = 0. \quad (4.66)$$

More generally, assuming that $\mathcal{Q}(\theta)$ is sufficiently smooth, we can expand it as a Fourier series,

$$\mathcal{Q}(\theta) = \frac{1}{2\pi} + \frac{1}{\pi} \sum_{n=1}^{\infty} (\omega_n \cos(n\theta) + \hat{\omega}_n \sin(n\theta)). \quad (4.67)$$

Assume further that $\omega_1 = \hat{\omega}_1 = 0$ so there is no velocity bias i.e. $\langle v_x \rangle = \langle v_y \rangle = 0$. Then

$$D_{xx} = \frac{av^2}{\beta} \int_0^{2\pi} \cos^2(\theta)\mathcal{Q}(\theta)d\theta = \frac{av^2}{2\beta} (1 + \omega_2)$$
$$D_{yy} = \frac{av^2}{\beta} \int_0^{2\pi} \sin^2(\theta)\mathcal{Q}(\theta)d\theta = \frac{av^2}{2\beta} (1 - \omega_2), \quad (4.68)$$
$$D_{xy} = \frac{av^2}{\beta} \int_0^{2\pi} \sin(\theta) \cos(\theta)\mathcal{Q}(\theta)d\theta = \frac{av^2}{2\beta}\hat{\omega}_2.$$
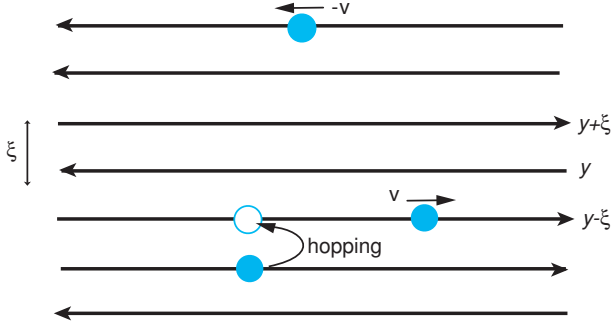
FIG. 21 Random velocity model of a microtubular network with quenched polarity disorder. Particles move ballistically along parallel tracks in a direction determined by the polarity of the given track. They also hop between tracks according to an unbiased random walk.

It follows that only the second terms in the Fourier series expansion contribute to the diffusion tensor.

An alternative formulation of transport on disordered microtubular networks has been developed by Kahana *et al.* (2008) in terms of random velocity fields (Ajdari, 1995; Redner, 1997; Zumofen *et al.*, 1990). In order to describe the basic idea, consider the simplified model analyzed by Zumofen *et al.* (1990). The latter model consists of a set of equally spaced parallel tracks along the x-axis, say, see Fig. 21. The tracks are assigned random polarities ± 1 with equal probabilities corresponding to quenched polarity disorder. A particle undergoes a random walk in the y–direction, whereas when a particle attaches to a certain track it moves ballistically with velocity ± 1 according to the track's polarity. It is assumed that when a particle hops to a neighboring track it binds immediately. Let $X(t)$ denote the displacement of a random walker in the longtitudinal direction at time t:

$$X(t) = \int_0^t v[y(t')]dt'. \qquad (4.69)$$

Taking the continuum limit in the y direction means that

$$p(y,t) = \frac{1}{\sqrt{4\pi Dt}}e^{-y^2/4Dt},$$

where D is the diffusion coefficient, and the velocity field is δ–correlated $\langle v(y)v(y')\rangle_c = v^2\xi\delta(y-y')$. Here averaging is taken with respect to the quenched polarity disorder and ξ is the infinitesimal spacing between tracks. Now consider the second moment $\langle\langle X^2(t)\rangle\rangle$ of the stochastic process averaged with respect to the quenched disorder and realizations of the random walk:

$$\langle\langle X^2(t)\rangle\rangle = 2\int_0^t dt_1 \int_0^{t_1} dt_2 \langle\langle v[y(t_1)]v[y(t_2)]\rangle\rangle, \quad (4.70)$$

where

$$\langle\langle v[y(t_1)]v[y(t_2)]\rangle\rangle = \int_{-\infty}^\infty dy_1 \int_{-\infty}^\infty dy_2 \langle v(y_1)v(y_2)\rangle_c$$
$$\times p(y_2,t_2)p(y_1-y_2,t_1-t_2). \qquad (4.71)$$

Using Laplace transforms and the velocity correlation function,

$$\langle\langle \widetilde{X^2}(s)\rangle\rangle = \frac{2v^2\xi}{s}\widetilde{p}(0,s)\int_{-\infty}^\infty \widetilde{p}(y,s)dy, \qquad (4.72)$$

with

$$\widetilde{p}(y,s) = \frac{1}{\sqrt{4Ds}}e^{-|y|\sqrt{s/D}}.$$

Performing the integration with respect to y thus shows that $\langle\langle\widetilde{X^2}(s)\rangle\rangle = v^2\xi D^{-1/2}s^{-5/2}$, which on inverting the Laplace transform gives

$$\langle\langle X^2(t)\rangle\rangle = \frac{4v^2\xi}{3\sqrt{\pi D}}t^{3/2}. \qquad (4.73)$$

An equivalent formulation of the problem is to treat $\langle\langle X^2(t)\rangle\rangle$ as the solution to the differential equation (Kahana *et al.*, 2008)

$$\frac{d^2}{dt^2}\langle\langle X^2(t)\rangle\rangle = 2v^2\xi yp(0,t), \qquad (4.74)$$

where $\xi p(0,t)$ is the probability of turn to the origin at time t within a single lattice spacing ξ, and $p(0,t) = 1/\sqrt{4\pi Dt}$. In conclusion, the random velocity model supports anomalous superdiffusion in the x direction.

Kahana *et al.* (2008) extended the above construction to 2D (and 3D) disordered networks where there are parallel tracks in the x and y directions. The distribution of polarities are unbiased in both directions. A self-consistent description of the dynamics is obtained by taking

$$\frac{d^2}{dt^2}\langle\langle X^2(t)\rangle\rangle = 2v^2\xi p_y(0,t), \quad \frac{d^2}{dt^2}\langle\langle Y^2(t)\rangle\rangle = 2v^2\xi p_x(0,t), \qquad (4.75)$$

where p_x and p_y are the probability densities of the x and y coordinates. From the symmetry of the network, $p_x(0,t) = p_y(0,t)$. Hence, assuming that $p_x(0,t) = C\langle\langle X^2(t)\rangle\rangle^{-1/2}$ for some constant C, and setting $\phi(t) = \langle\langle X^2(t)\rangle\rangle$ gives

$$\phi^{1/2}\frac{d^2}{dt^2}\phi = 2Cv^2\xi. \qquad (4.76)$$

It follows that $\phi(t) \sim t^{4/3}$ so that the diffusion is less enhanced than in the case of parallel tracks in one direction. Finally, note that active transport on the randomly oriented network of Fig. 20 exhibits normal rather than anomalous diffusion. A major difference from the random velocity model is that the latter has quenched polarity disorder, whereas the former has dynamical polarity disorder.

F. Virus trafficking

An interesting example of active transport in 2D or 3D is given by virus trafficking. An animal virus typically invades a mammalian cell by first undergoing membrane endocytosis from the exterior to the interior of the cell. It then has to navigate the crowded cytoplasm without being degraded in order to reach a nuclear pore and deliver its DNA to the cell nucleus (Damm and Pelkmans, 2006). Single particle tracking has established that virus trajectories within the cytoplasm consist of a succession of free or confined diffusion and ballistic periods involving active transport along microtubules or actin networks (Brandenburg and Zhuang, 2007). A macroscopic computational model of the trafficking of a population of viruses has been developed based on the law of mass action, which takes into account cell geometry but neglects stochastic effects (Dinh *et al.*, 2007, 2005). More recently, in a series of papers, Holcman and collaborators (Holcman, 2007; Lagache *et al.*, 2009a,b; Lagache and Holcman, 2008) have developed a stochastic model of a single virus trafficking inside a cell, which involves reducing an intermittent search model (see Sec. IV.H) to an effective Langevin equation, and using the latter to calculate the mean time to reach a nuclear pore based on a narrow escape problem (see Sec. II.C). The basic structure of a 2D version of the latter model is shown in Fig. 22.

Following (Lagache and Holcman, 2008), the cell is treated as a radially symmetric disc consisting of an annular region of cytoplasm of outer radius R and inner radius δ, surrounding a central nuclear disc. N microtubules radiate outwards from the nucleus to the cell membrane, and are assumed to be distributed uniformly so that the angle between two neighboring microtubules is $\Theta = 2\pi/N$. (A two-dimensional description of a cell would be reasonable in the case of cultured cells that are flattened due to adhesion to the substrate). The motion of a virus particle alternates between diffusive motion within a wedge region $\widehat{\Omega}$ subtending an angle Θ at the origin, and binding to one of the two microtubules at the boundary of the wedge. Suppose that a virus particle starts at some radius $r_0 < R$ and arbitrary angle within such a wedge. Let $\tau(r_0)$ denote the MFPT for the particle to bind to a microtubule, and let $\rho(r_0)$ be the mean radial position on the microtubule. Suppose that the particle moves with a fixed speed v for a time T towards the nucleus before being released to a new position with radius r_1 and arbitrary angle within another wedge. It follows that $r_1 = \rho(r_0) - vT$. Treating the domain $\widehat{\Omega}$ as an open wedge by ignoring the reflecting boundary at $r = R$, it can be shown that if $\Theta \ll 1$ then (Lagache *et al.*, 2009a)

$$\tau(r_0) \approx r_0^2 \Theta^2/12D, \quad \rho(r_0) \approx r_0(1 + \Theta^2/12).$$
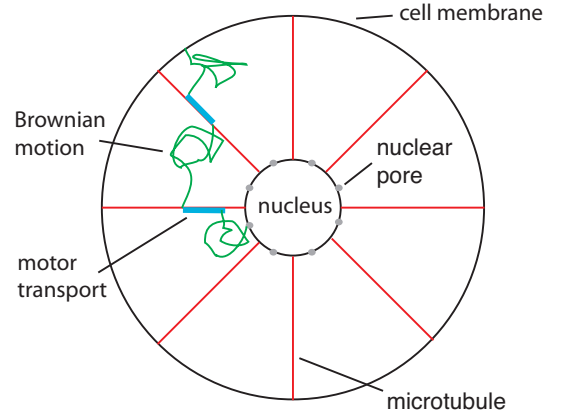
The reduction method of (Lagache *et al.*, 2009a; La-

FIG. 22 Model of Lagache and Holcman (2008). Diagram of a 2D radially symmetric cell with radially equidistant microtubes. A virus trajectory is shown that alternates between ballistic motion along a microtubule and diffusion the cytoplasm. Trajectory starts at the cell membrane and ends at a nuclear pore.

gache and Holcman, 2008) is to assume that on a coarse-grained time-scale the random intermittent motion of the virus can be approximated by a Langevin equation with a radial drift vector:

$$\frac{d\mathbf{r}}{dt} = b(r)\frac{\mathbf{r}}{|\mathbf{r}|} + \sqrt{2D}d\xi dt. \tag{4.77}$$

In order to estimate the drift function $b(r)$, the MFPT $\widehat{\tau}(r_0)$ for the effective Langevin particle to start at r_0 and end at r_1 is calculated using the standard theory of first passage times (see Sec. II.B and (Redner, 2001)), and then compared to $\tau(r_0)$. First, $\widehat{\tau}(r_0)$ satisfies the equation

$$D\nabla^2\widehat{\tau} - b(r)\nabla\widehat{\tau} = -1,$$

with boundary conditions

$$\frac{d\widehat{\tau}}{dr}(r) = 0, \quad \widehat{\tau}(r_1) = 0.$$

As a further simplification, it is assumed that $b(r)$ varies slowly with r so that $b(r) \approx b(r_0)$, leading to the solution

$$\widehat{\tau}(r_0) = \int_{r_1}^{r_0} \int_v^R \frac{u e^{-b(r_0)[u-v]/D}}{Dv} du dv.$$

Assuming that $D \ll 1$ the Laplace method can be used to evaluate the integral with respect to u, giving $\widehat{\tau}(r_0) \approx (r_0 - r_1)/b(r_0)$. Finally, setting $\widehat{\tau}(r_0) = \tau(r_0) + T$ yields

$$b(r_0) = \frac{r_0 - r_1}{\tau(r_0) + T} = \frac{d - r_0\Theta^2/12}{T + r_0^2\Theta^2/12D}. \tag{4.78}$$

A more detailed calculation of the effective drift function $b(r)$ under less restrictive assumptions can be found in (Lagache *et al.*, 2009a).

Having reduced the effective motion of the virus to a Langevin equation, the probability that the virus arrives at a nuclear pore before being degraded at a rate k_0 can now be calculated by solving a narrow escape problem. The assocated FP equation takes the form

$$\frac{\partial p}{\partial t} = D\nabla^2 p(\mathbf{r},t) - \nabla \cdot \mathbf{b}(\mathbf{r})p(\mathbf{r},t) - k_0 p(\mathbf{r},t) \quad (4.79)$$

on the annular region Ω of Fig. 22, together with the boundary conditions

$$p(\mathbf{r},t) = 0, \mathbf{r} \in \partial N_a, \quad J(\mathbf{r},t) \cdot \mathbf{n} = 0, \ \mathbf{r} \in \partial\Omega - \partial N_a.$$

The boundary $\partial\Omega$ of the annulus is taken to be reflecting everywhere except for the surface ∂N_a of the nucleus occupied by nuclear pores, which are taken to be perfect absorbers. Asymptotic analysis then shows that the hitting probability $\mathcal{P}$ and conditional MFPT $\mathcal{T}$ are (Lagache *et al.*, 2009a; Lagache and Holcman, 2008)

$$\mathcal{P} = \frac{b(\delta)}{b(\delta) + 2\delta k_0\nu}, \quad \mathcal{T} = \frac{2\delta\nu}{2\delta k_0\nu + b(\delta)}, \quad (4.80)$$

where $\nu = \log(1/\epsilon)$ with ϵ the fraction of the nucleus covered by nuclear pores.

G. Exclusion processes

So far we have considered a single molecular motor or motor/cargo complex moving along a filament track. However, in practice there could be many active particles moving along the same track, which could interact with each other and exhibit some form of collective behavior. This has motivated a number of studies that model the movement of multiple motor particles as an asymmetric exclusion process (ASEP) (Evans *et al.*, 2003; Klumpp and Lipowsky, 2003; Kolomeisky, 1998; Lipowsky *et al.*, 2001; Nowak *et al.*, 2007a; Parmeggiani *et al.*, 2003, 2004; Popkov *et al.*, 2003; Pronina and Kolomeisky, 2007). In the simplest version of such models, each particle hops unidirectionally at a uniform rate along a 1D lattice; the only interaction between particles is a hard-core repulsion that prevents more than one particle occupying the same lattice site at the same time. This so–called totally asymmetric exclusion process (TASEP) is combined with absorption/desorption (Langmuir) kinetics, in which individual particles can bind to or unbind from the track, see Fig. 23. The TASEP has become the paradigmatic model of non-equilibrium stochastic processes, and a variety of analytical methods have been developed to generate exact solutions for the stationary state, see (Blythe and Evans, 2007; Chou *et al.*, 2011; Schadschneider *et al.*, 2010) and references therein. However, when Langmuir kinetics or other biologically motivated extensions of TASEP are included, it is no longer possible to obtain exact solutions so that some form of mean-field approximation is required.

1. Asymmetric exclusion process and the hydrodynamic limit

Let us consider in more detail the system shown in Fig. 23, which consists of a finite 1D lattice of N sites labeled $i = 1, \ldots, N$. The microscopic state of the system is given by the configuration $\mathcal{C}$ that specifies the distribution of identical particles on the lattice. That is, $\mathcal{C} = \{n_1, \ldots, n_N\}$ where each occupation number $n_i = 1$ if the i-th site is occupied by a single particle and $n_i = 0$ if the site is vacant. Exclusion effects preclude more than one particle at any site. Thus, the state space consists of 2^N configurations. Let $\mathcal{P}(\mathcal{C},t)$ demote the probability of finding a particular configuration $\mathcal{C}$ at time t. The evolution of this probability distribution is described by a master equation:

$$\frac{d\mathcal{P}(\mathcal{C},t)}{dt} = \sum_{\mathcal{C}'\neq\mathcal{C}} [\mathcal{W}_{\mathcal{C}'\to\mathcal{C}}\mathcal{P}(\mathcal{C}',t) - \mathcal{W}_{\mathcal{C}\to\mathcal{C}'}\mathcal{P}(\mathcal{C},t)].$$
(4.81)

The transition rate $\mathcal{W}_{\mathcal{C}\to\mathcal{C}'}$ from configuration $\mathcal{C}$ to $\mathcal{C}'$ is determined from the following set of rules (Parmeggiani *et al.*, 2003):

(a) at sites $i = 1, \ldots, N-1$, a particle can jump to site $i+1$ at a unit rate if the latter is unoccupied;

(b) at site $i = 1$ ($i = N$) a particle can enter (exit) the lattice at a rate α (β) provided that the site is unoccupied (occupied);

(c) in the bulk of the lattice, a particle can detach from a site at a rate ω_D and attach to an unoccupied site at a rate ω_A.

Rules (a) and (b) constitute a TASEP with open boundary conditions, whereas rule (c) describes Langmuir kinetics. It follows that the evolution of the particle densities $\langle n_i \rangle$ away from the boundaries is given by the exact equation

$$\frac{d\langle n_i\rangle}{dt} = \langle n_{i-1}(1-n_i)\rangle - \langle n_i(1-n_{i+1})\rangle + \omega_A\langle 1-n_i\rangle - \omega_D\langle n_i\rangle.$$
(4.82)

Here $\langle n_i(t)\rangle = \sum_{\mathcal{C}} n_i \mathcal{P}(\mathcal{C},t)$ etc. Similarly, at the boundaries

$$\frac{d\langle n_1\rangle}{dt} = -\langle n_1(1-n_2)\rangle + \alpha\langle 1-n_1\rangle - \omega_D\langle n_1\rangle, \quad (4.83a)$$

$$\frac{d\langle n_N\rangle}{dt} = \langle n_{N-1}(1-n_N)\rangle + \omega_A\langle 1-n_N\rangle - \beta\langle n_N\rangle.$$
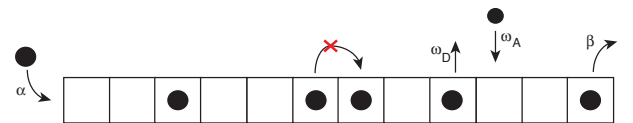(4.83b)

FIG. 23 Schematic diagram of TASEP with Langmuir kinetics, in which particles can spontaneously detach and attach at rates ω_D and ω_A, respectively.

Note that in the absence of any exclusion constraints, Eq. (4.82) reduces to a spatially discrete version of the unidirectional PDE Eq. (4.18a), with $p_+(n_i \Delta x, t) = \langle n_i \rangle$, $\beta_+ = \omega_D$, and $p_0 \alpha = \omega_A$ and $v_+/\Delta x = 1$. The goal is to find a non- equilibrium stationary state for which the current flux J along the lattice is a constant. It then follows that J has the exact form

$$J = \alpha \langle 1 - n_1 \rangle = \langle n_i(1 - n_{i+1}) \rangle = \beta \langle n_N \rangle, \quad i = 1, N-1.$$

Eqs. (4.82) and (4.83) constitute a non-trivial many-body problem, since in order to calculate the time evolution of $\langle n_i \rangle$ it is necessary to know the two-point correlations $\langle n_{i-1}(1 - n_i) \rangle$. The latter obey dynamical equations involving three–point and four-point correlations. Thus, there is an infinite hierarchy of equations of motion. However, progress can be made by using a mean-field approximation and a continuum limit in order to derive a PDE for the density of particles (Evans *et al.*, 2003; Parmeggiani *et al.*, 2004). The mean–field approximation consists of replacing two-point correlations by products of single–site averages:

$$\langle n_i n_j \rangle = \langle n_i \rangle \langle n_j \rangle.$$

Next introduce the infinitesimal lattice spacing ϵ and set $x = k\epsilon$, $\rho(x, t) = \rho_k(t) \equiv \langle n_k(t) \rangle$. The continuum limit is then defined according to $N \to \infty$ and $\epsilon \to 0$ such that the length of the track $L = N\epsilon$ is fixed. (Fix length scales by setting $L = 1$). Expanding $\rho_{k\pm1}(t) = \rho(x \pm \epsilon, t)$ in powers of ϵ gives

$$\rho(x \pm \epsilon, t) = \rho(x) \pm \epsilon \partial_x \rho(x, t) + \frac{1}{2} \epsilon^2 \partial_{xx} \rho(x, t) + \mathcal{O}(\epsilon^3).$$

Finally, rescaling the absorption/desorption rates according to $\omega_A = \Omega_A \epsilon, \omega_D = \Omega_D \epsilon$, and rescaling time $\tau = \epsilon t$, Eq. (4.82) becomes to $\mathcal{O}(\epsilon)$

$$\frac{\partial \rho}{\partial \tau} = \frac{\epsilon}{2} \frac{\partial^2 \rho}{\partial x^2} - (1 - 2\rho)\frac{\partial \rho}{\partial x} + \Omega_A(1 - \rho) - \Omega_D \rho. \quad (4.84)$$

Similarly, Eq. (4.83) reduces to the boundary conditions $\rho(0) = \alpha, \rho(1) = 1 - \beta$. In the continuum limit the flux takes the form

$$J(x, t) = -\frac{\epsilon}{2} \frac{\partial \rho}{\partial x} + \rho(1 - \rho). \quad (4.85)$$

Note that it is also possible to extend the mean-field approximation to ASEP with slowly spatially varying hopping rates, although now the effective diffusivity in the hydrodynamic limit now depends on the density (Lakatos *et al.*, 2006).

The next step is to find a stationary non equilibrium state for which the current J is constant, and to determine the corresponding stationary density profile. This then generates a phase diagram with respect to the parameters α, β and fixed Ω_A, Ω_D. In the case of a pure

TASEP, the phase diagram can be calculated explicitly (Blythe and Evans, 2007; Krug, 1991). Set $\Omega_A = \Omega_D = 0$ in Eq. (4.84), and consider constant current solutions $J(x, t) = J$. Rewrite Eq. (4.85) in the form

$$\frac{\partial \rho}{\partial x} = -\frac{2}{\epsilon}(\rho - r_+)(\rho - r_-), \quad (4.86)$$

with

$$r_\pm = \frac{1}{2} \left[1 \pm \sqrt{1 - 4J_0} \right], \quad (4.87)$$

Eq. (4.86) is easily integrated from the left-hand boundary, say, to give

$$\frac{(\rho(x) - r_+)(\rho(0) - r_-)}{(\rho(x) - r_-)(\rho(0) - r_+)} = e^{-2(r_+ - r_-)x/\epsilon}. \quad (4.88)$$

with $\rho(0) = \alpha$. The unknown current J is obtained by setting $x = 1$ and using the boundary condition $\rho(1) = 1 - \beta$. The stationary density profile can then be constructed explicitly by carrying out an asymptotic expansion with respect to the small parameter ϵ. First, suppose that $J < 1/4$ so $r_\pm$ are real. Denote the $\mathcal{O}(1)$ approximation of the current by J_0. If $r_+ \approx 1 - \beta$ so that $J_0 = \beta(1 - \beta)$ and $r_- \approx \beta$, then the bulk of the domain is in a high density (HD) phase. Since $r_+ > r_-$ it follows that $\beta < 1/2$. Eq. (4.86) implies that the density profile is flat except for a boundary layer close to $x = 0$. Similarly, there exists a low density (LD) phase when $r_- \approx \alpha$, for which $J_0 = \alpha(1 - \alpha)$, $\rho_+ \approx (1 - \alpha)$ and $\alpha < 1/2$; there is now a boundary layer at $x = 1$. Finally, in the case $J > 1/4$ (so $r_\pm$ are complex) one finds that the density profile consists of a flat region at the centre of the domain where $\rho \approx 1/2$ and $J_0 = 1/4$ with boundary layers now at both ends. Moreover, writing $J = 1/4 + \Delta J$ it can be seen that $r_+ - r_- = i\sqrt{\Delta J}$. In order to avoid fast spatial oscillations in the profile (4.88), one requires $\Delta J = \mathcal{O}(\epsilon^2)$. Carrying out a perturbation expansion of Eq. (4.85) in powers of ϵ then establishes that $\rho(x) - 1/2$ varies as $1/x$ as one moves away from the left-hand boundary. A schematic illustration of the phase diagram for pure TASEP is shown in Fig. 24.

2. Method of characteristics and shocks

Eq. (4.84) is mathematically similar in form to the viscous Burger's equation with additional source terms (Ockendon *et al.*, 2003). Thus, one expects singularities such as shocks in the density ρ to develop in the inviscid or non-dissipative limit $\epsilon \to 0^+$. This can be investigated more directly by setting $\epsilon = 0$ in Eq. (4.84), which then takes the form of a standard quasilinear PDE

$$\frac{\partial \rho}{\partial \tau} + (1 - 2\rho)\frac{\partial \rho}{\partial x} = \Omega_A(1 - \rho) - \Omega_D \rho. \quad (4.89)$$
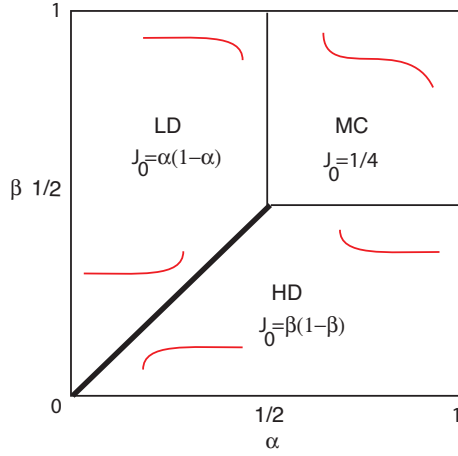
FIG. 24 Mean-field phase diagram for the TASEP showing the regions of α, β parameter space where the low-density (LD), high-density (HD) and maximal-current (MC) phases exist. Schematic illustrations of the density profiles in the various regions are shown in red.

A well known method for studying such equations is to construct characteristic curves $x = x(\tau)$ along which $\rho(\tau) \equiv \rho(x(\tau), \tau)$ satisfies

$$\frac{d\rho}{d\tau} = \frac{\partial \rho}{\partial \tau} + \frac{dx}{d\tau} \frac{\partial \rho}{\partial \tau}.$$

Comparison with Eq.n (4.89) leads to the characteristic equations (Evans *et al.*, 2003; Kolomeisky *et al.*, 1998)

$$\frac{dx}{d\tau} = 1 - 2\rho, \quad \frac{d\rho}{d\tau} = \Omega_A(1 - \rho) - \Omega_D\rho. \qquad (4.90)$$

These equations can be interpreted as kinematic waves that propagate changes in density that move at a variable speed $1 - 2\rho$.
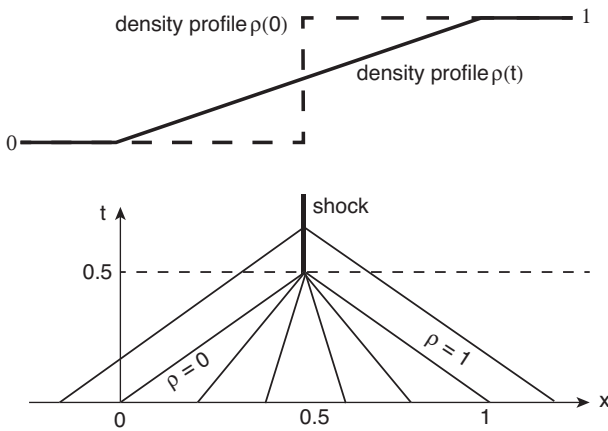

FIG. 25 Formation of a shock for Eq. (4.91). The characteristics are straight lines of speed $1 - 2\rho$ with ρ constant along a characteristic. The initial density profile evolves into a stationary shock solution.

In order to illustrate the basic method of analysis, let us return to a pure TASEP where $\Omega_A = \Omega_D = 0$. Eq. (4.89) then simplifies to the kinematic wave equation

$$\frac{\partial \rho}{\partial \tau} + \frac{\partial J_0(\rho)}{\partial x} = 0, \quad J_0(\rho) = \rho(1 - \rho) \qquad (4.91)$$

and the characteristic become straight lines along which ρ is constant. Ignoring boundary effects for the moment, the density profile at time t is determine by the propagation of the initial density $\rho(x, 0)$ along characteristics as illustrated in Fig. 25. Since higher densities propagate more slowly than lower densities, an initial linear density profile steepens until a shock is formed at the points of intersection where pairs of characteristics meet. In general, a shock propagates with a speed v_S determined by the so called Rankine-Hugonoit condition (Ockendon *et al.*, 2003):

$$v_S = \frac{J_0(\rho_2) - J_0(\rho_1)}{\rho_2 - \rho_1} = 1 - \rho_1 - \rho_2 \qquad (4.92)$$

where ρ_1, ρ_2 are the densities on either side of the shock. For the particular initial density profile shown in Fig. 25, $\rho_1 = 0$ and $\rho_2 = 1$ so that the shock is stationary ($v_S = 0$). The possibility of stationary shocks reflects the fact that the current $J_0(\rho) = \rho(1 - \rho)$ has a maximum, which means that two different densities can have the same current on either side of the shock.

The method of characteristics and kinematic wave theory yields insights into the dynamics underlying the formation of the various stationary phases shown in Fig. 24 (Blythe and Evans, 2007; Kolomeisky *et al.*, 1998; Krug, 1991). The basic idea is to consider kinematic waves propagating from the left-hand and right-hand boundaries, respectively, which act as particle reservoirs with corresponding densities $\rho(0) = \alpha$ and $\rho(1) = 1 - \beta$. A kinematic wave propagates from the left-hand (right-hand) boundary with speed $1 - 2\alpha$ ($2\beta - 1$). Hence, if $\alpha < 1/2, \beta < 1/2$, both waves propagate into the interior of the domain and meet somewhere in the middle to form a shock that propagates with speed $v_S = \beta - \alpha$. If $\beta > \alpha$ then the shock moves to the right-hand boundary and the bulk of the domain is in a low-density (LD) state with $\rho \approx \alpha < 1/2$. On the other hand, If $\beta < \alpha$ then the shock moves to the left-hand boundary and the bulk of the domain is in a high-density (HD) state with $\rho \approx 1 - \beta > 1/2$. Note that the line separating the HD and LD phases, $\alpha = \beta < 1/2$, is a coexistence line. The system consists of a low density region separated from a high density region by a shock. Once higher order dissipative effects are included, this shock diffuses freely between the ends of the domain, so that the average density profile is linear. In the case $\alpha > 1/2$ or $\beta > 1/2$, the kinematic wave associated with that boundary does not propagate into the interior so that the density associated with the other boundary dominates. Finally, if

both $\alpha > 1/2$ and $\beta > 1/2$ then the steady-state bulk solution has the maximal current density $\rho_m = 1/2$. In order to show this, and to determine how bulk solutions match the boundary conditions, it is necessary to include dissipation effects as in the previous section.

The above analytical arguments can be extended to the full molecular motor model that combines TASEP with Langmuir kinetics (Evans *et al.*, 2003; Parmeggiani *et al.*, 2003, 2004). When $\Omega_A, \Omega_D \neq 0$ the characteristics are curves in the $x - t$ plane. For example, consider the propagation of density fluctuations along a characteristic starting at the left boundary with $\rho = \alpha < 1/2$ and $\alpha < K/(K + 1)$, where $K = \Omega_A/\Omega_D$. It follows from Eq. (4.90) that initially the fluctuation propagates along the characteristic with decreasing speed and increasing density. If $K/(1 + K) < 1/2$ then ρ will approach the constant value $\rho = K/(K + 1)$ and the speed approaches a constant value. However, if $K/(1 + K) > 1/2$ then after a finite time the density reaches $\rho = 1/2$ and propagation ceases. A similar analysis holds for characteristics propagating from the right boundary. Furthermore, characteristics propagating from opposite boundaries can again intersect, implying multivalued densities and thus a breakdown of the quasilinear equation. The resulting shock has the same wave speed as pure TASEP. Of particular interest are stationary solutions for which the current $J = \rho(1 - \rho)$ is constant so that any shock solution is stationary ($v_S = 0$). To a first approximation, these can be obtained by finding steady–state solutions of the mean-field Eq. (4.89):

$$(1 - 2\rho)\frac{\partial \rho}{\partial x} - \Omega_D[K - (1 + K)\rho] = 0. \qquad (4.93)$$

The occurrence of stationary shocks is consistent with the observation that this is a first–order ODE but there are two boundary conditions. One thus proceeds by integrating from the left boundary where $\rho(0) = \alpha$ to obtain a density profile $\rho_L(x)$ and then integrating from the right boundary where $\rho(1) = 1 - \beta$ to obtain a second density profile $\rho_R(x)$. The full solution is constructed by matching the two profiles at a shock whose position also has to be determined. If the shock lies outside the unit interval, then it is necessary to include at least one boundary layer. A detailed analysis of the steady-state solutions with coexisting low and high density phases, and the corresponding phase-diagram with respect to the parameters $(\alpha, \beta, \Omega_D, \Omega_A)$ can be found in (Evans *et al.*, 2003; Parmeggiani *et al.*, 2004). If the effects of dissipation are also taken into account then the sharp interfaces and boundary layers become smooth fronts of size $\mathcal{O}(1/\epsilon)$.

3. mRNA translation by ribosomes

One of the first examples of a TASEP model in biology was proposed by Gibbs and collaborators in their study of
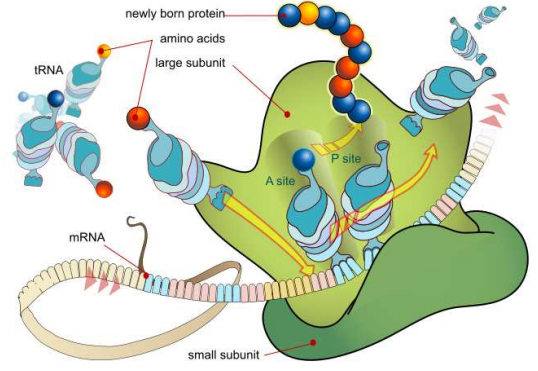

FIG. 26 Diagram showing how the translation of the mRNA and the synthesis of proteins is made by ribosomes. [By LadyofHats (Public domain), via Wikimedia Commons]

the translation of messenger RNA (mRNA) by ribosomes during protein synthesis (MacDonald and Gibbs., 1969; MacDonald *et al.*, 1968). Proteins are macromolecules formed from chains of amino acids, and the blueprint for how these proteins are synthesized is contained in the DNA of the cell nucleus. Protein synthesis involves two stages: transcription of genetic information from DNA to messenger RNA (mRNA) by RNA polymerase, and translation from mRNA to proteins through ribosome translocation. The mRNA carries genetic information, encoded as triplets of nucleotides known as codons. Since there are four nucleotides (A, U,C, G), there are 64 distinct codons, e.g., AUG, CGG, most of which code for a single amino acid. The process of translation consists of ribosomes moving along the mRNA without backtracking (from one end to the other, technically known as the 5' end to the 3' end) and is conceptually divided into three major stages: initiation, elongation and termination. Each elongation step invokes translating or 'reading' of a codon and the binding of a freely diffusing transfer RNA (tRNA) molecule that carries the specific amino acid corresponding to that codon. The basic translation machinery is illustrated in Fig. 26.

The simplest model of translation is a pure TASEP. However, as originally highlighted by MacDonald and Gibbs. (1969); MacDonald *et al.* (1968) and recently reviewed by Chou *et al.* (2011); Zia *et al.* (2011), this considerably oversimplifies the biology. For example, ribosomes are large molecules so that they extend over several codons or lattice sites (around $l = 12$). In order to extend TASEP to multi-site particles, it is first necessary to spec-
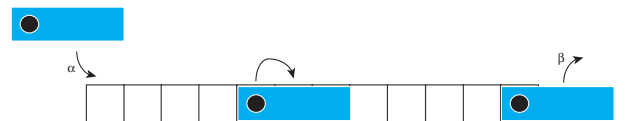

FIG. 27 A TASEP with extended particles of size $l = 3$.

ify the rules for entry and exit of a ribosome. One possibility is 'complete entry, incremental exit', which assumes that a ribosome enters completely provided the first l lattice sites are vacant, whereas it exits one step at a time (Chou and Lakatos, 2003). Inclusion of extended objects considerably complicates the analysis even though the basic structure of the phase diagram is preserved (Chou and Lakatos, 2003; Shaw *et al.*, 2003). In contrast to pure TASEP, there does not currently exist an exact solution, although mean field approximations do provide useful insights. A second biologically motivated modification of TASEP is to include site–dependent hopping rates (Chou and Lakatos, 2004; Dong *et al.*, 2007; Foulaadvand *et al.*, 2008; Kolomeisky, 1998). This is motivated by the fact that the local hopping rate depends on the relative abundance of specific amino-acid carrying tRNA. Using a combination of Monte Carlo simulations and mean field theory it can be shown, for example, that two defects (regions of slow hopping rates) decrease the steady-state current more when they are close to each other. Finally, note that a number of researchers have developed models that take into account intermediate steps in the translocation of a ribosome along the mRNA, including the binding of tRNA to the ribosome and hydrolysis (Basu and Chowdhury, 2007; Ciandrini *et al.*, 2010; Garai *et al.*, 2009; Reichenbach *et al.*, 2006).

H. Motor transport and random intermittent search processes

So far we have considered models of motor-driven intracellular transport without any reference to the process whereby the cargo or load carried by one or more motors is delivered to the correct location within a cell. It is unlikely that a target is selected according to where a mictrotubular track terminates, since a cargo could be released from its associated motors at any point along the track. Moreover, targeted delivery probably uses the same microtubular "highway" as more general, non–targeted intracellular trafficking. It would also be difficult to establish global chemical concentration gradients aimed at guiding a motor–driven cargo to a specific target, as such signals would be drowned out by the many other signals originating from additional intracellular targets. Therefore, instead of thinking of motor-driven cargo transport as a direct path to a given target, the random intermittent motion of motor–driven cargo observed in experiments suggests that the cell maintains a distribution of mobile cargo throughout its interior, and that delivery of a cargo to a specific target is a stochastic process (Bressloff and Newby, 2009; Loverdo *et al.*, 2008; Newby and Bressloff, 2010b). Some of the molecular mechanisms that cause a cargo to attach or detach from a molecular motor have been identified (Goldstein *et al.*, 2008). In most cases, a protein dissolved in the cytosol reacts with an adaptor protein that binds a cargo to the motor, causing the cargo to be released. However, when a cargo is pulled at a relatively high velocity it doesn't have much time to explore local space and is therefore much less likely to participate in such a reaction. Therefore, one possible interpretation of the frequent pauses observed during motor transport is that it provides a mechanism to improve the reaction kinetics required to localize the cargo to its target by giving it more time to explore local space. This then leads to a simple model of cargo delivery in which there are transitions of the internal state of the motor complex between directed movement states and stationary or slowly diffusing searching states. If the transitions between these states are governed by chemical reactions under the influence of thermodynamic fluctuations, then the model becomes a random intermittent search processs.

Random search has recently been used to model a wide range of problems (Benichou *et al.*, 2011b), including the behavior of foraging animals (Bell, 1991; Benichou *et al.*, 2005; Viswanathan *et al.*, 1999; Viswanathan *et al.*, 2011) and the active transport of reactive chemicals in cells (Bressloff and Newby, 2009; Loverdo *et al.*, 2008). The facilitated diffusion of protein-DNA interactions can also be thought of as a random intermittent search process, see Sec. II.E. Random intermittent search falls within a class of random processes characterized by a particle with both an 'internal' and 'external' state. The external state typically represents the spatial location or position of the particle, and one or more boundary conditions may apply to the process that represent the physical domain in which it moves. The motion of the particle depends on its internal state, which can be continuous but is usually discrete. For example, the tug-of-war model from Sec. IV.B is a process where the position, or external state, changes deterministically at a constant velocity, while the velocity depends upon the discrete internal state, the randomly changing number of motors bound to the microtubule. In general, the external state need not change deterministically, but could also fluctuate. For example, one could include diffusion of the cargo and add a continuous noise term whose amplitude depends on the internal state.

In order to formulate motor-cargo transport as a random intermittent search process, consider a single particle moving on a 1D track of length L as shown in Fig. 28. In contrast to the models considered in Sec. IV.A-IV.G, we now assume that there exists a hidden target of width $2l$ centered at X within the interior of the domain. We also assume that if the particle is within range of the target and is in a slowly moving search state then it can 'find' the target at a rate k. Within the context of motor-driven cargo transport, it is assumed that when the target is found the particle is immediately removed from the system, that is, the cargo (with or without its associated set of molecular motors) is delivered to the target. Hence, the target is treated as a partially absorbing

trap. One possible application of a 1D model would be to vesicular transport along the axons and dendrites of neurons, where microtubules are aligned in parallel with the (+) end oriented away from the cell body. (In the case of dendritic domains close to the cell body, the polarities may be randomly distributed). The hidden target could then be a synapse, an intracellular compartment such as an endosome, or the growth cone of an elongating axon, see Sec. IV.D. In general, the transport process is expected to be biased, with newly synthesized macromolecules transported away from the cell body (anterograde transport) whilst products requiring degradation are transported back to the cell body (retrograde transport).

It is straightforward to incorporate a hidden target into the general n-state PDE model (4.20) of a motor complex moving in a 1D domain by taking

$$\frac{\partial \mathbf{p}}{\partial t} = A\mathbf{p} + \mathcal{L}(\mathbf{p}), \qquad (4.94)$$

where $A \in \mathbb{R}^{n \times n}$ again specifies the transition rates between each of the n internal motor complex states, and the diagonal operator $\mathcal{L}$ now has the modified form

$$\mathcal{L}_j = [-v_j \partial_x + D_{0,j} \partial_x^2 + k_j \chi(x - X)]. \qquad (4.95)$$

As before, v_j is the velocity of internal state j and $D_{0,j}$ is the corresponding diffusivity. The additional term takes into account the probability flux into the target with k_j the rate for internal state j and χ is the indicator function

$$\chi(x) = \begin{cases} 1, & \text{if } |x| < l \\ 0, & \text{otherwise.} \end{cases} \qquad (4.96)$$

In general k_j will only be non-zero for a subset of states. For example, in the 3-state model of Eqs. (4.18), $k_j = k\delta_{j,0}$, that is, the unbound stationary or diffusing state is identified as the search state.

In the case of the more biophysically realistic tug-of-war model, see Sec. IV.B, the identification of the search

FIG. 28 Diagram depicting a motor-cargo complex performing a random intermittent search for a hidden target on a one–dimensional track of length L. The motor-cargo complex is transported along a microtubule by two populations of molecular motors with opposing directional preferences. When equal numbers of each type of motor are bound to the microtubule, the motor-cargo complex is in a slowly moving search state and can find the target provided that it lies within the target domain of width $2l$ centered at $x = X$. Target detection rate is k.

states is more complicated. The simplest scenario is that the cargo locates its target after it becomes fully detached from the microtubule and diffuses within distance of its target, where it binds to scaffolding proteins and is separated from its molecular motors. However, if many molecular motors are bound to the cargo, the waiting time between diffusive searching events can be too large to reliably deliver the cargo. Moreover, if the cargo is large so that its diffusivity is low or the cargo is moving through a crowded and confined domain, diffusive motion may be restricted, preventing the cargo from reaching the target. Another possibility is that subcellular machinery is present to detach the cargo from its motors or inhibit the activity of the motors so that scaffolding proteins can bind to and sequester the cargo. Delivery then changes from a diffusion limited reaction to a waiting time that depends on a reaction occurring between the motor-cargo complex and biomolecules (either freely diffusing or anchored) local to the target while its moving along the microtubule. If details of the localization mechanism are unknown then the simplest model is to assume that this waiting time is approximately exponential and to associate a target detection rate k_j with each motor state. The model can be simplified further by assuming that detection is unlikely while only one species of motors is engaged and pulling the cargo at its maximum (forward or backward) velocity. This suggests assigning a single target detection rate k to those states that have sufficiently low speeds (Newby and Bressloff, 2010c). Thus, $k_{(n_+, n_-)} = k\Theta(v_h - v(n_+, n_-))$, where $v(n_+, n_-)$ denotes the velocity when n_+ kinesin and n_- dynein motors are attached to the track and v_h is a velocity threshold.

The efficiency of a given search process can be characterized in terms of two important quantities. The first is the hitting probability Π that a particle starting at x_0 at time $t = 0$ finds the target, that is, the particle is absorbed somewhere within the domain $X - l \leq x \leq X + l$. The second is the conditional MFPT $\mathcal{T}$ for the particle to find the target given that it is eventually absorbed by the target. Let $J(t)$ denote the probability flux due to absorption by the target at X,

$$J(t) = \sum_{j=1}^n k_j \int_{X-l}^{X+l} p_j(x, t) dx, \qquad (4.97)$$

where we have suppressed the initial conditions. It follows that

$$\Pi = \int_0^\infty J(t) dt, \quad \mathcal{T} = \frac{\int_0^\infty t J(t) dt}{\int_0^\infty J(t) dt}. \qquad (4.98)$$

In the case of the 3-state model, it is possible to calculate these quantities directly from the system of PDEs (4.94)(Benichou et al., 2005, 2007, 2011b; Bressloff and Newby, 2009). For more complicated models, the QSS reduction technique presented in Sec. IV.C can be used to reduce the system of PDEs to a scalar FP equation.
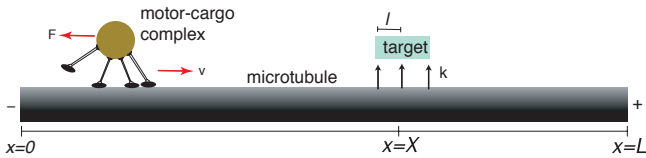
The target detection terms then lead to an inhomogeneous term in the reduced FP equation:

$$\frac{\partial u}{\partial t} = -\frac{\partial}{\partial x}(Vp) + \frac{\partial}{\partial x}\left(D\frac{\partial u}{\partial x}\right) - \lambda\chi(x - X)u, \quad (4.99)$$

with $\lambda = \sum_{j=1}^{n} k_j p_j^{\text{ss}}$, and the vector p_j^{ss} is the space-clamped steady-state distribution (see Sec. IV.C). For the three-state model,

$$\lambda = kp_0^{\text{ss}} = k\left(\frac{1/\alpha}{1/\beta_+ + 1/\beta_- + 1/\alpha}\right). \quad (4.100)$$

There are then three effective parameters that describe the random search process: the drift V, the diffusivity D, and the target detection rate λ. Each of these parameters are themselves functions of the various cargo velocities, transition rates, and target detection rates contained in the full model. The hitting probability and MFPT are still given by Eqs. (4.98) except that now the flux is

$$J(t) = \lambda \int_{X-l}^{X+l} u(x, t)dx. \quad (4.101)$$

1. Mean-field model

Further simplification can be obtained by considering a population of searchers and taking a mean-field limit (Bressloff and Newby, 2012). That is, consider N independent, identical searchers that all start at the origin at time $t = 0$. Each searcher evolves according to the system of PDEs (4.94) or the corresponding FP Eq. (4.99). Denote the FPT to find the target of the jth searcher by T_j, $j = 1, \ldots, N$, with each T_j an independent, identically distributed random variable drawn from the single searcher first passage time distribution $F^{(1)}(t) = \int_0^t J(s)ds$. The random time T to fill the trap is then given by $T = \min(T_1, T_2, ..., T_N)$, and the distribution for T is

$$\begin{aligned}F^{(N)}(t) &= \text{Prob}(T < t) = 1 - \text{Prob}(T > t) \\ &= 1 - \text{Prob}(T_1 > t, T_2 > t, ..., T_N > t) \\ &= 1 - (1 - F^{(1)}(t))^N.\end{aligned}$$

Furthermore, suppose that the rate of detection for a single searcher in internal state j scales as $k_j = \kappa_j/N$ with κ_j independent of j. Set $J(t) = J_0(t)/N$ with $J(t)$ given by Eq. (4.94). It follows that

$$F^{(N)}(t) = 1 - \left(1 - \frac{\kappa}{N}\int_0^t J_0(s)ds\right)^N. \quad (4.102)$$

In the limit $N \to \infty$, the detection rates $k_j \to 0$ so that the probability density functions $p_j(x, t)$ decouple from the target. Moreover, taking the large N limit shows that the FPT distribution for a population of identical searchers is

$$F_\infty(t) \equiv \lim_{N \to \infty} F^{(N)}(t) = 1 - e^{-\mu(t)}, \quad (4.103)$$

with

$$\mu(t) = \int_0^t J_0(s)ds = \sum_{j=1}^{n} \kappa_j \int_0^t \int_{X-l}^{X+l} p_j(x, s)dxds. \quad (4.104)$$

The corresponding hitting probability that at least one particle finds the target in the mean-field limit is

$$\Pi = \lim_{t \to \infty} F_\infty(t) = 1 - e^{-\mu(\infty)}. \quad (4.105)$$

Thus, $\Pi < 1$ if $\mu(\infty) < \infty$. The corresponding conditional MFPT is

$$\mathcal{T} = \frac{\int_0^\infty t\mu'(t)e^{-\mu(t)}}{1 - e^{-\mu(\infty)}}. \quad (4.106)$$

Combining the mean-field approximation with the QSS reduction leads to the FPT distribution (4.103) with

$$\mu(t) = \widehat{\lambda} \int_0^t \int_{X-l}^{X+l} u(x, s)dxds \quad (4.107)$$

and $\widehat{\lambda} = \sum_{j=1}^{n} \kappa_j p_j^{\text{ss}}$. Here $u(x, t)$ is the solution to the FP Eq. (4.99) with $\lambda = 0$. On a semi-infinite domain with a reflecting boundary at the origin, the method of images can then be used to obtain the explicit solution

$$\begin{aligned}u(x, t) = &\frac{1}{\sqrt{\pi Dt}}e^{-(x-Vt)^2/(4Dt)} \\ &- \frac{V}{2D}e^{xV/D}\text{erfc}(\frac{x + Vt}{2\sqrt{Dt}}).\end{aligned} \quad (4.108)$$

Unfortunately, it is not possible to derive an explicit analytical solution for $\mu(t)$, although the integral expressions can be evaluated numerically. Nevertheless, it is possible to determine the hitting probability Π and the large-time behavior of the waiting time density $f_\infty(t) = dF_\infty(t)/dt$ under the approximation $l \ll X$ for which

$$\mu(t) = c\int_0^t u(X, s)ds, \quad c = 2l\widehat{\lambda}. \quad (4.109)$$

First, taking the Laplace transform of $u(x, t)$ gives (Bressloff and Newby, 2012)

$$\widetilde{u}(x, s) = \frac{e^{-[\Gamma(s)-V/2D]x}}{\sqrt{V^2 + 4sD}}\left[2 - \frac{V}{D}\frac{1}{\Gamma(s) + V/2D}\right]$$

with

$$\Gamma(s) = \frac{1}{2}\sqrt{(V/D)^2 + 4s/D}. \quad (4.110)$$

Assuming that $l \ll X$, it follows that

$$\mu(\infty) \approx 2l\widehat{\lambda}\lim_{s \to 0}\widetilde{u}(X, s) = \frac{c}{V}. \quad (4.111)$$

Thus the corresponding hitting probability $\Pi < 1$ for $V > 0$ and $\Pi = 1$ for $V = 0$ (pure diffusion). Second, the large-time behavior of the waiting time density can be obtained by using the following asymptotic expansion of the complementary error function:

$$\text{erfc}(z) = \frac{e^{-z^2}}{\sqrt{\pi} z} \left[1 - \frac{1}{2z^2} \cdots \right].$$

Applying this to Eq. (4.108) with $z = (x+Vt)/(2\sqrt{Dt}) \approx V\sqrt{t}/(2\sqrt{D})$ for large t and $V > 0$, leads to the approximation

$$u(X,t) \sim \frac{2c\sqrt{D}}{V^2\sqrt{\pi t^3}} e^{-V^2 t/(4D)}, \tag{4.112}$$

which is independent of target location X. Substituting this expression into Eq. (4.109) gives

$$\mu(t) \sim \mu(\infty) - \frac{2c}{V\sqrt{\pi}} \left[\frac{4D}{tV^2}\right]^{3/2} e^{-V^2 t/(4D)}, \tag{4.113}$$

On the other hand, for $V = 0$,

$$\mu(t) = c \int_0^t \frac{1}{\sqrt{\pi Dt}} e^{-X^2/(4Dt)} \sim 2c\sqrt{t/\pi D}, \tag{4.114}$$

assuming that $e^{-X^2/(4Dt)} \sim 1$ for large t. The large-time asymptotic approximation for $\mu(t)$ determines how the waiting time density, $f_\infty(t)$, scales with time. For $V = 0$,

$$f_\infty(t) \propto t^{-1/2} e^{-\hat{c}\sqrt{t}}, \tag{4.115}$$

with $\hat{c} = 2c/\sqrt{\pi D}$, and for $V > 0$

$$f_\infty(t) \propto t^{-1/2} e^{-V^2 t/(4D)}. \tag{4.116}$$

For the sake of illustration, consider the 3-state model of Eqs. (4.18), for which V, D, λ are given by Eqs. (4.47) and (4.100). In the case of a single random intermittent searcher on a finite track of length L with reflecting boundary conditions at both ends $x = 0, L$ (so that $\Pi = 1$) and unbiased transport ($\beta_+ = \beta_- = \beta$), it can be shown that there exists an optimal search strategy in the sense that there exists a unique set of transition rates α, β for which the MFPT is minimized (Benichou et al., 2005, 2007, 2011b). On the other hand, for directed intermittent search ($\beta_+ > \beta_-$) on a semi–infinite domain or a finite domain with an absorbing boundary at $x = L$ (so that $\Pi < 1$), a unique optimal strategy no longer exists (Bressloff and Newby, 2009; Newby and Bressloff, 2010b). One finds that a similar situation holds if there is a population of N independent searchers (Bressloff and Newby, 2012). First, consider an unbiased random intermittent search process in the mean–field population model, for which $N \to \infty$ and $\beta_+ = \beta_- = \beta$ ($V = 0$). In Fig. 29(a) the MFPT is plotted as a function of (i) the
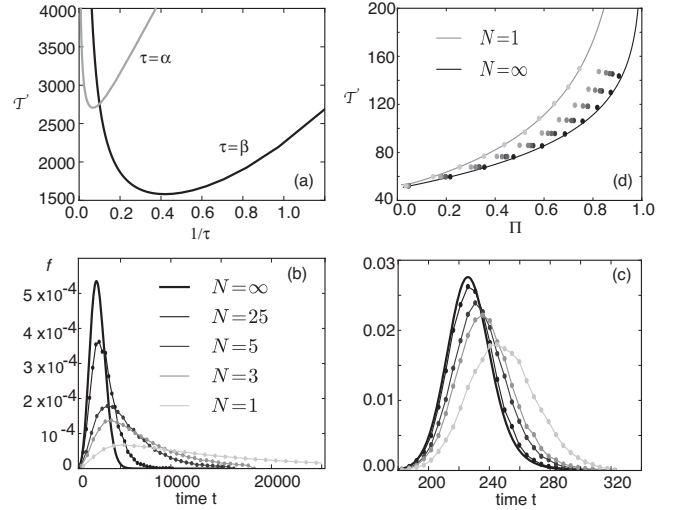

FIG. 29 (a) Unbiased ($\beta_+ = \beta_- = \beta$) random intermittent search in the mean–field population model. The MFPT vs (i) the average search time $1/\alpha$ with $\beta = 1/\epsilon$ and (ii) the average duration $1/\beta$ of the moving (forward and backward) state with $\alpha = 2/\epsilon$. Each curve has a minimum MFPT for a given value of α and β. Parameter values used are $\epsilon = 0.1$, $k = 5/N$, $X = 50$, and $l = 0.25$. (b) First passage time density for an unbiased search with same parameters as (a). The solid curve shows the analytical density function in the mean field limit and the remaining curves are histograms obtained from 10^4 Monte-Carlo simulations for different numbers of searchers N. (c) Corresponding first passage time density for a biased search with $\alpha = 1/\epsilon$, $\beta_+ = 1/\epsilon$, $\beta_- = 2/\epsilon$, $\epsilon = 0.1$, $k = 5/N$, $X = 50$, and $l = 0.25$. (d) The MFPT vs hitting probability for population model. Each curve is parameterized by $0 \le \beta_+ \le \beta_-$. Analytical results are shown as lines, with the single searcher in grey and the mean field limit ($N = \infty$) in black. Averaged Monte Carlo simulations (10^4 simulation each) are shown as symbols, sets ranging from grey to black, with a different value of N used in each set. From grey to black there are six sets of simulations with $N = 1, 2, 3, 4, 5, 25$, respectively. Parameter values are the same as c).

average duration of the search phase, $1/\alpha$, and (ii) the average duration of the ballistic phase, $1/\beta$. In both cases there exists a minimum MFPT for a particular choice of α, β, consistent with the single-searcher regime.

Next, consider how the search process changes as more searchers are added. In particular, the first passage time density is approximated by Monte-Carlo simulations for different values of N, and the results are compared to the analytical mean field results. This illustrates how the single-searcher process ($N = 1$) is related to the mean-field population search process ($N \to \infty$). In Fig. 29(b) the unbiased case is shown. The most significant difference is found in the large time behavior, with power-law scaling $t^{-3/2}$ for the single search and the so-called stretched exponential scaling $e^{-\hat{c}\sqrt{t}}$ (see Eqn. (4.115)) for the mean field $N \to \infty$ limit. A similar plot showing the first passage time density for a biased search ($\beta_+ < \beta_-$ so that $V > 0$) is shown in Fig. 29c). In this case, adding

more searchers has little qualitative effect on the first passage time density, each case having the same exponential large time scaling (see Eqn. (4.115)). In both cases, the results, show that adding more searchers decreases the mean search time and the variance. The analysis of the mean-field model showed that the hitting probability is less than unity when the velocity bias is positive (i.e. when $\beta_+ < \beta_-$ so that $V > 0$). In Fig. 29(d), the MFPT is plotted against the hitting probability for different values of N. Each curve is parameterized by β_+, the rate of leaving the forward-moving state, with $0 < \beta_+ < \beta_-$. By changing the value of β_+, any hitting probability can be achieved. As $\beta_+ \to \beta_-$ the searcher's motion becomes unbiased, and the hitting probability increases to unity. However, as the searchers become more unbiased the MFPT also increases, in other words, an optimal search strategy no longer exists. Analytical results for the single searcher case ($N = 1$) and the mean-field limit ($N = \infty$) are shown as solid curves (black and grey, respectively) and to connect the two, averaged Monte-Carlo simulations are shown (as dots) for different values of $N = 1, 2, 3, 4, 25$ (each dot is colored in greyscale from $N = 1$ in black to $N = 25$ in light grey). Ten different sets of Monte-Carlo simulations are run corresponding to ten different values of β_+, and in each set the hitting probability decreases and the MFPT increases as more searchers are added.

2. Local target signaling

In the case of directed intermittent search there is a playoff between minimizing the MFPT and maximizing the hitting probability. One way to enhance the efficiency of the search process would be for the target to generate a local chemical signal that increases the probability of finding the target without a significant increase in the MFPT. This issue has recently been explored using the QSS reduction of the tug-of-war model (Newby and Bressloff, 2010b,c). Two potential signaling mechanisms were considered by the authors, the second of which we will review in more detail here. The first was based on the observation that the stall force and other single motor parameters are strongly dependent on the level of [ATP], see Sec. IV.B. Since ATP concentration ([ATP]) is heavily buffered, a small region of intense ATP phosphorylation around a target could create a sharp, localized [ATP] gradient, which would significantly slow down a nearby motor complex, thus increasing the chances of target detection. The second signaling mechanism involved microtubule associated proteins (MAPs). These molecules bind to microtubules and effectively modify the free energy landscape of motor-microtubule interactions (Telley et al., 2009; Tokuraku et al., 2007). For example, tau is a MAP found in the axon of neurons and is known to be a key player in Alzheimer's disease (Kosik
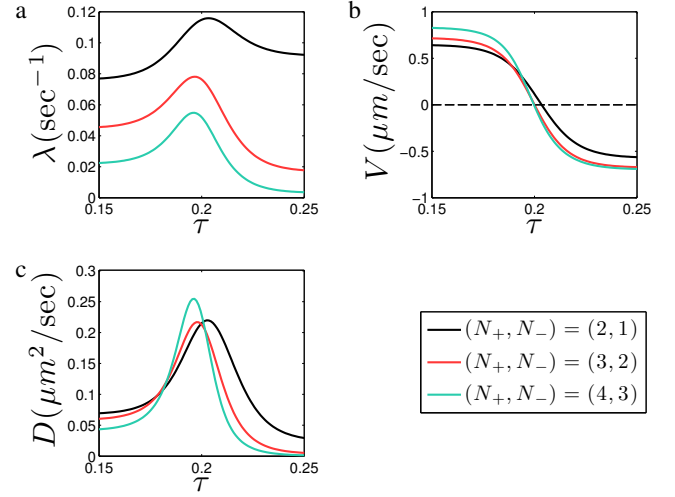

FIG. 30 Effects of tau concentration on the tug-of-war model with N_+ kinesin motors and N_- dynein motors. The stall force F_S, forward velocity v_f and unbinding rate γ_0 are given by Eqs. (4.31)-(4.33) with $[\text{ATP}] = 10^3 \mu M$. The other single motor parameters are (Muller et al., 2008b): $F_d = 3\ pN$, $\gamma_0 = 1\ \text{sec}^{-1}$, $\pi_0 = 5\ \text{sec}^{-1}$, and $v_b = 0.006\ \mu m/\text{sec}$. The corresponding parameters of the FP Eq. are obtained using a QSS reduction and plotted as a function of τ. (a) Effective capture rate λ. (b) Drift velocity V. (c) Diffusivity D.

et al., 1986). Another important MAP, called MAP2, is similar in structure and function to tau, but is present in dendrites (Shaft-Zagardo and Kalcheva, 1998); MAP2 has been shown to affect dendritic cargo transport (Maas et al., 2009). Experiments have shown that the presence of tau or MAP2 on the microtubule can significantly alter the dynamics of kinesin; specifically, by reducing the rate at which kinesin binds to the microtubule (Vershinin et al., 2007). Moreover, the tau- and MAP2-dependent kinesin binding rate have the same form (Seitz et al., 2002). It has also been shown that, at the low tau concentrations affecting kinesin, dynein is relatively unaffected by tau (Dixit et al., 2008).

Newby and Bressloff (2010c) modeled the effects of tau by introducing into the tug-of-war model, Sec. IV.B, the tau concentration-dependent kinesin binding rate

$$\pi_0(\tau) = \frac{\pi_0^{max}}{1 + e^{-\gamma(\tau_0 - \tau)}}, \qquad (4.117)$$

where τ is the dimensionless ratio of tau per microtubule dimer and $\pi_0^{max} = 5\text{s}^{-1}$. The remaining parameters are found by fitting the above function to experimental data (Vershinin et al., 2007), so that $\tau_0 = 0.19$ and $\gamma = 100$. Carrying out the QSS reduction of the tug-war-model then leads to the FP Eq. (4.99) with τ-dependent drift V, diffusivity D and capture rate λ as illustrated in Fig. 30. The most significant alteration in the behavior of the motor-complex is the change in the drift velocity V as a function of τ. The drift velocity switches sign when τ is increased past a critical point. That is, by reducing

the binding rate of kinesin, the dynein motors become dominant, causing the motor-complex to move in the opposite direction. The effects of local changes in τ concentration on the efficiency of random search can now be determined by assuming that within range of the target, $|x - X| < l$, $\tau = \tau_1 > \tau_0$, whereas $\tau = \tau_0$ outside the target, $|x - X| > l$. Carrying out the QSS reduction of the tug-war-model then leads to the FP Eq. (4.99) with x-dependent drift and diffusivity:

$$V(x) = V_0 + \Delta V \chi(x), \quad D(x) = D_0 + \Delta D \chi(x), \quad (4.118)$$

where $\chi(x)$ is the indicator function defined in (4.96), $V_0 = V(\tau_0), D_0 = D(\tau_0)$, $\Delta V = V(\tau_1) - V_0$, and $\Delta D = D(\tau_1) - D_0$. Solving the piecewise-continuous FP equation then determines the hitting probability Π and MFPT $\mathcal{T}$ as functions of τ_1 for fixed τ_0. In Fig. 31, the hitting probability Π and the MFPT $\mathcal{T}$ are plotted as a function of τ_1. As τ_1 is increased above the critical level $\tau_0 = 0.19$, there is a sharp increase in Π but a relatively small increase in the MFPT, confirming that τ can improve the efficacy of the search process.

Another interesting effect of a local increase in τ is that it can generate stochastic oscillations in the motion of the motor-complex (Newby and Bressloff, 2010c). As a kinesin driven cargo encounters the tau-coated trapping region the motors unbind at their usual rate and can't rebind. Once the dynein motors are strong enough to pull the remaining kinesin motors off the microtubule, the motor-complex quickly transitions to $(-)$ end directed transport. After the dynein-driven cargo leaves the tau-coated region, kinesin motors can then reestablish $(+)$ end directed transport until the motor-complex returns to the tau-coated region. This process repeats until the motor-complex is able to move forward past the tau-coated region. Interestingly, particle tracking experiments have observed oscillatory behavior during mRNA transport in dendrites (Dynes and Steward, 2007; Rook et al., 2000). In these experiments, motor-driven mRNA
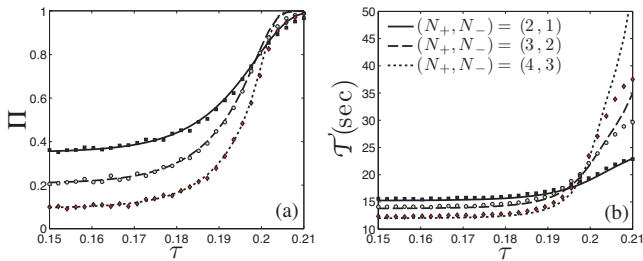
FIG. 31 Effect of adding tau to the target on the capture probability Π and MFPT $\mathcal{T}$ using parameters from Fig. 30. a) The analytical approximation P (solid line) and results from Monte-Carlo simulation. b) The analytical approximation T along with averaged Monte-Carlo simulations. The synaptic trap is located at $X = 10\mu m$, the trapping region has radius $l = 2\mu m$, and the MT track has length $L = 20\mu m$. The capture rate is taken to be $k_0 = 0.5\text{s}^{-1}$.
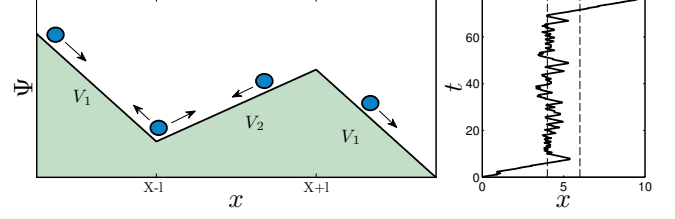
FIG. 32 Diagram showing the effective potential well created by a region of tau coating a MT, and a representative trajectory showing random oscillations.

granules move rapidly until encountering a fixed location along the dendrite where they slightly overshoot then stop, move backwards, and begin to randomly oscillate back and forth. After a period of time, lasting on the order of minutes, the motor-driven mRNA stops oscillating and resumes fast ballistic motion. The duration of the oscillations can be estimated by noting that the FP equation obtained by carrying out the QSS reduction describes a Brownian particle moving in an effective potential well $\Psi(x) = \int_{X-l}^{x} V(x')dx'$, where the drift $V(x)$ of Eq. (4.118) is reinterpreted as a piecewise constant force, see Fig. 32. Depending on the length of the region influenced by the trap, and the magnitude of the drift velocities, the time spent in the potential well can be quite long. Suppose that a Brownian particle starts at the bottom of the potential well. The corresponding mean exit time (MET) (see (2.30)) is

$$M_B = \int_{X-l}^{X+l} \exp\left(-\frac{\Psi(y)}{D(y)}\right) dy \int_{-\infty}^{y} \frac{\exp\left(\frac{\Psi(z)}{D(z)}\right)}{D(z)} dz$$
$$= \frac{2lD_2}{\nu}\left(e^{\frac{\nu}{D_2}} - 1\right)\left(\frac{1}{V_1} + \frac{2l}{\nu}\right) - \frac{4l^2}{\nu},$$

where $\nu = -V_2 2l$ is the depth of the well. In general, the MET will be an exponentially increasing function of the depth of the well. This means that any error generated by the QSS approximation will also grow exponentially. This is typical of large-deviation behavior in a stochastic process where it is well known that diffusion approximations break down. One can still obtain an approximation of the MET using perturbation methods, but they must be applied to the full CK equation (Keener and Newby, 2011; Newby and Keener, 2011).

I. Active transport on DNA

So far we have considered the case where ATP hydrolysis by a molecular motor facilitates active transport along a fixed track. However, it is also possible for ATP hydrolysis by a track to facilitate active transport. Active transport occurs when waves of ATP hydrolysis along the track push a passive element much like ocean waves

push a surfer toward the shore. Several studies have examined track-induced transport (Antal and Krapivsky, 2005; Artyomov *et al.*, 2008; Morozov, 2007; Saffarian *et al.*, 2006). Here, we discuss directed transport of a Holliday junction along DNA (Lakhanpal and Chou, 2007).

A Holliday junction is a site where two segments of double stranded DNA (dsDNA) bind and exchange one of their strands in what is known as genetic recombination. Strands with complimentary base pairs bind and form a junction. The junction then moves along both segments until it reaches a termination point. It is well known that translocation of this junction is an active transport process, requiring energy from ATP hydrolysis. A protein called RecA forms a helical polymer wrapped around a segment of DNA, and interactions between the RecA polymer and the dsDNA drive junction translocation (Klapstein and Bruinsma, 2000). When RecA monomers hydrolyze ATP, the nucleoprotein filament shifts into a different conformational state where the two strands rotate around each other. We refer to this as the activated state.

One possibility for how the Holliday junction moves along dsDNA is by hydrolysis waves along the nucleoprotein filament. This reaction proceeds in waves because activated RecA preferentially catalyzes ATP hydrolysis by the adjacent monomer on the $3'$ side. That is, a monomer hydrolyses ATP much more rapidly when its neighboring monomer (on the $5'$ side) is activated. This asymmetry creates waves of hydrolysis, with a resulting mechanical effect, from the $5'$ to the $3'$ end (hereafter specified as the forward direction) of the DNA strand. It is the mechanical stretching and unwinding of the DNA induced by the hydrolysis wave that propels the junction forward. Consider a model of Holliday junction transport along an infinite lattice of RecA monomers surrounding a dsDNA. Each lattice site can be in one of two states: activated or unactivated. Let S_j be a random variable associated with the jth lattice site. In the activated state $S_j = 1$, and in the unactivated state $S_j = 0$. Transitions between these two states are governed by a Markov switching process,

$$(S_j = 0) \underset{k_0}{\overset{\alpha(S_{j-1})}{\rightleftarrows}} (S_j = 1). \tag{4.119}$$

The rate of transitioning to the activated state depends on the state of the lattice site to the left, that is, $\alpha(0) = k_-$ and $\alpha(1) = k_+$, with $k_+ > k_-$ (see Fig. 33). Because of the coupling between neighboring lattice sites, one must consider transitions between states of the full system. If the track contains a finite number of n sites then the total number of states in the system is 2^n, with each possible state given by the different sequences of 0^{s} and 1^{s}. In other words, the state space corresponds to all of the possible binary words of length n.

As a first step, before including the motion of the junction on the track, one would like to characterize the
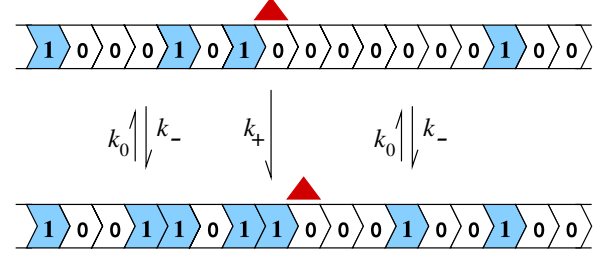

FIG. 33 Diagram describing stochastic hydrolysis dynamics.

steady state properties of the hydrolysis waves on the track. However, analytical solutions are only possible in thermodynamic equilibrium, where directed transport is not possible. Therefore an approximation must be found, and one approach is to use a mean field approximation. From the Master equation governing the process, one can derive a hierarchy of equations for the moments of S_j. This system of equation is not closed so that the equation for the mean, $\sigma_j \equiv \langle S_j \rangle$, depends upon terms such as $\langle S_{j-1}S_j \rangle$. The mean field approximation assumes that $\langle S_{j-1}S_j \rangle \approx \sigma_{j-1}\sigma_j$, and with this assumption, one obtains a system of n equations for each σ_j. However, since we must consider the $n \to \infty$ limit, solving the system of nonlinear differential equations is impractical. The simplest mean-field approximation is to assume that $\sigma_{j-1} \approx \sigma_j = \sigma$, which yields

$$\sigma = \frac{k_+ - 2k_- - k_0 + \sqrt{(k_+ - k_0)^2 + 4k_-k_0}}{2(k_+ - k_-)}. \tag{4.120}$$

When compared to Monte-Carlo simulation results, this approximation is only in qualitative agreement, which suggests that accounting for correlations between adjacent sites is necessary to correctly capture the steady-state behavior.

It is a reasonable assumption that the correlations between sites is short ranged. This motivates an approach called the finite segment mean field theory (FSMFT) approximation (Nowak *et al.*, 2007b). Consider a small segment within the track containing m sites so that the number of states in the system is $M = 2^m$. Clearly, It is much simpler to enumerate the Master equation for this segment than for an infinite lattice. Define the probability density vector $\mathbf{p} = (p_0, \cdots, p_{M-1})^T$ where each p_j corresponds to a different state of the track segment. The master equation is $d\mathbf{p}/dt = A\mathbf{p}$. The simplest mapping of the binary state to the index j is the binary representation of base-ten numbers. For example, if $m = 2$ then $j = 0$ corresponds to the state $(0 \cdot 0)$, $j = 1$ corresponds to $(0 \cdot 1)$, $j = 2 \leftrightarrow (1 \cdot 0)$, and $j = 3 \leftrightarrow (1 \cdot 1)$. In this

example, the matrix of transition rates is

$$
A = \begin{bmatrix}
-2k_- - \sigma\Delta & k_0 & k_0 & 0 \\
k_- & -k_0 - k_- - \sigma\Delta & 0 & k_0 \\
k_- + \sigma\Delta & 0 & -k_+ - k_0 & k_0 \\
0 & k_-\sigma\Delta & k_+ & -2k_0
\end{bmatrix},
$$

where $\Delta = k_+ - k_-$. Recall that the rate of activation for each site depends upon the state of its neighbor to the left. The approximation made by the FSMFT is to set the activation rate of the leftmost site in the finite segment to $k_-(1 - \sigma) + k_+\sigma$, where $0 \leq \sigma \leq 1$ is the mean activation level of the site immediately to the left of the segment. One way to determine σ is to set it equal to the mean activation level of the rightmost site in the segment. This results in the auxiliary equation,

$$
\langle S_m \rangle = \sum_{\substack{j=0 \\ j \text{ odd}}}^{M-1} p_j = \sigma. \tag{4.121}
$$

To find the steady state hydrolysis activity, one first solves the linear system of equations for the nullspace of A using standard methods. Then, combining the result with (4.121) results in a nonlinear equation to solve for σ. Notice that the simplest mean field approximation (4.120) is recovered by setting $m = 1$.

The movement of the Holliday junction can be incorporated into the model by considering a segment (with m odd), centered on the position of the junction, that moves with the junction. For simplicity take $m = 3$. The frame shifts whenever a wall passes through the junction. When the frame shifts, the state of the new site is determined by the far field mean activity, σ. This requires modification of transition from states $(1 \cdot 0 \cdot 0)$, $(1 \cdot 0 \cdot 1)$, and $(0 \cdot 0 \cdot 1)$ to appropriate frame-shifted states after activation of the center cite. Let the master equation be $d\mathbf{q}/dt = \hat{A}\mathbf{q}$, where $\mathbf{q}(t)$ is the probability distribution for the activation state of the sites surrounding the junction, with indexing the same as for $\mathbf{p}$. Assume that the only way to reach the $(1 \cdot 1 \cdot 1)$ state, where the center cite is activated, is from $(1 \cdot 0 \cdot 1)$; this transition does not result in movement of the junction. Note that transitions where the shifted segment has the same state as the original do not apear in the modified transition-rate matrix. For example, suppose a wall moves the junction to the right via a transition from $(1 \cdot 0 \cdot 0)$ when the center cite is activated. The shifted segment can be either $(1 \cdot 0 \cdot 1)$ or $(1 \cdot 0 \cdot 0)$. Transition to state $(1 \cdot 0 \cdot 1)$ occurs at a rate $k_+\sigma$, and transition to $(1 \cdot 0 \cdot 0)$ at a rate $k_+(1 - \sigma)$, but the transition to $(1 \cdot 0 \cdot 0)$ does not apear in the modified transition rate matrix because it has the same activation state as the pre-shifted segment.

Let q_+ correspond to state $(1 \cdot 0 \cdot 0)$ and q_- to state $(0 \cdot 0 \cdot 1)$ (or the sum of q_j over appropriate states if $m > 3$). Then, the steady state velocity and effective diffusivity of the junction is $V = k_+q_+ - k_-q_-$ and $D = k_+q_+ + k_-q_-$.

As long as m is chosen large enough so that σ is close to the far-field bulk value, the FSMFT approximation accurately captures the correlations near the junction; in practice the authors find the $m = 5$ is a good choice. One expects the velocity of the junction to depend strongly upon the catalyzed hydrolysis rate, k_+. As this rate is increased, the asymmetry should increase the speed of the forward hydrolysis waves. While this is true for small values of k_+, the velocity begins to *decrease* after a critical value of k_+ where the velocity is maximal. This is due to an increase in the total fraction of activated sites. A high fraction of activated sites means that the junction is more likely to be trapped within a long segment of purely activated sites where it does not move.

V. TRANSPORT AND SELF-ORGANIZATION IN CELLS

A. Axonal elongation and cellular length control

During neural development, the formation of synapses involves the elongation of an axon of one cell to locate the dendrites of another cell. Axon elongation is a consequence of the interplay between force generation at the growth cone that pulls the axon forward, pushing forces due to microtubule and actin polymerization and depolymerization, the rate of protein synthesis at the cell body, and the action of cytoskeletal motors (Baas and Ahmad, 2001; Goldberg, 2003; Lamoureux *et al.*, 1989; Mitchison and Kirschner, 1988; O'Toole *et al.*, 2008; Suter and Miller, 2011). Several models of axonal elongation have focused on the sequence of processes based on the production of tubulin dimers at the cell body, the active transport of these proteins to the the tip of the growing axon, and microtubule extension at the growth cone (Graham *et al.*, 2006; Kiddie *et al.*, 2005; McLean and Graham, 2004; Miller and Samuels, 1997; van Veen and van Pelt, 1994). One motivation for identifying the polymerization of microtubules as a rate limiting step is that axonal growth occurs at a similar rate to the slow axonal transport of tubulin, namely, around $1mm$ per day. (It is possible that short, freshly nucleated microtubules are also actively transported into axons (Baas and Buster, 2004)). For the sake of illustration, consider a continuum model of the active transport of tubulin (Graham *et al.*, 2006; McLean and Graham, 2004). Let $c(x, t)$ denote the concentration of tubulin at position x along the axon at time t. Suppose that at time t the axon has length $l(t)$ so that $x \in [0, l(t)]$. The transport of tubulin is modeled macroscopically in terms of an advection-diffusion equation with an additional decay term representing degradation at a rate g:

$$
\frac{\partial c}{\partial t} = D\frac{\partial^2 c}{\partial x^2} - V\frac{\partial c}{\partial x} - gc. \tag{5.1}
$$

Such a model can be derived from a more detailed stochastic model of active transport as detailed in Sec.

(IV.C), with V the effective drift due to motor-driven transport and D the effective diffusivity. It is assumed that there is a constant flux of newly synthesized tubulin from the cell body at $x = 0$ so that

$$\frac{\partial c}{\partial x} = -\epsilon_0 c_0 \text{ at } x = 0. \quad (5.2)$$

The flux at the growing end $x = l(t)$ is equal to the difference between the fluxes associated with microtubule assembly and disassembly:

$$\frac{\partial c}{\partial x} = -\epsilon_l c + \gamma_l \text{ at } x = l(t). \quad (5.3)$$

Finally, the rate of growth is also taken to be proportional to the difference between these two fluxes according to

$$\frac{dl}{dt} = \Omega \left[\epsilon_l c - \gamma_l \right], \quad x = l(t). \quad (5.4)$$

The constant Ω depends on the size of each tubulin dimer, the number of microtubules at the tip and the cross-sectional area of the axon.

It is straightforward to determine the steady-state length L of the axon (McLean and Graham, 2004). First, $dl/dt = 0$ implies that $c(L) = c_L \equiv \gamma_l/\epsilon_l$ and and $\partial c/\partial x = 0$ at $x = L$. The steady-state concentration profile takes the form $c(x) = Ae^{\lambda_+ x} + Be^{\lambda_- x}$ with $\lambda_\pm = (V/2D) \left[1 \pm \sqrt{1 + 4h} \right]$ and $h = Dg/V^2$. The coefficients A, B are determined from the boundary conditions at $x = L$. Finally, a transcendental equation for the steady-state length L is obtained by imposing the boundary condition (5.2):

$$F(L) \equiv e^{-\lambda_- L} - e^{-\lambda_+ L} = \frac{D\epsilon_0}{g} \frac{c_0}{c_L} (\lambda_+ - \lambda_-), \quad (5.5)$$

having used $\lambda_+ \lambda_- = -g/D$. For small L, the exponentials can be Taylor expanded to give $L \approx \frac{D\epsilon_0}{g} \frac{c_0}{c_L}$, whereas for large L the first exponential is dominant and $L = \frac{V}{g} \log \left(\frac{D\epsilon_0}{g} \frac{c_0}{c_L} \right)$. The last equation follows from taking $h \ll 1$ so that $\lambda_+ \approx V/D$ and $\lambda_- \approx -g/V$. In the first regime diffusion is dominant, whereas in the other active transport is dominant. Numerical simulations of the full time-dependent model show that these steady-states are stable and in both regimes the approach to steady-state is overdamped. On the other hand, for intermediate values of L damped oscillations occur resulting in overshoot (Graham et al., 2006).

There are a number of simplifications assumed in the above model (Goldberg, 2003; Vitriol and Zheng, 2012). First, the rate of elongation is based on the average rate of assembly and disassembly of a bundle of microtubules, which neglects the stochastic switching between periods of of elongation and rapid contraction exhibited by individual microtubules (Mitchison and Kirschner, 1984). Second, tensile forces acting on the microtubules within

the growth cone due to interactions with the actin cytoskeleton are neglected (Suter and Miller, 2011). Third, there are a number of other processes that could act as rate limiting steps in axonal growth, namely, the recycling of lipid membrane and the maintenance of the energy needs at the growth tip via the transport of mitochondria (Hollenbeck and Saxton, 2005; Miller and Sheetz, 2004; Morris and Hollenbeck, 1993; O'Toole et al., 2008). A recent stochastic model incorporates a number of these features (Atanasova et al., 2009). First, the rate of growth of the axon tip is determined by the rates at which newly delivered membrane proteins are inserted into the tip via exocytosis and are removed via endocytosis. Meanwhile, microtubules grow via polymerization until they reach the axon tip, where they are stabilized by interactions with the actin cytoskeleton. This in turn reduces the rate of endocytosis of membrane vesicles.

Axonal length control is one example of how cells regulate the size of their organelles and internal structures. Size control mechanisms, which are critical for proper cell function, can be distinguished according to whether the underlying structure is static (remains intact once assembled (Katsura, 1987; Keener, 2005)) or dynamic. Dynamic structures are constantly turning over so that in order for them to maintain a fixed size, there must be a balance between the rates of assembly and disassembly. If these rates depend on the size in an appropriate way then there will be a unique balance point that stabilizes the size of the organelle. Recent experimental work suggests that such a dynamic mechanism may also occur in eukaryotic flagella (Ishikawa and Marshall, 2011; Marshall et al., 2005; Marshall and Rosemblum, 2001). These are microtubule–based structures that extend to about 10 μm from the cell and are surrounded by an extension of the plasma membrane. They are at least an order of magnitude longer than bacterial flagella. Flagellar length control is a particularly convenient system for studying organelle size regulation, since a flagellum can be treated as 1D structure whose size is characterized by a single length variable. The length of a eukaryotic flagellum is important for proper cell motility, and a number of human diseases appear to be correlated with abnormal length flagella (Gerdes and Kasanis, 2005).

Radioactive pulse–labeling has been used to measure protein turnover in the flagella of Chlamydomonas, a unicellular green alga with genetics similar to budding yeast (Marshall and Rosemblum, 2001). Such measurements have suggested that turnover of tubulin occurs at the distal + end of flagellar microtubules, and that the assembly part of the turnover is mediated by intraflagellar transport (IFT). This is a motor-assisted motility within flagella in which large protein complexes move from one end of the flagellum to the other (Kozminski et al., 1993; Scholey, 2003). Particles of various size travel to the flagellar tip (anterograde transport) at 2.0 μm/s, and smaller particles return from the tip (retrograde trans-
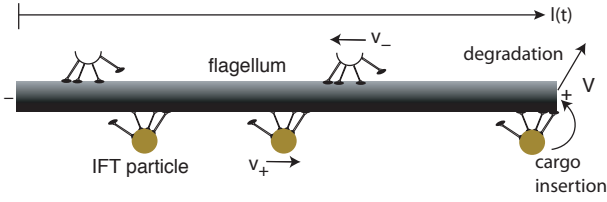
FIG. 34 Schematic diagram of intraflagellar transport (IFT), in which IFT particles travel with speed $v_\pm$ to the $\pm$ end of a flagellum. When an IFT particle reaches the + end it releases its cargo of protein precursors that contribute to the assembly of the flagellum. Disassembly occurs independently of IFT transport at a speed V.

port) at 3.5 μm/s after dropping off their cargo of assembly proteins at the + end. A schematic diagram of IFT transport is shown in Fig. 34. Immunoflourescence analysis indicates that the number of IFT particles (estimated to be in the range 1–10) is independent of length (Marshall *et al.*, 2005; Marshall and Rosemblum, 2001). If a fixed number of transport complexes M move at a fixed mean speed $\bar{v}$, then the rate of transport and assembly should decrease inversely with the flagellar length L. On the other hand, measurements of the rate of flagellar shrinkage when IFT is blocked indicate that the rate of disassembly is length–independent. This has motivated the following simple deterministic model for length control (Marshall and Rosemblum, 2001):

$$\frac{dL}{dt} = \frac{a\bar{v}M}{2L} - V, \qquad (5.6)$$

where a is the size of the precursor protein transported by each IFT particle and V is the speed of disassembly. Eq. (5.6) has a unique stable equilibrium given by $L^* = a\bar{v}M/2V$. Using the experimentally based values $M = 10$, $\bar{v} = 2.5$ μm/s, $L^* = 10$ μm and $V = 0.01$ μm/s, the effective precursor protein size is estimated to be $a \approx 10$ nm. A stochastic version of a model for flagellar length control has also been developed using the theory of continuous time random walks (Bressloff, 2006)

B. Cooperative transport of proteins in cellular organelles

The extensive secretory pathway of eukaryotic cells provides an alternative system for transporting newly synthesized lipids and proteins along axons and dendrites (Kennedy and Ehlers, 2006; Ramirez and Couve, 2011; Valenzuela *et al.*, 2011). One major organelle of the secretory pathway is the endoplasmic reticulum (ER), which tends to be dispersed throughout the cytoplasm of a cell (Lippincott-Schwartz *et al.*, 2000), see Fig. 35. Proteins and lipids destined for the plasma membrane enter the ER from the nucleus as they are translated by ER-associated ribosomes, where they fold into their
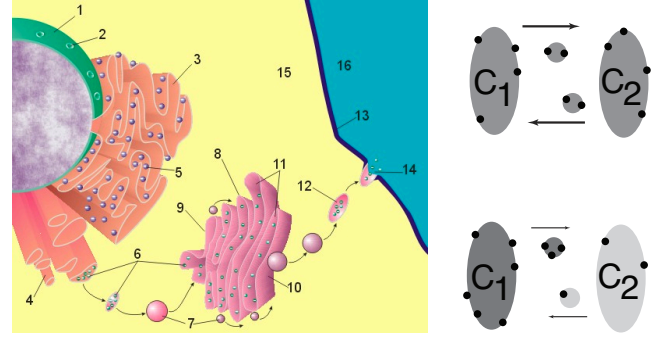

FIG. 35 LEFT: Diagram of secretory pathway including nucleus, ER and Golgi apparatus. 1. Nuclear membrane; 2. Nuclear pore; 3. RER; 4. SER; 5. Ribosome; 6. Protein; 7. Transport vesicles; 8. Golgi apparatus; 9. *Cis* face of Golgi apparatus; *Trans* face of Golgi apparatus ; 11 Cisternae of Golgi apparatus; 12. Secretory vesicle; 13. Plasma membrane; 14. Exocytosis; 15 Cytoplasm; 16. Extracellular domain. [Public domain image from WikiMedia Commons]. RIGHT: When two compartments continually exchange products via vesicular transport, a symmetry breaking mechanisms is needed to maintain nonidentical compartments ($C_1 \neq C_2$).

proper 3D structure. The ER can be partitioned into the rough ER (RER), which is rich in ribosomes, and the smooth ER (SER), which has only a few sparse ribosomes and tends to form a tubular structure. In neurons, the RER is present in the soma and proximal dendritic compartments, whereas the SER is distributed in distal dendrites (including some dendritic spines) and axons. The diffusivity of proteins within the tubular-like SER is 3-6 times smaller than within the cytoplasm. However, the ER is constantly being remodeld by motor-driven sliding along microtubules, for example, which could add an active component to protein transport (Ramirez and Couve, 2011; Valenzuela *et al.*, 2011). Moreover, the thin tubular structure of the SER reduces the effective spatial dimension of diffusion, thus enhancing progression along a dendrite. Another important aspect of the secretory pathway is that it is tightly regulated (Lippincott-Schwartz *et al.*, 2000). Proteins accumulate at specific exit sites and leave the ER in vesicles that transfer the cargo to organelles forming the Golgi network where final packaging and sorting for target delivery is carried out. In most eucaryotic cells the Golgi network is confined to a region around the nucleus known as the Golgi apparatus, whereas in neurons there are Golgi "outposts" distributed throught the dendrite. Thus it is possible that some proteins travel long distances within the SER (rather than via active transport along microtubules) before being sorted for local delivery at a synapse.

One of the significant features of the secretory pathway is that there is a constant active exchange of molecules between organelles such as the ER and Golgi apparatus, which have different lipid and protein compositions. Such

an exchange is mediated by motor-driven vesicular transport. Vesicles bud from one compartment or organelle, carrying various lipids and proteins, and fuse with another compartment. Transport in the anterograde direction has to be counterbalanced by retrograde transport in order to maintain the size of the compartments and to reuse components of the transport machinery. Since bidirectional transport would be expected to equalize the composition of both compartments, there has been considerable interest in understanding the self-organizing mechanisms that allow such organelles to maintain their distinct identities while constantly exchanging material (Mistelli, 2001), see Fig. 35. One model for generating stable, non-identical compartments has been proposed by Heinrich and Rapoport (2005), (see also Binder *et al.* (2009); Dmitrieff and Sens (2011); Gong *et al.* (2010); Klann *et al.* (2012)), based on the observation that vesicular transport involves a complex network of molecular interactions between vesicles, transported molecules and recipient organelles (Barlowe, 2000; Lippincott-Schwartz and Phair, 2010; Pelham, 2001). That is, the rates of vesicle exchange between compartments are influenced by their composition. An inutitive understanding of the basic mechanism can be obtained by considering the exchange of four types of protein (SNARES), X, U, Y, V say, between two compartments. Suppose that in steady-state many vesicles with a low content of X, U move in one direction (from the first to the second compartment), whereas a few vesicles with a large content of X, U move in the opposite direction so that the total protein fluxes are balanced. This would reflect differences in composition of X, U in the two compartments. However, lipid balance would not be maintained because there would be a net flux of vesicles in one direction. However a balance of lipid fluxes can also be achieved by having a complemetary transport of Y, V molecules in the opposite direction. The asymmetric states are stablilized by taking the rates of budding and fusion to depend on interactions between vesicles and compartments mediated by the protein pairs (X, U) and (Y, V) (Heinrich and Rapoport, 2005).

C. Cell polarity

Many cellular processes depend critically on the stable maintenance of polarized distributions of signaling proteins on the plasma membrane. These include cell motility, epitheleal morphogenesis, embryogenesis, and stem cell differentiation. In many cases cell polarity can occur spontaneously in the absence of pre-existing spatial cues. Various experimental studies suggest that there are at least two independent but coordinated positive feedback mechanisms that can establish cell polarity (Wedlich-Soldner *et al.*, 2004). One involves the reinforcement of spatial asymmetries by the directed transport of signal-

ing molecules along the cytoskeleton to specific locations on the plasma membrane (Altschuler *et al.*, 2008; Layton *et al.*, 2011; Marco *et al.*, 2007), whereas the other involves the coupling of membrane diffusion with bistable enzymatic dynamics (Gamba *et al.*, 2009; Mori *et al.*, 2008; Semplice *et al.*, 2012).

One example of the first class of model is shown in Fig. 36. Here the asymmetric distribution of a signaling molecule within the plasma membrane $\partial\Omega$ and the orientation of actin filaments are mutually enhanced through a positive feedback loop (Marco *et al.*, 2007). Let $u(\mathbf{r}, t)$ denote the concentration of signaling molecules within the plasma membrane. Then u depends on six physically interpretable quantities: (i) the membrane diffusivity D; (ii) the index function $\chi(\mathbf{r})$ indicating the region of the plasma membrane to which cytoskeletal tracks are attached, that is, the cluster within which u is high; (iii) the total amount of signaling molecule N_{tot}; (iv) the rate of directed transport h; (v) the endocytosis rate k within the cluster; and (vi) the endocytosis rate K outside the cluster with $K < k$. The density u evolves according to the macroscopic equation (Marco *et al.*, 2007)

$$\frac{\partial u}{\partial t} = D\Delta u - [k\chi + K\bar{\chi}] u + hN_{\text{cyt}}\frac{\chi}{\int_{\partial\Omega} \chi d\mathbf{r}}, \quad (5.7)$$

where Δ is the Laplace-Beltrami operator for diffusion in the membrane, $\bar{\chi}(\mathbf{r}) = 1 - \chi(\mathbf{r})$, and N_{cyt} is the total amount number of signaling molecules within the cytoplasm: $N_{\text{cyt}} = N_{\text{tot}} - \int_{\partial\Omega} u d\mathbf{r}$. The cytoplasmic pool is assumed to be homogeneous due to the fast dispersion of vesicles in the cytosol. Numerical simulations show that a stable spatially asymmetric distribution of signaling molecules within the plasma membrane can be maintained. Moreover, the degree of polarization can be optimized by varying the rates of endocytosis. One limitation of the model, however, is that the packaging of signaling molecules into discrete vesicles is ignored, that is, the model treats transport as a continuous flux of proteins. As highlighted by Layton *et al.* (2011), incorporating vesicular transport into the model makes cell polarization more difficult to sustain. A simple argument for this proceeds as follows. Exocytic vesicles need to have higher concentrations of the signaling molecule than the polarization site in order to enhance the concentration. A dynamic equilibrium of recycling can only be maintained if endocytic vesicles also have an enhanced concentration of signaling molecules. This appears to put unrealistically strong constaints on the mechanisms for loading vesicles with cargo prior to transport.

The second basic mechanism for establishing cell polarity does not depend on active transport, and can be modeled in terms of a reaction–diffusion system. One example of such a model is described in Fig. 37 (Gamba *et al.*, 2009; Semplice *et al.*, 2012). Consider a macroscopic version of the model, in which $\phi^{\pm}$ denote the concentration of activated and inactivated signaling molecules within

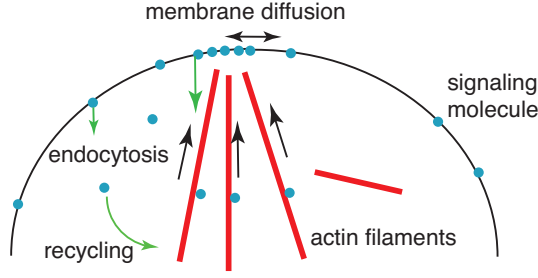FIG. 36 Model of Marco et al. (2007). Signaling molecules can attach and orient actin filaments that deliver vesicles carrying the signaling molecule from the cytoplasm to the plasma membrane. The additional signaling molecules orient more actin filaments that transport more molecules in a positive feedback loop. The local orientation of actin filaments also increases the rate of endocytosis within the cluster.

the plasma membrane. Let x_c, y_c be the concentration of the counteracting enzymes in the cytosol (which is assumed to be homogeneous), let x', y be the concentrations of membrane associated enzymes activated by Φ^+ and Φ^-, respectively, and let x'' denote the concentration of membrane associated enzyme activated by a distribution of receptors s. The model equations take the form (Semplice et al., 2012)

$$\partial\phi^\pm/\partial t = D\Delta\phi^\pm \pm g(\phi^+, \phi^-, x', x'', y) \quad (5.8a)$$

$$\partial x'/\partial t = k'_a s x'_c - k'_d x' \quad (5.8b)$$

$$\partial x''/\partial t = k''_a \phi^+ x_c - k'_d x'', \quad (5.8c)$$

$$\partial y/\partial t = k_a \phi^- y_c - k_d y. \quad (5.8d)$$

Here Δ is the Laplace-Beltrami operator, k'_a, k''_a, k_a and k'_d, k''_d, k_d are the forward and backward reaction rates of the signaling and feedback pathways, and

$$g = k'_c \frac{x'\phi^-}{K' + \phi^-} + k''_c \frac{x''\phi^-}{K'' + \phi^-} - k_c \frac{y\phi^+}{K + \phi^-} \quad (5.9)$$

is the enzymatic conversion rate of Φ^+ to Φ^-. The total amount of Φ^+ and Φ_- is conserved, $\phi^+ + \phi^- = c$, as are the total amounts of each enzyme X, Y. Using a time-scale separation in which the equilibria for the concentrations x', x'', y, x_c, y_c are reached much faster than the equilibria for the surface distributions $\phi^\pm$, the dynamics for the concentration difference $\phi = \phi^+ - \phi^-$ reduces to the system (Semplice et al., 2012)

$$\frac{\partial\phi}{\partial t} = D\Delta\phi + V'(\phi), \quad (5.10)$$

where

$$V'(\phi) = (c^2 - \phi^2)[\Gamma'(\phi) + \Gamma''(\phi) + \Gamma(\phi)], \quad (5.11)$$

with

$$\Gamma' = \frac{2(k'_c k'_a/k'_d)x_c s}{(2K' + c - \phi)(c + \phi)}, \Gamma'' = \frac{2(k''_c k''_a/k'_d)x_c}{2K'' + c - \phi}$$
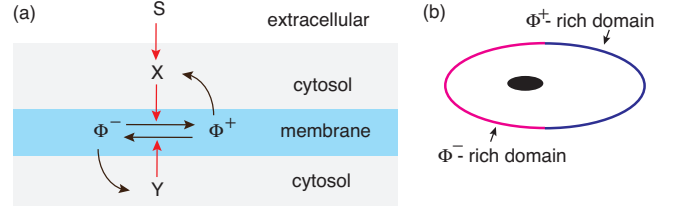
$$\Gamma = \frac{2(k_c k_a/k_d)y_c}{2K + c - \phi}.$$

FIG. 37 Model of Semplice et al. (2012). (a) A set of receptors transduce an external distribution of chemotactic cues into an internal distribution of activated enzymes X that catalyze the switch of a signaling molecule from an unactivated state Φ^- to an activated state Φ^+. A counteracting enzyme Y transforms Φ^+ back to Φ^-. Amplifying feedback loops, in which Φ^+ activates X and Φ^- activates Y, result in chemical bistability. The signaling molecules are permanently bound to the plasma membrane, where they exhibit lateral diffusion, whilst the enzymes are free to move between the membrane and the cytosol. (b) Cell polarization occurs when there is phase separation into two stable chemical states.

Under the adiabatic approximation, the dynamics can be written in the variational form

$$\frac{\partial\phi}{\partial t}(\mathbf{r}, t) = -\frac{\delta\mathcal{F}[\phi]}{\delta\phi(\mathbf{r}, t)} \quad (5.12)$$

with $\mathcal{F}$ an effective energy functional

$$\mathcal{F}[\phi] = \int_{\partial\Omega} \left[D(\nabla\phi)^2 + V(\phi)\right] dS. \quad (5.13)$$

Here integration is with respect to the membrane surface. Stable homogeneous solutions correspond to minima of the potential $V(\phi)$ for which $V'(\phi) = 0$. One finds that for a range of parameter values, the system exhibits bistability. That is, there exist two stable equilibria $\varphi_\pm$ corresponding to phases enriched in $\Phi^\pm$ separated by an unstable equilibrium.

The polarization of the cell membrane can now be understood in terms of the theory of phase separation kinetics familiar from the study of condensed matter systems (Gamba et al., 2009; Semplice et al., 2012). A polarized state will exist when the cell membrane is divided into two complementary regions, see Fig. 37(b), that correspond to two distinct stable chemical phases, separated by a thin diffusive interface. Such a spatially inhomogeneous solution has to minimize both terms in the functional (5.13). One condition for stability is phase coexistence, that is,

$$\Delta V = V(\varphi_+) - V(\varphi_-) = \int_{\varphi_-}^{\varphi_+} V'(\phi)d\phi = 0. \quad (5.14)$$

A second condition is that the diffusive "energy" associated with the interface is minimized. Even when a stable polarized state exists, the evolution to such a state involves a complex process of nucleation and competitive growth of heterogeneous patches. Suppose, for example,

that the membrane is initially in a metastable state consiting of the φ_- phase. External stimulation may make the φ_+ phase energetically more favorable but there is an energy barrier to overcome, which blocks a continuous transition to the φ_+ phase. Instead, patches of the φ_+ phase are nucleated by thermal fluctuations and start expanding due to front propagation, see also (Mori *et al.*, 2008). In fact, one finds that only patches larger than a critical size $r_c \sim 1/\Delta V$ can expand into the background φ_- phase with a front velocity $\sim \Delta V$. However, the growth of the φ_+ phase decreases x_c and increases y_c, resulting in a reduction of the barrier height. Thus, growth slows, the critical radius increases, and large patches grow at the expense of smaller patches until only a single φ_+ patch remains, which coexists with the φ_- phase. A microscopic version of the model has also been developed (Semplice *et al.*, 2012), in which the cell membrane is represented by a 2D lattice with sites populated by a discrete number of molecules of each chemical species. The probability distribution of the discrete populations evolves according to a master equation that keeps track of all possible chemical reactions and diffusive jumps.

VI. DISCUSSION

In this review we have focused on analytically tractable microscopic and macroscopic models of intracellular transport. A complementary approach is to develop more biologically realistic multi-scale computational models, which include details of the structure of individual macromolecules, the biochemical network of signaling pathways, the acqueous environment of the cytoplasm, the mechanical properies of the cytoskeleton, and the geometry of the cell. One major challenge in stochastic simulations is how to efficiently couple stochastic chemical reactions with diffusion in complex environments (Andrews and Bray, 2004; Bhalla, 2004a,b; Erban and Chapman, 2009; Isaacson and Peskin, 2006; Turner *et al.*, 2004). Many approaches are based on spatial extensions of the Gillespie algorithm for well-mixed chemical reactions (Gibson and Bruck, 2000; Gillespie, 1977, 2001). Several stochastic simulation packages have also been developed including MCell (Franks *et al.*, 2001, 2002) and smoldyn (Andrews, 2012). In addition to the example of phase separation during cell polarity, macroscopic reaction-diffusion systems can exhibit complex spatiotemporal dynamics including coherent oscillations, wave propagation and Turing pattern formation (Falcke, 2003; Igoshin *et al.*, 2001; Keener and Sneyd, 2009; Lenz and Sogaard-Andersen, 2011; Loose *et al.*, 2011). These are thought to play an important role in a variety of cellular processes including morphogenesis, cell division, and embryogenesis (Murray, 2002). Understanding the affects of noise at the microscopic level on reaction-diffusion dynamics is an active area of current research.

REFERENCES

Ajdari, A., 1995, Europhys. Lett. **31**, 69.

Alberts, B., A. Johnson, J. Lewis, M. Raff, and K. R. amd P Walter, 2008, *Molecular Biology of the Cell* (Garland, New York), 5th edition.

Altschuler, S. J., S. B. Angenent, Y. Wang, and L. F. Wu, 2008, Nature **454**, 886.

Ambjornsson, T., and R. Metzler, 2004, Phys. Biol. **1**, 77.

Andrews, S. S., 2012, Meth. Mol. Biol. **804**, 519.

Andrews, S. S., and D. Bray, 2004, Phys. Biol. **1**, 137.

Antal, T., and P. L. Krapivsky, 2005, Phys. Rev. E **72**, 046104.

Artyomov, M. N., A. Y. Morozov, and A. B. Kolomeisky, 2008, Phys. Rev. E **77**, 040901.

Ashby, M. C., S. R. Maier, A. Nishimune, and J. M. Henley, 2006, J. Neurosci. **26**, 7046.

Atanasova, K. T., A. Burgo, T. Galli, and D. Holcman, 2009, Biophys. J. **96**, 840.

Baas, P., and D. Buster, 2004, J. Neurobiol. **58**, 3.

Baas, P. W., and F. J. Ahmad, 2001, Trends Cell. Biol. **11**, 244.

Baas, P. W., J. S. Deitch, M. M. Black, and G. A. Banker, 1988, Proc. Natl. Acad. Sci. USA **85**, 8335.

Banks, D. S., and C. Fradin, 2005, Biophys. J. **89**, 2960.

Bannai, H., T. Inoue, T. Nakayama, M. Hattori, and K. Mikoshiba, 2004, J Cell Sci **117**, 163.

Barbi, M., C. Place, V. Popkov, and M. salerno, 2004a, Phys. Rev. E **70**, 041901.

Barbi, M., C. Place, V. Popkov, and M. Salerno, 2004b, J Biol. Phys. **30**, 203.

Barkai, E., and R. Silbey, 2009, Phy. Rev. Lett. **102**, 050602.

Barlowe, C., 2000, Traffic **1**, 371.

Basu, A., and D. Chowdhury, 2007, Phys. Rev. E **75**, 021902.

Becalska, A. N., and E. R. Gavis, 2009, Development **136**, 2493.

Becskei, A., and I. W. Mattaj, 2005, Curr Opin Cell Biol **17**, 27.

Bell, J. W., 1991, *Searching Behaviour, The Behavioural Ecology of Finding Resources* (Chapman and Gall, London).

Benichou, O., C. Chevalier, B. Meyer, and R. Voituriez, 2011a, Phys. Rev. Lett. **106**, 038102.

Benichou, O., M. Coppey, M. Moreau, P. Suet, and R. Voituriez, 2005, Phys. Rev. Lett. **94**(198101).

Benichou, O., C. Loverdo, M. Moreau, and R. Voituriez, 2007, J. Phys. A **19**(065141).

Benichou, O., C. Loverdo, M. Moreau, and R. Voituriez, 2011b, Rev. Mod. Phys. **83**, 81.

Benichou, O., and R. Voituriez, 2008, Phys Rev Lett **100**, 168105.

Berezhkovskii, A. M., and S. M. Bezrukov, 2005, Chem. Phys. **319**, 342.

Berezhkovskii, A. M., M. A. Pusovoit, and S. M. Bezrukov, 2003, J. Chem. Phys. **119**, 3943.

Berezhkovskii, A. M., M. A. Pustovoit, and S. M. Bezrukov, 2002, J. Chem. Phys. **116**, 9952.

Berg, O. G., and P. H. von Hippel, 1985, Ann. Rev. Biophys.Biophys. Chem. **14**, 131.

Berg, O. G., R. B. Winter, and P. H. von Hippel, 1981, Biochem. **20**, 6929.

Bezrukov, S. M., A. M. Berezhkovskii, M. A. Pustovoit, and A. Szabo, 2000, J. Chem. Phys. **113**, 8206.

Bhalla, U. S., 2004a, Biophys. J. **87**, 733.

Bhalla, U. S., 2004b, Biophys. J. **87**, 745.

Bickel, T., and R. Bruinsma, 2002, Biophys J. **83**, 3079.

Biess, A., E. Kerkotian, and D. Holcman, 2007, Phys. Rev. E **76**, 021922.

Biess, A., E. Korkotian, and D. Holcman, 2011, PLoS Comp Bio. **7**, e1002182.

Binder, B., A. Goede, N. Berndt, and H.-G. Holzhutter, 2009, PLoS One **4**, e8295.

Bloom, O. E., and J. R. Morgan, 2011, Mol. Cell. Neurosci. **48**, 339.

Blum, J., and M. C. Reed, 1989, Cell Motil. Cytoskeleton **12**, 53.

Blythe, R. A., and M. R. Evans, 2007, J. Phys. A **40**, R333.

Bouchaud, J. P., and A. Georges, 1990, Phys. Rep. **195**, 127.

Brandenburg, B., and X. Zhuang, 2007, Nat. Rev. Microbiol. **5**, 197.

Bredt, D. S., and R. A. Nicoll, 2003, Neuron **40**, 361.

Bressloff, P. C., 2006, Phys. Rev. E **73**, 061916.

Bressloff, P. C., 2009, Phys. Rev. E **79**, 041904.

Bressloff, P. C., and B. A. Earnshaw, 2007, Phys. Rev. E **75**, 041916.

Bressloff, P. C., and B. A. Earnshaw, 2009, Biophys. J. **96**, 1786.

Bressloff, P. C., B. A. Earnshaw, and M. J. Ward, 2008, SIAM J. Appl. Math. **68**, 1223.

Bressloff, P. C., and J. M. Newby, 2009, New J. Phys. **11**, 023033.

Bressloff, P. C., and J. M. Newby, 2011, Phys. Rev. E. **83**, 061139.

Bressloff, P. C., and J. M. Newby, 2012, Phys. Rev. E **85**, 031909.

Bringuier, E., 2009, Physica A **388**, 2588.

Bronstein, I., Y. Israel, E. Kepten, S. Mai, Y. Shav-Tal, E. Barkai, and Y. Garini, 2009, Phys. Rev. Lett. **103**, 018102.

Brooks, E., 1999, Annals of Applied Probability **9**, 719.

Brown, A., 2000, Nat. Rev. Mol. Cell Biol. **1**, 153.

Brown, A., 2003, J. Cell Biol. **160**, 817.

Brown, F. L. H., D. M. Leitner, J. A. McCammon, and K. R. Wilson, 2000, Biophys. J. **78**, 2257.

Burada, P. S., P. Hanggi, F. Marchesoni, G. Schmid, and P. Talkner, 2009, Chem. Phys. Chem. **10**, 45.

Burada, P. S., G. Schmid, D. Reguera, J. M. Rubi, and P. Hanggi, 2007, Phys. Rev. E **75**, 051111.

Burlakov, V. M., N.Emptage, A.Goriely, and P. C. Bressloff, 2012, Phys. Rev. Lett. **108**, 028101.

Burov, S., J. H. Jeon, R. Metzler, and E. Barkai, 2011, Phys. Chem. Chem. Phys. **13**, 1800.

Centres, P. M., and S. Bustingorry, 2010, Phys. Rev. E **81**, 061101.

Cherstvy, A. G., A. B. Kolomeisky, and A. A. Kornyshev, 2008, J. Phys. Chem. **112**, 4741.

Chevalier, C., O. Benichou, B. Meyer, and R. Voituriez, 2011, J. Phys. A **44**, 025002.

Cheviakov, A. F., M. J. Ward, and R. Straube, 2010, SIAM J. Multiscal Mod. Sim. **8**, 836.

Choquet, D., and A. Triller, 2003, Nat. Rev. Neurosci. **4**, 251.

Chou, T., 1998, J. Chem. Phys. **110**, 606.

Chou, T., and G. Lakatos, 2003, J. Phys. A **36**, 2027.

Chou, T., and G. Lakatos, 2004, Phys. Rev. Lett. **93**, 198101.

Chou, T., K. Mallick, and R. K. P. Zia, 2011, Rep. Prog. Phys. **74**, 116601 (41pp).

Ciandrini, L., I. Stansfield, and M. C. Romano, 2010, Phys. Rev. E **81**, 051904.

Collinridge, G. L., J. T. R. Isaac, and Y. T. Wang, 2004, Nat. Rev. Neurosci. **5**, 952.

Collins, F. C., and G. E. Kimball, 1949, J. Colloid Sci. **4**, 425.

Coombs, D., R. Straube, and M. J. Ward, 2009, SIAM J. Appl. Math **70**, 302.

Coppey, M., O. Benichou, R. Voituriez, and M. Moreau, 2004, Biophys J. **87**, 1640.

Craciun, G., A. Brown, and A. Friedman, 2005, J. Th. Biol. **237**, 316.

Cronshaw, J. M., and M. J. Matunis, 2004, Trends Endocrinol Metab **15**, 34.

Czondora, K., M.Mondina, M. Garciaa, M. Heinec, R. Frischknechtc, D. Choqueta, J. B. Sibaritaa, and O. R. Thoumine, 2012, Proc. Nat. Acad. Sci. USA **109**, 3522.

Damm, E. M., and L. Pelkmans, 2006, Cell Microbiol. **8**, 1219.

Derrida, B., 1983, J. Stat. Phys. **31**, 433.

Dinh, A. T., C. Pangarkar, T. Theofanous, and S. Mitragotri, 2007, Biophys. J. **92**, 831.

Dinh, A. T., T. Theofanous, and S. Mitragotri, 2005, Biophys. J. **89**, 1574.

Dix, J. A., and A. S. Verkman, 2008, Annu. Rev. Biophys. **37**, 247.

Dixit, R., J. L. Ross, Y. E. Goldman, and E. L. F. Holzbaur, 2008, Science **319**, 1086.

Dmitrieff, S., and P. Sens, 2011, Phys. Rev. E **83**, 041923.

Doherty, G. J., and H. T. McMahon, 2009, Ann. Rev. Biochem. **78**, 857.

Dong, J., B. Schmittmann, and R. K. P. Zia., 2007, Phys. Rev. E **76**, 051113.

D'Orsogna, M. R., T. Chou, and T. Antal, 2007, J. Phys. A **40**, 5575.

Driver, J. W., A. R. Rodgers, D. K. Jamison, R. K. Das, A. B. Kolomeisky, and M. R. Diehl, 2010, Phys. Chem. Chem. Phys. **12**, 10398.

Dynes, J., and O. Steward, 2007, The Journal of Comparative Neurology **500**(3), 433.

Earnshaw, B. A., and P. C. Bressloff, 2006, J. Neurosci. **26**(47), 12362.

Earnshaw, B. A., and P. C. Bressloff, 2008, J. Comput. Neurosci. **25**, 366.

Eggert, U. S., T. J. Mitchison, and C. M. Field, 2006, Ann. Rev. Biochem. **75**, 543.

Ehlers, M. D., 2000, Neuron **28**, 511.

Ehlers, M. D., M. Heine, L. Groc, M.-C. Lee, and D. Choquet, 2007, Neuron **54**(3), 447, ISSN 0896-6273 (Print).

Elf, J., G. W. Li, and X. S. Xie, 2007, Science **316**, 1191.

Elston, T. C., 2000a, J. Math. Biol. **41**, 189.

Elston, T. C., 2000b, Biophys. J. **79**, 2235.

Erban, R., and J. Chapman, 2009, Phys. Biol. **6**, 046001.

Evans, M. R., and T. Hanney, 2005, J. Phys. A **38**, R195.

Evans, M. R., R. Juhasz, and L. Santen, 2003, Phys. Rev. E **68**, 026117.

Fahrenkrog, B., J. Koser, and U. Aebi, 2004, Trends Biochem Sci **29**, 175.

Falcke, M., 2003, N. J. Phys. **5**, 96.1.

Feder, T. J., I. BrustMascher, J. P. Slattery, B. Baird, and W. W. Webb, 1996, Biophys. J. **70**, 2797.

Fedotov, S., H. Al-Shami, A. Ivanov, and A. Zubarev, 2010, Phys. Rev. E **82**, 041103.

Fisher, M., and A. Kolomeisky, 2001, Proc. Natl. Acad. Sci. U. S. A. **98**, 7748.

Foulaadvand, M. E., A. B. Kolomeisky, and H. Teymouri, 2008, Phys. Rev. E **78**, 061116.

Franks, K. M., T. M. Bartol, and T. J. Sejnowski, 2001, Neurocomputing **38**, 9.

Franks, K. M., T. M. Bartol, and T. J. Sejnowski, 2002, Biophys. J. **83**, 2333.

Freche, D., U. Pannasch, N. Rouach, and D. Holcman, 2011, PLoS one **6**(10), e25122.

Friedman, A., and G. Craciun, 2005, J. Math. Biol. **51**, 217.

Friedman, A., and G. Craciun, 2006, SIAM J. Math. Anal. **38**, 741.

Friedman, A., and B. Hu, 2007, Indiana University Mathematics Journal **56**, 2133.

Fulton, A., 1982, Cell **30**, 345.

Gamba, A., I. Kolokolov, V. Lebedev, and G. Ortenzi, 2009, J. Stat. Mech. **P02019**.

Gao, Y. Q., 2006, Biophys. J. **90**, 811.

Garai, A., D. Chowdhury, and T. V. Ramakrishnan, 2009, Phys. Rev. E **80**, 011908.

Gardiner, C. W., 2009, *Handbook of stochastic methods, 4th edition* (Springer, Berlin).

Gennerich, A., and D. Schild, 2006, Phys. Biol. **3**, 45.

Gerdes, J. M., and N. Kasanis, 2005, Cell Mol. Life Sci. **62**, 1556.

Gerland, U., R. Bundschuh, and T. Hwa, 2004, Phys. Biol. **1**, 19.

Gerrow, K., and A. Triller, 2010, Curr. Opin. Neurobiol. **20**, 631.

Gibson, M. A., and J. Bruck, 2000, J. Chem. Phys. **104**, 1876.

Gillespie, D. T., 1977, J. Phys. Chem. **81**, 2340.

Gillespie, D. T., 2001, J. Chem. Phys. **115**, 1716.

Glotzer, M., 2009, Nat. Rev. Mol. Cell Biol. **10**, 9.

Goldberg, J. L., 2003, Genes Dev. **17**, 941.

Golding, I., and E. C. Cox, 2006, Phys. Rev. Lett. **96**, 098102.

Goldstein, A. Y. N., X. Wang, and T. L. Schwarz, 2008, Current Opinion In Neurobiology **18**, 495.

Goldstein, L., and Z. Yang, 2000, Ann. Rev. Neurosci. **23**, 39.

Gong, H., Y. Guo, A. Linstedt, and R. Schwartz, 2010, Phys. Rev. E **81**, 011914.

Gorman, J., and E. C. Greene, 2008, Nat. Struct. Mol. Biol. **15**, 768.

Gorski, S. A., M. Dundr, and T. Mistelli, 2006, Curr Opin Cell Biol **18**, 284.

Gowers, D. M., G. G. Wilson, and S. E. Halford, 2005, Proc. Nat. Acad. Sci. USA **102**, 15883.

Graham, B. P., K. Lauchlan, and D. R. Mclean, 2006, J. Comput. Neurosci. **20**, 43.

Grigoriev, I. V., Y. A. Makhnovskii, A. M. BereZhkovskii, and V. Y. Zitserman, 2002, J. Chem. Phys. **116**, 9574.

Groc, L., M. Heine, L. Cognet, K. Brickley, F. Stephenson, B. Lounis, and D. Choquet, 2004, Nat. Neurosci. **7**, 695.

Grunwald, D., and R. H. Singer, 2011, Curr. Opin. Cell Biol. **24**, 1.

Gundelfinger, E. D., M. M. Kessels, and B. Qualmann, 2003, Nat. Rev. Mol. Cell Biol. **4**, 127.

Halford, S. E., 2009, Biochem. Soc. Trans. **37**, 343.

Halford, S. E., and J. F. Marko, 2004, Nucl. Acid Res. **32**, 3040.

Hanggi, P., P. Talkner, and M. Borkovec, 1990, Rev. Mod. Phys. **62**, 251.

Harris, T. E., 1965, J. Appl. Prob. **2**, 323.

He, Y., S. Burov, R. Metzler, and E. Barkai, 2008, Phys. Rev. Lett. **101**, 058101.

Heinrich, R., and T. A. Rapoport, 2005, J. Cell Biol. **168**, 271.

Hendricks, A. G., E. Perlson, J. L. Ross, H. W. S. III, M. Tokito, and E. L. K. Holzbaur, 2010, Cur. Opin. Biol. **20**, 697.

Henley, J. M., E. A. Barker, and O. O. Glebov, 2011, Trends Neurosci. **34**, 258.

Hille, B., 2001, *Ionic channels of excitable membranes* (Sinauer Associates, Massachusetts), 3rd edition.

Holcman, D., 2007, J. Stat. Phys. **127**, 471.

Holcman, D., A. Marchewka, and Z. Schuss, 2005, Phys. Rev. E **72**, 031910.

Holcman, D., and Z. Schuss, 2004, J. Stat. Phys. **117**, 975.

Holcman, D., and A. Triller, 2006, Biophys. J. **91**, 2405.

Hollenbeck, P. J., and W. M. Saxton, 2005, J. Cell Sci. **11**, 5411.

Howard, J., 2001, *Mechanics of motor proteins and the cytoskeleton* (Sinauer, MA).

Hu, T., A. Y. Grossberg, and B. I. Shklovskii, 2006, Biophys J. **90**, 2731.

Hu, T., and B. Shklovskii, 2006, Phys. Rev. E **74**, 021903.

Hughes, B. D., 1995, *Random walks and random environments volume 1: random walks* (Oxford University, Oxford).

Igoshin, O. A., A. Mogilner, R. D. Welch, D. Kaiser, and G. Oster, 2001, Proc. Nat. Acad. Sci. USA **98**, 14913.

Isaacson, S. A., D. M. McQueen, and C. S. Peskin, 2011, Proc. Natl. Acad. Sci. U. S. A. **108**, 3815.

Isaacson, S. A., and C. S. Peskin, 2006, SIAM J. Sci. Comput. **28**, 47.

Ishikawa, H., and W. F. Marshall, 2011, Nat. Rev. Mol. Cell Biol. **12**, 222.

Jacobs, M. H., 1967, *Diffusion processes* (Springer-Verlag, New York).

Jacobson, K., O. G. Mouritsen, and R. G. W. Anderson, 2007, Nat. Cell Biol. **9**, 7.

Jeon, J.-H., and R. Metzler, 2012, Phys. Rev. E **85**, 021147.

Jeon, J.-H., V. Tejedor, S. Burov, E. Barkai, C. Selhuber-Unkel, K. Berg-Sorensen, L. Oddershede, and R. Metzler, 2011, Phys. Rev. Lett. **106**, 048103.

Jepsen, D. W., 1965, J. Math. Phys. **6**, 405.

Julicher, F., A. Ajdari, and J. Prost, 1997, Rev. Mod. Phys. **69**, 1269.

Jung, P., and A. Brown, 2009, Phys. Biol. **6**, 046002.

Kahana, A., G. Kenan, M. Feingold, M. Elbaum, and R. Granek, 2008, Phys. Rev. E **78**, 051912.

Kalay, Z., P. E. Parris, and V. M. Kenkre, 2008, J. Phys. Cond. Matt. **20**, 245105.

Kalinay, P., and J. K. Percus, 2006, Phys. Rev. E **74**, 041203.

Kampen, N. G. V., 1992, *Stochastic processes in physics and biology* (North-Holland, Amsterdam), second edition.

Katsura, I., 1987, Nature **327**, 73.

Keener, J., and J. Sneyd, 2009, *Mathematical Physiology I: Cellular Physiology* (Springer), 2nd edition.

Keener, J. P., 2005, J. Theor. Biol. **234**, 263.

Keener, J. P., and J. M. Newby, 2011, Phys. Rev. E **84**, 011918.

Keizer, J., 1982, J. Phys. Chem. **86**, 5052.

Keller, D., and C. Bustamante, 2000, Biophys. J. **78**, 541.

Kenkre, V. M., L. Giuggioli, and Z. Kalay, 2008, Phys. Rev. E **77**, 051907.

Kennedy, M. J., and M. D. Ehlers, 2006, Ann. Rev. Neurosci. **29**, 325.

Kerr, J. M., and T. A. Blanpied, 2012, J. Neurosci. **32**, 658.

Keyser, U. F., B. N. Koeleman, S. van Dorp, D. Krapf, R. M. M. Smeets, S. G. Lemay, N. H. Dekker, and C. Dekker, 2006, Nat. Phys. **2**, 473.

Kiddie, G., D. McLean, A. van Ooyen, and B. Graham, 2005, Prog. Brain Res. **147**, 67.

King, S. J., and T. A. Schroer, 2000, Nat. Cell Biol. **2**, 20.

Klann, M., H. Koeppl, and M. Reuss, 2012, PLoS One **7**, e29645.

Klapstein, K., and R. Bruinsma, 2000, J. Biol. Chem. **275**, 16073.

Klumpp, S., and R. Lipowsky, 2003, J. Stat. Phys. **113**, 233.

Knowles, R., J. Sabry, M. Martone, T. Deerinck, M. Ellisman, G. Bassell, and K. Kosik, 1996, J. Neurosci. **16**, 7812.

Kolomeisky, A., and M. Fisher, 2007, Ann. Rev. Phys. Chem. **58**(1), 675.

Kolomeisky, A. B., 1998, J. Phys. A **31**, 1159.

Kolomeisky, A. B., 2007, Phys. Rev. Lett. **98**, 048105.

Kolomeisky, A. B., 2011, Phys. Chem. Chem. Phys. **13**, 2088.

Kolomeisky, A. B., G. M. Schutz, E. B. Kolomeisky, and J. P. Straley, 1998, J. Phys. A **31**, 6911.

Kosik, K. S., C. L. Joachim, and D. J. Selkoe, 1986, Proc. Natl. Acad. Sci. U.S.A. **83**, 4044.

Kou, S. C., 2008, Annals Appl. Stat. **2**, 501.

Kozminski, K. G., J. K, A, P. Forscher, and J. L. Rosenblum, 1993, Proc. Natl. Acad. Sci. U. S. A. **90**, 5519.

Krapivsky, P. L., and K. Mallick, 2010, J. Stat. Mech. **7**, P07007.

Krug, J., 1991, Phys. Rev. E **67**, 1882.

Kubo, R., 1962, in *Fluctuation, relaxation and resonance in magnetic systems*, edited by D. TerHaar (Oliver and Boyd, Edinburgh), pp. 23–68.

Kural, C., H. Kim, S. Syed, G. Goshima, V. I. Gelfand, and P. R. Selvin, 2005, Science **308**, 1469.

Kustanovich, T., and Y. Rabin, 2004, Biophys J. **86**, 2008.

Kusumi, A., C. Nakada, K. Ritchie, K. Murase, and K. S. et al., 2005, Annu. Rev. Biophys. Biomol. Struct. **34**, 351.

Kusumi, A., Y. M. Shirai, I. Koyama-Honda, K. G. N. Suzuki, and T. K. Fujiwara, 2010, FEBS Lett. **584**, 1814.

Kuznetsov, A. V., and A. A. Avramenko, 2008, Proc. Roy. Soc. A **464**, 2867.

Lacayo, C. I., Z. Pincus, M. M. VanDuijn, C. A. Wilson, D. A. Fletcher, F. B. Gertler, A. Mogilner, and J. A. Theriot, 2007, PLoS Biol. **5**, 2035.

Lagache, T., E. Dauty, and D. Holcman, 2009a, Curr. Opin. Microbiol. **12**, 439.

Lagache, T., E. Dauty, and D. Holcman, 2009b, Phys. Rev. E **79**, 011921.

Lagache, T., and D. Holcman, 2008, SIAM J. Appl. Math **68**, 1146.

Lakatos, G., J. O'Brien, and T. Chou, 2006, J. Phys. A **39**, 2253.

Lakhanpal, A., and T. Chou, 2007, Phys. Rev. Lett. **99**, 248302.

Lamoureux, P., R. E. Buxbaum, and S. R. Heidemann, 1989, Nature **340**, 159.

Lauffenburger, D. A., 1996, *Receptors: models for binding, trafficking, and signaling* (Oxford University Press, Oxford).

Layton, A. T., N. S. Savage, A. S. Howell, S. Y. Carroll, D. G. Durbin, and D. J. Lew, 2011, Curr. Biol. **21**, 184.

Lebowitz, J. L., and J. K. Percus, 1967, Phys. Rev. **155**, 122.

Leitner, D. M., F. L. H. Brown, and K. R. Wilson, 2000, Biophys. J. **78**, 125.

Lenz, P., and L. Sogaard-Andersen, 2011, Nat. Rev. Microbiol. **9**, 565.

Levitt, D. G., 1973, Phys. Rev. A **8**, 3050.

Li, G.-W., O. G. Berg, and J. Elf, 2009, Nat. Phys. **4**, 294.

Li, Y., P. Jung, and A. Brown, 2012, J. Neurosci. **32**, 746.

Liepelt, S., and R. Lipowsky, 2007, Phys. Rev. Lett. **98**, 258102.

Lim, R. Y., B. Fahrenkrog, J. Koser, K. Schwarz-Herion, and W. Z. et. al., 2007, Science **318**, 640.

Lim, R. Y., N. P. Huang, J. K. J, J. Deng, and K. H. Lau, 2006, Proc. Natl. Acad. Sci. USA **103**, 9512.

Lipowsky, R., and S. Klumpp, 2005, Physica A Statistical Mechanics and its Applications **352**(1), 53.

Lipowsky, R., S. Klumpp, and T. M. Nieuwenhuizen, 2001, Phys. Rev. Lett. **87**, 108101.

Lippincott-Schwartz, J., and R. D. Phair, 2010, Ann. Rev. Biophys. **39**, 559.

Lippincott-Schwartz, J., T. H. Roberts, and K. Hirschberg, 2000, Ann. Rev. Cell Dev. Biol. **16**, 557.

Lizana, L., and T. Ambjornsson, 2008, Phys. Rev. Lett. **100**, 200601.

Loose, M., K. Kruse, and P. Schwille, 2011, Annu. Rev. Biophys. **40**, 315.

Loverdo, C., O. Benichou, M. Moreau, and R. Voituriez, 2008, Nat. Phys. **4**, 134.

Lowe, A. R., J. J. Siegel, P. K. abd M Siu, K. Weis, and J. T. Liphardt, 2010, Nature **467**, 600.

Luby-Phelps, K., 2000, Int. Rev. Cytol **192**, 189.

Lutz, E., 2001, Phys. Rev. E **64**, 051106.

Maas, C., D. Belgardt, H. K. Lee, F. F. Heisler, C. Lappe-Siefke, M. M. Magiera, J. van Dijk, T. J. Hausrat, C. Janke, and M. Kneussel, 2009, Proc. Natl. Acad. Sci. U.S.A. **106**, 8731.

Macara, I. G., 2001, Microbiol Mol Biol Rev **65**, 570.

MacDonald, C. T., and J. H. Gibbs., 1969, Biopolymers **7**, 707.

MacDonald, C. T., J. H. Gibbs, and A. C. Pipkin, 1968, Biopolymers **6**, 1.

MacGillavry, H. D., J. M. Kerr, and T. A. Blanpied, 2011, Mol. Cell. Neurosci. **48**, 321.

Magdziarz, M., A. Weron, K. Burnecki, and J. Kalfter, 2009, Phys Rev Lett **103**, 180602.

Mallik, R., and S. P. Gross, 2004, Current Biology **14**(22), R971.

Mandelbrot, B. B., and J. W. V. Ness, 1968, SIAM Rev. **10**, 422.

Marco, E., R. Wedlich-Soldner, R. Li, S. J. Altschuler, and L. F. Wu, 2007, Cell **129**, 411.

Marshall, W. J., H. Qin, M. R. Brenni, and J. L. Rosemblum, 2005, Mol. Cell Biol. **16**, 270.

Marshall, W. J., and J. L. Rosemblum, 2001, J. Cell Biol. **155**, 405.

Matlack, K. B., B. Misselwitz, K. Plath, and T. Rapoport, 1999, Cell **97**, 553.

Maxfield, F. R., and T. E. McGraw, 2004, Nat. Rev. Mol. Cell Biol. **5**, 121.

McLean, D. R., and B. P. Graham, 2004, Proc. Roy. Soc. Lond. A **460**, 2437.

Metzler, R., and J. Klafter, 2000, Phys. Rep. **339**, 1.

Metzler, R., and J. Klafter, 2004, J. Phys. A **37**, R161.

Miller, K. E., and D. C. Samuels, 1997, J. Th. Biol. **186**, 373.

Miller, K. E., and M. P. Sheetz, 2004, J. Cell Sci. **117**, 2791.

van Milligen, B. P., B. A. Carreras, and R. Sanchez, 2005, Plasma Phys. Control. Fusion **47**, B743.

Mirny, L., M. Slutsky, Z. Wunderlich, A. Tafvizi, J. Leith, and A. Kosmrlj, 2009, J. Phys. A **42**, 434013.

Mistelli, T., 2001, J. Cell Biol. **155**, 181.

Mistelli, T., 2008, Histochem Cell Biol **129**, 5.

Mitchison, T., and M. Kirschner, 1984, Nature **312**, 237.

Mitchison, T. J., and M. Kirschner, 1988, Neuron **1**, 761.

Mogilner, A., A. F. A, and R. Baskin, 2001, J. Theor. Biol. **211**, 143.

Mogilner, A., and L. Edelstein-Keshet, 2002, Biophys. J. **83**, 1237.

Mori, Y., A. Jilkine, and L. Edelstein-Keshet, 2008, Biophys. J. **94**, 3684.

Morozov, 2007, Physical Review E **75**, 031910.

Morris, R. L., and P. J. Hollenbeck, 1993, J. Cell Sci. **104**, 917.

Moussavi-Baygi, R., Y. Jamali, R. Karimi, and M. R. K. Mofrad, 2011, PLoS Comp. Biol. **7**, e1002049.

Muller, M. J. I., S. Klumpp, and R. Lipowsky, 2008a, J. Stat. Phys. **133**(1059-1081).

Muller, M. J. I., S. Klumpp, and R. Lipowsky, 2008b, Proc. Natl. Acad. Sci. U. S. A. **105**, 4609.

Murray, J. D., 2002, *Mathematical Biology*, volume I and II (Springer, New York), 3rd edition.

Nadler, B., Z. Schuss, A. Singer, and R. S. Eisenberg, 2004, J. Phys. Cond. Matt. **16**, S2153.

Newby, J. M., and P. C. Bressloff, 2010a, Phys. Biol. **7**, 036004.

Newby, J. M., and P. C. Bressloff, 2010b, Bull Math Biol **72**, 1840.

Newby, J. M., and P. C. Bressloff, 2010c, J. Stat. Mech. **P04014**.

Newby, J. M., and J. P. Keener, 2011, Multiscale Model. Simul. **9**, 735.

Newpher, T. M., and M. D. Ehlers, 2008, Neuron **58**(4), 472, ISSN 1097-4199 (Electronic).

Novak, I. L., P. Kraikivski, and B. M. Slepchenko, 2009, Biophys. J. **97**, 758.

Nowak, S., P.-W. Fok, and T. Chou, 2007a, Phys. Rev. E **76**, 031135.

Nowak, S. A., P.-W. Fok, and T. Chou, 2007b, Phys. Rev. E **76**, 031135.

Ockendon, J., S. Howison, A. Lacey, and A. Movchan, 2003, *Applied partial differential equations* (Oxford University, Oxford).

O'Toole, M., R. Latham, R. M. Baqri, and K. E. Miller, 2008, J. Th. Biol. **255**, 369.

Parmeggiani, A., T. Franosch, and E. Frey, 2003, Phys. Rev. Lett. **90**, 086601.

Parmeggiani, A., T. Franosch, and E. Frey, 2004, Phys. Rev. E **70**, 046101.

Parmeggiani, A., F. Julicher, A. Ajdari, and J. Prost, 1999, Phys. Rev. E **60**, 2127.

Pavliotis, G. A., and A. M. Stuart, 2008, *Multiscale methods: averaging and homogenization* (Springer, New York).

Pelham, H. R., 2001, Trends Cell Biol. **11**, 99.

Percus, J. K., 1974, Phys. Rev. A **9**, 557.

Peskin, C., and G. Oster, 1995, Biophys. J. **65**, 202.

Peskin, C. P., G. M. Odell, and G. F. oster, 1993, Biophys. J. **65**, 316.

Peters, R., 2005, Traffic **6**, 421.

Pillay, S., M. J. Ward, A. Peirce, and T. Kolokolnikov, 2010, SIAM Multiscale Model. Sim. **8**, 803.

Popkov, V., A. Rakos, R. D. Williams, A. B. Kolomesisky, and G. M. Schutz, 2003, Phys. rev. E **67**, 066117.

Porra, J. M., K. G. Wang, and J. Masoliver, 1996, Phys. Rev. E **53**, 5872.

Posta, F., M. R. D'Orsogna, and T. Chou, 2009, Phys. Chem. Chem. Phys. **11**, 4851.

Pronina, E., and A. Kolomeisky, 2007, J. Phys. A **40**, 2275.

Prost, J., J. F. Chauwin, L. Peliti, and A. Ajdari, 1994, Phys. Rev. Lett. **72**, 2652.

Rafelski, S. M., and J. A. Theriot, 2004, Ann. Rev. Biochem. **73**, 209.

Ramirez, O. A., and A. Couve, 2011, Trends Cell Biol. **21**, 219.

Redner, S., 1997, Phys. Rev. E **56**, 4967.

Redner, S., 2001, *A guide to first-passage processes* (Cambridge University Press, Cambridge, UK).

Reed, M. C., S. Venakides, and J. J. Blum, 1990, SIAM J. Appl. Math. **50**(1), 167, ISSN 0036-1399.

Reguera, D., and J. M. Rubi, 2001, Phys. Rev. E **64**, 061106.

Reguera, D., G. Schmid, P. S. Burada, J. M. Rubi, PReimann, and P. Hanggi, 2006, Phys. Rev. Lett. **96**, 130603.

Reichenbach, T., T. Franosch, and E. Frey, 2006, Phys. Rev. Lett. **97**, 050603.

Reimann, P., 2002, Phys. Rep. **361**, 57.

Reimann, P., C. van den Broeck, H. Linke, P. Hanggi, J. M. Rubi, and A. Perez-Madrid, 2002, Phys. Rev. E **65**, 031104.

Reingruber, J., and D. Holcman, 2010, J. Phys. Cond. Matt. **22**, 065103.

Ribbeck, K., and D. Gorlich, 2001, EMBO J **21**, 2664.

Ribbeck, K., and D. Gorlich, 2002, EMBO J **21**, 2664.

Rice, S. A., 1985, *Diffusion-limited reactions* (Elsevier, Amsterdam).

Richter, P. H., and M. Eigen, 1974, Biophys. Chem. **2**, 255.

Riggs, A. D., S. Bourgeois, and M. Cohn, 1974, J. Mol. Biol. **53**, 401.

Rodenbeck, C., J. Karger, and K. Hahn, 1998, Phys. Rev. E **57**, 4382.

Rook, M. S., M. Lu, and K. S. Kosik, 2000, The Journal of Neuroscience **20**(17), 6385.

Rout, M. P., J. D. Aitchiso, M. O. Magnasco, and B. T. Chait, 2003, Trends Cell Biol **13**, 622.

Roux, B., T. Allen, S. Berneche, and W. Im, 2004, Q. Rev. Biophys. **37**, 15.

Rubi, J. M., and D. Reguera, 2010, Chem. Phys. **375**, 518.

Sabatini, B. L., M. Maravall, and K. Svoboda, 2001, Curr. Opin. Neurobiol. **11**, 349.

Saffarian, S., H. Qian, I. Collier, E. Elson, and G. Goldberg, 2006, Phys. Rev. E **73**.

Saffman, P., and M. Delbruck, 1975, Proc. Natl. Acad. Sci. USA **72**, 3111.

Salman, H., A. Abu-Arish, S. Oliel, A. Loyter, J. Klafter, R. Granek, and M. Elbaum, 2005, Biophys. J. **89**, 2134.

Santamaria, F., S. Wils, E. de Schutter, and G. J. Augustine, 2006, Neuron **52**, 635.

Saxton, M. J., 1989, Biophys. J. **55**, 21.

Saxton, M. J., 1990, Biophys. J. **57**, 1167.

Saxton, M. J., 1994, Biophys. J. **66**, 394.

Saxton, M. J., 1995, Biophys. J. **69**, 389.

Saxton, M. J., 1996, Biophys. J. **70**, 1250.

Saxton, M. J., 2007, Biophys. J. **92**, 1178.

Saxton, M. J., and K. Jacobson, 1997, Annu. Rev. Biophys. Biomol. Struct. **26**, 373.

Schadschneider, A., D. Chowdhury, and K. Nishinari, 2010, *Stochastic transport in complex systems: from molecules to vehicles* (Elsevier, Amsterdam).

Scher, H., and E. W. Montroll, 1975, Phys. Rev. B **12**, 2455.

Schnell, S., and T. Turner, 2004, Prog Biophys Mol Biol **85**, 235.

Schnitzer, M., K. Visscher, and S. Block, 2000, Nat. Cell Biol. **2**, 718.

Scholey, J. M., 2003, Ann. Rev. Cell Dev. Biol. **19**, 423.

Schreiber, G., G. Haran, and H.-X. Zhou, 2009, Chem. Phys. Rev. **109**, 839.

Schuss, Z., B. Nadler, and R. S. Eisenberg, 2001, Phys. Rev. E **64**, 036116.

Schuss, Z., A. Singer, and D. Holcman, 2007, Proc. Natl. Acad. Sci. USA **104**, 16098.

Seisenberger, G., M. U. Ried, T. Endress, H. Buning, M. Hallek, and C. Brauchle, 2001, Science **294**, 1929.

Seitz, A., H. Kojima, K. Oiwa, E.-M. Mandelkow, Y.-H. Song, and E. Mandelkow, 2002, EMBO J **21**, 4896.

Sekimoto, K., and A. Triller, 2009, Phys. Rev. E **79**, 031905.

Semplice, M., A. Veglio, G. Naldi, G. Serini, and A. Gamba, 2012, PLoS one **7**, e30977.

Shaft-Zagardo, B., and N. Kalcheva, 1998, Mol. Neurobiol. **16**, 149.

Shaw, L. B., R. K. P. Zia, and K. H. Lee, 2003, Phys. Rev. E **68**, 021910.

Sheetz, M., K. Pfister, J. Bulinski, and C. Cotman, 1998, Progress In Neurobiology **55**, 577.

Sheinman, M., O. Benichou, Y. Kafri, and R. Voituriez, 2012, Rep. Prog. Phys. **75**, 026601.

Shepherd, J. D., and R. L. Huganir, 2007, Annu. Rev. Cell Dev. Biol. **23**, 613.

Shouval, H. Z., 2005, Proc. Natl. Acad Sci. USA **102**, 14440.

Singer, A., Z. Schuss, and D. Holcman, 2006a, J. Stat. Phys. **122**(465-489).

Singer, A., Z. Schuss, and D. Holcman, 2006b, J. Stat. Phys. **122**, 491.

Singer, S. J., and G. L. Nicolson, 1972, Science **175**, 720.

Slutsky, M., and L. A. Mirny, 2004, Biophys J. **87**, 4021.

Smith, D. A., and R. M. Simmons, 2001, Biophys. J. **80**, 45.

Smoluchowski, M. V., 1917, Z. Phys. Chem. **92**, 129.

Soldati, T., 2006, Nat. Rev. Mol. Cell Biol. **7**, 897.

Soppina, V., A. K. Rai, A. J. Ramiaya, P. Barak, and R. Mallik, 2009, Proc. Natl. Acad. Sci. U. S. A. **106**, 19381.

Sorra, K. E., and K. M. Harris, 2000, Hippocampus **10**, 501.

Stratonovich, R. L., 1958, Radiotekhnika i elektronika **3**, 497.

Straube, R., M. J. Ward, and M. Falcke, 2007, J. Stat. Phys. **129**, 377.

Sung, B. J., and A. Yethiraj, 2008, J. Phys. Chem. B **112**, 143.

Suter, D. M., and K. E. Miller, 2011, Prog. Neurobiol. **94**, 91.

Szymanski, J., and M. Weiss, 2009, Phy. Rev. Lett. **103**, 038102.

Tafvizi, A., F. Huang, J. S. Leith, A. R. Ferscht, L. A. Mirny, and A. M. van Oijen, 2008, Biophys. J. **94**, 3323.

Taloni, A., and M. A. Lomholt, 2008, Phys. Rev. E **78**, 051116.

Taloni, A., and F. Marchesoni, 2006, Phys. Rev. Lett. **96**, 020601.

Telley, I. A., P. Bieling, and T. Surrey, 2009, Biophys. J. **96**, 3341.

Tokuraku, K., T. Q. Noguchi, M. Nishie, K. Matsushima, and S. Kotani, 2007, J. Biochem. **141**, 585.

Torquato, S., 2002, *Random heterogeneous materials* (Springer, New York).

Tothova, J., G. Vaszlova, L. Glod, and V. Lisy, 2011, Eur. J. Phys. **32**, 645.

Tran, E. J., and S. R. Wente, 2006, Cell **125**, 1041.

Triller, A., and D. Choquet, 2005, Trends Neurosci. **28**, 33.

Turner, T. E., S. Schnell, and K. Burrage, 2004, Comp. Biol. Chem. **28**, 165.

Valenzuela, J. I., M. Jaureguiberry-Bravo, and A. Couve, 2011, Mol. Cell. Neurosci. **48**, 269.

van Veen, M. P., and J. van Pelt, 1994, Bull. Math. Biol. **56**, 247.

Vereb, G., J. Szollosi, J. M. P. Nagy, and T. Farkas, 2003, Proc. Natl. Acad. Sci. USA **100**, 8053.

Vershinin, M., B. C. Carter, D. S. Razafsky, S. J. King, and S. P. Gross, 2007, Proc. Natl. Acad. Sci. U.S.A. **104**, 87.

Visscher, K., M. Schnitzer, and S. Block, 1999, Nature **400**, 184.

Viswanathan, G., S. Buldyrev, S. Havlin, M. da Luz, E. Raposo, and H. Stanley, 1999, Nature **401**, 911.

Viswanathan, G. M., M. G. E. da Luz, E. P. Raposo, and H. E. Stanley, 2011, *The physics of foraging: An introduction to random Searches and biological encounters* (Cambridge University Press, Cambridge).

Vitriol, E. A., and J. Q. Zheng, 2012, Neuron **73**, 1068.

de Vos, K. J., A. J. Grierson, S. Ackerley, and C. C. J. Miller, 2008, Ann. Rev. Neurosci. **31**, 151.

Wang, H., T. C. Elston, A. Mogilner, and G. oster, 1998, Biophys. J. **74**, 1186.

Wang, K. G., 1992, Phys. Rev. A **45**, 833.

Wang, K. G., and C. W. Lung, 1990, Phys. Lett. A **151**, 119.

Wang, L., and A. Brown, 2001, Mol. Cell Biol. **12**, 3257.

Wang, L., C. L. Ho, D. Sun, R. K. H. Liem, and A. Brown, 2000, Nat. Cell. Biol. **2**, 137.

Ward, M. J., 2000, Nat. Res. Model. **13**, 271.

Ward, M. J., W. D. Henshaw, and J. B. Keller, 1993, SIAM J. Appl. Math **53**, 799.

Weber, S. C., A. J. Spakowitz, and J. A. theriot, 2010, Phys. Rev. Lett. **104**, 238102.

Wedlich-Soldner, R., S. C. Wai, T. Schmidt, and R. Li, 2004, J. Cell. Biol. **166**, 889.

Weigel, A. V., B. Simon, M. M. Tamkun, and D. Krapf, 2011, Proc. Nat. Acad. Sci. USA **108**, 6438.

Weiss, M., M. Elsner, F. Kartberg, and T. Nilsson, 2004, Biophys. J. **87**, 3518.

Welte, M., 2004, Current Biology **14**(13), R525.

Whittaker, G. R., M. Kann, and A. Helenius, 2000, Annu. Rev. Cell Dev. Biol. **16**, 627.

Wiley, H. S., S. Y. Shvartsman, and D. A. Lauffenburger, 2003, Trends Cell Biol. **13**, 43.

Winter, R. B., , and P. H. von Hippel, 1981, Biochem. **20**, 6948.

Yang, Y. M., R. H. Austin, and E. C. Cox, 2006, Phys. Rev. Lett. **97**, 048302.

Yuste, R., A. Majewska, and K. Holthoff, 2000, Nat. Neurosci. **3**, 653.

Zhou, H. X., 2005, Biophys. J. **88**, 1608.

Zhou, H.-X., G. Rivas, and A. P. Minton, 2008, Annu. Rev. Biophys. **37**, 375.

Zia, R. K. P., J. J. Dong, and B. Schmittmann, 2011, J. Stat. Phys. **144**, 405.

Zilman, A., S. D. Talia, B. T. Chait, M. P. Rout, and M. O. Magnasco, 2007, PLoS Comp. Biol. **3**, e125.

Zumofen, G., J. Klafter, and A. Blumen, 1990, Phys. Rev. A **42**, 4601.

Zwanzig, R., 1990, Acc. Chem. Res. **23**, 148.

Zwanzig, R., 1992, J. Phys. Che,. **96**, 3926.